EFFECTS OF LARGE-EDDY BREAKUP DEVICES IN A TURBULENT FLOW

by

PONNAMPALAM BALAKUMAR

B.Sc(Eng)Hons., University of Sri Lanka, Peradeniya (1977)
M.S., University of Missouri, Rolla (1981)

SUBMITTED IN PARTIAL FULFILLMENT OF THE REQUIREMENTS FOR
THE DEGREE OF
DOCTOR OF PHILOSOPHY

at the

MASSACHUSETTS INSTITUTE OF TECHNOLOGY

September 1986

Signature redacted

Signature of Author --
Department of Aeronautics and Astronautics August, 1986

Signature redacted

Certified by --
Professor Sheila E.Widnall
Thesis Supervisor, Professor of Aeronautics and Astronautics

Signature redacted

Certified by --
Professor Marten T.Landahl
Professor of Aeronautics and Astronautics

Signature redacted

Certified by ---- -----------------
Professor Joseph H.Haritonidis
Associate Professor of Aeronautics and Astronautics

Signature redacted

Accepted by -- ---
Professor Harold Y.Wachman
Chairman, Department Graduate Committee

p.231-233 contain text that runs off the edge of the page margin.

EFFECTS OF LARGE-EDDY BREAKUP DEVICES IN A TURBULENT FLOW

by

Ponnampalam Balakumar

Submitted to the Department of Aeronautics and Astronautics, June, 1986 in partial fulfillment of the requirements for the Degree of Doctor of Philosophy in Aeronautics and Astronautics.

ABSTRACT

Effects of large-eddy breakup devices (LEBU) in a turbulent boundary layer are investigated using analytical and numerical techniques. The modifications to the vertical velocity of a turbulent flow by the large-eddy breakup devices (LEBU) were analyzed using linear three-dimensional unsteady aerodynamics. A Fourier component of the input turbulence convected over these devices was considered and the modified vertical velocity in the far downstream wake was solved. It is shown that the amplitude of the vertical velocity behind the device is reduced, the effect increasing with increasing stream and spanwise wavenumber. Two plates placed far apart in series produce a reduction that is the square of that for a single plate. The presence of the ground plane decreases the effectiveness of the LEBU in reducing the amplitude of the vertical velocity in the far wake.

To study the effect of the wake, interaction of a vortex pair and a wake which has a velocity defect in the Gaussian form is investigated. It is shown that the wake reduces the motion of the eddy towards the wall and spreads the eddy in the streamwise direction. This is observed in two and three-dimensional cases. Due to the mean shear the vorticity in the wake accumulates only in the upper part of the wake and forms concentrated shear layer regions.

Thesis Supervisor: Dr. Sheila E.Widnall
Title: Professor of Aeronautics and Astronautics

ACKNOWLEDGEMENTS

The author wishes to thank his sincere gratitude to his thesis supervisor, Professor Sheila Widnall for her patience and understanding in the course of this investigation.

Special thanks are also due to Professors Marten Landahl, Joseph Haritonidis and Judson Baron for their comments and support: to fellow graduate students for their interest and discussions: and to my roommates and many other friends near and far for their friendship and support.

The work reported in this thesis was funded by Airforce Office of Scientific Research under contract F-49620-83c-0019.

CONTENTS

CHAPTER NO. PAGE NO.

Figures

Chapter 1

Introduction:

Growing energy conciousness has generated interest in developing techniques for reducing drag forces on aerodynamic bodies. The drag force appears in three forms: (1) viscous drag (2) form drag, and (3) induced drag (vortex drag). Viscous drag ranges from 25% of the total drag for supersonic fighters to 50% for long haul transports and 54% for general aviation jets. Bushnell (1983) reviews many of the drag reduction concepts currently available and being considered for practical applications. In this thesis one of the above techniques known as large-eddy breakup devices (LEBU) is investigated. This method is presently being investigated in the laboratories as a feasible method to reduce the skin friction in a turbulent boundary layer. A LEBU may consist of horizontal and vertical plate elements, having various planforms and cross-sectional geometries and mounted within the turbulent boundary layer to directly interact with the large-scale motion. A schematic diagram of this device when two plates are used in tandem is depicted in Fig. 1.

The original experimental research on this type of technique to modify the structure of turbulence was conducted by Yanik and Acharya (1977), who inserted a 18x18 mesh screen fence within the turbulent boundary layer across the flow of a low-speed wind tunnel and obtained local skin friction reductions in excess of 50% over a distance of 100-150 boundary layer thicknesses downstream of the device. In this approach the drag associated with the fence was much higher than the total reduction in the skin friction; hence no net drag reduction was obtained. In 1979 Hefner, Weinstein and Bushnell at Nasa Langeley Research Center and Nagib (1979) at IIT tested LEBU devices with a few horizontal elements and found a 20% reduction in downstream average skin friction with much lower device drag, but still no net drag reduction was obtained within a 50 boundary layer thickness downstream. Corke (1982), testing with two plates in tandem, obtained a net drag reduction of up to 20% accompanied by a decrease in the number of burst rate of approximately 18% within 55 boundary layer thickness. The geometrical configuration used in the experiment is shown in Fig. 1. Following this there were a series of experiments done using tandem configuration (Bertelrud and Truong, 1982, Hefner et al. ,1983, Mangus ,1983, Anders et al. ,1984, Plesniak and Nagib ,1985, Guezennec and Nagib ,1985, Anders and Watson ,1985). These experiments were primarialy parametric studies and produced the following results. The average skin friction reduction behind the devices is about 20% and this reduction persists for 100-120 boundary layer thickness. A more modest value of 0-20% net drag reduction could be obtained using tandem configuration. The intensity of the streamwise velocity component is reduced below the device height and is increased above the device (Bertelrud et al. ,1982). The normal velocity component and the bursting frequency are reduced behind the plate. Recently, Sahlin et al. (1986) directly measured the drag force on a plate equipped with LEBU devices in a towing tank for a range of Reynolds numbers based on LEBU length of 25,000-100,000. Their main results show that there is no net drag reduction for this Reynolds number range and there was mainly a drag increase. Only for the lowest Reynolds number of 25,000 was a 2% drag reduction obtained.

Though the results obtained at different laboratories show quantitative differences, they all agree that the local skin friction is reduced behind the devices and this reduction persists for long distances downstream of the LEBU devices. One of the major concerns among the researchers is the question of whether net drag reduction can be obtained. In this work, it is attempted to explain, how the skin friction is reduced behind these devices using theoretical models.

A turbulent boundary layer may be divided into four regions: viscous sublayer ($y^+<5$), buffer region ($5<y^+<50$), logarithmic region ($50<y^+$, $y<.2\delta$) and wake region ($y>.2\delta$) Fig. 2. The viscous sublayer, the buffer region, and the logarithmic region is called the wall region and the wake region is called the outer region or the large-scale region. Many investigators using flow visualization techniques and hot-wire anemometer techniques investigated these two regions in the last two decades. Kline et al. (1967), Kim et al. (1971), Rao et al. (1971), Wallace et al. (1972), Willmarth et al. (1972), Lu et al. (1973), Nychas et al. (1974), Blackwelder et al. (1976), Thomas et al. (1983) and many others investigated the wall region using flow visualization and conditional sampling techniques. Willmarth (1975) reviewed the status and extend of the knowledge of the structure of turbulence in boundary layers. The picture that emerges from these investigation is as follows. The wall layer is dominated by intermittent events called bursts and sweeps. These events happen in stages. In the first stage low-speed fluid appears in the sublayer as elongated streaks. The width of a streak is about 10-30y^+ units and the spacing between the streaks is about 80-100z^+. This low speed streak is surrounded on either side by two counter rotating vortices. The rotation of these vortices is such as to lift up the low-speed fluid away from the wall. In the next stage the low-speed streak migrates slowly downstream and at the same time slowly lifts away from the wall. After it travels some distance the streak fluid ejects as a jet into the outer high speed region. This forms an inflexional profile in the buffer region $5<y^+<50$. This inflexional profile becomes unstable, oscillates, and finally breaks up. Then high speed fluid moves towards the wall from upstream and sweeps the debris from the burst. This is called the sweep event. The whole process is called bursting. Most of the turbulence and Reynolds stress are produced during this bursting. About 70% of the average Reynolds stress is produced during the ejection-like event and 70% during the sweep-like event. The remainder is made up by wallward and outward interactions. During the breakup process high mixing between the low speed fluid near the wall and the high speed fluid in the outer region takes place.

Klebanoff (1954), Kovasznay et al. (1970), Antonia (1972), Head et al. (1981), Chen et al. (1978) and many others investigated the flow properties and the structures in the outer region of a turbulent boundary layer. Fig. 3 shows the distribution of the statistical properties of the turbulent velocities in a turbulent boundary layer (Klebanoff ,1954). The outer region consists of a collection of horse-shoe or hair-pin vortices which are inclined at 45° to the free stream. Collectively this structure has a very slow rotational motion towards the wall. These horse-shoe vortices exist to very near the wall and have the dimensions of viscous units.

At this stage, the interaction between the inner region and the outer region and the function of the outer region on the bursting process are not well understood. But there are some speculative answers which are based on some flow visualization and hot-wire measurements studies. Nychas et al. (1973) in their investigation observed that a large scale, high speed, fluid from the outer region moves towards the wall before the ejection starts. Falco (1983) from his experimental ovservations suggested that the outer flow brings down the so called "typical eddies" towards the wall which later initiate the lift up process. From the conditional sampling and visual counting techniques Kim et al. (1971), Rao et al. (1971) and Lu et al. (1973) determined the bursting frequency and their results showed that the bursting frequency scaled with the outer variables. But contradictory to this, Blackwelder and Haritonidis (1983), Mangus (1983) show that the bursting frequency scaled with the wall variables. Alfredson et al. (1982) from their experimental results obtained in a channel flow found that the governing timescale for the wall region to be a mixture (the geometric mean) of inner and outer scales. From these observations it is suggestive that the large-scale outer motion has some influence on the bursting process.

Hence, when the LEBU devices are placed in the outer part of the turbulent boundary layer, the devices directly interact with the large-scale motion and modify or alter it. Due to this interaction the devices interfere with the bursting process and hence can produce a skin friction reduction downstream. In the following chapters, the effects of the LEBU devices on the outer part of the boundary layer is determined using analytical and numerical techniques and from these results possible mechanisms for the skin friction reduction are discussed.

At a more basic level there is still no complete structural picture of the interaction between the plates and the incoming boundary layer eddies or the mechanism whereby the skin friction is reduced. It has generally been stated (Hefner et al. ,1983) that the LEBU devices suppress the large-scales by restricting vertical fluctuations when the large-scales are advected over the plate. Munford and Savill (1983) postulated from their flow visualization studies that the wake which is generated behind the device acts like a barrier between the upper and lower regions of the boundary layer and this causes the reduction in the skin friction. But it is argued, on the other hand by Anders et al. (1985), that the long-lasting wake is the result of suppressing the large-scale turbulent structures and, thus the coherent wake is the effect rather than the cause. At this stage it is not clear which of these, if any, mechanisms is most important for the skin friction reduction.

We will investigate these two effects which are introduced by these devices. One is the unsteady aerodynamic effect in which the LEBU functions as an airfoil, responding to the upwash fluctuations of the incoming turbulent flow. As the large-eddy in the outer flow is advected over the LEBU, vortices are shed at the trailing edge. This vorticity modifies the velocity field behind the device. The other effect is the wake effect. When the flow is advected over the LEBU a wake is generated at the trailing edge. This wake interacts with the large-scale motion and modifies it. In the first part of this report the unsteady aerodynamic effect is analysed using analytical methods. In the second part the effects of the wake are investigated using numerical techniques.

First we will discuss the unsteady aerodynamic effect. For simplicity, it is assumed that the turbulent fluctuations are "frozen" (i.e. Taylor's Hypothesis) and advected with a constant velocity. It is considered that LEBU devices consisting of thin plane horizontal elements of finite chord located a finite distance above an infinite horizontal surface. It is assumed that the elements behave as airfoils, with rounded leading edges and sharp trailing edges at which the Kutta condition is satisfied. Initially the effects of the ground plane are neglected. Later the effects of the ground plane are included in the analysis through the method of images. When the eddy is advected over the plate it imposes an unsteady upwash on the plate. To balance this upwash, and to satisfy the Kutta condition at the trailing edge, circulation, the strength of which varies with time, is formed around the plate. Since the circulation varies with time, vortices are shed from the trailing edge and are advected downstream by the mean flow. They induce a velocity field and hence modify the eddy velocity field. In chapters 2-6 it is attempted to determine how these shed vortices from the LEBU devices modify the vertical velocity component of the eddy as it is advected downstream. Since the turbulent fluctuations are small in the region of the boundary layers where LEBU's are placed, the governing equations and the boundary conditions are linearized. The magnitude of the mean vorticity is small in the outer part of the boundary layer, and hence, its effect will be neglected in this preliminary analysis where potential flow theory is used. Within the framework of linearized theory, when the vertical velocity distribution is known, the solution can be obtained by Fourier analysis. A Fourier component $w(k_x,k_y)\exp(i\omega t-ik_x x+ik_y y)$ of the input turbulence is considered and the vertical velocity in the far wake is solved for in the form $w(k_x,k_y)\exp(i\omega t-ik_x x+ik_y y)S(k_x,k_y)$. $S(k_x,k_y)$ acts as the LEBU transfer function for the amplitude and phase of the vertical velocity of the eddy.

In chapter (2), advection of a two-dimensional eddy over a single plane element is considered. This problem is also solved using an approximate method as a prelude to the study of the effects of the ground plane. Next the effect of the tandem configuration is determined for the case when the distance between the plates becomes large. In chapters (3)-(5), advection of a three-dimensional eddy over a single plane element is considered. In chapter (3), the problem is formulated in terms of an integral equation and is solved for the case when the spanwise wavenumber k_y becomes small. In chapter (4) this case is treated in terms of an acceleration potential and is solved using matched asymptotic expansion for small k_y. In chapter (5) the case when the spanwise wavenumber k_y is large is considered. In chapter (6) the effect of the ground plane is included through the method of images and is solved for the normal velocity component in the far wake for the two and three-dimensional cases using approximate theory.

The wavenumbers k_x,k_y are non-dimensionalised by the semi-chord of the plate, c/2. The chord length of the LEBU devices used in the laboratory is of the order of the boundary layer thickness, δ ($c=0.8\delta-1.2\delta$). The one dimensional spectral distribution for the longitudinal velocity component has been measured in a turbulent boundary layer on a flat plate (Fig. 3, Klebanoff, 1954). From this, an approximate distribution for the two-dimensional spectrum for the normal velocity component is obtained using isotropic relations (Hinze, 1975). It is observed that the energy containing eddies have the non-dimensional wavenumbers $\sqrt{k_x^2 + k_y^2}$ based on half the boundary layer thickness, in the range 0.3 to 3.0.

The results for all the cases considered show that the LEBU devices reduce the amplitude of the vertical velocity in the far wake. The reduction increases with increasing k_x and k_y. For a two-dimensional disturbance it is shown that when two plates are placed far apart, this reduction is squared. The analysis incorporating the effect of the ground plane shows a decrease in the effectiveness of the LEBU in reducing the amplitude of the vertical velocity in the far wake. The effectiveness of the LEBU devices decreases as they are moved towards the plane.

Next the effect of the wake is considered. In the operating conditions the Reynolds numbers based on the length of the LEBU devices is 30,000. For this range of Reynolds number the characteristics of the wake behind the plate can be summarised as follows, Sato and Kuriki (1958). The laminar boundary layers which form on the surfaces of the plate merge and form a laminar wake at the trailing edge. This laminar wake becomes unstable and the disturbances grow exponentially with downstream distance. The frequency of oscillation corresponds to the maximum growth rate. In the next stage, nonlinear effects set in and a Karman vortex street forms. The dimensions of the vortex street depend on the Reynolds number and are shown in Fig. 5, Taneda (1957). Further downstream, three-dimensional disturbances set in and the vortex street breaks-up and forms a turbulent wake with an approximately Gaussian velocity defect. The length of the different regions depend on the Reynolds number.

In chapters 7-9 it is attempted to investigate how this wake interacts with the outer part of the turbulent boundary layer and what are the effects of this interaction on the bursting cycle. The wake is simulated in two ways. First, the wake is simulated by a Karman vortex street and second with a continuous vorticity distributions with a Gaussian velocity defect. Munford and Savill (1984), in the interpretation of their flow visualization studies, is the only paper which made an attempt to investigate the mechanisms through flow visualization studies, quoted that the wake behind the device consists of a coherent vortex street which persists upto 60 boundary layer thickness downstream. Further they discussed that the counter rotating vortices below the devices lift the fluid near the wall across the wake and the wake prevents that fluid from coming towards the wall.

Downstream of the plate this wake interacts with the large-eddies moving towards the wall and with the ejected fluid coming from the wall. To study this effect the interaction of a vortex pair with the wake is considered. The vortex pair can simulate the ejection process or the wallward movement of the outer fluid towards the wall. The problem is solved numerically and the motion of the vortex pair and the evolution of the wake is followed in time. In chapter (7) the interaction of the vortex pair and the vortex street is considered. In chapter (8) the interaction of the vortex pair and the continuous wake is solved using the cloud-in-cell technique. Here, the effect of the mean shear is also analysed. In chapter (9) the interaction of the vortex pair and the continuous wake is analysed using linear theory for two-dimensional and three-dimensional cases.

The results from all the cases considered show that the wake spreads the large-eddy and slows down its motion towards the wall. Due to the interaction the wake is disturbed and concentrated vorticity regions are formed on either side of the wake. When the mean shear is introduced, there is not much change in the motion of the eddy but the wake deforms differently. The vortices are formed only above the wake and the deformation below the wake disappears and the disturbance is confined to the region above the wake.

Chapter 2

The LEBU devices which are placed in the outer part of the boundary layer behave as airfoils, with rounded leading edges and sharp trailing edges at which the Kutta condition is satisfied. When the eddy is advected over the plate it imposes an unsteady upwash on the plate. To balance this upwash, and to satisfy the Kutta condition at the trailing edge, circulation, the strength of which varies with time, is formed around the plate. Since the circulation varies with time, vortices are shed from the trailing edge and are advected downstream by the mean flow. They induce a velocity field and hence modify the eddy field. In this chapter we will investigate the interaction of a two-dimensional eddy and the LEBU devices. We assume linear potential theory and consider one Fourier component of the advecting eddy.

2.1 Analysis of a two-dimensional model

A two dimensional thin rectangular plate of chord length 'c' is placed in the x,y plane and its mid chord is positioned with the y axis, as shown in Fig. 6. A turbulent gust with a normal velocity component of the form $w(k_x)\exp(i\omega t-ik_x x)$ is convected by a uniform stream of velocity U. We assume invisid, irrotational flow. Frozen convection (ie, Taylor's hypothesis) is assumed; therefore the wavenumber is

$$k_x = \omega/U$$

and the non-dimensionalised wavenumber is

$$\bar{k}_x = k_x \, c/2$$

The approach we follow is first given by Schwarz (1940) and is discussed in Bisplinghoff et al. (1955). For the linearized theory the governing equation for the perturbed potential ϕ is given by

$$\phi_{xx} + \phi_{zz} = 0;$$

the pressure coefficient by

$$c_p = -2 \, \phi_x - 2 \, \phi_t / U$$

The boundary conditions are

(1) For $-c/2 \leq x \leq c/2 \; ; \; z = \pm 0$

$$\phi_z = -w(k_x) \exp(i\omega t - ik_x x)$$

(2) $\phi \to 0$ as $x^2 + y^2 \to \infty$

and

(3) zero pressure discontinuity across the wake ($x \geq c/2$, $z = 0$)

From the boundary condition (1) it is evident that ϕ is antisymmetric about z=0. Therefore, a discontinuity in horizontal velocity exists across the plane z=0. We replace the wing and the wake by a vortex sheet of strength $\gamma(x,t)$, Fig. 6, where

$$\begin{aligned}\gamma(x,t) &= u(x,+0,t) - u(x,-0,t)\\ &= 2\ u(x,+0,t)\\ &= 2\ \phi_x(x,+0,t)\end{aligned}$$

Define the circulation as

$$\begin{aligned}\Gamma\ (x,t) &= \int_{-\infty}^{x} \gamma(x_1,t)\ dx_1\\ &= 2 \int_{-\infty}^{x} \phi_x(x_1,+0,t)\ dx_1\end{aligned}$$

Hence $\Gamma(x,t) = 2\ \phi(x,+0,t)$ (1)

Therefore, the total circulation around the plate

$$\Gamma(c/2,t) = \int_{-c/2}^{c/2} \gamma(x_1,t)\ dx_1$$

is equal to

$$\Gamma(c/2,t) = 2\ \phi(c/2,+0,t) \qquad (2)$$

Since the ϕ is antisymmetric about z=0, no pressure jump across the wake requires

$$c_p = 0.0 \qquad \text{for } x \geq c/2\ ,\quad z=0.$$

This gives

$$\phi_x(x,+0,t) + \phi_t(x,+0,t)/U = 0$$

The solution of this equation satisfies the relation

$$\phi(x,+0,t) = \phi(c/2,+0,t - x-c/2) \qquad (3)$$

i.e., the disturbance propagates downstream with the velocity U.

From equations (1),(2) and (3) we obtain

$$\Gamma(x,t) = \Gamma(c/2,t - x-c/2)$$

and

$$\gamma(x,t) = -\Gamma_t(c/2,t - x-c/2)/U \qquad (4)$$

Since this is a linear problem and the time appears in the boundary condition as simple harmonic oscillation, all the variables will have the simple harmonic time dependent.

$$\Gamma(c/2,t) = \bar{\Gamma}(c/2) \exp(i\omega t)$$

$$\gamma(x,t) = \bar{\gamma}(x) \exp(i\omega t)$$

Then, from eq.(4) we obtain an expression for $\bar{\gamma}(x)$

$$\bar{\gamma}(x) = -ik_x \bar{\Gamma}(c/2) \exp(i\bar{k}_x) \exp(-ik_x x) \quad \text{for } x \geq c/2 \qquad (5)$$

The boundary condition on the plate is written as

$$-w(k_x)\, e^{(\iota\omega t - \iota k_x x)} = -\frac{1}{2\pi}\int_{-c/2}^{c/2} \frac{\gamma(x_1,t)}{x-x_1}\,dx_1$$

$$-\frac{1}{2\pi}\int_{c/2}^{\infty}\frac{\gamma(x_1,t)}{x-x_1}\,dx_1$$

Substituting eq.(5) into this equation we obtain

$$-w(k_x)\, e^{-\iota k_x x} = -\frac{1}{2\pi}\int_{-c/2}^{c/2}\frac{\bar{\gamma}(x_1)}{x-x_1}\,dx_1 + \iota \bar{k}_x\, \frac{\bar{\Gamma}(c/2)}{c/2}\, e^{\iota \bar{k}_x}\int_{c/2}^{\infty}\frac{e^{-\iota k_x x_1}}{x-x_1}\,dx_1$$

Schwartz (1940) used Sohngens inversion formula (Bisplinghoff et al. 1955) to solve this integral equation to obtain $\bar{\gamma}(x)$. Integrating this expression for $\bar{\gamma}(x)$ the circulation around the plate $\bar{\Gamma}(c/2)$ is obtained. Since we are interested only in the circulation $\bar{\Gamma}(c/2)$ we continue as follows. Non-dimensionalize the x-variable through division by c/2, multiply the whole equation by $\sqrt{(1.+x)/(1.-x)}$, and integrate it from -1 to +1. One then obtains

$$W(k_x)\int_{-1}^{+1}\sqrt{\frac{1+x}{1-x}}\;e^{-i k_x x}\,dx = \frac{1}{2\pi}\int_{-1}^{+1}\left\{\sqrt{\frac{1+x}{1-x}}\int_{-1}^{+1}\frac{\bar{\gamma}(x_1)}{x-x_1}\,dx_1\right\}dx$$

$$-\frac{i}{2\pi}\,\bar{k}_x\,\frac{\bar{\Gamma}(c/2)}{c/2}\,e^{i\bar{k}_x}\int_{-1}^{+1}\left\{\sqrt{\frac{1+x}{1-x}}\int_{1}^{\infty}\frac{e^{-i k_x x_1}}{x-x_1}\,dx_1\right\}dx$$

We evaluate these integrals in closed form (appendix A) and find that

$$W(k_x)\,\pi\left\{J_0(\bar{k}_x) - i\,J_1(\bar{k}_x)\right\} = \frac{1}{2}\,\frac{\bar{\Gamma}(c/2)}{c/2}$$

$$-\,i\,\bar{k}_x\,e^{i\bar{k}_x}\,\frac{\bar{\Gamma}(c/2)}{c/2}\left\{\frac{1}{2}\,\frac{e^{-i\bar{k}_x}}{i\bar{k}_x} + \frac{1}{2}\,\frac{\pi}{2}\left[H_1^{(2)}(\bar{k}_x) + i\,H_0^{(2)}(\bar{k}_x)\right]\right\}$$

where J_0, J_1 are Bessel functions of first kind and $H_0^{(2)}$, $H_1^{(2)}$ are Hankel functions of second kind.

After simplifying this expression we obtain the known results

$$\frac{\bar{\Gamma}(c/2)}{c/2} = -\,\frac{4\,W(k_x)\left\{J_0 - i\,J_1\right\}e^{-i\bar{k}_x}}{i\,\bar{k}_x\left\{H_1^{(2)} + i\,H_0^{(2)}\right\}} \qquad (6)$$

Substituting this into eq.(5) we obtain for the strength of the shed vortices as

$$\bar{\gamma}(x) = \frac{4\, w(k_x)\left\{ J_0 - i J_1 \right\} e^{-i k_x x}}{\left\{ H_1^{(2)} + i H_0^{(2)} \right\}} \tag{7}$$

Having this, one may determine the velocity field in the far wake. Consider a vortex sheet of strength $\bar{y}$ exp($-ik_x x$) which lies on the xy-plane. Outside this vortex sheet the flow is governed by the potential equation and the solution is given by(Appendix B)

$$\phi = i\, \bar{y}\,|z|/z \, \exp(-ik_x x)\, \exp(-k_x\, z\,)/(2k_x)$$

The normal velocity component is

$$\phi_z = -i\, \bar{y}\, \exp(-ik_x x)\, \exp(-k_x\, z\,) \tag{8}$$

Using eq.(7) for $\bar{y}$ we obtain the induced velocity due to the shed vortices at z=0 as

$$W_{IN}(x) = -\frac{2i\left\{ J_0 - i J_1 \right\}}{\left\{ H_1^{(2)} + i H_0^{(2)} \right\}}\, w(k_x)\, e^{-i k_x x}$$

The total velocity in the wake at z=0 is the sum of the induced velocity and the gust velocity, and is given by

$$w_T(x,t) = w(k_x) \exp(i\omega t) \exp(-ik_x x) S(\bar{k}_x)$$

where

$$S(\bar{k}_x) = 1.0 - \frac{2i\left\{J_0 - iJ_1\right\}}{\left\{H_1^{(2)} + iH_0^{(2)}\right\}} \qquad (9)$$

The $S(\bar{k}_x)$ functions as a transfer function and measures the change in amplitude and phase of the normal velocity in the far wake with respect to that upstream of the LEBU. Amplitude and phase angle of $S(\bar{k}_x)$ are calculated and shown in Figs. 9,10. The results show that the amplitude of $S(\bar{k}_x)$ decreases from 1.0 to 0.2 rapidly when $\bar{k}_x$ varies from 0.0 to 1.0. After that the amplitude decreases slowly with increasing $\bar{k}_x$ and reaches a value of 0.04 for $\bar{k}_x = 5.0$.

2.2 Analysis using quarter-chord theory

In this section as a prelude to study the effect of the ground plane we derive an approximate expression for the circulation around the plate and compare this with the exact solution obtained in the previous section. As often done in the steady airfoil theory we replace the airfoil as a loaded line placed at x = -c/4 (quarter chord from leading edge) and satisfy the vertical boundary condition at x = c/4 (3/4 quarter chord from the leading edge). In the following we refer to this as the 'Quarter chord theory'. The boundary condition on the plate takes the form

$$-w(k_x)\, e^{-i k_x c/2} = -\frac{1}{2\pi}\,\frac{\bar{\Gamma}(c/2)}{c/2} - \frac{1}{2\pi}\int_{c/2}^{\infty} \frac{\bar{\gamma}(x_1)}{\frac{c}{4} - x_1}\, dx_1$$

From the previous analysis the shed vorticity $\bar{\gamma}(x)$ is given by eq.(5). Substituting this in the above expression and solve for the circulation , we obtain

$$\frac{\bar{\Gamma}(c/2)}{c/2} = \frac{2\pi w(k_x)\, e^{-i \bar{k}_x/2}}{1.0 + \bar{k}_x\, e^{i \frac{\bar{k}_x}{2}} \left\{ \left[\frac{\pi}{2} - S_i\left(\frac{\bar{k}_x}{2}\right) \right] - i\, C_i\left(\frac{\bar{k}_x}{2}\right) \right\}}$$

where

$$S_i\left(\frac{\bar{k}_x}{2}\right) = \int_0^{\bar{k}_x/2} \frac{\sin \xi}{\xi}\, d\xi$$

$$C_i\left(\frac{\bar{k}_x}{2}\right) = -\int_{\bar{k}_x/2}^{\infty} \frac{\cos \xi}{\xi}\, d\xi$$

Substituting this value for the circulation in the expression for the total velocity in the far wake at z=0, we obtain

$$w_T(x) = w(k_x)\ \exp(i\omega t)\ \exp(-ik_x x)\ S(\bar{k}_x)$$

where

$$S(\bar{k}_x) = 1.0 - \frac{\pi \bar{k}_x\, e^{i\bar{k}_x/2}}{1.0 + \bar{k}_x\, e^{i\frac{\bar{k}_x}{2}} \left\{ \left[\frac{\pi}{2} - S_i\left(\frac{\bar{k}_x}{2}\right) \right] - i\, C_i\left(\frac{\bar{k}_x}{2}\right) \right\}}$$

The amplitude and phase of $S(\bar{k}_x)$ is calculated and plotted for a range of $\bar{k}_x$ values. The results are shown in Figs. 9,10. Comparing it with the exact linearized theory solutions one sees that the quarter chord theory solution is quite accurate for small wave numbers $\bar{k}_x < 0.25$.

2.3 Analysis for two tandem plates

We now consider the case where two plates are placed in tandem at a distance Nc/2 in the two-dimensional gust Fig. 7. The shed vortices from the first plate, covers the wake between the two plates. The shed vortices from the second plate covers the wake extending from the trailing edge of the second plate. The strength of these vortices can be determined in terms of the circulations Γ_1, Γ_2 and of k_x and N using the condition that there is no pressure jump across the wake. To determine the two unknowns Γ_1 and Γ_2 we use the boundary conditions on the plates resulting in two integral equations in terms of the vorticity distributions.

These integral equations are difficult to solve in closed form. If we consider the limiting case where the distance between the plates becomes large the mutual effects between the plates is negligible and we may consider the plates separately Fig. 8. In this case the reduction in velocity downstream of the second plate should be the square of that for a single plate. To estimate the minimum distance between the plates for which this approximation could be used, we considered a single plate and evaluated the induced velocity at its 3/4 chord point by its wake vorticity. Then the length of this wake which is required to obtain ±10% accuracy of this induced velocity is calculated. As we expect, this length was a function of the wavenumber and decreases with increasing wavenumber. For $k_x = 0.1, 0.25, 0.5, 1.0, 3.0, 5.0$ the required lengths were 14,7,6,4.5,3.5,3 chord-lengths respectively. The distance between the plates used in the laboratory is about 8-10 chord-lengths. Threfore, except for very small wavenumbers the above approximations can be used to determine the effect of the tandem plates. We may consider the plates separately. The strength of the shed vortices from the first plate is known from the analysis of that plate only and is given by eq.(5)

$$y_1(x,t) = -i\bar{k}_x \left(\Gamma_1/c/2 \right) \exp(ik_x) \exp(-ik_x x) \exp(i\omega t)$$

and Γ_1 is given by eq.(6)

$$\frac{\Gamma_1}{c/2} = - \frac{4\, w(k_x) \left\{ J_0 - i J_1 \right\} e^{-i\bar{k}_x}}{i \bar{k}_x \left\{ H_1^2 + i H_0^2 \right\}} \tag{10}$$

The shed vortices from the second plate is

$$\begin{aligned} y_2(x,t) &= -i\bar{k}_x (\Gamma_1/c/2) \exp(i3\bar{k}_x/2) \exp(-ik_x x) \exp(i\omega t) \\ &\quad - i\bar{k}_x (\Gamma_2/c/2) \exp(i\bar{k}_x/2) \exp(-ik_x x) \exp(i\omega t) \end{aligned} \tag{11}$$

With the use of these expressions for y_1 and y_2 the boundary condition on the plate takes the form

$$w(k_x)\, e^{-i k_x x} = -\frac{1}{2\pi}\, i \bar{k}_x\, \frac{\Gamma_1}{c/2}\, e^{i\bar{k}_x} \int_{-\infty}^{-1} \frac{e^{-i k_x \xi}}{x-\xi}\, d\xi$$

$$+ \frac{1}{2\pi} \int_{-1}^{+1} \frac{\bar{\gamma}(\xi)}{x-\xi}\, d\xi - \frac{i\bar{k}_x}{2\pi}\, \frac{\Gamma_1}{c/2}\, e^{i3\bar{k}_x} \int_{1}^{\infty} \frac{e^{-i k_x \xi}}{x-\xi}\, d\xi$$

$$- \frac{i \bar{k}_x}{2\pi} \frac{\Gamma_2}{c/2} e^{i\bar{k}_x} \int_1^\infty \frac{e^{-i \bar{k}_x \xi}}{x-\xi} \, d\xi$$

This integral equation is similar to the one which appears in the section 2.1. Using Sohngen's inversion formula this equation can be solved to obtain $\bar{\gamma}(x)$. Since we are interested only in the circulation Γ_2 we continue as follows: we multiply this equation by $\sqrt{(1+x)/(1-x)}$ and integrate it from -1 to +1. This gives us the following expression for Γ_2: (For evaluation of the integrals see Appendix A)

$$\frac{\Gamma_2}{2\pi w c/2} = - \frac{\pi\{J_0 - i J_1\} + \frac{\Gamma_1}{2\pi w c/2} i\bar{k}_x \left\{e^{i\bar{k}_x} I_2 + e^{i3\bar{k}_x} I_1\right\}}{\frac{\pi^2}{2} i\bar{k}_x e^{i\bar{k}_x} \left\{H_1^{(2)} + i H_0^{(2)}\right\}} \qquad (12)$$

where

$I_1 = \pi \left[\exp(-i\bar{k}_x)/(i\bar{k}_x) + \pi/2 \left(H_1^2 + H_0^2 \right) \right]$

$I_2 = \pi \left[-\exp(-i\bar{k}_x)/(i\bar{k}_x) + \pi/2 \left(H_1^1 + H_0^1 \right) \right]$

Hence the total normal velocity in the far wake is obtained from eqs.(8), (11) as

$$w_T = w(k_x)\ \exp(-ik_x x)\ \exp(i\omega t) S(\bar{k}_x)$$

where

$$S(\bar{k}_x) = 1. - \pi\bar{k}_x\ [\ \Gamma_1/(2\pi wc/2)\ \exp(i3\bar{k}_x) + \Gamma_2/(2\pi wc/2)\ \exp(i\bar{k}_x)\ ]$$

With the substitution of Γ_1 and Γ_2 in this expression from eq.(10) and eq.(12) this is simplified to

$$S(\bar{k}_x) = \left\{ 1.0 - 2i\,\frac{J_0 - iJ_1}{H_1^{(2)} + iH_0^{(2)}} \right\}^2$$

We note that this is equal to the square of the expression eq.(9) which we obtained for the single plate case. This confirms that the factor by which the amplitude of the normal velocity is reduced for the case of tandem plates is equal to the square of that for the single plate case. The amplitude and phase of $S(\bar{k}_x)$ is plotted in Fig. 11.

We now consider the effect of increased chord. The non-dimensional wavenumber is obtained by multiplying the wavenumber (2π/wavelength) by the semichord c/2. When a wave with a particular wavelength is convected over longer plate it will have higher non-dimensional wavenumber than that for a smaller plate. Since the amplitude reduction increases with the increasing non-dimensional wavenumbers the amplitude reduction for a particular wave is higher when it is convected over a longer plate than over a smaller one. The results doubling the length of the plate is shown in the Fig. 11:

enchanced reduction is obtained by doubling the length of the plate but less than when two plates are used in tandem.The results that the amplitude reduction increases with the increasing non-dimensional wavenumbers implies that the amplitude reduction for a particular wave is higher when it is convected over a longer plate than over a smaller one.

CHAPTER 3

Analysis of a three-dimensional model using integral method

A turbulent gust with a normal velocity component of the form $w(k_x,k_y)\exp(i\omega t-ik_x x+ik_y y)$ is convected by a uniform stream of velocity U over a thin rectangular plate as shown in Fig. 6. Frozen convection (i.e., Taylor's hypothesis) is assumed, therefore the wave number in the x direction is

$$k_x = \omega/U$$

and the non-dimensional wave numbers are

$$\bar{k}_x = k_x\ c/2$$
$$\bar{k}_y = k_y\ c/2\ .$$

We assume inviscid irrotational flow. For the linearized theory the governing equation for the perturbed potential is

$$\phi_{xx} + \phi_{yy} + \phi_{zz} = 0$$

The pressure coefficient to first order is given by

$$c_p = -2\ \phi_x - 2\ \phi_t/U$$

The boundary conditions are

1. $\phi_z = -w(k_x,k_y)\exp(i\omega t-ik_x x+ik_y y)$ for $-c/2 \leq x \leq +c/2$; $z=\pm 0$

2. $\phi \to 0$ as $x^2 + y^2 \to \infty$

and

3. pressure is continuous across the wake ($x \geq c/2$, $z = 0$).

Reissner (1947) derived a formula for the pressure distribution on an oscillating finite wing. The mechanics of this problem is similar to the one we consider in this chapter. In the first part we formulate this problem in terms of an integral equation with a similar procedure as by Reissner(1947). Graham (1970) derived this integral equation and solved by means of a Chebyshev expansion of part of the kernel function that appears in that equation.

From the boundary condition (1) it is evident that ϕ is antisymmetric about z=0. Therefore there is a discontinuity in streamwise and spanwise velocity components exists across the plane z=0. We replace the wing and the wake by a vortex sheet which consists the spanwise component γ and streamwise component δ as shown in the Fig. 6.

Here

$$\gamma(x,y,t) = 2\ u(x,y,+0,t)$$

$$\delta(x,y,t) = 2\ v(x,y,+0,t) \tag{13}$$

and u,v are streamwise and spanwise velocity components. Outside this singularity region flow is irrotational, therefore

$$u_y = v_x$$

With this equation and eq.(13) we obtain the relation between γ and δ in the form

$$\gamma_y = \delta_x \tag{14}$$

Since this is a linear problem and the time and the spanwise variations appear in the boundary condition as simple harmonic varitation, all the dependent variables become products of $\exp(i\omega t)$ $\exp(ik_y y)$. Thus the amplitudes are independent of y and t. We write

$$\gamma(x,y,t) = U\ f_1(x)\ \exp(ik_y y)\ \exp(i\omega t) \tag{15}$$

From eq.(14) we deduce that δ takes the form

$$\delta(x,y,t) = U\ i\bar{k}_y\ f_2(x)\ \exp(ik_y y)\ \exp(i\omega t) \tag{16}$$

where

$$f_2(x) = \int_{-1}^{x} f_1(x)\ dx \tag{17}$$

The pressure differences across the plane z=0 takes the form

$$\Delta c_p = - \int_{-\infty}^{x} \gamma(x_1,t)dx_1 - U\,\gamma(x,t)$$

In the wake pressure difference is zero. Since $\gamma(x,t)$ is zero for $x < -c/2$ we can replace the lower limit to $x = -c/2$. We obtain the equation

$$\int_{-c/2}^{x} \gamma(x_1,t)\,dx_1 + U\,\gamma(x,t) = 0 \quad \text{for } x \geq c/2$$

Substituting for γ from eq.(15) and using eq.(17)

$$i\bar{k}_x\, f_2(x) + f_1(x) = 0 \tag{18}$$

When x = 1, this relation gives

$$f_1(1) = -i\bar{k}_x\, f_2(1) \tag{19}$$

Differentiating eq.(18) we get

$$f'_1(x) = -i\bar{k}_x\, f_1(x)$$

The solution of this with the condition eq.(19), gives

$$f_1(x) = -i\bar{k}_x \exp(i\bar{k}_x)\, f_2(1)\exp(-ik_x x) \quad \text{for } x \geq c/2$$

$$f_2(x) = \exp(i\bar{k}_x)\, f_2(1)\exp(-ik_x x) \quad \text{for } x \geq c/2 .$$

Hence, the strength of the shed vorticity γ_w and the trailing vorticity δ_w

is given by

$$\gamma_w = - U\, i\bar{k}_x\, f_2(1)\, \exp(i\bar{k}_x)\, \exp(-ik_x x)\, \exp(ik_y y)\, \exp(i\omega t)$$
$$\delta_w = U\, i\bar{k}_y\, f_2(1)\, \exp(i\bar{k}_x)\, \exp(-ik_x x)\, \exp(ik_y y)\, \exp(i\omega t)$$

We observe that in the wake the vortex lines are parallel to the convecting gust direction. The total circulation around the plate is defined by

$$\Gamma(y,t) = \int_{-c/2}^{c/2} \gamma(x_1,t)\, dx_1$$

and is equal to

$$\Gamma(y,t) = Uc/2\, f_2(1)\, \exp(ik_y y)\, \exp(i\omega t)$$

We can derive these expressions for γ_w and δ_w with a different procedure (Appendix C). We derive the expressions for the strength of the vortices eq.(20) in terms of the circulation around the plate $f_2(1)$. To evaluate this circulation we write the boundary condition on the plate. Using the Biot-Savart law the normal velocity at any point due to the vortex sheet is

$$w(x,y,z,t) = -\frac{1}{4\pi} \iint \frac{\gamma(\xi,\eta,t)(x-\xi) + \delta(\xi,\eta,t)(y-\eta)}{\{(x-\xi)^2 + (y-\eta)^2 + z^2\}^{3/2}}\, d\xi\, d\eta$$

In the limit as z → 0 we obtain the imposed upwash on the airfoil surface by the vortex sheet

$$w(x,y,0,t) = -\frac{1}{4\pi}\iint \frac{\gamma(\xi,\eta,t)(x-\xi)+\delta(\xi,\eta,t)(y-\eta)}{\left\{(x-\xi)^2+(y-\eta)^2\right\}^{3/2}}\,d\xi\,d\eta$$

We substitute for y and δ from eqs. (15), (16), (20) and non-dimensionalise the variables with half the chord length c/2. For simplicity we take y = 0. Then the boundary condition on the plate takes the form

$$-w(k_x,k_y)\,e^{-i\bar{k}_x x} = -\frac{1}{\pi}\int_{\xi=-1}^{+1}\int_{\eta=-\infty}^{+\infty}\frac{f_1(\xi)\,e^{i\bar{k}_y\eta}(x-\xi)}{\left\{(x-\xi)^2+\eta^2\right\}^{3/2}}\,d\xi\,d\eta$$

$$+\frac{i\bar{k}_y}{4\pi}\int_{\xi=-1}^{+1}\int_{\eta=-\infty}^{+\infty}\frac{f_2(\xi)\,\eta\,e^{i\bar{k}_y\eta}}{\left\{(x-\xi)^2+\eta^2\right\}^{3/2}}\,d\eta\,d\xi$$

$$+\frac{i\bar{k}_x f_2(1)}{4\pi}\,e^{i\bar{k}_x}\int_{\xi=+1}^{\infty}\int_{\eta=-\infty}^{\infty}\frac{e^{-i\bar{k}_x\xi}\,e^{i\bar{k}_y\eta}(x-\xi)}{\left\{(x-\xi)^2+\eta^2\right\}^{3/2}}\,d\eta\,d\xi$$

$$+\frac{i\bar{k}_y f_2(1)}{4\pi}\,e^{i\bar{k}_x}\int_{\xi=+1}^{\infty}\int_{\eta=-\infty}^{\infty}\frac{e^{-i\bar{k}_x\xi}\,e^{i\bar{k}_y\eta}\,\eta}{\left\{(x-\xi)^2+\eta^2\right\}^{3/2}}\,d\eta\,d\xi$$

We evaluate some of the integrals and modify this equation into a different form (Appendix D). This expression is equivalent to the one which appears in Graham (1970).

$$-w\, e^{i\bar{k}_x x} = -\frac{\bar{k}_y}{2\pi}\int_{-1}^{+1} f_1(\xi)\, K_1\left\{\bar{k}_y\,|x-\xi|\right\}\,\mathrm{sgn}\,(x-\xi)\, d\xi$$

$$-\frac{\bar{k}_y^{2}}{2\pi}\int_{-1}^{+1} f_2(\xi)\, K_0\left\{\bar{k}_y\,|x-\xi|\right\} d\xi$$

$$-\, f_2(1)\left\{\bar{k}_x^{2}+\bar{k}_y^{2}\right\} Q\, e^{i\bar{k}_x}\, e^{-i\bar{k}_x x}$$

$$+\frac{f_2(1)}{2\pi}\left\{\bar{k}_x^{2}+\bar{k}_y^{2}\right\} e^{i\bar{k}_x(1-x)}\int_{0}^{1-x} e^{-i\bar{k}_x \xi}\, K_0\left\{\bar{k}_y\,\xi\right\} d\xi$$

$$-\frac{i\bar{k}_x}{2\pi}\, f_2(1)\, K_0\left\{\bar{k}_y\,(1-x)\right\} \qquad (21)$$

$$Q = \frac{1}{\left\{\bar{k}_x^{2}+\bar{k}_y^{2}\right\}^{1/2}}\left\{\frac{\pi}{2} - i\log_e \frac{\bar{k}_x+\sqrt{\bar{k}_x^{2}+\bar{k}_y^{2}}}{\bar{k}_y}\right\}$$

This integral equation and the relation eq.(17)

$$f_2(x) = \int_{-1}^{x} f_1(x)\, dx$$

defines the problem completely to determine the vorticity distribution $f_1(x)$. But it is difficult to obtain a closed form expression in a general case. Hence we consider a case where $\bar{k}_y$, the non-dimensional wave number in the y direction, is small and derive a closed form expression for $f_2(1)$ to $O(\bar{k}_y)$ accuracy.

If we assume $\bar{k}_y$ is small some of the integrals in eq.(21) can be simplified using the properties of the Bessel functions (Abramowitz and Stegun 1975).

(a)

Since $x-\xi \leq 2$, for small $\bar{k}_y$ we have

$$K_1\left\{ \bar{k}_y |x-\xi| \right\} = \frac{1}{\bar{k}_y |x-\xi|} + \bar{k}_y |x-\xi| \ln \frac{\bar{k}_y |x-\xi|}{2} + O(\bar{k}_y^2)$$

$$K_0\left\{ \bar{k}_y |x-\xi| \right\} = -\left\{ \log_e \frac{\bar{k}_y |x-\xi|}{2} + \gamma \right\} + O\left(\bar{k}_y^2 \log \bar{k}_y\right)$$

$$\frac{\bar{k}_y}{2\pi}\int_{-1}^{+1} f_1(\xi)\, K_1\left\{\bar{k}_y |x-\xi|\right\} \operatorname{sgn}(x-\xi)\, d\xi = \frac{1}{2\pi}\int_{-1}^{+1} \frac{f_1(\xi)}{x-\xi}\, d\xi + O(\bar{k}_y^2 \ln \bar{k}_y)$$

$$\frac{\bar{k}_y^2}{2\pi}\int_{-1}^{+1} K_0\left\{\bar{k}_y |x-\xi|\right\} f_2(\xi)\, d\xi = O(\bar{k}_y^2 \ln \bar{k}_y)$$

Both these results are equivalent to the assumption that the induced velocity due to the vortices on the plate is equal to the two-dimensional case value.

(b)

$$I = \int_0^{1-x} e^{-\iota \bar{k}_x x} K_0\{\bar{k}_y \xi\}\, d\xi$$

$$= \frac{e^{-\iota \bar{k}_x \xi}}{-\iota \bar{k}_x} K_0\{\bar{k}_y \xi\}\Bigg|_{\varepsilon}^{1-x} - \frac{\bar{k}_y}{\iota \bar{k}_x}\int_{\varepsilon}^{1-x} e^{-\iota \bar{k}_x \xi} K_1\{\bar{k}_y \xi\}\, d\xi$$

For small $\bar{k}_y$ we simplify this to

$$\bar{k}_x^2 I = +i\bar{k}_x e^{-i\bar{k}_x \varepsilon}\left\{\gamma + \ln\frac{\bar{k}_y \varepsilon}{2}\right\}$$

$$+ i\bar{k}_x e^{-i\bar{k}_x (1-x)} K_0\left\{\bar{k}_y (1-x)\right\} + i\bar{k}_x \int_{\varepsilon}^{1-x} \frac{e^{-i\bar{k}_x \xi}}{\xi}\, d\xi .$$

$$= i\bar{k}_x e^{-i\bar{k}_x \varepsilon}\left\{\gamma + \ln\frac{\bar{k}_y \varepsilon}{2}\right\} + i\bar{k}_x e^{-i\bar{k}_x (1-x)} K_0\left\{\bar{k}_y (1-x)\right\}$$

$$+ i\bar{k}_x \left[Ci\,(\bar{k}_x \varepsilon) - Ci\left\{\bar{k}_x (1-x)\right\}\right]$$

$$+ \bar{k}_x \left[Si\left\{\bar{k}_x (1-x)\right\} - Si\,(\bar{k}_x \varepsilon)\right]$$

where

$$Ci\,(z) = \int_{z}^{\infty} \frac{\cos t}{t}\, dt \quad \text{and} \quad Si\,(z) = \int_{0}^{z} \frac{\sin t}{t}\, dt$$

When $\varepsilon \longrightarrow 0$

$$Ci\,(\bar{k}_x \varepsilon) = -\left\{\gamma + \ln\,(\bar{k}_x \varepsilon)\right\}$$

Substituting these results we obtain the folowing relation for small $\bar{k}_y$

$$\bar{k}_x^2 \, I = i \bar{k}_x \, e^{-i \bar{k}_x (1-x)} \, K_0 \{ \bar{k}_y (1-x) \}$$

$$+ \; i \bar{k}_x \, \ln \frac{\bar{k}_y}{2 \bar{k}_x}$$

$$+ \; \bar{k}_x \left\{ Si \{ \bar{k}_x (1-x) \} - i \, Ci \{ \bar{k}_x (1-x) \} \right\}$$

With the simplifications (a) and (b) eq.(21) becomes

$$- \frac{W \, e^{-i \bar{k}_x x}}{U} = - \frac{1}{2\pi} \int_{-1}^{+1} \frac{f_1(\xi)}{x - \xi} \, d\xi$$

$$- \frac{f_2(1)}{2\pi} \left\{ \bar{k}_y^2 + \bar{k}_x^2 \right\}^{1/2} \left\{ \frac{\pi}{2} - i \log_e \frac{\bar{k}_x + \sqrt{\bar{k}_x^2 + \bar{k}_y^2}}{\bar{k}_y} \right\} e^{i \bar{k}_x} \, e^{-i \bar{k}_x x}$$

$$+ \frac{f_2(1)}{2\pi} \, i \bar{k}_x \, \ln \frac{\bar{k}_y}{2 \bar{k}_x} \, e^{i \bar{k}_x} \, e^{-i \bar{k}_x x}$$

$$+ \frac{f_2(1)}{2\pi} \, \bar{k}_x \left\{ Si \{ \bar{k}_x (1-x) \} - i \, Ci \{ \bar{k}_x (1-x) \} \right\} e^{i \bar{k}_x} \, e^{-i \bar{k}_x x}$$

From this equation we may obtain the expression for $f_2(1)$. To do this we multiply the equation by $\sqrt{(1+x)/(1-x)}$ and integrate it from -1 to +1 making use of the integrals in Appendix A to give

$$\bar{k}_x \int_{-1}^{+1} \sqrt{\frac{1+x}{1-x}} \; e^{i\bar{k}_x(1-x)} \left\{ Si\{\bar{k}_x(1-x)\} - i\, Ci\{\bar{k}_x(1-x)\} \right\}$$

$$= \pi \quad + \pi\cdot\frac{\pi}{2} \; e^{i\bar{k}_x} \; \bar{k}_x \left\{ Y_1(\bar{k}_x) + i\, Y_0(\bar{k}_x) \right\}$$

Using this results we solve for $f_2(1)$ and which becomes

$$f_2(1) = - \frac{w(\bar{k}_x, \bar{k}_y)}{U} \; \frac{4\, e^{i\bar{k}_x} \left\{ J_0(\bar{k}_x) - i\, J_1(\bar{k}_x) \right\}}{i\bar{k}_x \left\{ H_1^{(2)}(\bar{k}_x) + i\, H_0^{(2)}(\bar{k}_x) \right\}} \; \frac{1}{1+\varepsilon} \tag{2.2}$$

where

$$\mathcal{E} = \frac{2}{\pi} \frac{J_0 - i J_1}{H_1^{(2)} + i H_0^{(2)}} \left\{ \log \frac{a}{2} + \sqrt{1+a^2} \log \frac{1+\sqrt{1+a^2}}{a} + i \frac{\pi}{2} \left\{ \sqrt{1+a^2} - 1 \right\} \right\} \qquad (23)$$

and

$$a = \bar{k}_y / \bar{k}_x$$

After the strength of the shed vortices and the trailing vortices are obtained the velocity field in the far wake may be calculated. Consider a vortex sheet of strength $\gamma \exp(-ik_x x) \exp(ik_y y)$ in the spanwise direction (shed vorticity) and of strength $\delta \exp(-ik_x x) \exp(ik_y y)$ in the streamwise direction (trailing vorticity), which is positioned in the xy-plane. Outside this vortex sheet the flow is irrotational and the velocity potential is given by (Appendix B)

$$\phi = i|z|/z \ \gamma/(2k_x) \exp(-ik_x x) \exp(ik_y y) \exp(- \sqrt{k_x^2 + k_y^2}|z|)$$

From this we obtain the induced normal velocity due to the vortex sheet at $z = 0$ which is

$$w_{in} = -i \ \gamma/(2\bar{k}_x) \sqrt{\bar{k}_x^2 + \bar{k}_y^2} \exp(-ik_x x) \exp(ik_y y)$$

Substituting for γ from eq.(20) we obtain

$$w_{in}/U = -\ f_2(1)/2 \sqrt{\bar{k}_x^2 + \bar{k}_y^2}\ \exp(i\bar{k}_x)\ \exp(-ik_x x)\ \exp(ik_y y)$$

The total velocity in the wake at z = 0 is the sum of the induced velocity and the gust velocity and is given by

$$w_T/U = w(k_x,k_y)/U\ \exp(-ik_x x)\ \exp(ik_y y)\ S(\bar{k}_x,\bar{k}_y)$$

where

$$S(\bar{k}_x,\bar{k}_y) = 1. - f_2(1)\ \exp(i\bar{k}_x) \sqrt{\bar{k}_x^2 + \bar{k}_y^2}\ /2 \qquad (24)$$

and $f_2(1)$ is given by eq.(22). The amplitude and phase of $S(\bar{k}_x,\bar{k}_y)$ is calculated for a range of $\bar{k}_x$ and $\bar{k}_y$ values and is plotted in Figs. 12,13. The results show that the percentage reduction in amplitude increases with incresing $\bar{k}_x$ and the reduction is more for larger $\bar{k}_y$. For $\bar{k}_x >> 1.$ the results approach the two dimensional value.

CHAPTER 4

Analysis of the three-dimensional model using acceleration potential method

In Chapter 3 we formulated the three-dimensional problem in terms of an integral equation and solved it for small $\bar{k}_y$. In this section we formulate this problem in terms of an acceleration potential. Ahmadi (1980) developed an unsteady lifting line theory for an oscillating finite wing using the acceleration potential. We follow the same procedure and obtain a closed form expression for the circulation when $\bar{k}_y$ is small.

The acceleration potential ψ is defined as

$$\psi(\vec{X},t) = [\ p_\infty - p(\vec{X},t)\ ]\ /\rho \qquad (25)$$

where $\vec{X} = (x,y,z)$, p is pressure, ρ is fluid density and p_∞ is the free stream pressure. For a linearized theory the Euler equations become

$$\begin{aligned} u_t + U\,u_x &= \psi_x \\ v_t + U\,v_x &= \psi_y \\ w_t + U\,w_x &= \psi_z \end{aligned} \qquad (26)$$

and the continuity equation

$$u_x + v_y + w_z = 0. \qquad (27)$$

It follows that ψ is governed by the Laplace equation

$$\psi_{xx} + \psi_{yy} + \psi_{zz} = 0. \tag{28}$$

Boundary conditions are

(1) for $-c/2 \leq x \leq c/2$ and $z = \pm 0$

$$w(x,y,\pm 0) = -w(k_x,k_y)\exp(i\omega t - ik_x x + ik_y y) \tag{29}$$

In terms of ψ from eq.(26) we obtain the condition

$$\psi_z = 0 \qquad \text{on the plate.} \tag{30}$$

(2) $x^2 + y^2 + z^2 \to \infty \qquad \psi \to 0$ (31)

(3) Pressure discontinuity is zero across the wake. Since ψ is antisymmetric across the wake, this condition gives $\psi = 0$ for $x \geq c/2$; $z = 0$. (32)

The formal solution of this boundary value problem is

$$\psi(\vec{x},t) = -\frac{1}{4\pi\rho}\int_{-\infty}^{\infty} d\eta \int_{-c/2}^{+c/2} \frac{\partial}{\partial z}\left(\frac{1}{R}\right)\Delta p(\xi,\eta)\,d\xi \tag{33}$$

where

$$\Delta p(\xi,\eta) = \rho \left[\psi(x,y,0+) - \psi(x,y,0-) \right] \tag{34}$$

and

$$R = \frac{1.0}{\left\{ (x-\xi)^2 + (y-\eta)^2 + z^2 \right\}^{1/2}} \tag{35}$$

In the following sections , using matched asymptotic expansions , we solve for ψ when $\bar{k}_y$ is small . Let us assume

$b = 1/k_y$ (this is proportional to the wave length in the spanwise direction.)

$= O(1)$

$c =$ width of the plate

$= O(\varepsilon)\ b$

Define

$$A = 1/(\ k_y\ c/2) = 1/\ \bar{k}_y = O(1/\varepsilon) \tag{36}$$

These A and b are similar to aspect ratio and span length in a finite wing. Now consider the outer solution and the inner solutions of the problem.

OUTER SOLUTION

In the outer region distances from the plate is of the order of b (= $O(A^0)$). Then we expand 1/R in Taylor series for small ξ [$(-c/2 \leq \xi \leq c/2) = O(1/A)$] and obtain

$$\frac{1}{R} = \frac{1}{R_o} - \xi \frac{\partial}{\partial x}\left(\frac{1}{R_o}\right) + \frac{\xi^2}{2!}\frac{\partial^2}{\partial x^2}\left(\frac{1}{R_o}\right) + O(\xi^3) \qquad (37)$$

where

$$R_0 = \sqrt{x^2 + (y-\eta)^2 + z^2}$$

$$= \sqrt{r^2 + y_0^2}$$

and

$$r^2 = x^2 + z^2$$

$$y_0 = y - \eta \qquad (38)$$

Substituting this expansion in the eq.(33) we obtain an outer solution for ψ valid in the outer region

$$\psi^{o}(\vec{x},t) \sim -\frac{1}{4\pi\rho}\left\{ -\int_{-\infty}^{\infty} \frac{\bar{\ell}(\eta)\, z}{\left\{ r^{2}+Y_{0}^{2}\right\}^{3/2}}\, d\eta - \int_{-\infty}^{\infty} \frac{\bar{m}(\eta)\, 3xz}{\left\{ r^{2}+Y_{0}^{2}\right\}^{5/2}}\, d\eta \right.$$

$$+ \int_{-\infty}^{\infty} \frac{\bar{q}(\eta)\, 3z\left\{ z^{2}-4x^{2}+Y_{0}^{2}\right\}}{2\left\{ r_{0}^{2}+Y_{0}^{2}\right\}^{7/2}}\, d\eta + \text{--------} \qquad (39)$$

where

$$l(\eta) = \int_{-c/2}^{c/2} \Delta p(\xi,\eta)\, d\xi \qquad O(1/A) \qquad (40)$$

$$m(\eta) = -\int_{-c/2}^{c/2} \Delta p(\xi,\eta)\, \xi\, d\xi \qquad O(1/A^{2}) \qquad (41)$$

$$q(\eta) = \int_{-c/2}^{c/2} \Delta p(\xi,\eta)\, \xi^{2}\, d\xi \qquad O(1/A^{3}) \qquad (42)$$

Here $l(\eta)$ represents the sectional lift. $m(\eta)$, $q(\eta)$, etc. represents the higher order moments of the loading about the mid-chord. The order of magnitude of these terms are also shown next to the expressions.

When r becomes small (of the order of the chord length) the

outer solution ceases to apply. This region corresponds to the inner region. To analyze this part we magnify the variables .
Define the inner variables as

$$\bar{x} = A\,x$$

$$\bar{z} = A\,z$$

$$y = y$$

$$\bar{r} = A\,r$$

and

$$\bar{x} = \bar{r}\cos\theta$$

$$\bar{z} = \bar{r}\sin\theta$$

In the inner variables the plate is positioned at $-\bar{c}/2 \leq \bar{x} \leq \bar{c}/2$; $z = 0$ where $\bar{c} = A\,c = O(1)$.

Later for the purpose of matching, we need the inner expansion of this outer expansion. We substitute for the outer variables r,x,z in terms of the inner variables $\bar{r},\bar{x},\bar{z}$ and A and expand for small (1/A). We obtain the inner expansion of the outer solution

$$\psi^{oi} \sim \frac{1}{2\pi\rho}\left\{ A\,\ell(Y)\,\frac{\sin\theta}{\bar{r}} + \frac{1}{4A}\,\bar{r}\,\sin\theta\left[\frac{\partial^3}{\partial Y^3}\right.\right. \int_{-\infty}^{\infty}$$

$$\ell(\eta) \log (Y-\eta) \operatorname{sgn}(Y-\eta)\, d\eta + \left(1 + 2 \log \frac{2A}{\bar{r}}\right) \ell''(Y) \Big] + O(A^{-3} \ell)$$

$$- \frac{1}{2\pi\rho} \left\{ A^{2} m(Y) \frac{\sin 2\theta}{\bar{r}^{2}} + \frac{1}{4} m''(Y) \sin 2\theta + O(A^{-2} m) \right\}$$

$$+ \frac{1}{2\pi\rho} \left\{ A^{3} q(Y) \frac{\sin 3\theta}{\bar{r}^{3}} - \frac{A}{8} q''(Y) \frac{\sin\theta - \sin 3\theta}{\bar{r}} + O(A^{-1} q) \right\}$$

(44)

INNER SOLUTION

Writing the governing eq.(28) and the boundary conditions in terms of the inner variables we obtain

$$\psi_{\bar{x}\bar{x}} + \psi_{\bar{z}\bar{z}} + \psi_{yy}\ 1./A^{2} = 0$$

$\psi_{\bar{z}} = 0$ on the plate

$\psi = 0$ in the wake. (45)

We expand the inner solution in an asymptotic series of the form

$$\psi^{i} \sim \psi_{0}^{i} + A^{-1} \log A\, \psi_{1}^{i} + A^{-1} \psi_{2}^{i} + \text{(higher order terms)}. \qquad (46)$$

Substituting this expansion in the governing equations (45) and collecting the terms with the same order we obtain a series of simplified two-dimensional problems for ψ_n^i.

(1)

For ψ_0^i , ψ_1^i , ψ_2^i , ψ_3^i

$$\psi^i_{\bar{x}\bar{x}} + \psi^i_{\bar{z}\bar{z}} = 0$$

$\psi^i_{\bar{z}} = 0$ on the plate

$\psi = 0$ in the wake (47)

(2)

$$\psi^i_{4,\bar{x}\bar{x}} + \psi^i_{4,\bar{z}\bar{z}} = -\psi^i_{o,yy}$$

$\psi^i_{4,\bar{z}} = 0$ on the plate

$\psi = 0$ in the wake (48)

We note that in all these problems (1) ,(2) etc. the conditions at infinity is not defined. Therefore the solutions are not unique and leads to many eigensolutions. One of those eigensolutions is the classical Sear's solution. Later we see that this is the only eigensolution important to us.

When a two dimensional gust of the form $w_g(y)\exp(i\omega t - ik_x x)$ is convected over an infinite plate the governing equation and the boundary conditions are

(1) $$\psi_{\bar{x}\bar{x}} + \psi_{\bar{z}\bar{z}} = 0 \qquad (49)$$

(2) $w(\bar{x},y,\pm 0,t) = -w_g(y)\exp(i\omega t - ik_x\bar{x}/A)$ on the plate. And this codition is equivalent to

$$\psi_{\bar{z}} = 0 \quad \text{on the plate} \qquad (50)$$

(3) $\psi = 0$ in the wake

(4) $\psi \to 0$ at infinity

The solution of this problem is

$$\psi^{i}_{sears} = \mathrm{Real}[\, f(\bar{\xi},y) \,] \qquad (51)$$

where

$$f(\bar{\xi},y) = -jU\, w_g(y)\, P(\bar{k}_x)\, (\Lambda - 1) \qquad (52)$$

$$P(\bar{k}_x) = i\, J_1(\bar{k}_x) + [\, J_0(\bar{k}_x) - i\, J_1(\bar{k}_x)\,]\, C(\bar{k}_x) \qquad (53)$$

$$C(\bar{k}_x) = H^2_1(\bar{k}_x) \,/\, [\, H^2_1(\bar{k}_x) + i\, H^2_0(\bar{k}_x)\,] \qquad (54)$$

= Theodorsen function

$$\Lambda = \left\{ \frac{\bar{\xi} - \bar{c}/2}{\bar{\xi} + \bar{c}/2} \right\}^{1/2} \tag{55}$$

$\bar{\xi} = \bar{x} + j\,\bar{z}$

$\bar{k}_x = k_x\, c/2$

We do the analysis assuming $\bar{k}_x = O(1/A)$ and later improve it to the case when $\bar{k}_x = O(1)$

$$\bar{k}_x = \left(\frac{\omega}{U}\,\frac{\bar{c}}{2}\right)\frac{1}{A}$$

$$\nu = \frac{\omega}{U}\,\frac{\bar{c}}{2} = O(1) \tag{56}$$

$$\bar{k}_x = \nu \cdot \frac{1}{A} \tag{57}$$

We expand $P(\bar{k}_x)$ for small $\bar{k}_x$ and obtain

$$\begin{aligned} P(\bar{k}_x) = 1. + [\, i\nu \log(\gamma\nu/2) - \pi\nu/2 \,]\, A^{-1} \\ - i\nu\, A^{-1}\log A + O(A^{-2}\log A) \end{aligned} \tag{58}$$

Therefore for small $\bar{k}_x$, ψ^{i}_{sears} takes the form

$$\psi^{i}_{sears} = U\, w_g(y)\, [\, 1.+(i\nu \log(\gamma\nu/2) - \pi\nu/2\,)\, A^{-1} - i\nu\, A^{-1}\log A \;\; \mathrm{Im}(\Lambda) \; + \; ---- \tag{59}$$

When $w_g(y) = w(k_x,k_y)\exp(ik_y y)$, ψ^i_{sears} satisfies the boundary condition on the plate eq.(29). We separate out this solution because this simplifies our analysis later. We denote this as ψ^i_{2D}.

For small $\bar{k}_x$

$$\psi^i_{2D} = \psi^i_{2D,0} + \psi^i_{2D,1}\, A^{-1}\log A + \psi^i_{2D,2}\, A^{-2} + --- \qquad (60)$$

where

$$\psi^i_{2D,0} = U\, w\, \mathrm{Im}(\Lambda)$$

$$\psi^i_{2D,1} = -i\nu\, U\, w\, \mathrm{Im}(\Lambda)$$

$$\psi^i_{2D,2} = [\, i\nu \log(\gamma\nu/2) - \pi\nu/2 \,]\, U\, w\, \mathrm{Im}(\Lambda). \qquad (61)$$

For later calculations we need the $l_{2D}(y)$, the two dimensional lift function. This is equal to

$$l_{2D}(y) = \int_{-c/2}^{+c/2} \Delta p_{2D}(\xi,y)\, d\xi$$

$$= 2\,(\,\bar{c}/2A\,)\,\rho \int_{-1}^{+1} \psi^i_{2D}(\xi)\, d\xi$$

From eq.(51), substituting for ψ^i_{2D}, we obtain

$$l_{2D}(y) = 2\pi\ \rho\ (\ \bar{c}/2\ )\ U\ w\ P(\bar{k}_x) \tag{62}$$

If we expand this for small $\bar{k}_x$ we find

$$\begin{aligned} l_{2D}(y) = 2\pi\rho\ (\ \bar{c}/2A\ )\ \Big[\ & U\ w \\ & + U\ w\ (\ i\nu\ \log(y\nu/2) - \pi\nu/2\ )\ A^{-1} \\ & - U\ w\ i\nu\ A^{-1}\ \log A + \text{-----}\Big] \end{aligned} \tag{63}$$

Define

$$\begin{aligned} F_{2D} &= \text{lift}\ /(\ 2\pi\rho\ \bar{c}/2A\ ) \\ &= U\ w\ P(\bar{k}_x) \end{aligned} \tag{64}$$

The inner solution consists only of the eigensolutions. ψ^{i}_{2D} is the two-dimensional solution. We consider this as the primary solution and the other eigensolutions as a three-dimensional correction. Hence we write the inner solution as

$$\psi^{i} \sim \psi^{i}_{2D,1} + F_0 \psi_{sears} + f_0 \psi_1 + g_0 w_2 + \text{-------}$$

$$+ A^{-1} \log A \; [\; \psi^{i}_{2D,2} + F_1 \psi_{sears} + f_1 \psi_1 + g_1 \psi_1 + \text{-----}$$

$$+ A^{-1} \; [\; \psi^{i}_{2D,3} + F_2 \psi_{sears} + f_2 \psi_1 + g_2 \psi_2 + \text{-------}$$

$$+ O(\; A^{-2} \log A \;) \qquad (65)$$

here

$$\psi_{sears} = \text{Im} \; (\Lambda) \qquad (66)$$

and Λ is given by eq.(55)

ψ_1, ψ_2,----are other possible eigensolutions

and F_0, f_0, g_0, ---- are arbitary constants.

For convenience we combine ($\psi^{i}_{2D,1} + F_0 \psi_{sears}$) etc. as one term and will separate them in a later stage. Define

$$\bar{F}_0 = F_0 + U \; w$$

$$\bar{F}_1 = F_1 - i\nu \; U \; w$$

$$\bar{F}_2 = F_2 + [\; i\nu \log(\gamma\nu/2) - \pi\nu/2 \;] \; U \; w \qquad (67)$$

Then the inner solution becomes

$$\psi^{i} \quad \bar{F}_0 \psi_{sears} + f_0 \psi_1 + g_0 \psi_2 + \text{----------}$$

$$+ A^{-1} \log A \left[\bar{F}_1 \psi_{sears} + f_1 \psi_1 + g_1 \psi_2 + \text{-------} \right.$$

$$+ A^{-1} \left[\bar{F}_2 \psi_{sears} + f_2 \psi_1 + g_2 \psi_2 + \text{-----------} \right.$$

$$+ O(A^{-2} \log A) \qquad (68)$$

For matching purposes we need the outer expansion of the inner solution. This is obtained by substituting for the inner variables $\bar{r}, \bar{x}, \bar{z}$ in terms of the outer variables r,x,z and expanding the solution for small (1/A). From eq.(43), (55) and (66) we obtain the outer expansion of the Sears solution.

$$\psi^{io}_{sears} \sim \left(\frac{\bar{c}/2}{A}\right) \frac{\sin\theta}{r} - \frac{1}{2}\left(\frac{\bar{c}/2}{A}\right)^2 \frac{\sin 2\theta}{r^2}$$

$$+ \frac{1}{2}\left(\frac{\bar{c}/2}{A}\right)^3 \frac{\sin 3\theta}{r^3} + O(A^{-4}) \qquad (69)$$

After obtaining the inner expansion of the outer solution eq.(44) and the outer expansion of the inner solution eq.(69) we apply the matching principle and determine l, m, q in terms of $\bar{F}_0$, $\bar{F}_1$, $\bar{F}_2$. The asymptotic matching principle reads: (Van Dyke, 1964)

m-term inner expansion (n-term outer expansion) = n-term outer expansion (m-term inner expansion)

ⓐ 1 - term outer expansion from eq. (99)

$$\frac{1}{4\pi\rho}\int_{-\infty}^{\infty}\frac{\ell(\eta)\,z}{\left\{r^{2}+Y_0^{2}\right\}^{3/2}}\,d\eta$$

Expanded in inner variables, from eq. (104)

$$\frac{1}{2\pi\rho}\left\{A\,\ell(Y)\,\frac{\sin\theta}{\bar{r}}+\frac{1}{4A}\,\bar{r}\,\sin\theta\left[\frac{\partial^{3}}{\partial Y^{3}}\int_{-\infty}^{\infty}\bar{\ell}(\eta)\log(y-\eta)\,\mathrm{sgn}(Y-\eta)\,d\eta\right.\right.$$

$$\left.\left.+\left(1+2\log\frac{2A}{r}\right)\ell''(Y)\right]\right\}$$

1 - term inner expansion from eq. (125)

$$\bar{F}_0\,\psi_{\text{Sears}}+f_0\,\psi_1+g_0\,\psi_2+\text{--------}$$

Expanded in outer variables, from eq. (126)

$$\bar{F}_0\left(\frac{\bar{c}/2}{A}\right)\frac{\sin\theta}{r}-\frac{\bar{F}_0}{2}\left(\frac{\bar{c}/2}{A}\right)^{2}\frac{\sin 2\theta}{r^{2}}+\frac{1}{2}\left(\frac{\bar{c}/2}{A}\right)^{3}\frac{\sin 3\theta}{r^{3}}+\text{----}$$

Matching these two expressions, we obtain

$$\bar{F}_0 \left(\frac{\bar{C}/2}{A}\right) \frac{\sin\theta}{r} = \frac{1}{2\pi\rho} \, A \, \bar{\ell}(Y) \, \frac{\sin\theta}{\bar{r}}$$

$$f_0 = g_0 = \cdots\cdots = 0$$

$$\bar{\ell}(Y) = \bar{F}_0 \cdot 2\pi\rho \left(\frac{\bar{C}/2}{A}\right) \qquad (130)$$

ⓑ

2 - term outer expansion from eq. (99)

$$\frac{1}{4\pi\rho}\left\{\int_{-\infty}^{\infty} \frac{\ell(\eta)}{\left\{r^2 + Y_0^2\right\}^{3/2}}\, d\eta + \int_{-\infty}^{\infty} \frac{m(\eta)\; 3\,x\,z}{\left\{r^2 + Y_0^2\right\}^{5/2}}\, d\eta\right\}$$

1 - term inner expansion of 2 - term outer expansion from eq. (104)

$$\frac{1}{2\pi\rho} \, A \, \ell(Y) \, \frac{\sin\theta}{\bar{r}} - \frac{1}{2\pi\rho} \, m(Y) \, A^2 \, \frac{\sin 2\theta}{\bar{r}^2}$$

1 - term inner expansion from eq. (125)

$$\bar{F}_0 \, \psi_{\text{sears}}$$

2 - term outer expansion of 1 - term inner expansion, from eq. (126)

$$\overline{F_0}\left(\frac{\bar{c}/2}{A}\right)\frac{\sin\theta}{A} \quad - \quad \frac{\overline{F_0}}{2}\left(\frac{\bar{c}/2}{A}\right)^{2}\frac{\sin 2\theta}{r^{2}}$$

Matching these two terms we obtain

$$\ell(Y) = 2\pi\rho\left(\frac{\bar{c}/2}{A}\right)\overline{F_0}$$

$$m(Y) = \pi\rho\left(\frac{\bar{c}/2}{A}\right)^{2}\overline{F_0} \qquad (131)$$

ⓒ

2 - term outer expansion from eq. (99)

$$\frac{1}{4\pi\rho}\left\{\int_{-\infty}^{\infty}\frac{\ell(\eta)}{\left\{r^{2}+Y_0^{2}\right\}^{3/2}}\,d\eta \quad + \int_{-\infty}^{\infty}\frac{m(\eta)\,3xz}{\left\{r^{2}+Y_0^{2}\right\}^{5/2}}\,d\eta\right\}$$

2 - term inner expansion of 2 - term outer expansion from eq. (104)

$$\frac{1}{2\pi\rho}\left\{\left(\frac{\bar{c}/2}{A}\right)\frac{\sin\theta}{\bar{r}}A\ell - A^{2}m(Y)\frac{\sin 2\theta}{\bar{r}^{2}}\right\}$$

2 - term inner expansion from eq. (125)

$$\overline{F}_0 \, \psi_{sears} + A^{-1} \log A \; F_1 \, \psi_{sears} + A^{-1} F_2 \, \psi_{sears} \, .$$

2 - term outer expansion of 2 - term inner expansion from eq. (126)

$$\overline{F}_0 \left\{ \left(\frac{\overline{c}/2}{A} \right) \frac{\sin \theta}{r} - \frac{1}{2} \left(\frac{\overline{c}/2}{A} \right)^2 \frac{\sin 2\theta}{r^2} \right\}$$

$$+ A^{-1} \log A \left(\frac{\overline{c}/2}{A} \right) \frac{\sin \theta}{r} \overline{F}_1 + A^{-1} \left(\frac{\overline{c}/2}{A} \right) \frac{\sin \theta}{r} \overline{F}_2 \, .$$

Matching these two expressions we obtain

$$l(Y) = 2 \pi \rho \left(\frac{\overline{c}/2}{A} \right) \left\{ \overline{F}_0 + A^{-1} \log A \, \overline{F}_1 + A^{-1} F_2 \right\} \quad (132)$$

$$m(Y) = \pi \rho \left(\frac{\overline{c}/2}{A} \right)^2 \overline{F}_0 \, .$$

If we do the next order matching, we will obtain the higher order expressions for l, m and q.

Eq.(72) gives the expression for the sectional lift $l(y)$ to order A^{-2}. Now we separate $\bar{F}_0$, $\bar{F}_1$, $\bar{F}_2$ into the two-dimensional contribution and eigensolution contribution as explained earlier eq.(67). We obtain for the lift

$$\begin{aligned} l(y) &= 2\pi\rho \left[U w + F_0 \right] (\bar{c}/2A) \\ &+2\pi\rho \left[-U w i\nu + F_1 \right] (\bar{c}/2A) A^{-1} \log A \\ &+2\pi\rho \left[U w (i\nu \log(y\nu/2) - \pi\nu/2) +F_2 \right] (\bar{c}/2A) A^{-1} \\ &+ O(A^{-2} \log A) \end{aligned} \tag{73}$$

Substituting this results in the expression for outer expansion eq.(39) we obtain the outer solution in terms of F_0, F_1, F_2. After determine the inner solution and outer solution in terms of F_0, F_1, F_2 we form the composite solution ψ^c to $O(A^{-1})$ accuracy.

$$\psi^c = \psi^i + \psi^o - \psi^{oi} \tag{74}$$

where

$$(1) \quad \psi^i \sim \psi^i_{2D,1} + F_0 \psi_{sears} + A^{-1} \log A \left[\psi^i_{2D,2} + F_1 \psi_{sears} \right]$$

$$+ A^{-1} [\psi^{i}_{2D,3} + F_2 \psi_{sears}]$$

Using eq.(60), without loosing the accuracy we write this as

$$\psi^{i} \quad \psi^{i}_{2D} + [F_0 + F_1 A^{-1} \log A + F_2 A^{-1} \} \Psi_{sears} \tag{75}$$

where ψ^{i}_{2D} is given by eq.(51).

(2) ψ^{o} = outer solution to order A^{-1} accuracy

$$\psi^{o} = -\frac{1}{4\pi\rho} \frac{\partial}{\partial z} \int_{-\infty}^{\infty} \frac{l(\eta)}{\{ x^2 + (y-\eta)^2 + z^2 \}^{1/2}} d\eta \tag{76}$$

(3) ψ^{oi} = common solution to order A^{-1} accuracy

$$\psi^{oi} = \frac{1}{2\pi\rho} \, l(y) \, \frac{z}{x^2 + z^2} \tag{77}$$

and

$$l_0(y) = \bar{F}_0 \, 2\pi\rho \quad \bar{c}/2A \tag{78}$$

This composite solution is uniformly valid for the whole region. The expression for this ψ^{c} consists the arbitrary constants F_0, F_1, F_2. To determine these constants we use the condition that ψ^{c} has to satisfy the velocity boundary condition on the plate,

$$w^c(x,y,o) = -w(k_x,k_y)\ \exp(-ik_x x+ik_y y) \qquad (79)$$

where w^c is the normal velocity corresponding to the composite acceleration potential ψ^c. To obtain the velocity from the acceleration potential we have to solve the Euler equations, eq.(26).

$$w_t + U\ w_x = \psi_z$$

Since this is a linear problem, and the time and the spanwise variations appear in the boundary condition as simple harmonic variation, all the dependent variables become proportional to $\exp(i\omega t)\ \exp(ik_y y)$ with amplitudes that are independent of y and t. We write

$$w(x,y,z,t) = w(x,z)\ \exp(i\omega t)\ \exp(ik_y y)$$

$$l(y) = l\ \exp(ik_y y)$$

$$m(y) = m\ \exp(ik_y y)\ \text{etc.}$$

Then $w(x,z)$ satisfies the D.E.

$$i\omega\ w + U\ w_x = \psi_z$$

The solution of this equation is

$$w(x,z) = 1/U\ \exp(-ik_x x)\ \int_{-\infty}^{x} \Psi_{,z}\ \exp(ik_x \xi)\ d\xi \qquad (80)$$

where the integration is along a line parallel to the x axis. If we substitute ψ_c for ψ in eq.(140) and take the limit $z \to 0$ we obtain $w^c(x,0)$. We write $w^c = w^i + w^o - w^{oi}$, where w^i, w^o, w^{oi} are the velocities corresponding to ψ^i, ψ^o, ψ^{oi}. In the next step we evaluate these velocities.

(a) EVALUATION OF w^i

From eq.(75)

$$\psi^i = \psi^i_{2D} + (F_0 + F_1\, A^{-1} \log A + F_2\, A^{-1}\,)\, \Psi_{sears}.$$

The vertical velocity due to ψ_{sears} is

$$w^i_{sears}(\bar{x},\bar{z}) = 1/U \exp(-i\bar{k}_x \bar{x}/A\,)\ (\,F_0 + A^{-1}\log A\ F_1 + A^{-1}\ F_2)\int_{-\infty}^{x} \psi_{sears',z}\ \exp(ik_x\bar{\xi})\ d\bar{\xi} \tag{81}$$

We have to evaluate this integral at z=0. Since $\psi_{sears',z}$ has a non-integrable singularity at the leading edge we transform this into an integrable form. From eq.(55)

$$\Lambda = \left\{ \frac{\bar{x} + j\bar{z} - \bar{c}/2}{\bar{x} + j\bar{z} + \bar{c}/2} \right\}^{1/2} \tag{82}$$

$$\Lambda = \Phi + \psi_{sears}$$

Since Λ is an analytic function of $(\bar{x}+j\bar{z})$ from Cauchy - Riemann relation we have

$$\Phi,_{\bar{x}} = \psi_{\text{sears}'\bar{z}} \qquad (83)$$

and, when z=0, we obtain

$$\Phi = \left\{ \frac{\bar{x} - \bar{c}/2}{\bar{x} + \bar{c}/2} \right\} \qquad \text{for} |x| > c/2$$

$$= \quad 0 \qquad \text{for} |x| < c/2 \qquad (84)$$

Substituting eq.(83) in eq.(81), integrating by parts and use the results from eq.(84) we obtain

$$w^{i}_{\text{sears}}(x,0) = i\pi/(2U)\ \bar{k}_x \exp(-ik_x x)\ [\ F_0 + F_1\ A^{-1}\log A + F_2\ A^{-1}\ ]\ (\ H^2_1 + i\ H^2_0\ ) \qquad (85)$$

The velocity due to ψ^{i}_{2D} is the gust velocity. Hence the boundary condition eq.(79) becomes

$$-w(k_x,k_y)\cancel{e}xp(-ik_x x) = \cancel{-w^{i}_{2D}}$$

$$+\ i\pi/(2U)\ \bar{k}_x \exp(-jk_x x)\ [\ F_o + A^{-1}\ \log A\ F_1 + A^{-1}\ F_2\ ]\ (\ H^2_1 + i\ H^2_0\ )$$

$$+\ \lim\ [\ w^{o}(x,z) - w^{oi}(x,z)\ ]\ \exp\ (-ik_x x) \qquad (86)$$

where

$$w^{o}(x,z) = 1/U \int_{-\infty}^{x} \Psi^{o},_{z} \exp(ik_{x}\xi)\, d\xi \qquad (87)$$

and

$$w^{oi}(x,z) = 1/U \int_{-\infty}^{x} \Psi^{oi},_{z} \exp(ik_{x}\xi)\, d\xi \qquad (88)$$

From eq.(86) we observe $(w^{o} - w^{oi})$ is independent of x. Therefore, for convenience we evaluate w^{o} and w^{oi} at x=0.

(b) EVALUATION OF w^{oi}

Substituting for ψ^{oi} in eq.(88) from eq.(77) and (78) we obtain

$$W^{oi} = \frac{1}{U} \bar{F}_0 \frac{\bar{c}/2}{A} \frac{\partial}{\partial z} \int_{-\infty}^{0} \frac{z\, e^{ik_x \xi}}{\xi^2 + z^2}\, d\xi \qquad (89)$$

In the limit z → 0 this becomes (Appendix E)

$$w^{oi} = ik_{x}/U\, \bar{F}_{0}\, (\, \bar{c}/2A\,)\, [\, \gamma + \log\, (k_{x}z) + \pi/2\ i\,] \qquad (90)$$

(c) EVALUATION OF w^o

Substituting for ψ^o in eq.(87) from eq.(76) and eq.(78) and simplifying we obtain

$$W^o = -\frac{\bar{F}_o}{U}\,\frac{\bar{c}/2}{A}\int_0^\infty \cos k_y\eta\, d\eta\,\frac{\partial^2}{\partial z^2}\int_0^\infty \frac{e^{i k_x \xi}}{\left\{r^2+\eta^2\right\}^{1/2}}\, d\xi \qquad (91)$$

Substitution of the integrals from Appendix F gives

$$w^o = \bar{F}_0/U\ (\bar{c}/2A)\ [\, w^{o1} + w^{o2} + w^{o3} + w^{o4}\,] \qquad (92)$$

where

$$W^{o1} = \int_0^\infty \cos k_y\eta \left\{ -\frac{i k_x}{r} + i\,\frac{k_x z^2}{r^3} \right\} d\eta$$

$$W^{o2} = \int_0^\infty \cos k_y\eta \left\{ \frac{k_x}{r} K_1(k_x r) - \frac{z^2 k_x^2}{r^2} K_2(k_x r) \right\} d\eta$$

$$W^{o3} = \int_0^\infty \cos k_y\eta \left\{ \frac{i k_x}{r}\left[I_1(k_x r) - L_1(k_x r) \right]\frac{\pi}{2} + \frac{\pi}{2}\left[I_2(k_x r) - L_2(k_x r) \right]\frac{k_x^2 z^2}{r^2} \right\} d\eta$$

$$W_o^{04} = \int_0^{\infty} \cos k_y \eta \left\{ - \frac{i z^2 k_x^3}{3 r} \right\} d\eta \qquad (93)$$

When z → 0 we obtain (Appendix G)

$$w^{01} = i k_x \left\{ \gamma + \ln \frac{k_y}{2} + \ln z + 1 \right\}$$

$$w^{02} = k_x \int_{\varepsilon}^{\infty} \frac{\cos k_y \eta \; K_1(k_y \eta)}{\eta} d\eta - \frac{1}{\varepsilon}$$

$$w^{03} = i k_x \frac{\pi}{2} \int_0^{\infty} \frac{\cos k_y \eta}{\eta} \left\{ I_1(k_x \eta) - L_1(k_x \eta) \right\} d\eta$$

$$w^{04} = 0 \qquad (94)$$

Combination with the expression for w^{0}, eq.(94) and w^{0i}, eq.(93) yields

$$w^{0} - w^{0i} = \frac{\bar{F}_o}{U} \left(\frac{\bar{c}/2}{A} \right) \left\{ i k_x \left\{ \ln \frac{k_y}{2 k_x} + 1.0 - \frac{\pi}{2} i \right\} \right.$$

$$+ \; \bar{k}_x \int_{\varepsilon}^{\infty} \frac{\cos k_y \eta \; K_1(k_y \eta)}{\eta} \, d\eta \; - \; \frac{1}{\varepsilon}$$

$$+ \; j \, k_x \frac{\pi}{2} \int_{0}^{\infty} \frac{\cos k_y \eta}{\eta} \left\{ I_1(k_x \eta) - L_1(k_x \eta) \right\} d\eta \; \Bigg] \qquad (95)$$

We evaluate these integrals in closed form (Appendix H) and reduce this equation to the simplified form

$$w^{o} - w^{oi} = \bar{F}_0/U \;\; \bar{c}/2A \;\; T \qquad (96)$$

where

$$T \; = \; i \, k_x \left\{ \sqrt{1+a^2} \, \log \, \frac{1+\sqrt{1+a^2}}{a} \; + \; \ln \frac{a}{2} \right\}$$

$$- \; \frac{\pi}{2} \; k_x \left\{ \sqrt{1+a^2} - 1 \right\} \qquad (97)$$

After deriving the expression for $(w^{o} - w^{oi})$, from eq.(86) we obtain a relation involving F_0, F_1 and F_2

$$w^{o} - w^{oi} = -i \; \pi/(2U) \; k_x \; [\; F_0 + F_1 \; A^{-1} \; \log A + F_2 \; A^{-1} \;] \; (\; H_1^2 + i \; H_0^2 \;) \qquad (98)$$

$$= \bar{F}_0/U \quad \bar{c}/2A \quad T$$

Using the relation

$$P(\bar{k}_x) = j J_1 + (J_0 - j J_1) \frac{H_1^{2}}{H_1^{2} + j H_0^{2}}$$

$$= \frac{1}{-j \frac{\pi}{2} \left\{ H_1^{2} + j H_0^{2} \right\} k_x} \tag{99}$$

we may rewrite eq.(98) in the form

$$[\, F_0 + A^{-1} \log A \; F_1 + A^{-1} \; F_2 \,] = \bar{F}_0 \;(\bar{c}/2A)\; T \; P(\bar{k}_x) \tag{100}$$

From this relation we determinate the constants F_0, F_1, F_2. For small $\bar{k}_x$ from eq.(58)

$$P(\bar{k}_x) = 1.0 + O(A^{-1} \log A)$$

Using this result from eq.(100) we deduce that

$$F_0 = F_1 = 0$$

and

$$F_2/A = \bar{F}_0 \quad \bar{c}/2A \quad T \tag{101}$$

From eq.(67)

$$\bar{F}_0 = U\ w$$
$$= \text{quasi steady lift} /(\ 2\pi\rho\ c/2\ ) \qquad (102)$$

After determine these constants F_0 ,F_1 , F_2 the composite solution is known to $O(A^{-1})$ accuracy. We can modify the above results without loosing the accuracy as follows.

Comparing eq.(63) and eq.(73) we note that without loosing the loss ofaccuracy eq.(73) may be written as

$$l(y) = l_{2D} + F_0\ 2\pi\rho\ \bar{c}/2A$$
$$+ F_1\ 2\pi\rho\ \bar{c}/2A\ A^{-1}\ \log A$$
$$+ F_2\ 2\pi\rho\ \bar{c}/2A\ A^{-1} \qquad (103)$$

Therefore, in eq.(78), instead of F_0 we substitute F_{2D} (eq.(64)), and the function $P(\bar{k}_x)$ is left without expansion for small $\bar{k}_x$. If we assumed $\bar{k}_x = O(1)$ we would have obtained these expressions.

Hence we obtain the new expression for F_2/A from eq.(100).

$$F_2/A = F_{2D}\ \bar{c}/2A\ T\ P(\bar{k}_x)$$
$$= U\ w\ P(\bar{k}_x)\ \bar{c}/2A\ T\ P(\bar{k}_x) \qquad (104)$$

Substituting these results in eq.(75) we obtain the expression for inner solution

$$\psi^{i} = U\, w\, P(\bar{k}_x)\ \mathrm{Im}(\Lambda)$$

$$+\ U\, w\, P(\bar{k}_x)\ \bar{c}/2A\ T\ P(\bar{k}_x)$$

$$= U\, w \left[\ 1. + \bar{c}/2A\ T\ P(\bar{k}_x)\ \right] P(\bar{k}_x)\ \mathrm{Im}(\Lambda) \qquad (105)$$

From this expression we observe that the inner solution is the Sear's solution with an amplitude of the form

$$w_g = w \left[\ 1. + \bar{c}/2A\ T\ P(\bar{k}_x)\ \right] \qquad (106)$$

When a two dimensional gust $w_g \exp(i\omega t - ik_x x)$ is convected over a plate the circulation is (eq.6)

$$\frac{\bar{\Gamma}}{c/2} = -\ \frac{4\, w_g \left\{ J_0 - i J_1 \right\} e^{-i\bar{k}_x}}{i\bar{k}_x \left\{ H_1^{(2)} + i H_0^{(2)} \right\}} \qquad (107)$$

When $w_g = w\ (1 - \varepsilon)$

$$f_2(1) = \frac{\bar{\Gamma}}{U\,\bar{c}/2} = -\frac{4\,\frac{w}{U}\,(1-\varepsilon)\left\{J_0 - i J_1\right\} e^{-i\bar{k}_x}}{i\,\bar{k}_x\left\{H_1^{(2)} + i\,H_0^{(2)}\right\}} \tag{108}$$

where

$$\varepsilon = -\bar{c}/2A\ T\ P(\bar{k}_x) \tag{109}$$

Substituting for T from eq.(97) and for $P(\bar{k}_x)$ from eq.(99) we find

$$\varepsilon = \frac{2}{\pi}\,\frac{1}{H_1^{(2)} + i\,H_0^{(2)}}\left\{\log\frac{a}{2} + \sqrt{1+a^2}\,\log\frac{1+\sqrt{1+a^2}}{a} + i\,\frac{\pi}{2}\left[\sqrt{1+a^2} - 1\right]\right\} \tag{110}$$

where

$a = k_y/k_x$

$= \bar{k}_y/\bar{k}_x$

Eq.(22) gives the expression for $f_2(1)$ which we obtained using the integral method. Comparing eq.(23) and eq.(110) we see that the expressions are the same for small $\bar{k}_y$.

Since for small ε

$$\frac{1}{1+\varepsilon} = 1 - \varepsilon + O(\varepsilon^2)$$

we derive the same expression for the circulation $f_2(1)$ using the both methods to O(1/A) accuracy. We obtain the velocity field in the far wake as explained in Chapter 3 and is given by

$$w_T/U = w(k_x,k_y)/U \exp(-ik_x x) \exp(ik_y y) \, S(\bar{k}_x,\bar{k}_y) \qquad (171)$$

where

$$S(\bar{k}_x,\bar{k}_y) = 1.0 - f_2(1) \exp(ik_x) \sqrt{\bar{k}_x^2 + \bar{k}_y^2} /2 \qquad (112)$$

and $f_2(1)$ is given by eq.(108). The amplitude and phase of $S(\bar{k}_x,\bar{k}_y)$ is calculated for a range of $\bar{k}_x$ and $\bar{k}_y$ values and is plotted in Fig. 14. The results show that for small $\bar{k}_y < 0.2$ both method give the same curves. When $\bar{k}_y$ becomes larger, and for small $\bar{k}_x < 0.2$, they deviate from one another. This is because when $\bar{k}_y$ becomes large the difference between the two expressions, which is of order $\bar{k}_y^2$, becomes large.

CHAPTER 5

Analysis of a three-dimensional model for high spanwise wavenumbers

In Chapter 3 we formulated the three-dimensional problem in terms of integral equations and obtained a closed form expression for the normal velocity in the far wake, for the case when the spanwise wave number k_y is small. In Chapter 4 we formulated this problem in terms of the acceleration potential and analysed using asymptotic matching principle for small k_y. In this Chapter we derive an expression for the normal velocity in the far wake for the case when the spanwise wavenumber, k_y, is high. For this case an approximate closed form expression for the pressure distribution on the plate is derived in Amiet (1976). The solution procedure is based on the work by Schwartzchild (1902) and Landahl (1958). We use the results derived in Amiet (1976) in the calculations.

We assume the flow is incompressible and irrotational. For linearized theory the governing equation and the boundary conditions are

$$\phi_{xx} + \phi_{zz} + \phi_{yy} = 0 \tag{113}$$

$$\phi(x,y,z) = 0 \qquad \text{for } -\infty \leq x \leq 0 \tag{114}$$

$$\phi_z = -w(k_x,k_y)\exp(i\omega t)\exp(-i\bar{k}_x x)\exp(i\bar{k}_y y) \qquad \text{for } 0 \leq x \leq 2,\ z=0 \tag{115}$$

and

$$\phi_t + U \phi_x = 0 \quad \text{for } 2 \leq x \leq \infty; \ z = 0 \tag{116}$$

The spatial coordinates are non-dimensionalised with the semi-chord c/2 and the axis is placed at the leading edge. We observe from these equations that ϕ is antisymmetric about the x axis and takes the form

$$\phi(x,y,z) = \phi(x,z) \exp(i\bar{k}_y y) \exp(i\omega t). \tag{117}$$

We solve this problem for $z \geq 0$. Substituting the expression eq.(117) into eq.(113-116) we obtain

$$\phi_{xx} + \phi_{zz} - \bar{k}_y^2 \phi = 0 \tag{118}$$

$$\phi(x,0) = 0 \quad \text{for} \quad -\infty \leq x \leq 0 \tag{119}$$

$$\phi_z = -w \exp(-i\bar{k}_x x) \quad \text{for} \quad 0 \leq x \leq 2, \ z = 0 \tag{120}$$

and

$$\phi_x + i\bar{k}_x \phi = 0 \quad \text{for} \quad 2 \leq x \leq \infty \tag{121}$$

An approximate solution of this equation is, from Amiet (1976)

$$\phi = \Phi_1(x,0) + \Phi_2(x,0) \tag{122}$$

where

$$\Phi_1(x,0) = \frac{w}{\sqrt{\bar{k}_x^2 + \bar{k}_y^2}}\, e^{-i\bar{k}_x x}\, \mathrm{erf}\sqrt{\mu x} \qquad x > 0 \tag{123}$$

$$\Phi_2(x,0) = -\frac{w}{\pi}\,\frac{e^{-ik_x x}}{\sqrt{\pi(\bar{k}_y + i\bar{k}_x)}}\int_0^\infty \frac{d\xi\, e^{-2\xi\bar{k}_y}}{\sqrt{2+\xi}\,\sqrt{\xi}}\int_{-\infty}^{x}\frac{\sqrt{r}}{\xi + r}\, e^{-k_y(2+r)}\, e^{ik_x t}\, dt \tag{124}$$

and $r = 2 - t$; $x \leqq 2$.

Here

$$\lambda = \bar{k}_y + i\bar{k}_x$$

$$\mu = \bar{k}_y - i\bar{k}_x \tag{125}$$

This solution satisfies the boundary condition on the plate eq.(120) and the downstream boundary condition eq.(121). But the third boundary condition is not satisfied by this solution. Comparing with the numerical solutions of Graham (1970) it is noted that for $\bar{k}_y > 1.0$ the accuracy of this solution is of the order of a few parts in 10^3, and reasonable accuracy is obtained for $\bar{k}_y$ as small as o.25. Landahl (1958) has shown that this iterative scheme converges uniformly for all $\bar{k}_y$, but many terms are needed to obtain good approximate solution for small $\bar{k}_y$.

The circulation around the plate is equal to

$$\Gamma = 2\,\phi(2,0) \tag{126}$$

We define

$$\Gamma/(U\,c/2) = w/U\, f_2(1)$$

Substituting for $\phi(2,0)$ from eq.(122-125) in eq.(126) we obtain (Appendix I)

$$f_2(1) = \frac{2\,e^{-2i\bar{k}_x}}{\sqrt{\bar{k}_x^2 + \bar{k}_y^2}}\ \operatorname{erf}\sqrt{2\mu} - \frac{2\,e^{-2i\bar{k}_x}}{\sqrt{\pi\lambda}}\, e^{-2\mu} \left\{ \frac{1}{\sqrt{\lambda\pi}}\, K_0(2\bar{k}_y)\, e^{2\bar{k}_y} - C \right\} \tag{127}$$

where

$$C = \int_0^\infty \frac{e^{-\rho\mu}}{\sqrt{2+\rho}}\ \operatorname{erfc}\sqrt{\lambda\rho}\ d\rho \tag{128}$$

and K_0 is the modified Bessel function of zero order.

When we derive these expressions we fixed the axis at the trailing edge. In the previous chapters the axis were fixed at the mid-chord. If we move the axis to the mid-chord there will be phase change equal to $\bar{k}_x$. Multiplying the eq.(127) by $\exp(i\bar{k}_x)$ we obtain the new expression for $f_2(1)$

$$f_2(1) = \frac{2\, e^{-i\bar{k}_x}}{\sqrt{\bar{k}_x^2 + \bar{k}_y^2}} \operatorname{erf}\sqrt{2\mu}$$

$$- \frac{2\, e^{-i\bar{k}_x}}{\sqrt{\pi\lambda}}\, e^{-2\mu} \left\{ \frac{1}{\sqrt{\lambda\pi}} K_0(2\bar{k}_y)\, e^{2\bar{k}_y} - C \right\} \qquad (129)$$

The total normal velocity in the far wake is derived in Chapter 3 and is given by eq. (24) as

$$w_T/U = w/U \exp(-ik_x x) \exp(ik_y y) S(\bar{k}_x,\bar{k}_y) \qquad (130)$$

and

$$S = 1.- f_2(1) \exp(i\bar{k}_x) \sqrt{\bar{k}_x^2 + \bar{k}_y^2}\,/2 \qquad (131)$$

The amplitude and the phase of $S(\bar{k}_x,\bar{k}_y)$ is calculated for a range of $\bar{k}_x$ and k_y values and are plotted in Figs. 15, 16. As mentioned earlier this solution gives reasonable accurate results for $\bar{k}_y > 0.25$ and gives better accuracy for larger $\bar{k}_y$(>1.0). The results show that the amplitude of $S(\bar{k}_x,\bar{k}_y)$ is very small for high spanwise wavenumbers. The amplitude decreases with increasing $\bar{k}_y$ and $\bar{k}_x$. For $\bar{k}_y$=1.0 it decreases from 0.07 to 0.025 when $\bar{k}_x$ increases from 0.0 to 4.0. For $\bar{k}_y$ larger than 2.0 the amplitude decreases to values less than 0.01.

CHAPTER 6

Analysis including ground plane

In the previous analysis we neglected the effect of the horizontal ground plane. In this chapter we will include its effect (Fig. 17). In addition to the boundary condition on the plate we also have to satisfy the boundary condition on the plane. We satisfy this condition by considering the mirror image of the plate on the horizontal plane. The present configuration is shown in Fig. 18. The boundary condition on the upper plate takes the form

$$-w(k_x)\, e^{-i k_x x} = -\frac{1}{2\pi}\int_{-c/2}^{+c/2} \frac{\gamma_1}{x-\xi}\,d\xi - \frac{1}{2\pi}\int_{c/2}^{\infty}\frac{\gamma_2}{x-\xi}\,d\xi$$

$$+\frac{1}{2\pi}\int_{-c/2}^{c/2}\frac{\gamma_1 (x-\xi)}{\left\{(x-\xi)^2+h^2\right\}}\,d\xi + \frac{1}{2\pi}\int_{c/2}^{\infty}\frac{\gamma_2 (x-\xi)}{\left\{(x-\xi)^2+h^2\right\}}\,d\xi \qquad (132)$$

Using the condition that there cannot be any pressure discontinuity across the wake we can solve for the vorticity distribution γ_2. This expression was derived in Chapter 2 and is given by eq.(5)

$$\gamma_2 = -\, i\, \bar{k}_x \left(\frac{\Gamma}{c/2}\right) \exp\left(i\,\bar{k}_x\right) \exp\left(-i\,k_x x\right) \qquad (133)$$

where

$$\Gamma = \int_{-c/2}^{c/2} \bar{\gamma}_1 \, d\xi$$

Substituting for y_2 and non-dimensionalising using c/2 as reference length we find from eq.(132)

$$w\, e^{-i\bar{k}_x x} = \frac{1}{2\pi}\int_{-1}^{+1} \frac{\gamma_1}{x-\xi}\, d\xi - \frac{1}{2\pi}\int_{-1}^{+1} \frac{\gamma_1 (x-\xi)}{\left\{(x-\xi)^2+h^2\right\}}\, d\xi$$

$$i\bar{k}_x \left(\frac{\Gamma}{2\pi\, c/2}\right) e^{i\bar{k}_x} \int_{1}^{\infty} \frac{e^{-i\bar{k}_x \xi}}{\xi - x}\, d\xi - i\bar{k}_x \left(\frac{\Gamma}{2\pi\, c/2}\right) \int_{1}^{\infty} \frac{e^{-i\bar{k}_x \xi}(\xi - x)}{\left\{(\xi-x)^2+h^2\right\}}\, d\xi \tag{134}$$

We have to solve this integral equation to estimate the circulation Γ. Since it is difficult to solve it in closed form we use the 'Quarter chord theory' to obtain an approximate expression for the circulation Γ. After some simplifications we obtain

$$\left\{\frac{\Gamma}{2\pi w\, c/2}\right\} = \frac{e^{-i\bar{k}_x/2}}{\left\{\frac{h^2}{1+h^2} + I_1 + I_2\right\}} \tag{135}$$

where

$$I_1 = i\bar{k}_x\, e^{i\frac{\bar{k}_x}{2}} \left\{ \int_{\frac{\bar{k}_x}{2}}^{\infty} \frac{\cos\xi}{\xi}\, d\xi - i \int_{\frac{\bar{k}_x}{2}}^{\infty} \frac{\sin\xi}{\xi}\, d\xi \right\} \tag{136}$$

$$I_2 = -\frac{i\bar{k}_x}{2}\, e^{\frac{i\bar{k}_x}{2}} \left\{ e^{-\bar{k}_x h}\, E_i(\mu_1) + e^{\bar{k}_x h}\, E_i(\mu_2) \right\} \qquad (137)$$

$$\mu_1 = \bar{k}_x \left\{ -h + \frac{i}{2} \right\}$$

$$\mu_2 = \bar{k}_x \left\{ h + \frac{i}{2} \right\} \qquad (138)$$

and

$$E_i(\mu) = \int_{\mu}^{\infty} \frac{e^{-z}}{z}\, dz \qquad (139)$$

After obtaining the expression for the circulation we can calculate induced normal velocity in the far wake. There is induced velocity contributions from both the lower and the upper wake vortices given by (Appendix B)

$$W_{in}\big)_{upper} = -i\,\frac{\gamma_2}{2}\, e^{-i k_x x} \qquad (140)$$

$$W_{in}\big)_{lower} = +i\,\frac{\gamma_2}{2}\, e^{-i k_x x}\, e^{-k_x h} \qquad (141)$$

Substituting for y_2 from eq.(133) and adding the induced velocity and the gust velocity we obtain the total normal velocity in the far wake as

$$W_T = w(k_x)\, e^{-\iota k_x x}\, e^{\iota \omega t}\, S(\bar{k}_x, H) \qquad (142)$$

where

$$S(\bar{k}_x, H) = 1.0 - \pi \bar{k}_x\, e^{\iota \bar{k}_x} \left(\frac{\Gamma}{2\pi w\, c/2}\right)\left\{1.0 - e^{-\bar{k}_x h}\right\} \qquad (143)$$

The amplitude and the phase of $S(\bar{k}_x,H)$ is calculated for a range of $\bar{k}_x$ and H values and is plotted in Fig.19. It is seen that the reduction in the amplitude is reduced by the inclusion of the plate. For H=2.0 and $\bar{k}_x$=0.5 the reduction in the amplitude is reduced by a factor of 1.5 of compared to the value without the surface. This factor is about the same for the lower wavenumbers. The other point observed is that when the height H becomes smaller this factor increases. For the purpose of understanding these results further we calculated the circulation and the shed vortices from eq.(133), (135). The amplitude of the circulation is shown in Fig. 20. We find that the amplitude of the circulation and the shed vortices in this case are larger than those without the ground plane. This leads to higher induced velocity from the upper and lower shed vortices. Since the shed vortices from the lower plate induce the velocity in the upper wake in the opposite direction to the above we effectively obtain a decrease in the reduction of the amplitude.

In the previous section we considered the interaction of the two-dimensional gust with the plate and the surface. In this part we extend this to the three-dimensional gust. Due to variations in the y-direction in addition to the shed vortices there is also trailing vortices. The strength of these and of the trailing vortices are derived in Chapter 3 (eq. 20) in terms of the circulation. As we did in the two-dimensional case we consider the mirror image of the plate on the horizontal surface and solve for the circulation using the 'Quarter chord theory'. After this approximation the equivalent vortex sheet representation for the upper plate is shown in Fig.10. For the lower plate we have the same figure with the vortices in the opposite direction. Using the Biot-Savart law the normal velocity due to these vortex sheets is determined at the 3/4 chord point. Satisfying the boundary condition at that point we derive the expression for the circulation (see Appendix J). After determine the circulation we calculate the induced normal velocity in the far wake and adding the gust velocity to this we obtain the total normal velocity in the far wake and is given by

$$W_T = w\, e^{-i\bar{k}_x x}\, e^{i\bar{k}_y y}\, e^{i\omega t}\, S(\bar{k}_x, \bar{k}_y, H) \qquad (144)$$

where

$$S(\bar{k}_x, \bar{k}_y, H) = 1.0 - \frac{\sqrt{\bar{k}_x^2 + \bar{k}_y^2}}{2}\, f_2(1)\, e^{i\bar{k}_x} \left\{ 1.0 - e^{-\sqrt{\bar{k}_x^2 + \bar{k}_y^2}\, h} \right\} \qquad (145)$$

and $f_2(1)$ is the circulation around the plate and is given by eq.(J13).

In Figs.22-24 we have plotted the amplitude of $S(\bar{k}_x,\bar{k}_y,H)$ for different $\bar{k}_x,\bar{k}_y$ and H values. In Fig.22 we compare the 'Quarter chord theory' results (without the surface ie $H=\infty$) with that obtained using the integral equation method eq.(24). As mentioned before, the 'Quarter chord theory' approximation is valid for small wavenumbers $\bar{k}_x$ less than 0.3. Fig.23, 24 show the amplitude for $\bar{k}_y=0.1$ and 0.2, and it is seen that except for small $\bar{k}_x<0.1$ there is not much difference from the conclusion made for the two-dimensional case.

CHAPTER 7

In this chapter the interaction of a vortex street and a vortex pair is considered. The vortex street simulates the wake behind the LEBU devices. The vortex pair models the ejection process or the wallward movement of the outer fluid towards the wall. In the absence of the vortex street the vortex pair moves with constant induced velocity. When the wake is introduced the vortex pair and the vortex street interact and the motion of the vortex pair is altered. In this section we will determine, how the motion of the vortex pair is altered and, how the wake is modified due to the interaction. We employed the two-dimensional model to gain some insight into the effects and the mechanism. The initial arrangement of the vortex system is shown in Fig. 25. First an approximate estimate is made for the magnitudes of the variables A, B, a, Γ_1 and Γ_2 where A, B are the longitudinal and lateral spacing of the vortex street, Γ_1 is the strength of the vortex street, 'a' is the distance between the vortex pair and Γ_2 is the strength of the vortex pair. The primary length and velocity scales involved in the problem is length of the plate 'c', the boundary layer thickness δ and the free stream velocity U. In most of the LEBU applications tested in the laboratories the length of the plate is equal to the boundary layer thickness $c = \delta$.

For B/A the Karman's theoretical stability condition ratio 0.28 is assumed. The velocity of the vortex street relative to the free stream is given by

$$\Gamma_1/2A \tanh \pi B/A = F_1 U \qquad (135)$$

From experimental results F_1 is approximately 0.08, Taneda (1958). Let

$$A = \delta/N \tag{136}$$

where N is the factor which determined the longitudinal spacing of the vortex street and it is a function of the Reynolds number. The variation of N with the Reynolds number is shown in Fig. 5, Taneda(1958). For the Reynolds number 30,000, N is approximately 8.

In the absence of the vortex street the vortex pair moves downward with the velocity $\Gamma_2/(2\pi a)$ and it carries with it an oval shape of fluid. The axis of the oval are 2.09a and 1.73a . The magnitude of a is determined by simulating the oval shape with a large-eddy of scale δ. Hence

$$a = F_2\ \delta \tag{137}$$

where F_2 takes a value of 1/4. To determine the strength of the pair, the velocity of the vortex pair $\Gamma_2/(2\pi a)$ is equated to the normal turbulent velocity in the outer part of the boundary layer.

$$\Gamma_2/(2\pi a) = F_3\ U \tag{138}$$

where F_3 measures the normal turbulent velocity in the outer part of the boundary layer and is in the order of 0.02 - 0.04, Fig. 3. From eqs. (135)-(138) we obtain

$$a/A = N\ F_2 \tag{139}$$

and

$$\Gamma_2\ /\ \Gamma_1 = \pi\ (F_3/F_1)\ NF_2\ \tanh\ (\pi B/A) \tag{140}$$

Substituting for F_1, F_2, F_3 and N the values which are evaluated, it is obtained

$$a/A = 2 \tag{141}$$

and Γ_2/Γ_1 is in the range 1.0 to 2.0.

In the calculations the variables are non-dimensionalised with length A, velocity $\Gamma_1/(2\pi a)$ and time $A/(\Gamma_1/(2\pi a))$ and the variables are 'a' and Γ_2 are varied in the above range. The initial and the distorted vortex systems are shown in Figs. 25, 26. Here, the axis are fixed to the vortex street and hence there is a free stream velocity in the x-direction with magnitude U which is equal to

$$U = \Gamma_1 /2A \ \tanh \pi B/A \tag{143}$$

The coordinates of the vortices in the undisturbed vortex street are

$$x_j = (L-j)\ A$$
$$y_j = 0.0 \qquad \text{for the lower row} \tag{144}$$

and

$$x_j = (L-j)\ A + A/2$$
$$y_j = B \qquad \text{for the upper row} \tag{145}$$

Here L^{th} vortex on the lower row locates at the origin and 'j' varies from $-\infty$ to $+\infty$. If we denote the coordinates of a vortex at a time t as (x_i,y_i) and the induced velocities on the vortex by other vortices as u_i,v_i then the motion of the vortex is governed by

$$\frac{dx_i}{dt} = u_i$$

and

$$\frac{dy_i}{dt} = v_i \tag{146}$$

Each row in the vortex street consists of an infinite number of vortices in either direction. It is reasonable to assume that far away from the vortex pair the influence of the vortex pair on the vortex street is negligible and the vortices will be stationary. Thus we can consider only the middle part of of the vortex street, between the sections LL' and RR', Fig. 25 , and assume that the vortices outside this region are stationary. ML is the number of the vortex which is at the left boundary and MR is the vortex at the right boundary. The induced velocity on a vortex which is inside the region is composed of three parts:

(1) Uniform free stream velocity given by eq.(143)

(2) Due to the vortices which are to the left of LL' and right of RR'. The induced velocity due to this part can be obtained by substracting the part due to the vortices inside the domain from the known solution for a vortex row. The velocity field due to the lower row vortices are (Lamb, 1932)

$$u = -\frac{\Gamma_1}{2A} \frac{\sinh \frac{2\pi y}{A}}{\cosh \frac{2\pi y}{A} - \cos \frac{2\pi x}{A}}$$

$$V = \frac{\Gamma_1}{2A} \frac{\sin \frac{2\pi}{A}}{\cosh \frac{2\pi y}{A} - \cos \frac{2\pi x}{A}} \qquad (147)$$

The induced velocity at a point (x,y) due to a point vortex which acts in the counterclockwise direction located at (x_0, y_0) is

$$u = -\frac{\Gamma_1}{2\pi} \frac{y - y_0}{(x - x_0)^2 + (y - y_0)^2}$$

$$V = \frac{\Gamma_1}{2A} \frac{x - x_0}{(x - x_0)^2 + (y - y_0)^2} \qquad (148)$$

Hence the induced velocity on a vortex which is located at a point (x_i, y_i) due to the lower row vortices which lie outside the domain is

$$u_i = -\frac{\Gamma_1}{2A}\,\frac{\sinh\frac{2\pi y_i}{A}}{\cosh\frac{2\pi y_i}{A} - \cos\frac{2\pi x_i}{A}} + \frac{\Gamma_1}{2\pi}\sum_{j=ML}^{MR}\frac{y_i}{(x_i-x_j)^2 + y_i^2}$$

$$v_i = \frac{\Gamma_1}{2A}\,\frac{\sin\frac{2\pi x_i}{A}}{\cosh\frac{2\pi y_i}{A} - \cos\frac{2\pi x_i}{A}} - \frac{\Gamma_1}{2\pi}\sum_{j=ML}^{MR}\frac{x_i - x_j}{(x_i-x_j)^2 + y_i^2} \tag{149}$$

Here x_j is the coordinate of the lower row vortices given by eq.(144). Similarly, due to the upper row vortices are

$$u_i = \frac{\Gamma_1}{2A}\,\frac{\sinh\frac{2\pi(y_i-B)}{A}}{\cosh\frac{2\pi(y_i-B)}{A} - \cos\frac{2\pi(x_i-B/2)}{A}} - \frac{\Gamma_1}{2\pi}\sum_{j=ML}^{MR}\frac{y_i - B}{(x_i-x_j)^2 + (y_i-B)^2}$$

$$v_i = -\frac{\Gamma_1}{2A}\,\frac{\sin\frac{2\pi(x_i-A/2)}{A}}{\cosh\frac{2\pi(y_i-B)}{A} - \cos\frac{2\pi(x_i-A/2)}{A}} + \frac{\Gamma_1}{2\pi}\sum_{j=ML}^{MR}\frac{x_i - x_j}{(x_i-x_j)^2 + (y_i-B)^2} \tag{150}$$

Here x_j is the coordinate of the upper row vortices given by eq.(144). When these equations are used to evaluate the velocities, in some instances, the vortex x_i, y_i locates near one of the vortices on the rows. Though u,v are finite, the expressions in the right hand side of eqs. (149), (150) become singular individually. To alleviate this problem, the expressions in eq.(149) and eq.(150) are expanded for small distance x_i, y_i and the singularity is removed.

Consider the lower vortex row which is located on the x axis, Fig. 25. The induced velocity due to this row on a point x_i, y_i is given by eq.(147). If the point x_i, y_i locates near the origin, vortex L, the induced velocity by the row can be expanded for small x_i, y_i and becomes

$$u_i = -\frac{\Gamma_1}{2\pi}\frac{y_i}{x_i^2 + y_i^2} + \frac{\Gamma_1}{2A} C_1$$

$$v_i = \frac{\Gamma_1}{2\pi}\frac{x_i}{x_i^2 + y_i^2} + \frac{\Gamma_1}{2A} C_2 \qquad (151)$$

where

$$C_1 = -\frac{Y}{3!}\sin^2\theta + \frac{2Y}{4!}\left(\sin^2\theta - \cos^2\theta\right)$$
$$-\frac{Y^3}{5!}\sin^2\theta + \frac{2Y^3}{3!\,4!}\left(\sin^2\theta - \cos^2\theta\right)$$

$$+ Y r^2 \left\{ 2 \frac{(\sin^4\theta - \sin^2\theta\cos^2\theta + \cos^4\theta)}{6!} - \frac{4}{4!\,4!} (\sin^2\theta - \cos^2\theta)^2 \right\}$$

$$+ O(X^5, Y^5)$$

$$C_2 = - \frac{X}{3!} \cos^2\theta - \frac{2X}{4!} (\sin^2\theta - \cos^2\theta)$$

$$+ \frac{X^3}{5!} \cos^2\theta + \frac{2X^3}{3!\,4!} (\sin^2\theta - \cos^2\theta)$$

$$+ X r^2 \left\{ 2 \frac{(\sin^4\theta - \sin^2\theta\cos^2\theta + \cos^4\theta)}{6!} - \frac{4}{4!\,4!} (\sin^2\theta - \cos^2\theta)^2 \right\}$$

$$+ O(X^5, Y^5) \qquad (153)$$

and

$X = 2\pi x_i = r \cos\theta$

$Y = 2\pi y_i = r \sin\theta.$

Singular terms $-\frac{\Gamma_\ell}{2\pi} \frac{y_\ell}{x_\ell^2 + y_\ell^2}$ and $\frac{\Gamma_1}{2\pi} \frac{x_\ell}{x_\ell^2 + y_\ell^2}$ are the induced velocities on the vortex (x_i, y_i) due to the vortex L. Hence when the contribution from the vortex L is substracted, this singularity will be removed and the eq.(149) takes the form

$$u_\ell = \frac{\Gamma_1}{2A} C_1 + \frac{\Gamma_1}{2\pi} \sum_{j=ML}^{MR}{}' \frac{y_\ell}{(x_\ell - x_j)^2 + y_\ell^2}$$

$$v_l = \frac{\Gamma_1}{2A} C_2 - \frac{\Gamma_1}{2\pi} \sum_{j=ML}^{MR}{}' \frac{x_l - x_j}{(x_l - x_j)^2 + y_l^2} \tag{154}$$

$\sum'$ means that the vortex L is excluded in the summation. Similarly eq.(150) for the upper row vortices can be modified.

(3) Induced velocity due to the vortices inside the domain. This includes vortex pair, upper and the lower vortex rows. This is given by

$$u_l = -\frac{\Gamma_1}{2\pi} \sum_{x_o, y_o} \frac{y_l - y_o}{(x_l - x_o)^2 + (y_l - y_o)^2}$$

$$v_l = \frac{\Gamma_1}{2\pi} \sum_{x_o, y_o} \frac{x_l - x_o}{(x_l - x_o)^2 + (y_l - y_o)^2} \tag{155}$$

The above procedure can simply be summarized as follows. Determine the velocity at a vortex x_i, y_i using the expression for the unperturbed vortex street and then add the difference due to the perturbation. After the induced velocities u_i, v_i are determined the new positions of the vortices are calculated using Euler scheme.

$$\begin{aligned} x_i(t+\Delta t) &= x_i(t) + \Delta t \,.\, u_i \\ y_i(t+\Delta t) &= y_i(t) + \Delta t \,.\, v_i \end{aligned} \tag{156}$$

where Δt is the time step. A program was written to solve this numerically. About 25-50 vortices on either side of the vortex pair were considered in the middle region of the vortex street. A time step of 0.01

was used in the calculations. All the conservations laws such as linear momentum, angular momentum and energy were calculated to check the numerical calculations. The linear momentum and energy were conserved to 0.1% accuracy. Motion of the vortex pairs and the distortion of the vortex street are followed in time.

The results are shown in Figs. 27-37. Figs. 27,28,29 show the motion of the vortex pair for different strength of the vortex pair Γ_2/Γ_1 = 0.5,1.0 and 2.0 respectively. The distance between the vortices is a = 2.5. X-axis represents the time and the Y-axis represents the Y-coordinate of the vortex pair. Curve 'Q' is the path which the pairs would have taken in the absence of the vortex street. 'L' and 'R' are the paths taken by the left vortex and the right vortex respectively due to the presence of the vortex street. It is seen from the results shown that when the strength of the vortex pair is small 0.5, 1.0 the vortex pair bounces back from the vortex street. When the strength of the vortex pair is 2.0, the vortex pair goes through the vortex street.

The turbulent intensity of the normal velocity component in the inner part of the boundary layer is about two times larger than that in the outer part of the boundary layer (at $y=0.2\delta$, $v'=0.04U_\infty$ and at $y=0.8\delta$, $v'=0.02U_\infty$). The vortex strength $\Gamma_2/\Gamma_1=1.0$ approximately represents the eddy with the normal velocity $v'=0.014U_\infty$. During the ejection process the ejected fluid moves away from the wall with the velocity which is about two, three times larger than that the outer fluid. Hence it will move across the wake and will reach the outer region. Since the outer fluid moves with low velocity, it will be blocked by the wake vortices. When the length of the plate is increased the longitudinal distance between the vortices and the strength of the vortices increase. Therefore the vortex street behind a longer plate will block more effectively than a shorter plate. The experimental results show that when the length of the plate is increased the local skin friction reduction is increased (Anders et al., 1985).

Figs. 30-33 show the position of the vortices in the vortex street and the vortex pair at different instants of time. Figs. 30-33 show the results for the case $\Gamma_2 = 0.5$ and $c = 2.5$. It is seen that the clockwise vortex in the pair interacts with the vortices in the lower row of the vortex street which are in the anticlockwise direction and bounces back from the wake. Similarly the anticlockwise vortex is kept above the wake by the upper row clockwise vortices Figs. 31,32. Due to the highly unstable character of the vortex street and due to the vortex pairing, the vortex street becomes very distorted (Fig. 33) and the calculations cannot be continued for longer times. In some cases, a vortex in the vortex pair and a vortex in the vortex street pair and move away from the wake due to the large induced velocities Figs. 28 and 34. To alleviate this problem different core radii were introduced for the vortex pair and the vortex street. The magnitudes of the radii are determined through energy considerations of the system.

A wake profile as shown in Fig. 35a is represented by an equivalent vortex street as shown in Fig. 35b. It is assumed that the vortices have circular cross sections and constant vorticity. The kinetic energy associated with one pair of vortices S_1 and S_2 is equivalent to the kinetic energy in the equivalent wake length and is given by

$$\text{Kinetic energy} = \rho \; (\Gamma_1^2/8\pi^3\;)\; 34.73 \tag{157}$$

Consider a vortex system as shown in Fig. 35c which consists of two circular vortices with constant vorticity. The core radius is r_c and half the distance between the vortices is R. The kinetic energy associated with that system is given by (Lamb 1940)

$$\text{Kinetic energy} = \rho \; (\Gamma^2/8\pi^3)\; F \tag{158}$$

where

$$F = -\left(\frac{R}{r_c}\right)^4 \int\!\!\int \xi\,(x,y)\,\xi\,(x',y')\,\log\left\{(x-x')^2+(y-y')^2\right\} dx\,dy\,dx'\,dy' \tag{159}$$

The variables x,y are non-dimensionalised with R and the integration is over the circular vortex sections S_1 and S_2. ξ is the strength of the vorticity in the circular regions. Equating eq.(157) and eq.(158) the core radius r_c can be determined. The above integral was numerically evaluated and for F = 34.73, r_c/R takes the value 0.55. Substituting for R, one obtains $r_c = 0.154$. Since the length scales in the vortex pair is about twice the scale in the vortex street the core radius of the vortex pair is taken as 0.3. After the sizes of the core radii are approximately determined the program was modified to include the effect of the core radius. The induced tangential velocity by a vortex which has a core radius r_c and circulation Γ is given by

$$\begin{aligned} V_\theta &= (\Gamma/2\pi r_c)\;(r/r_c) && \text{for} \quad r \leq r_c \\ &= \Gamma/2\pi r && \text{for} \quad r \geq r_c . \end{aligned} \tag{160}$$

The case $\Gamma_2 = 1.0$ is run again with this modification and the results are shown in Figs. 36, 37. It is seen that due to the different core radii for the vortex pair and the vortex streets, the vortex pairing is removed and the results show that the vortex pairs bounces back from the wake.

A large-eddy is a localised three-dimensional region with distributed vorticity over the region. In the above model we simulated the large-eddy with a vortex-pair. The results show that the strong interaction between the clockwise vortex and the vortex street occurs after the clockwise vortex moves inside the region between the upper and the lower vortex rows. During the interaction the clockwise vortex interacts with the vortices close to it and bounces back to above the wake region. From the above results we infer that some part of the large-eddy will be pulled inside the region between the lower and the upper vortices. In the point vortex model the clockwise vortex bounces back to above the wake. In the distributed vorticity case the results may be different. It would be an interesting study to investigate the above model replacing the vortex pair with a distributed vorticity model. It is felt that the part of the eddy which moves inside the wake region will be kept inside the wake. We can extend this model to three-dimensional case. For that we have to replace the point vortices with vortex filaments. The large-eddy can be simulated by a vortex ring. As discussed previously it is felt that depending on the relative strengths of the wake and the eddy, some part of the eddy will be pulled inside the wake and will be kept inside the wake region.

Chapter 8

In chapter 7 the interaction of a vortex street and a vortex pair is studied. The vortex street simulates the wake behind the plate. Munford and Savill (1983) flow visualization experiments, which show that the wake behind the LEBU devices consists of a coherent vortex street, were done at a low Reynolds number of 10,000 based on chord length of the plate. The length of the vortex street region decreases with increasing Reynolds number and at higher Reynolds number the wake behind the plate becomes turbulent at a shorter distance downstream of the plate. Therefore in this chapter we will consider the interaction of a continuous wake and a vortex pair. The turbulent wake behind a plate has the velocity defect approximately in the Gaussian form. The vortex pair simulates the ejection process or the wallward movement of the outer fluid towards the wall. In the absence of the wake the vortex pair will move with the constant induced velocity. When the wake is included the vortex pair and the wake interact and the motion of the vortex pair is altered. In this chapter we will determine, how the motion of the vortex pair is altered and, how the wake is modified due to the interaction. We employed the two-dimensional model to gain some insight into the effects and the mechanisms. The problem is solved using cloud-in-cell (CIC) method. There are basically two methods to solve the incompressible two-dimensional fluid flow problems. One is the stream function vorticity equation method, Roache (1975), and the second is the vortex method. In the first method the stream function is solved from the Poisson equation and then the vorticity equation is solved to obtain the new values of the vorticity at the Eulerian points. This procedure is continued till desired time is reached or steady state convergence is reached. When there are only concentrated vorticity regions imbedded in an otherwise irrotational fluid this method becomes unstable (Fromm and Harlow, 1963) and it is very convenient to use the vortex method Leonard (1980).

Vortex method simulates flows with concentrated voricity regions. By the theorems of Helmholtz and Kelvin it is known that the inviscid motion of the vorticity in these regions is given by the local fluid velocity which in turn is determined kinematically from the vorticity field. Thus in this method, the vorticity region is discretized into parcels of vorticity and this discretization is tracked in a Lagrangian reference frame. Leonard (1980) reviews the vortex methods and discusses the advantages and the disadvantages of the different vortex methods. The simplest method among them is the point vortex method. In this method the vorticity region is discretized into a finite number of point vortices. The induced velocity at a vortex by the remaining vortices is calculated by Biot-Savart formulae. After the induced velocities at all the vortices have been evaluated, the positions of the vortices are integrated in time. For N point vortices the above procedure requires $O(N^2)$ operations to compute all the required velocities. When the number of point vortices becomes large the computing time increases enormusly. One method which is used to decrease the computing time is cloud-in-cell (CIC) method. This method is widely used in Plasma dynamics Birdsell et al. (1969), and is recently used in fluid dynamics, Christianson (1973) ,Baker (1979). This method is described below and later this technique is applied to the wake problem.

A given vortex, say at (x_n, y_n) with circulation Γ_n, resides within a certain mesh cell, as depicted in Fig. 38. In the CIC method the vortex coordinate (x_n, y_n) is taken to be at the centre of the vorticity cloud of finite extent. Using a cloud the same size as a grid cell, Δx by Δy, the vorticity is distributed over the region as shown in Fig. 38. The strength of the vorticity is given by $\omega_n = \Gamma_n / \Delta x \Delta y$. In the next step this vorticity in this cloud is distributed to the spatial grid points. This is done by drawing a cell the same size as grid cell at the grid point and the common cloud to this cell and the vorticity cloud is assigned to that grid. For example, in the above case, the vorticity in the area shaded (   ) is assigned to grid point (i,j); that shaded (   ), to (i+1,j); that shaded (   ) to (i+1,j+1); that shaded (   ) to (i,j+1). This can be written as

$$\omega(i,j) = a_{i,j}\,\omega_n$$

where

$$a_{i,j} = (\Delta x - x_n)\,(\Delta y - y_n) / \Delta x \Delta y$$

$$a_{i+1,j} = x_n\,(\Delta y - y_n) / \Delta x \Delta y$$

$$a_{i+1,j+1} = x_n\, y_n / \Delta x \Delta y$$

$$a_{i,j+1} = (\Delta x - x_n)\, y_n / \Delta x \Delta y$$

and (x_n, y_n) is taken as the distance of the point vortex from the spatial grid point (i,j). For a large number of clouds, the vorticity at (i,j) is obtained by summing over the clouds as

$$\omega(i,j) = \sum_n a_{i,j}\, \omega_n.$$

After all the vorticity has been distributed among the mesh points Poisson equation for the stream function, ψ, is solved with appropriate boundary conditions

$$\psi_{xx} + \psi_{yy} = -\omega$$

With the stream function in hand, velocities at the mesh points can be calculated, for example, by central differences

$$u_{i,j} = (\psi_{i,j+1} - \psi_{i,j-1})/2\Delta y$$

$$v_{i,j} = - (\psi_{i+1,j} - \psi_{i-1,j})/2\Delta x.$$

To determine the velocity of the vortex 'n' bilinear interpolation (area weighting) can be used.

$$u_n = a_{i,j}u_{i,j} + a_{i+1,j}u_{i+1,j} + a_{i+1,j+1}u_{i+1,j+1} + a_{i,j+1}u_{i,j+1}.$$

After determine the velocities of all the vortices the vortex positions are moved forward in time by the formulae

$$x_n(t+\Delta t) = x_n(t) + u_n\Delta t$$

$$y_n(t+\Delta t) = y_n(t) + v_n \Delta t.$$

This concludes the description of the CIC method.

This method conserves total vorticity and the linear momentum, but the angular momentum is not conserved. The distribution of vorticity to the mesh and the bilinear interpolation to obtain the vortex velocities are subject to error. Due to this error small scale fluctuations are produced on a scale compared to the grid size. Christianson (1973) applied this method to few interesting cases, formation of Karman vortex street, Kelvin-Helmholtz instability and evolution of two finite area regions of vorticity in proximity, and reported good results. Baker (1979) applied this method to the roll-up of vortex sheet and obtained results which compared well with other numerical results. It is demonstrated in those calculations that the large-scale features are very well resolved by this method and is independent of grid size. One proposal to improve the numerics of CIC method has been put forth by Hockney et al. (1974). In the following, CIC method is applied to study the interaction of the continuous wake and the vortex pair. Using this method large-scale distortions of the wake and the motions of the vortex pairs are investigated.

The wake behind a plate has a Gaussian form and is given by

$$U = - \exp (-18y^2)$$

where y is the transverse coordinate Fig. 39. The vorticity distribution in the wake is given by

$$\omega = - 36y \exp(-18y^2)$$

The width of the wake which is defined as the distance between the points where the velocities are 0.01 is taken as one unit. The velocity at the centre of the wake is one unit. The wake behind the LEBU devices when they are used in tandem is measured by Bertelrud et al. (1982) and Mangus (1983). The measurements show that at 10δ (δ = boundary layer thickness) downstream the wake velocity is $0.2U_1$ (U_1 = free stream velocity) and width of the wake is 0.3δ and at 25δ downstream they are $0.1U_1$ and 0.4δ respectively. If the distance between the vortex pairs is taken as $\delta/4$, and the eddy velocity as $0.02U_1$ then the strength of the vortex pair $\Gamma_2 = 0.03\delta U_1$. Non-dimensionalising the variables by the wake velocity and by the width of the wake the strength of the vortex Γ_2 becomes 0.5 - 1.0. To study the mean shear a constant mean shear profile $U=\omega y$ is added to the wake profile, Fig. 39. The mean shear in the outer part of the boundary layer is $du/dy = 0.2U_1/\delta$. The non-dimensionalised value for ω based on the wake velocity and the width of the wake is in the range of 0.25- 1.0.

For the numerical calculations a rectangular grid as shown in Fig. 39 is used. The vorticity above the lines $y = \pm 0.5$ is assumed zero. This implies that the wake vorticity is assumed to concentrate within this region $-0.5<y<0.5$. In the next step every grid cell is divided into several small cells and the vorticity in those small cells are replaced by point vortices located at the centre of the small cells. This way the continuous vorticity in the wake is simulated by equivalent point vortices.

The upper boundary BC (Fig. 39) and the lower boundary AD are placed far away from the vortex system and are assumed to be streamlines. If the stream function at the lower boundary is taken as zero the stream function at the upper boundary takes the value

$$\psi = - \int_{-\infty}^{\infty} \exp(-18y^2)\, dy$$

$$= -0.4177$$

Two types of boundary conditions are tried at the left boundary AB and at the right boundary DC. One is that the disturbances are zero at those boundaries and the flow crosses those boundaries undisturbed and the second type is that the flow conditions are periodic at both boundaries. Both type of boundary conditions produce the same results. This we expect also because the interaction between the wake vorticity and the vortex pair is a localised effect and the boundary effect is small. To study the effect of the wall the lower boundary AD is moved closer to the wake accordingly.

Poisson equation is solved using Fast Poisson Solver routine. We used the code which was developed at National Center for Atmospheric Research (1975). The numerical procedure can be explained as follows:

(1). using the CIC method solve for the induced velocities on the point vortices in the wake and on the vortex pair by the point vortices in the wake

(2) add the induced velocity by the vortex pair on the vortices

(3) add the mean shear velocity

(4) move the vortices to the new positions.

The procedure is continued till desired time is required. To study the effect of the eddies coming from below and above the wake, the effect of the wall and the effect of the mean shear, the following cases as shown in Fig. 40 are considered. Except cases (1) and (4) in all other cases (2), (3), (5) and (6) wall is placed at a height $y=-2.0$.

The following parameters are used in the numerical calculations $\Delta x=0.1$, $\Delta y=0.05$, $M=257$ and $N=129$ where Δx, Δy are grid sizes and M, N are the number of nodal points in the X, Y directions. For discretization every mesh cell is divided into 4 small cells. The results are shown in Figs. 41-69b. In these figures deformation of the wake and the position of the vortex pairs are shown at different instants of time. Figs. 41-49 show the results for the case (1). In this case a vortex pair with the strength $\Gamma_2 = 0.5$ and the distance between the pairs $c = 1.0$ is placed at a height $H=1.5$ above the centre of the wake. Fig. 41 shows the motion of the right and the left vortices in the vortex pair with time and also shown is the path taken by the vortices in the absence of the wake. It is seen that due to the interaction with the wake the vortices move slowly towards the wake. In Figs. 42-46 the distortion of the wake and the paths taken by the vortex pair are depicted. The wake region which is plotted is the part of the wake which was initially in the region $-0.5<y<0.5$. There are two observations that have to be made. One is what changes take place in the wake and the other is the motion of the vortex pairs. It is seen that the distance between the vortices in the vortex pair increases with time. This means that due to the interaction the vortices move slowly and spreads in the streamwise direction. It is very interesting to observe the changes that take place in the wake. The disturbance introduced by the vortices grows with time and at the same time is swept by the mean wake velocity to the left side. Concentrated vorticity regions are formed on the upper and lower part of the wake. It is observed in Fig. 46 that when the anticlockwise vortex in the vortex pair moves close to the wake it lifts the fluid in the upper part of the wake. If the calculation is continued the vorticity in this lifted fluid which is in the clockwise direction moves the anticlockwise vortex away from the wake and therefore we terminated the calculations at this time. Figs. 47, 48 show the results for the case Γ_2=1.0 and c=1.0. Fig. 49a and Fig. 49b show the results for the case Γ_2=3.0 and c=1.0. It is seen that when the strength of the vortex increases it moves as undisturbed until it moves very close to the wake. Fig. 49a and Fig. 49b show that when Γ_2=3.0 the vortex pairs go through the wake. Another observation is that in the initial stages when the strength of the vortex is doubled the displacement of the wake also doubled. This can be noted in Figs. 42, 47. Fig. 50 depicts the results for the case (2). This is same as the case (1) but with a wall which is placed below the wake at y=-2.0. There was no difference on the motion of the vortex pair. Fig. 50 shows the distortion of the wake and the path of the vortices at the non-dimensional time T=15.0. It is seen that due to the presence of the wall the growth in the lower part of the wake is suppressed. Figs. 51, 52 show the results for the case (3). This case is same as case (2) but in this case vortices are moving up from the region between the wake and the wall. The results are similar to the case (1) in that the vortices move with reduced velocities and the streamwise distance between the vortices increases with time.

Next we will discuss the effect of mean shear. This case models the boundary layer problem better than the case without the mean shear. Case (4) and case (5) did not show any substantial differences and we present the results for the case (5). This is same as case (2) with the addition of a constant mean shear profile to the wake profile. The results are shown in Figs. 53-63 for the case $\Gamma_2 = 0.5$, $c=1.0$, mean shear = 0.5 and the wall is placed at $y=-2.0$. The vortices were initially located at $y=1.5$. Since there is a mean shear the vortices are advected to the right by the shear. Figs. 53-55 show the results for the case without the wake i.e., the strength of the wake is zero. In this case, if the wall is away from the vortices, then the vortices move on parabolas.

Fig. 56 shows the motion of the vortices with time with the wake. It is seen that as in previous cases the vortices move slowly due to the interaction with the wake. Figs. 57-60 show the distortion of the wake and the positions of the vortex pair. It is observed that the distance between the vortices increases with time. In this case we obtain somewhat different picture about the distortion of the wake. As in the previous cases the disturbances introduced by the vortex pair grows in time. But the important difference is that the disturbances in the lower part of the wake disappeared and concentrated vorticity regions are formed only in the upper part of the wake. In Figs. 61-63 we plotted the streamwise velocity distributions at different x locations. The solid lines show the modified velocity distribution and the dotted lines show the undisturbed velocity distributions. It is very interesting to observe how a shear layer is developing in the upper part of the wake. In Fig. 63 this shear layer appears in region $12.0<x<15.0$. Figs. 63a-63c show the results for the case $\Gamma_2=3.0$, $c=1.0$ and mean shear $=0.5$ and the wall is placed at $y=-2.0$. It is seen from Fig. 63a that the vortices go through the wake in this case. Fig. 63b and 63c show the distortion of the wake. It is seen that due to the large strength of the vortices the wake is distorted violently.

From above results we make the following general conclusions about the changes occur above the wake. The eddy which moves from above the wake towards the wall due to the interaction with the wake moves with reduced vertical velocity and spreads in the streamwise direction. When the strength of the vortex $\Gamma_2=0.5$, the distance between the vortices is doubled after the non-dimensional time interval $T=12.0$ and the vertical distance which is travelled is reduced by about 40% from the undisturbed value. When $\Gamma_2=3.0$ the vortices go through the wake. It is observed for the case $\Gamma_2=0.5$ that the disturbances introduced by the eddy in the wake grows with time and forms shear layers above the wake. The region below the wake is not much affected by the interaction. For $\Gamma_2=3.0$, the wake is distorted violently and it spreads to lower and upper regions.

The vertical velocity of the eddy corresponding to the case $\Gamma_2=0.5$ and $c=1.0$ is $0.5U_m/2\pi$ (U_m is the center line velocity of the wake). Hence when the wake velocity U_m is $0.2U_1$, the vertical velocity of the eddy is $0.016U_1$. The turbulent intensity of the vertical at $y=0.8\delta$ is $0.02U_1$. Therefore we can conclude from the above results that the wake behind the

LEBU devices reduces the motion of the outer part of the fluid towards the wall.

Next we will consider the results for the case (6) in which the vortices move from the region between the wake and the wall. Figs. 64-69 depicts the results of the distortion of the wake. The vortices are advected by the mean shear to the left. Figs. 64-67 show the results for the case $\Gamma_2 = 0.5$, c=1.0 and mean shear 0.5. The vortices were initially located at the height y=-1.5. It is seen that the vortices move differently than when they move from above the wake. The vortices are tilted towards the wall when they move away from the wall. The reason is due to the interaction the counter rotating vortex in the left is induced with a larger vertical velocity than the clockwise vortex in the right. Hence the vortices move with different vertical velocities and due to the mean shear they are tilted towards the wall. Figs. 68-69 show the results for the case $\Gamma_2=2.0$. Since the strength of the vortex is large it moves undisturbed until it moves very close to the wake Fig. 68. When it moves closer to the wake it strongly interacts with the wake and disturbes the whole outer region, Fig. 69. Fig. 69a, 69b show the results for the case $\Gamma_2=3.0$. It is observed that the vortices move across the wake and reach the outer region of the wake.

We did several calculations with smaller grid sizes and smaller time steps to see the influence of the grid size and time steps. There were no significance differences observed in the distortion of the wake or in the motion of the vortex pairs. One difficulty we encountered is that when the point vortices move close to the wake they induce large velocities on the wake fluid. Due to this the wake fluid lifts away from the wake and wraps around the point vortices. This is observed in Figs. 46, 48, 52, 60, 63b and 63c. An alternative may be to simulate the large-eddy with continuous vorticity distributions instead of point vortices.

Chapter 9

In this chapter we analyze the interaction of the vortex pair and the continuous wake using linear theory. In the next section we will extend this analysis to study the three-dimensional effects. The problem is solved as an initial value problem using Fourier and Laplace transforms. This can be considered as a hydrodynamic stability problem. Case (1960) discusses the stability of inviscid plane couette flow as an initial value problem. Since it involved large amount of work and it gives the same stability criteria it is not widely attempted. The flow field considered for the analysis is shown in Fig. 70. A wake which has the velocity defect in the Gaussian form $U=-\exp(-18y^2)$ is flowing parallel to the x-axis. Two point vortices of strength $-\Gamma$ and $+\Gamma$ are located at the points $(0.0,H)$ and (D,H) respectively. Taking the Fourier and Laplace transforms to the linearized Euler equations we obtain

$$\frac{d^2\bar{v}}{dy^2} - k^2\bar{v} - \frac{\bar{v}}{U-c}\frac{d^2U}{dy^2} = -\frac{1}{ik(c-U)}\left\{\frac{d^2\tilde{v}_o}{dy^2} - k^2\tilde{v}_o\right\} \qquad (161)$$

This is the familiar Rayleigh equation with source term. The source term is introduced by the vortex pair. Here $\bar{v}(k,y,c)$ is the Fourier and Laplace transforms of the perturbation velocity in the y-direction $v(x,y,t)$. $v_0(k,y)$ is the Fourier transform of the initial perturbation velocity in the y-direction $v_0(x,y)=v(x,y,t=0.0)$. k and c are the Fourier and Laplace transform variables which are defined as:

Fourier transform

$$\tilde{\phi}(k,t) = \int_{-\infty}^{\infty} \phi(x,t)\, e^{-ikx}\, dx$$

Fourier inverse transform

$$\phi(x,t) = \frac{1}{2\pi} \int_{-\infty}^{\infty} \tilde{\phi}(k,t)\, e^{ikx}\, dk$$

Laplace transform

$$\tilde{\phi}(k,s) = \int_{-\infty}^{\infty} \tilde{\phi}(k,t)\, e^{-st}\, dt$$

Laplace inverse transform

$$\tilde{\phi}(k,t) = \frac{1}{2\pi i} \int_{a-i\infty}^{a+i\infty} \bar{\phi}(k,s)\, e^{st}\, ds$$

and s=-cik.

The boundary conditions are

$$\frac{d\bar{v}}{dy} + |k|\,\bar{v} = 0 \qquad \text{when } y \to \infty$$

$$\frac{d\bar{v}}{dy} - |k|\,\bar{v} = 0 \qquad \text{when } y \to -\infty.$$

The vorticity ξ_0 is defined as

$$\xi_0 = \frac{\partial v_0}{\partial x} - \frac{\partial u_0}{\partial y}$$

The Fourier transform of this gives

$$\tilde{\xi}_0 = \frac{1}{i k}\left\{ \frac{d^2\tilde{v}_0}{dy^2} - k^2 \tilde{v}_0 \right\}$$

In the problem we analyse two point vortices initialy located at (0.0,H) and (D,H). Therefore we have

$$\xi_0 = -\Gamma\,\delta(x)\delta(y-H) + \Gamma\,\delta(x-D)\delta(y-H)$$

and the Fourier transform of this yields

$$\tilde{\xi}_0 = \Gamma\,(\,e^{-ikD} - 1.0\,)\,\delta(y-H).$$

Substituting this relation in the eq.(161) we get

$$\frac{d^2\bar{v}_0}{dy^2} - k^2\bar{v} - \frac{\bar{v}}{U-c}\frac{d^2U}{dy^2} = -\frac{\Gamma}{c-U}\left\{ e^{-ikD} - 1.0 \right\}\delta(y-H) \tag{162}$$

This equation is solved using Green's function technique. Let $\phi_1(y,k,c)$ and $\phi_2(y,k,c)$ be two independent solutions of the homogeneous equation of eq.(162). We can select ϕ_1 and ϕ_2 as

$$\phi_1(0,k,c) = 1; \quad \phi'_1(0,k,c) = 0$$

$$\phi_2(0,k,c) = 0; \quad \phi'_2(0,k,c) = 1.$$

Hence ϕ_1 will give a symmetric solution and ϕ_2 will give an antisymmetric solution. Define

$$\psi_1(y,k,c) = \phi_1(y,k,c)\left\{ \phi_2'(-\infty,k,c) - |k|\,\phi_2(-\infty,k,c) \right\}$$

$$- \phi_2(y,k,c)\left\{ \phi_1'(-\infty,k,c) - |k|\,\phi_1(-\infty,k,c) \right\}$$

$$\psi_2(y,k,c) = \phi_1(y,k,c)\left\{ \phi_2'(+\infty,k,c) + |k|\,\phi_2(+\infty,k,c) \right\}$$

$$- \phi_2(y,k,c)\left\{ \phi_1'(+\infty,k,c) + |k|\,\phi_1(+\infty,k,c) \right\} \tag{163}$$

The solution of eq.(162) can be obtained using classical Green's function method (See Appendix K). We obtain

$$\bar{V}(y,k,c) = -\frac{\Gamma}{c - U(H)}\left\{ e^{-ikD} - 1.0 \right\} G(y,k,c,H)$$

where

$$G(y,k,c,H) = -\frac{\psi_2(H,k,c)\,\psi_1(y,k,c)}{2\left\{ \phi_1'(+\infty,k,c) + |k|\,\phi_1(+\infty,k,c)\right\}\left\{ \phi_2'(+\infty) + |k|\,\phi_2 \right\}} \qquad y < H$$

$$= -\frac{\psi_2(y,k,c)\,\psi_1(H,k,c)}{2\left\{ \phi_1'(+\infty,k,c) + |k|\,\phi_1(+\infty,k,c)\right\}\left\{ \phi_2'(+\infty) + |k|\,\phi_2 \right\}} \qquad y > H$$

Applying the Laplace inverse transformation to the above equations we get

$$\bar{V}(y,k,t) = -\frac{1}{2\pi i}\,\frac{\Gamma i k}{2}\int_{\infty + ia}^{-\infty + ia} \frac{[e^{-ikD} - 1]}{c - U(H)}\,\frac{\psi_2(H,k,c)\,\psi_1(y,k,c)\,e^{-iktc}\,dc}{\left\{ \phi_1'(+\infty) + |k|\,\phi_1 \right\}\left\{ \phi_2'(+\infty) + |k|\,\phi_2(+\infty) \right\}}$$

for y<H

$$\bar{V}(y,k,t) = -\frac{1}{2\pi i}\,\frac{\Gamma i k}{2}\int_{\infty+ia}^{-\infty+ia}\frac{\left[e^{-ikD}-1\right]\psi_2(y,k,c)\,\psi_1(H,k,c)\,e^{-iktc}\,dc}{(c-U(H))\left\{\phi_1'(+\infty)+|k|\,\phi_1\right\}\left\{\phi_2'(+\infty)+|k|\,\phi_2(+\infty)\right\}}$$

for $y>H$.

Integration has to be taken in the lower half plane if k is positive and in the upper half plane if k is negative. Singular points of the equation are introduced from different part of the integrand. The zeros of $(\phi'_1(+\infty,k,c)+k\phi_1(+\infty,k,c))$ and $(\phi'_2(+\infty,k,c)+k\phi_2(+\infty,k,c))$ introduce poles in the integrand. These poles give rise to the exponential behaviour. These are the symmetric and the antisymmetric normal modes which we would have obtained if we had done the normal mode analysis. The other singulaities are due to $c-U(H)=0$, $\psi_1(H,k,c)$ and $\psi_2(y,k,c)$. The singularity $c-U(H)=0$ gives rise to an oscillating solution if U(H) is other than zero and gives a time independent solution if U(H) is zero. When we integrate in the k space the oscillating solution will decay as 1/t and the time independent solution will give a solution which is only function of x and y. The components $\psi_1(H,k,c)$ and $\psi_2(y,k,c)$ will have logarithmic singularities and the inverse transform will decay as 1/t, Case (1960).

The singularity regions in the c-plane are shown in Fig. 71. $(\phi'_1(+\infty,k,c)+k\phi_1(+\infty,k,c))$ and $(\phi'_2(+\infty,k,c)+k\phi_2(+\infty,k,c))$ are equal to zero along the lines RST and PQR respectively. These give the symmetric and antisymmetric growing modes solutions. Points 1 and 2 are eigenvalues for a particular wavenumber k. The conjugate solutions are shown in the upper half plane. Point R corresponds to the inflection point. Point 5 represents the singularity c=U(H) and the singularities associated with $\psi_1(H,k,c)$ and $\psi_2(y,k,c)$ lie on the line PRT. In the following calculations we will first calculate the contributions from the exponentially growing solutions and will then compare them with the numerical results which we obtained in the previous chapter. Next we will include the contribution from all the terms in the calculations.

The eigenvalues for the wake profile $U = \exp(-18y^2)$ is shown in the Figs. 72-75. Here c_R and c_I are the real and imaginary parts of the eigenvalue and α is the wavenumber. The velocities at the edges of the wake $y=\pm0.5$ are obtained from eq.(163) using residue integral method.

$$\begin{aligned} v(y=0.5,k,t) &= R_1 + R_2 \\ v(y=-0.5,k,t) &= R_1 - R_2 \end{aligned} \qquad (163)$$

where

$$R_1 = -\frac{\Gamma \iota k}{2} \; \frac{e^{-\iota k D} - 1.0}{c_S - U(H)} \; \frac{\psi_2(H,k,c_S)\, \psi_1(y,k,c_S)\, e^{-\iota k t c_S}}{\left\{ \phi_2'(+\infty) + |k|\, \phi_2(+\infty) \right\}_{c=c_S} \dfrac{d}{dc} \left\{ \phi_1'(+\infty) + |k|\, \phi_1(+\infty) \right\}_{c=c_S}}$$

$$-k_{0S} < k < k_{0S}$$

$$R_2 = -\frac{\Gamma \iota k}{2} \; \frac{e^{-\iota k D} - 1.0}{c_A - U(H)} \; \frac{\psi_2(H,k,c_A)\, \psi_1(y,k,c_A)\, e^{-\iota k t c_A}}{\left\{ \phi_1'(+\infty) + |k|\, \phi_1(+\infty) \right\}_{c=c_A} \dfrac{d}{dc} \left\{ \phi_2'(+\infty) + |k|\, \phi_2(+\infty) \right\}_{c=c_A}}$$

$$-k_{0A} < k < k_{0A} \qquad (164)$$

and c_S, c_A are the eigenvalues for the symmetric and antisymmetric modes and k_{0S} and k_{0A} are the wavenumbers correspond to the neutral solutions in the symmetrical antisymmetrical modes. For the Gaussian wake profile of the form $\exp(-18.y^2)$, $k_{0S} = 8.1439$ and $k_{0A} = 4.7432$.

After determine the velocities at the edges of the wake using the kinematic conditions we can determine the evolution of the wake with time. The kinematic boundary condition at the edges of the wake is

$$\frac{\partial \eta}{\partial t} + U \frac{\partial \eta}{\partial x} = V$$

Here η is the displacement of the edge of the wake in the y-direction U is the wake velocity at the edge of the wake and v is the normal velocity. Taking the Fourier transform of this equation we get

$$\bar{\eta} = \frac{1}{ik} \frac{\bar{V}}{U - c}$$

Substituting for v from eq.(164) and (165) we obtain the expressions for the upper and the lower edges of the wake.

$$\bar{\eta}_{upper} = \frac{1}{ik} \frac{R_1}{U - c_S} + \frac{1}{ik} \frac{R_2}{U - c_A}$$

$$\bar{\eta}_{lower} = \frac{1}{ik} \frac{R_1}{U - c_S} - \frac{1}{ik} \frac{R_2}{U - c_A} \qquad (166)$$

Taking the Fourier inverse transform of these expressions we obtain the solution for η_{upper} and η_{lower}. The results are shown in Figs. 76-78 for the case Γ=0.5, H=1.5 and D=1.0.. From the stability diagram Figs. 72-75 we note that the wavelength corresponds to the maximum growth rate is about 1.6. It is observed that the deformed wake also has the length scale in that order. Also shown in the Figs. 76-78 are the solutions obtained using the cloud-in-cell method. It is observed that below the vortex pair the results from the linear theory considering only exponentially solution differ by a small amount from the numerical calculation results. The reason is that, as mentioned previously, since U(H) is approximately zero in this case, c-U(H)=0 singularity introduces a time independent velocity field. This will give rise to an algebraically growing solution for η_{upper} and η_{lower}. The physical reason is that since the mean velocity U(H) at the vortex locations is zero the vortices are stationary and induce a steady velocity field. Some part of this velocity field is associated with the c-U(H)=0 singularity solution and produces an algebraically growing solution η_{upper} and η_{lower}.

Next we will calculate the contribution from all the terms. For that we have to take Laplace inverse transform integration in the c-plane to include all the singularities. We considered the contour 'C', as shown in Fig. 71, and evaluated the Laplace inverse transform integration along this contour. The results are shown in Figs. 76-78. At time T=1.5 we obtain the same results as the CIC results. When the time increases the difference between the two solutions increases.

From the linear theory results we check the numerical calculations and further we observed that the larger part of the solution is contributed by the exponentially growing solution. The algebraically growing solution is significant directly below the vortex pairs. Even at larger times, T=6.0, the linear theory solution compares quite well with the numerical calculations.

Three-dimensional theory

In the previous chapters we investigated the response of a wake to two-dimensional disturbances. A large-eddy is a localised three-dimensional region with distributed vorticity over the region. The interaction of the large-eddy and the wake behind the LEBU devices is a three-dimensional phenomena. Therefore in this section we will investigate the interaction of a wake and a three-dimensional eddy. Specifically we try to determine the response of the wake to a three-dimensional disturbance and the modification to the motion of the eddy due to the interaction. Since the nonlinear calculations of three-dimensional rotational flow is much more difficult, we will do a linear analysis. Since it is not possible to find the dispersion relation for a continuous mean profile in closed form, in the analysis we replace the continuous wake by linear profile for which dispersion relation can be found in closed form. In two-dimensions we simulated the eddy by a vortex pair. The extension of this structure in three-dimension will be a vortex ring. Since the Fourier transform of the velocity field induced by the vortex ring is not easy to evaluate we consider a three-dimensional dipole instead of a vortex ring to simulate a three-dimensional eddy. The effects of the dipole and the vortex ring on the wake are qualitatively same in the initial stages of the interaction. To study the effect of the mean shear we add a constant mean shear profile to the wake profile. Therefore we have the model problem as shown in Fig. 79, to be analysed. For the analysis we consider the frame of reference where the dipole is at rest. The mean velocity profile is given by

$$U(y) = w(y-H) \qquad y > h$$

$$U(y) = -U\,(h-y)/h + w(y-H) \qquad 0 < y < h.$$

A dipole of strength μ is located at a height H on the Y-axis. The normal velocity field induced by this dipole is

$$V_0 = \frac{\mu}{4\pi}\,\frac{1}{\{x^2+z^2+(y-H)^2\}^{3/2}} - \frac{\mu}{4\pi}\,\frac{3(y-H)^2}{\{x^2+z^2+(y-H)^2\}^{5/2}}$$

Two-dimensional Fourier transform pair is defined by

$$\tilde{f}(k_x, k_z, y, t) = \int_{-\infty}^{\infty}\int_{-\infty}^{\infty} f(x, z, Y, t)\, e^{-ik_x x}\, e^{-ik_z z}\, dx\, dz$$

$$f(x, z, Y, t) = \frac{1}{(2\pi)^2}\int_{-\infty}^{\infty}\int_{-\infty}^{\infty} \tilde{f}(k_x, k_z, Y, t)\, e^{ik_x x}\, e^{ik_z z}\, dk_x\, dk_z$$

The Fourier transform of the velocity field v_0 is given by

$$\tilde{v}_0 = -\mu/2\ \alpha\ e^{-\alpha(y-H)},$$

here $\alpha^2 = k_x^2 + k_z^2$.

Hence the Fourier transforms of the induced velocities by the dipole at the interfaces a,b,c are

$$\tilde{v}_{0a} = -\mu/2\ \alpha\ e^{-\alpha(H-h)}$$

$$\tilde{v}_{0b} = -\mu/2\ \alpha\ e^{-\alpha H}$$

$$\tilde{v}_{0c} = -\mu/2\ \alpha\ e^{-\alpha(H+h)}. \tag{167}$$

Taking the Fourier transforms of the linearized Euler equations, we obtain

$$\imath k_x \tilde{u} + \imath k_z \tilde{w} + \frac{\partial \tilde{v}}{\partial y} = 0 \tag{168}$$

$$\frac{\partial \tilde{u}}{\partial t} + U(Y)\,\imath k_x \tilde{u} + \tilde{v}\frac{dU}{dy} = -\frac{1}{\rho}\,\imath k_x \tilde{p} \tag{169}$$

$$\frac{\partial \tilde{v}}{\partial t} + U(Y)\,\imath k_y \tilde{v} = -\frac{1}{\rho}\frac{\partial \tilde{p}}{\partial y} \tag{170}$$

$$\frac{\partial \tilde{w}}{\partial t} + U(Y)\,\imath k_x \tilde{w} = -\frac{1}{\rho}\, i\ \tilde{p} \tag{171}$$

Here $\tilde{u}$, $\tilde{v}$ and $\tilde{w}$ are the Fourier transforms of the perturbations u, v and w. Combining eqs.(169) and (171) we get

$$\frac{\partial}{\partial t}\left(\tilde{u}\,\imath k_x + \tilde{w}\,\imath k_z\right) + U(Y)\,\imath k_x\left\{\imath k_x \tilde{u} + \imath k_z \tilde{w}\right\} + \imath k_x \tilde{v}\frac{dU}{dY}$$

$$= \frac{1}{\rho}\left(k_x^2 + k_z^2\right) p \tag{172}$$

Equations (168), (170) and (172) provide the equivalent two-dimensional equations of motion in the rotated frame of reference. This we expect from Squire's equivalent theorem. Eliminating u,v and p from the above equatins we obtain

$$\frac{\partial}{\partial t}\left\{ \frac{\partial^2 \tilde{v}}{\partial y^2} - \alpha^2 \tilde{v} \right\} + U(Y)\, i k_x \left\{ \frac{\partial^2 \tilde{v}}{\partial y^2} - \alpha^2 \tilde{v} \right\} = 0 \qquad (173)$$

where $\alpha^2 = k_x^2 + k_y^2$. Let us define

$$\tilde{v} = \bar{v} + v_0$$

where v_0 is the induced velocity field by the dipole given by eq.(167). Hence $\bar{v}$ represents the disturbance due to the presence of the wake. Eq.(172) becomes

$$\frac{\partial}{\partial t}\left\{ \frac{\partial^2 \bar{v}}{\partial y^2} - \alpha^2 \bar{v} \right\} + U(Y)\, i k_x \left\{ \frac{\partial^2 \bar{v}}{\partial Y^2} - \alpha^2 \bar{v} \right\} = 0 \qquad (174)$$

Laplace transform pair is defined by

$$\tilde{f}(k_x, k_z, Y, s) = \int_0^\infty \bar{f}(k_x, k_z, Y, t)\, e^{-st}\, dt$$

$$\bar{f}(k_x, k_z, Y, t) = \frac{1}{2\pi i}\int_{a-i\infty}^{a+i\infty} \tilde{f}(k_x, k_z, Y, s)\, e^{st}\, ds$$

Laplace transform of eq.(174) yields

$$\frac{\partial^2 \bar{v}}{\partial y^2} - \alpha^2 \bar{v} = 0 \tag{175}$$

Taking Laplace transform of the eq.(172) we obtain an expression for pressure. Changing the variables s=-cik, we get

$$-ik_x(U-c)\frac{\partial \bar{v}}{\partial y} + ik_x \bar{v}\frac{dU}{dY} + \frac{U(Y)}{c}\frac{\partial \tilde{v}_0}{\partial Y} - \frac{\tilde{v}_0}{c}\frac{dU}{dY} = \frac{1}{\rho}\left(k_x^2 + k_z^2\right)\tilde{p} \tag{176}$$

Kinematic boundary condition at an interface takes the form

$$\frac{\partial \eta}{\partial t} + U\frac{\partial \eta}{\partial x} = V$$

where η is the displacement of the interface in the y direction, U is the mean velocity at the interface and v is the normal velocity at the interface. Taking the Laplace and Fourier transforms of this equation yields

$$\tilde{\eta}\, ik_x(U-c) = \bar{v} - \frac{\tilde{v}_0}{cik_x} \tag{177}$$

Next we apply these equations (175), (175) and (177) at the interfaces a,b,c (Fig. 79) and obtain three simultaneous equations for the displacement of the interfaces η_a,η_b and η_c (See Appendix L for detail).

$$\tilde{\eta}_a\left\{(w(H-h)+c)^2\alpha+(w(H-h)+c)^2\alpha\coth\alpha h+(w(H-h)+c)\frac{U}{h}\right\}(ik_x)^2$$

$$+\tilde{\eta}_b\left\{-(w(H-h)+c)(wH+c+U)\alpha\operatorname{cosech}\alpha h\right\}(ik_x)^2$$

$$=-\frac{w(H-h)+C}{C}\mu\alpha^2 e^{-\alpha(H-h)} \qquad (178)$$

$$\tilde{\eta}_a\left\{-(wH+c+U)(w(H-h)+c)\alpha\operatorname{cosech}\alpha h\right\}(ik_x)^2$$

$$+\tilde{\eta}_b\left\{2(wH+c+U)^2\alpha\coth\alpha h-2(wH+c+U)\frac{U}{h}\right\}(ik_x)^2$$

$$+\tilde{\eta}_c\left\{-(wH+c+U)(w(H+h)+c)\alpha\operatorname{cosech}\alpha h\right\}=0 \qquad (179)$$

$$\tilde{\eta}_b\left\{-(w(H+h)+c)(wH+c+U)\alpha\operatorname{cosech}\alpha h\right\}(ik_x)^2$$

$$+\tilde{\eta}_c\left\{(w(H+h)+c)^2\alpha\coth\alpha h+(w(H+h)+c)\frac{U}{h}\right.$$

$$\left.+(w(H+h)+c)^2\alpha\right\}(ik_x)^2=0 \qquad (180)$$

From these three simultaneous equation we can solve for η_a, η_b and η_c.

$$\eta_a=\Delta_a/\Delta$$

and

$$\eta_b = \Delta_c/\Delta$$

where

$$\Delta = c\Big\{(WH+c)^3\alpha^3(1+\coth\alpha h)^2 + (WH+c)^2\alpha^3 U(1+\coth\alpha h)^2$$

$$+ (WH+c)\alpha\Big[\frac{U}{h}\cdot U\alpha(1+\coth\alpha h)^2 - \frac{U^2}{h^2}(1+\coth\alpha h) - \frac{U^2}{h^2}$$

$$- W^2h^2\alpha^2(1+\coth\alpha h)^2\Big]$$

$$+ \Big[\frac{U^2}{h^2}\Big(U\alpha\coth\alpha h - \frac{U}{h}\Big) + W^2h^2\alpha^2(1+\coth\alpha h)^2\Big(\frac{U}{h} - U\alpha\Big)\Big]\Big\} \qquad (181)$$

$$\Delta_a = \frac{\mu\alpha^2}{2k_x^2}e^{-\alpha(H-h)}\Big\{2\Big[(WH+c+U)\alpha\coth\alpha h - \frac{U}{h}\Big]\Big[(W(H+h)+c)$$

$$\alpha(1+\coth\alpha h) + \frac{U}{h}\Big] - (WH+c+U)(W(H+h)+c)\alpha\,\mathrm{cosech}^2\alpha h\Big\}$$

$$\Delta_b = \frac{\mu\alpha^2}{2k_x^2}e^{-\alpha(H-h)}(W(H-h)+c)(WH+c+U)\alpha^2\,\mathrm{cosech}^2\alpha h$$

To determine η_a and η_c first we take the Laplace inverse transform and then take the Fourier inverse transform. The singularities of η_a and η_c are determined by $\Delta = 0$. This is the dispersion relation for the linear wake profile considered. One root of this equation is $c = 0$ and the other three roots are the roots of a cubic polynomial. This can be determined in closed form (Abramowitz and Stegun 1970). Δ can be written as

$$\Delta = c\, \alpha^3 \,(1+\coth \alpha h)^2 \,(\, x^3 + a_2\, x^2 + a_1\, x + a_0 \,)$$

where

$$X = W H + C$$

$$a_2 = U$$

$$a_1 = \frac{1}{\alpha^2 (1+\coth \alpha h)^2} \left\{ \frac{U}{h}\, U\alpha \,(1+\coth \alpha h)^2 - \frac{U^2}{h^2}(1+\coth \alpha h) - \frac{U^2}{h^2} - w^2 h^2 \alpha^2 \,(1+\coth \alpha h)^2 \right\}$$

$$a_0 = \frac{1}{\alpha^2 (1+\coth \alpha h)} \left\{ \frac{U^2}{h^2}\left(U\alpha \coth \alpha h - \frac{U}{h}\right) + w^2 h^2 \alpha^2 (1+\coth \alpha h)\left(\frac{U}{h} - U\alpha\right) \right\}$$

Let

$$q = a_1 \ / \ 3 - a_2^2 \ / \ 3$$

$$r = 1/6 \ (a_1 a_2 - 3a_0) - a_2^3 \ / \ 27$$

$$s_1 = [\ r + (q^3 + r^2)^{1/2 \ 1/3}$$

$$s_2 = [\ r - (q^3 + r^2)^{1/2 \ 1/3}$$

then the roots are

$$x_1 = (s_1+s_2)-a_2/3$$

$$x_2 = - \ 1/2 \ (s_1+s_2) \ -a_2/3 \ +i\sqrt{3}/2 \ (s_1 - s_2)$$

$$x_3 = - \ 1/2 \ (s_1+s_2) \ -a_2/3 \ -i\sqrt{3}/2 \ (s_1-s_2)$$

When the mean shear w=0, we can obtain the roots in the simple form

$$C_1 = - U$$

$$C_2 = U \ \frac{\alpha^2 h\,(1+\coth\alpha h) - \alpha + \sqrt{\left\{\alpha^2(1+\coth\alpha h) - \alpha\right\}^2 - 4\alpha^2(1+\coth\alpha h)(1-\alpha h\coth\alpha h)}}{2\alpha^2\,(1+\coth\alpha h)}$$

$$C_3 = U \frac{\alpha^2 h\,(1+\coth\alpha h) - \alpha - \sqrt{\left\{\alpha^2 h\,(1+\coth\alpha h) - \alpha\right\}^2 - 4\alpha^2 (1+\coth\alpha h)(1-\alpha h\coth\alpha h)}}{2\,\alpha^2 h\,(1+\coth\alpha h)}$$

There is a cut off wavenumber beyond which the imaginary part of the roots are zero. For the case w=0 this wavenumber is 1.77. After we calculate the roots of the equation, we do the Laplace inverse transformation using residue integral method. Fourier inverse transformation is done employing Fast Fourier Transform (FFT) routines. When we apply the FFT routines the infinite integral in the wavenumber space is curtailed to a finite integral. Integration range was increased to larger range to verify that the aliasing effect did not affect the results. In the calculations the variables are non-dimensionalised by

Length	- h
Velocity	- U
Time	- h/U
Mean shear	- U/h

The results are shown in Figs. 80-103. These results are for the case H =

3.0. For plotting we consider the frame of reference where mean shear profile is zero at the centre. Hence the dipole is advected by the mean shear velocity at its location. We calculated and plotted $\eta_a(x,z,t)$ and $\eta_c(x,z,t)$ at different instants of time. We made two plots (1) $\eta_a(x,0,t)$ and $\eta_c(x,0,t)$ which are the wake heights at the centre and (2) constant height contours in (x,z) plane. To study the effects of the wake and the mean shear we consider the following cases.

(1) without the wake and without the mean shear
(2) without the wake and with the mean shear
(3) with the wake and without the mean shear
(4) with the wake and with the mean shear

Case (1). without the wake and without the mean shear

The results are shown in Figs. 80 and 81. For this case $\eta_a = v_{0a}.t$ and $\eta_c = v_{0c}.t$ where v_{0a} and v_{0c} are the induced velocities by the dipole on the interfaces 'a' and 'c'.

Case (2). without the wake and with the mean shear

The results are shown in Figs. 82 and 83. This is different from case (1). Because the dipole is advected by the mean flow the growth rate is not linear with time but the disturbed wake region extends in the streamwise direction. In both cases (1) and (2) the disturbed normal velocity $\bar{v}$ is zero.

Case (3). with the wake and without the mean shear

Figs. 84 and 85 show the two-dimensional calculations, i.e., we place a two-dimensional dipole above the wake. Figs. 86-89 show the three-dimensional results. Due to the unstable character of the wake profile the disturbances grow exponentially with time and the disturbances are advected by the wake velocity. As expected the growth rate is smaller in three-dimensions than in two-dimensions. In two-dimensional numerical calculations we observed that the wake disturbances grow with time and form concentrated vorticity regions in the upper and lower part of the wake. Hence in the three-dimensional calculations we may expect that the initial disturbances grow with time and form concentrated vorticity regions in the upper and lower part of the wake. The disturbed wake region has a triangular shape in the xz- plane and this triangle increases in size with time.

Case (4). with the wake and with the mean shear

Figs. 90 and 91 show the two-dimensional results. Figs. 92-95 show the three-dimensional results. The important observation is that the growth in the lower part of the wake is reduced by the mean shear. The growth in the upper part of the wake is not much altered. This was also observed in the previous two-dimensional calculations. Hence we may say that the disturbances will grow with time and eventually form concentrated vorticity regions in the upper part of the wake. Due to the mean shear the disturbed wake region in the xz plane is elongated in the spanwise direction.

When there is a symmetric mean velocity profile any disturbance can be separated into symmetric and antisymmetric parts. The symmetric part has a larger growth rate than the antisymmetric part. Hence when there is no mean shear the disturbances in the lower and in the upper parts of the wake are similar. When there is mean shear the mean velocity profile is no longer symmetric and the magnitude of the vorticity is reduced in the lower part of the wake. Hence the growth rate of the wake also may be reduced in the lower part.

Next we will determine how the vertical motion of the dipole is affected by the interaction. The vertical velocity on the plane y=H is given by (Appendix L)

$$\bar{v}(k_x, k_z, y=H, c) = -e^{-\alpha(H-h)} \left\{ \frac{\mu}{2} \frac{\alpha e^{-\alpha(H-h)}}{c i k_x} + \tilde{\eta}_a i k_x (w(H-h)+c) \right\}$$

As we did previously by taking Laplace inverse transform and Fourier inverse transform of this expression we can obtain the normal velocity field $\bar{v}(x,z,H,t)$ at y=H plane. When there is no wake for linear theory the disturbed velocity field $\bar{v}$ is zero. Figs. 96-98 show the disturbed velocity distribution $\bar{v}(x,z=0,y=H,t)$ at different times. The results are for the case (4) i.e., with the wake and with the mean shear. The non-dimensional mean shear w=0.25. The interesting observation is that there is always an upward velocity field is induced around the dipole region. This means that downward motion of the eddy is reduced by the wake.

To investigate this observation further, let us consider the kinematic boundary condition at the interface 'a'.

$$\frac{\partial \eta_a}{\partial t} + U \frac{\partial \eta_a}{\partial x} = \bar{v} + v_{0a}$$

where v_{0a} is the normal velocity field due to the dipole, $\bar{v}$ is the disturbed normal velocity field and U=-w(H-h) the mean velocity at the interface 'a'. Hence

$$\bar{v} = - v_{0a} + \frac{\partial \eta_a}{\partial t} + U \frac{\partial \eta_a}{\partial x} \qquad (181)$$

The normal velocity field $\bar{v}$ is governed by the Laplace equation $\nabla^2 \bar{v} = 0$. Therfore we can think of the solution $\bar{v}$ as that due to the sources located at the interface a with the strength distribution given by eq.(181). There are three contributions to the source strength, $-v_{0a}$, which give the image solution, $\frac{\partial \eta_a}{\partial t}$ and $U \frac{\partial \eta_a}{\partial x}$. We calculated $\frac{\partial \eta_a}{\partial t}$ and $U \frac{\partial \eta_a}{\partial x}$ at different times along the centre line z=0 and plotted the results in Figs. 99-101. Initially at t=0, $\frac{\partial \eta_a}{\partial t} = v_{0a}$ and $\eta_a = 0$. The results show that there are two separate regions where $\frac{\partial \eta_a}{\partial t}$ and $U \frac{\partial \eta_a}{\partial x}$ are large in magnitusde. The region in the left is the part where the large distortion in the wake occurs. The region in the right is directly below the dipole, where $\frac{\partial \eta_a}{\partial t} \approx 0$ and $U \frac{\partial \eta_a}{\partial x}$ has a negative value. Since the dipole is advected by the mean shear the induced velocity field due to the distorted wake region will be small and the normal velocity near the dipole is mainly induced by the source strength below the dipole which is approximately ($-V_{oa} + U\frac{\partial \eta_a}{\partial x}$). Since this source strength ($-V_{oa} + U\frac{\partial \eta_a}{\partial x}$) is positive in this region there is always an upward motion induced near the dipole.

Next we will determine the motion near the dipole when it is placed below the wake. The non-dimensional mean shear w is 0.25 and the dipole is placed at y=-3.0. The results are shown in Figs. 102, 103 at time T=9.0 and T=12.0. It is seen that near the dipole there is an antisymmetric normal velocity distribution is induced. To the left side of the dipole a positive velocity is induced and to the right side a negative velocity is induced. Hence when an eddy is moving towards the wake from below the wake the region in the left side travels with larger vertical velocity than the right side and due to the mean shear the eddy will be tilted in the clockwise direction towards the wall. We also made these observations in the two-dimensional numerical calculations, Figs. 65, 66.

Chapter 10

Conclusion and Discussion

In summary, the effects of LEBU devices in a turbulent boundary layer are investigated using analytical and numerical techniques. The modifications to the vertical velocity of a turbulent flow by the LEBU devices are analyzed using linear, three-dimensional unsteady aerodynamics. To study the effects of the wake, the interaction of a vortex pair and a wake which has a Gaussian velocity defect is investigated using numerical techniques.

As far as the unsteady aerodynamics effects are concerned, in all the cases considered, the results show that when a Fourier component of an eddy is advected over the LEBU devices, the shed vortices from these devices reduce the amplitude of the vertical velocity behind the device to varying degrees depending on the wavenumbers k_x and k_y. This reduction increases with increasing wavenumbers k_x and k_y. However it should be noted that only the modification of low wavenumber disturbances will have a substantial effect throughout the entire boundary layer. Modification to higher wavenumber fluctuations will be confined to the wake of the devices.

The two-dimensional results show that the amplitude is reduced as the wavenumber k_x increases. From the three-dimensional results we note that the amplitude is further reduced with increasing spanwise variations. This indicates that the LEBU devices are more effective at modifying vertical velocities for a 3-D disturbance than for a 2-D one.

When the eddy is advected over two plates which are far apart, the reduction in amplitude is squared. In a recent experiment (Guezennec and Nagib 1985) it was observed that in the tandem configuration immediately downstream of the first plate, the vertical velocity fluctuations are reduced, and after the second plate the vertical component is further reduced. This reduction of the vertical component is in qualitative agreement with our results. If we assume, in accordance with what was also postulated by others (Hefner et al. (1979), Corke (1983), Anders et al. (1984)) as the probable mechanism, that the reduction in the amplitude of the vertical velocity is the basic cause for the apparent reduction in the skin friction downstream of the LEBU devices, the above results show that the two plates which are used in tandem are more effective in reducing the drag than a single plate. We note that the only configuration which produced net drag reduction in experiments (Corke, 1985, Anders et al. 1984) so far, has this arrangement.

The analysis considering the effect of the ground plane shows that this decreases the effectiveness of the LEBU devices in reducing the amplitude of the vertical velocity in the wake. This effect increases when the LEBU devices are moved towards the plane. It is appropriate to mention here of the experimental results of Anders et al. (1984). When the LEBU devices which were used in tandem at 10δ, spacing were tested at the heights 0.3δ, 0.5δ and 0.8δ they obtained 0.0, 5.0 and 7.0 percent net drag reduction, respectively.

At this stage we cannot establish that this apparent reduction in the amplitude of the vertical velocity is the cause for the measured skin friction reduction downstream of the LEBU devices. It was observed in the experiments (Nychas et al.,1973) that high speed fluid from the outer flow moves towards the wall region before the ejection starts. It was suggested by Falco (1983) that the outer flow brings down the so called "typical eddies" towards the wall which later initiate the lift up process. Our results suggest that when the LEBU devices are introduced the shed vortices from the device reduce the level of vertical velocity fluctuations downstream of the devices and thus inhibit this large-scale wallward movement from occuring and prevent some fraction of the turbulent production. Therefore a corresponding reduction in the skin friction is obtained.

The wake which forms behind the LEBU devices interacts with the eddies in the outer part of the boundary layer and alters the motion of these eddies. During this interaction the motion in the wake is also modified. During the ejection process the low speed fluid which ejects from the wall interacts with the high speed outer fluid and forms large-eddies in the inner part of the boundary layer. This large eddy grows in size and moves towards the outer part of the boundary layer (Nychas et al., 1973). Downstream, the large-eddies which formed during these bursting events in the upstream region, form large-scale motions which have a very slow rotational motion towards the wall (Head and Bandyopadhyay 1981). It is observed that the dye which is placed near the wall reaches the outer region of the boundary layer and the dye which is placed near the outer region is found near the wall region. Even though these observations do not explain how the large-scale outer motion influences the bursting or the formation of low speed streaks and liftup, it is agreed that the large-scale outer motion towards the wall has some influence on the burst-sweep events. Falco (1983, 1984) from his series of experiments suggested that, during the bursting process, vortex rings are generated in the wall region and the vortex rings move away from the wall due to self induced velocities. These vortex scale wiyh the displacement thickness and are called "typical eddies". After these eddies reach the outer part of the boundary layer they are brought back towards the wall by the large-scale outer fluid which has the motion towards the wall. Later these vortex rings influence the next bursting process. This way the burst-sweep cycle is closed. With this assesment in background we will interpret our results.

In chapter 8 we investigated the two-dimensional, nonlinear interaction of the wake which has a Gaussian velocity defect with a vortex pair. The vortex pair simulates the large-eddy which moves towards the wall or away from the wall. We solved to determine two effects, one how the motion of the vortex pair is modified due to the presence of the wake and two, how the wake is modified due to the interaction. To study the influence of the mean shear, we included a constant mean shear profile in the analysis.

First we will discuss the changes that occur when the eddy moves from above the wake towards the wall. As expected, the effects depend on the relative strengths of the eddy and the wake. If the wake strength is weak or the eddy moves with large velocity, the presence of the wake will not influence the eddy motion and the eddy will cross the wake. Otherwise our results show that due to the interaction with the wake the eddy moves with reduced velocity. This result was obtained with and without the mean shear present. In the calculations we observed that the distance between the vortices, in the vortex pair, increases in the streamwise direction.

In chapter (9) we considered the two-dimensional and three-dimensional case and solved it using linear theory. The results show that near the eddy there is always a vertical velocity induced in the direction opposite to the motion of the eddy. Further we noted in the linear theory that, the solution for the vertical velocity consists of two separate parts. One governs the flow field near the disturbed wake and the other governs the flow field near the eddy. Due to the mean shear these two solutions split and move away from each other in time. The solution near the dipole opposes the motion of the eddy towards the wall.

As far as the motion of the wake is concerned the wake responds differently with and without the mean shear. When there is no mean shear the disturbances introduced by the eddy grow with time and at the same time they are advected to the left by the mean wake velocity. As expected, growth of the wake is observed in the lower and in the upper part of the wake. When the mean shear is included the growth of the wake in the lower part of the wake disappeared and concentrated vorticity regions are formed only in the upper part of the wake. It is noted from the velocity distributuions that these concentrated vorticity regions are shear layers with large velocity gradients.

When there is a symmetric mean velocity profile any disturbance in linear theory can be separated into symmetric and antisymmetric parts. The symmetric part has a larger growth rate than the antisymmetric part. Hence, when there is no mean shear the disturbances in the lower and in the upper part of the wake are similar. When there is mean shear the mean velocity profile is no longer symmetric and the magnitude of the vorticity is reduced in the lower part of the wake. Hence the growth of the lower part of the wake is reduced in the lower part.

Next we will discuss the results when the eddy moves from below the wake. The normal turbulence intensity in the inner part of the boundary layer is about 3-4 times larger than that in the outer part of the boundary layer. The eddy moving from below the wake has a larger velocity than that coming from above the wake. When the eddy with large velocity moves from below the wake it moves as undisturbed and when it moves across the wake it strongly interacts with the wake and disturbs the whole outer region. When the strength of the eddy is small, the motion of the eddy is modified differently than when it moves from above the wake. We will discuss the results with the mean shear. When the vortex pair interacts with the wake the vortex in the left side is induced with the positive vertical velocity and the vortex in the right side is induced with a negative vertical velocity. Therefore the left part moves with the larger velocity than the right one and due to the mean shear the vortex pair is rotated in the clockwise direction towards the wall. This was observed in the two and three-dimensional cases.

The overall picture that comes out of this study is as follows. The eddy which moves away from the wall due to its larger vertical velocity will strongly interact with the wake and will reach the outer region of the boundary layer. It has generally been stated that the eddies which reach the outer region collectively form a large-scale motion towards the wall. Since this motion is weak in magnitude the wake inhibits the motion of the eddy towards the wall. Due to the interaction the vorticity in the wake accumulates in the upper part of the wake and forms concentrated shear layer regions.

At this stage we are not able to explain the direct consequences of these modifications in the wall region. But from the previous discussion we infer that since the motion of the outer fluid towards the wall is reduced some reduction in the skin friction is expected. The results of Bertelrud and Truong (1982), Guezennec and Nagib (1985) show that the turbulence intensity in the streamwise direction increases above the wake. This may be due to the formation of shear layers above the wake during the interaction as predicted by the analysis.

From this investigation the following recommendations are suggested for future study.

(1) We investigated the unsteady aerodynamic effect and the blockage effect of the wake in the outer part of a turbulent boundary layer. In the future, one needs to investigate how these modifications affect the flow conditions in the wall region. The experiments should include surveys with multiple sensor rakes oriented in the transverse direction located close to the wall in order to study the instantaneous velocity profiles during the bursting event in regular and manipulated boundary layers. With this

velocity measurements and the flow visualization studies near the wall region, we can infer the effect of the LEBU devices in the wall region. These experiments will also provide clues about the interactions between the outer region and the wall region in a turbulent boundary layer. One should also modify the above experiments in order to differentiate the unsteady effect from the wake effect in the wall region.

(2) One has to do an experiment to verify the results obtained in this report. It would be interesting to investigate experimentally the interaction of the wake with a vortex pair or a vortex ring with and without the mean shear.

(3) In the unsteady aerodynamic analysis we considered only one Fourier component. It is recommended to study how an eddy with known vertical velocity distribution is modified downstream when it is advected over the plate. To obtain the results one has to take the Fourier transform of the known vertical velocity distribution, multiply the Fourier components by the transfer function $S(k_x,k_y)$ and then take the Fourier inverse transform.

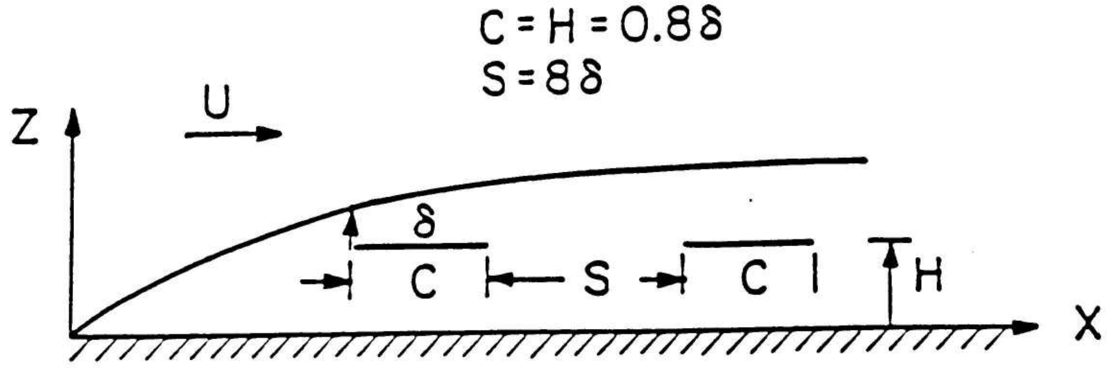

Fig. 1. Plate configuration for LEBU devices.

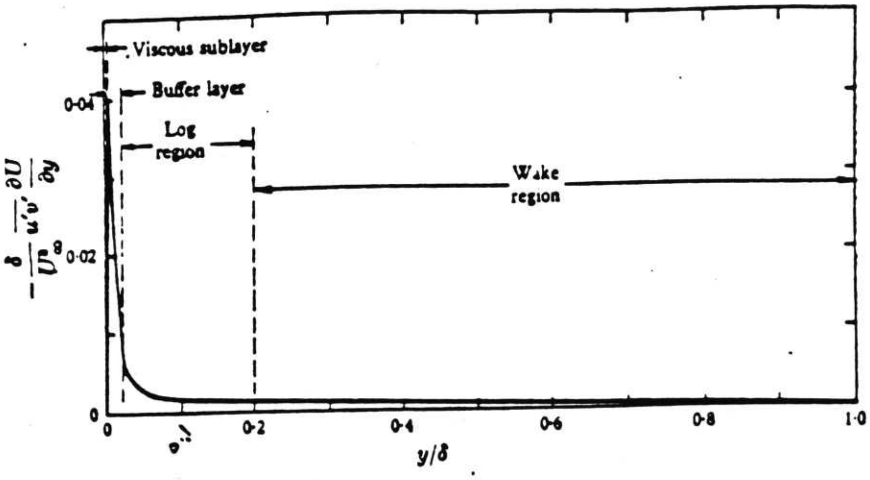

Fig. 2a. Normalized turbulence energy production per unit volume in a typical boundary layer (Klebanoff 1954).

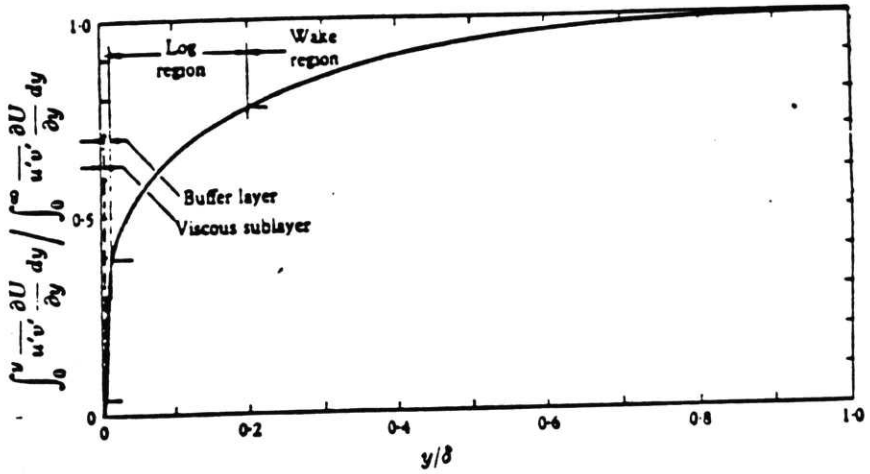

Fig. 2b. Cumulative turbulence energy production rate in a typical turbulent boundary layer (Klebanoff 1954).

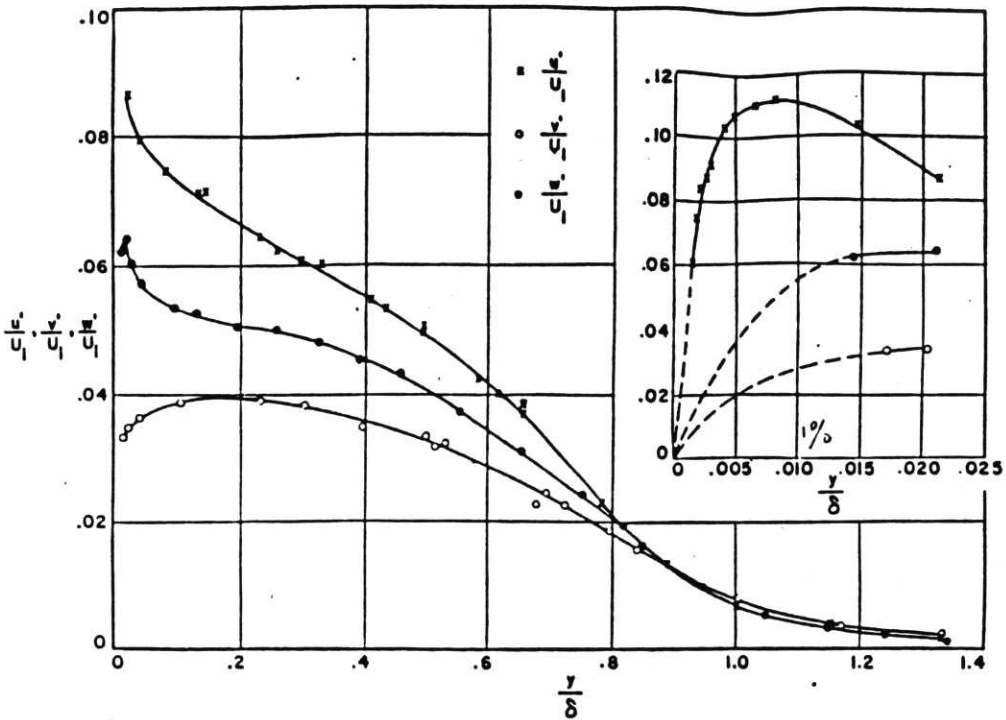

Fig. 3. Distribution of turbulence intensities in a typical turbulent boundary layer (Klebanoff 1954).

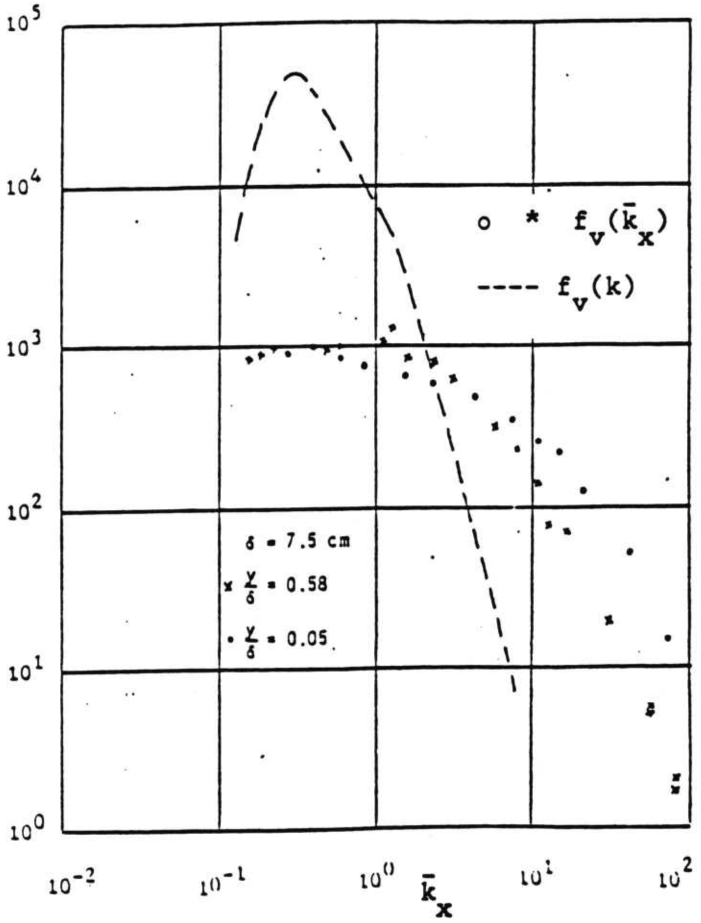

$$k = \sqrt{\bar{k}_x^2 + \bar{k}_y^2}$$

Fig. 4. Spectra of a turbulent normal velocity (Klebanoff 1954).

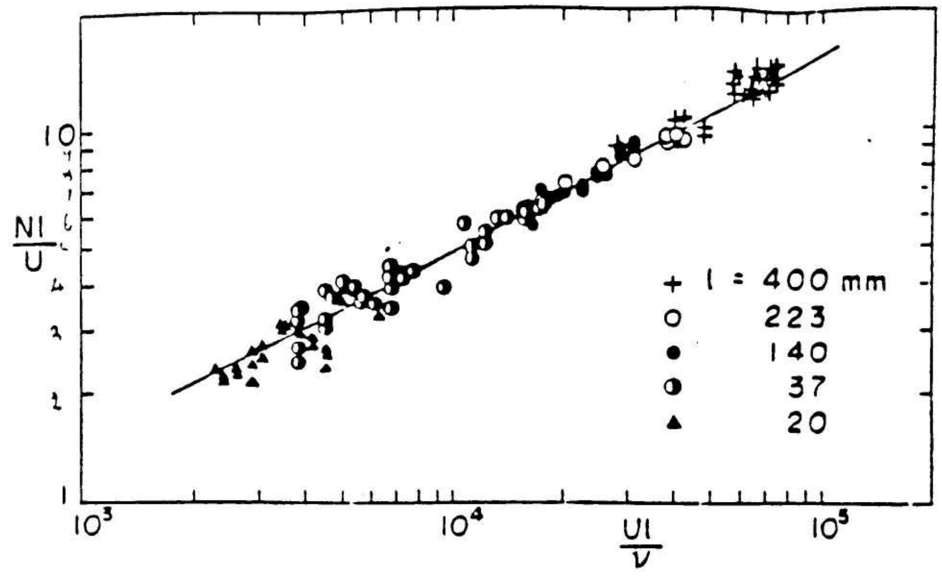

Fig. 5a. Plot of log S against log R.

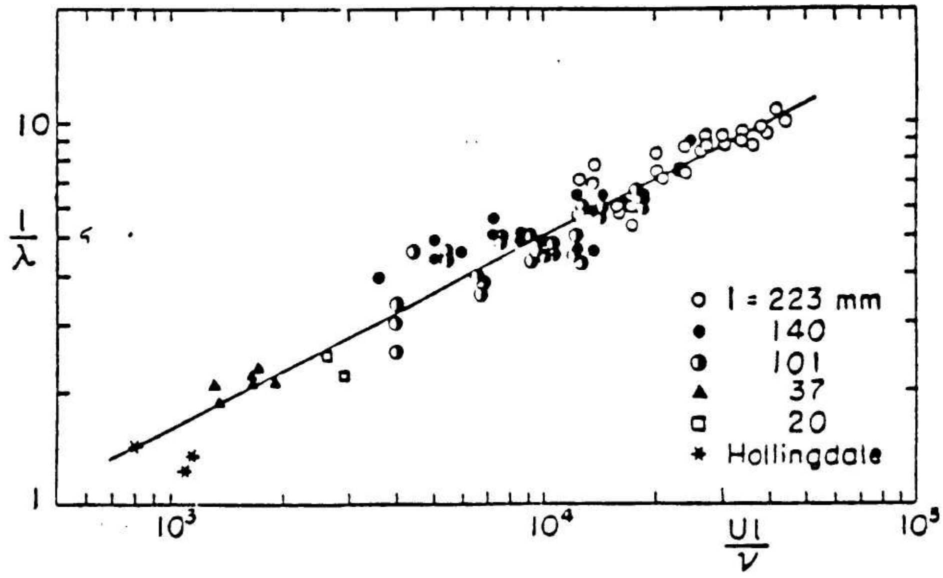

Fig. 5b. Plot of log $1/\lambda$ against log R.

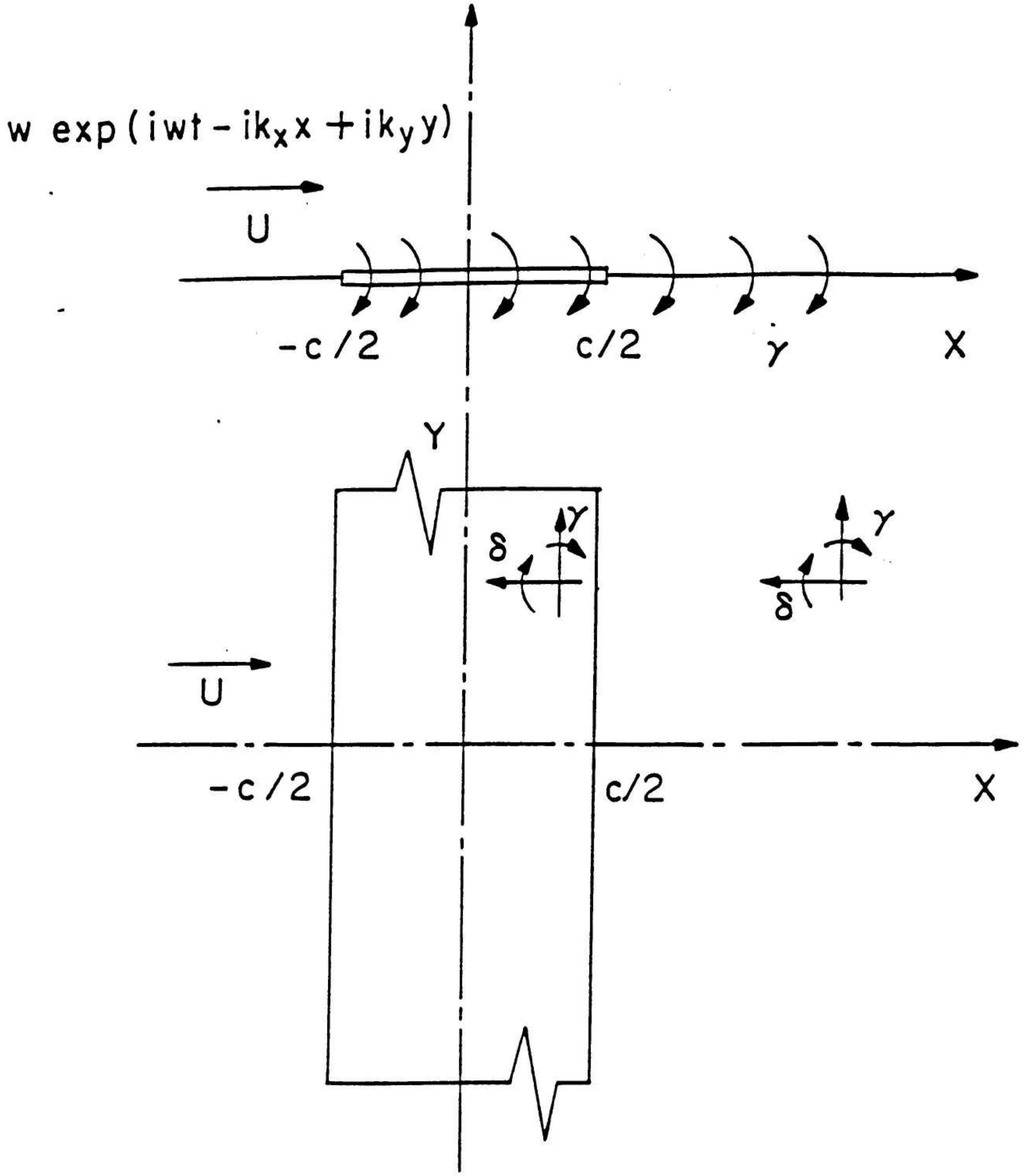

Fig. 6. Interaction of an oblique gust and a plate.

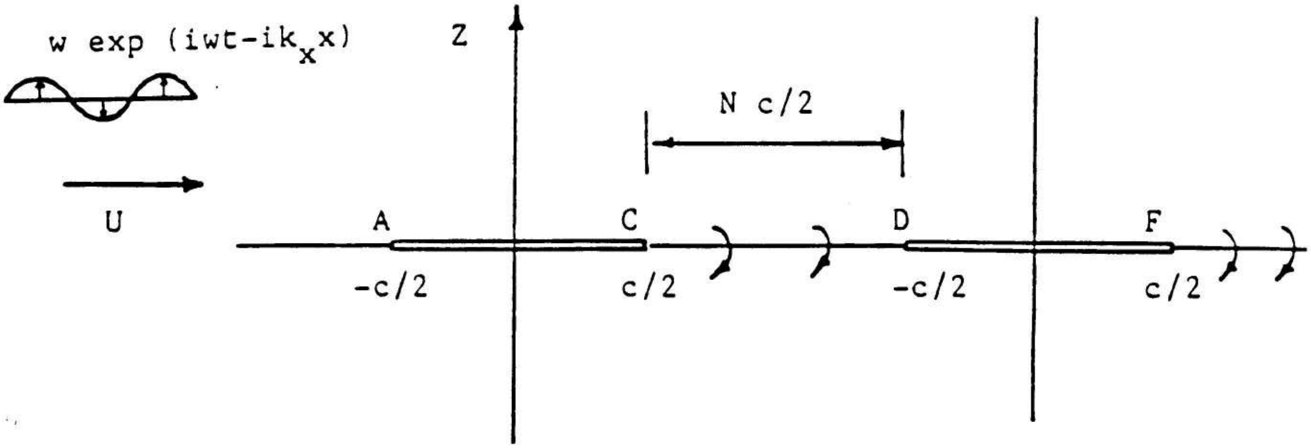

Fig. 7. Interaction of a gust and two plates.

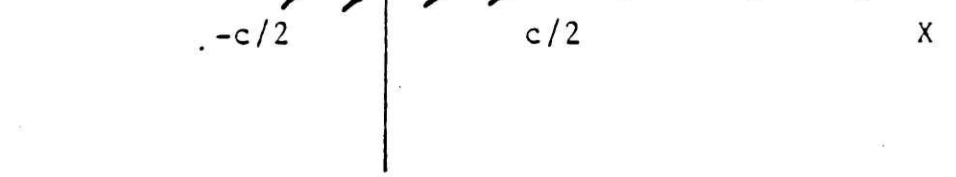

Fig. 8. Vortex sheet representation when the distance between the plates becomes large.

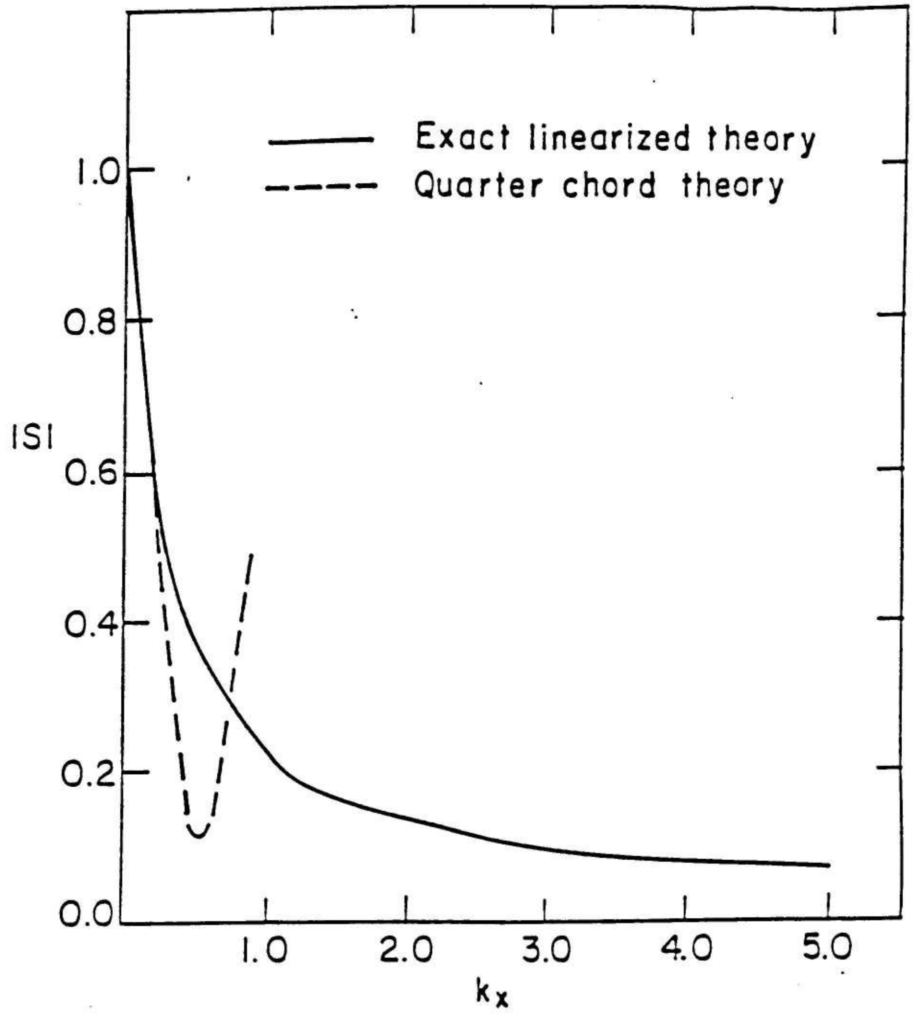

Fig. 9. Amplitude of the function $S(\bar{k}_x)$ versus wavenumber $\bar{k}_x$.

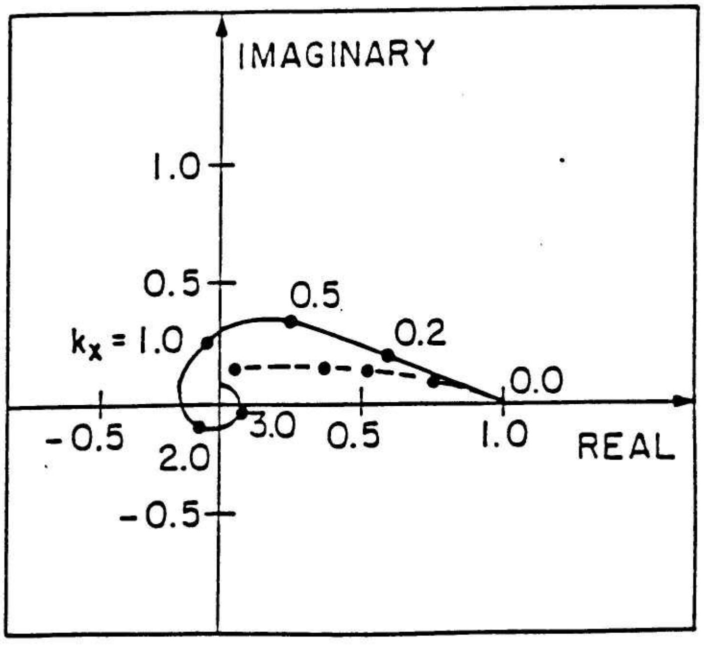

Fig. 10. Phase plane of the function $S(\bar{k}_x)$.

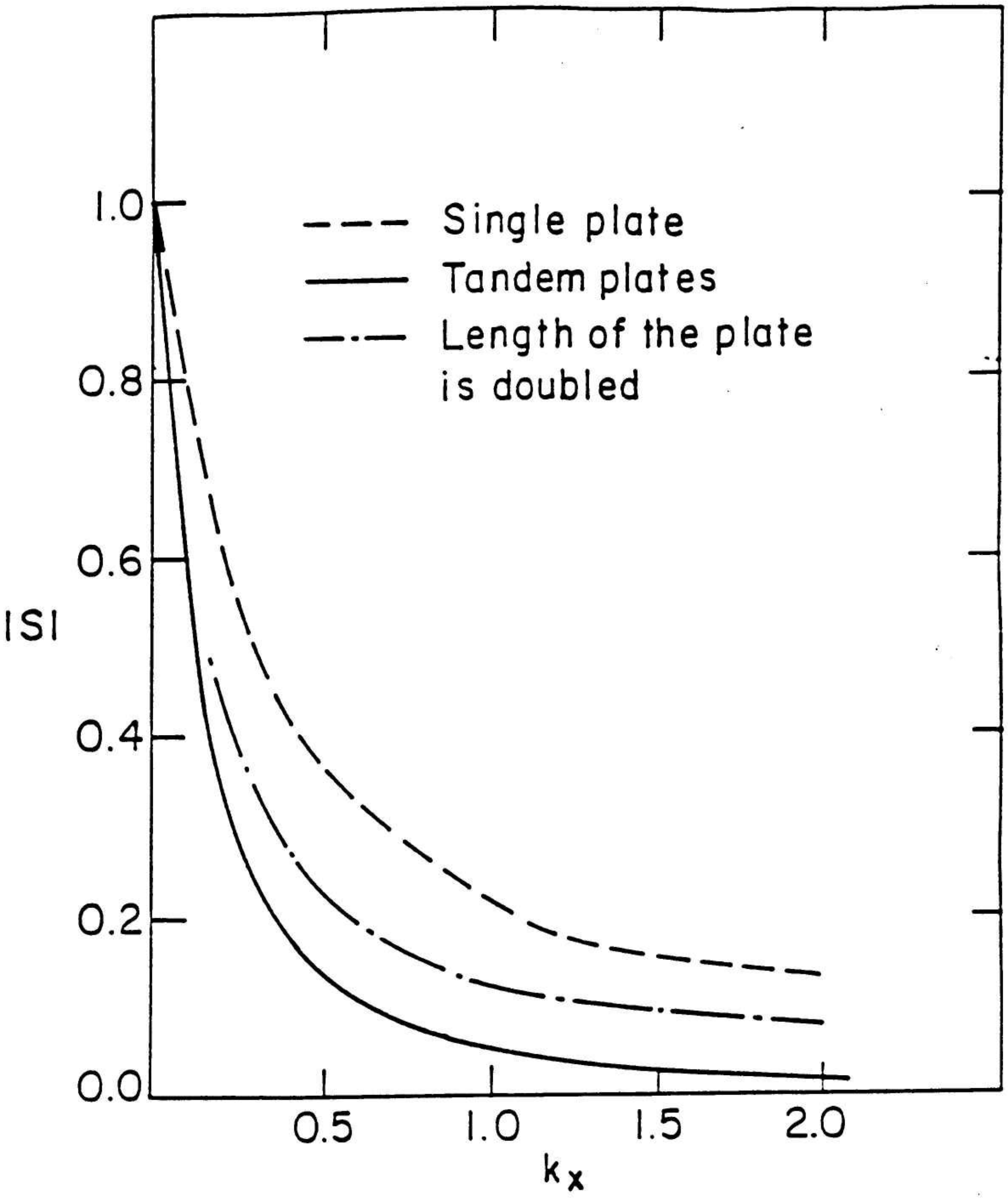

Fig. 11. Amplitude of the function $S(\bar{k}_x)$ when the distance between the plates becomes large.

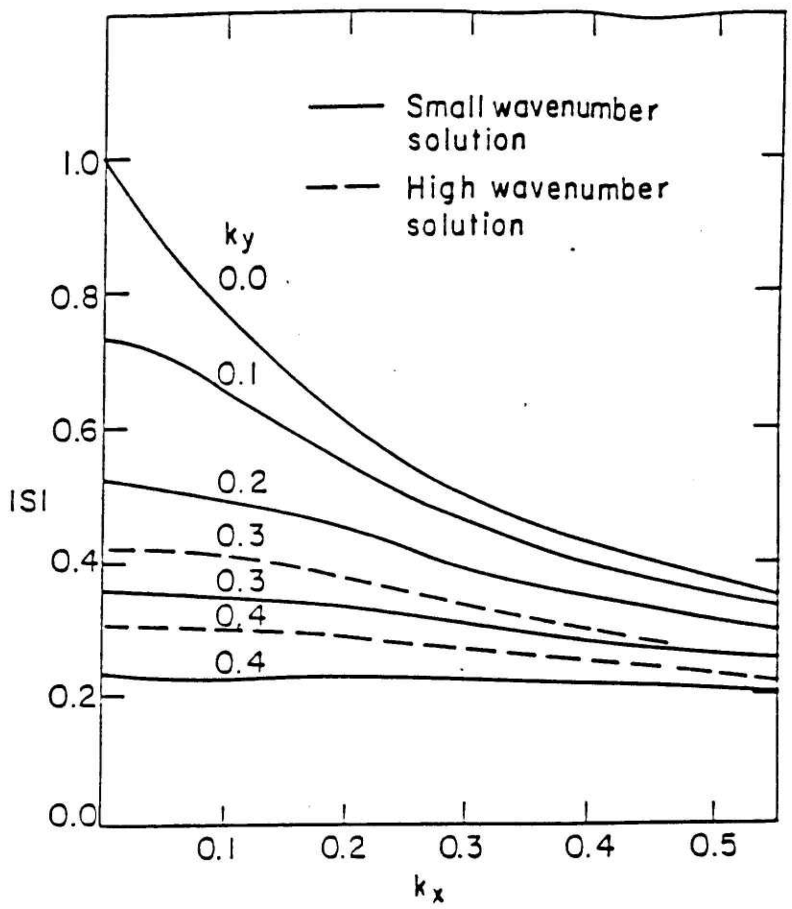

Fig. 12. Amplitude of the function $S(\bar{k}_x,\bar{k}_y)$ for small $\bar{k}_y$ using integral method.

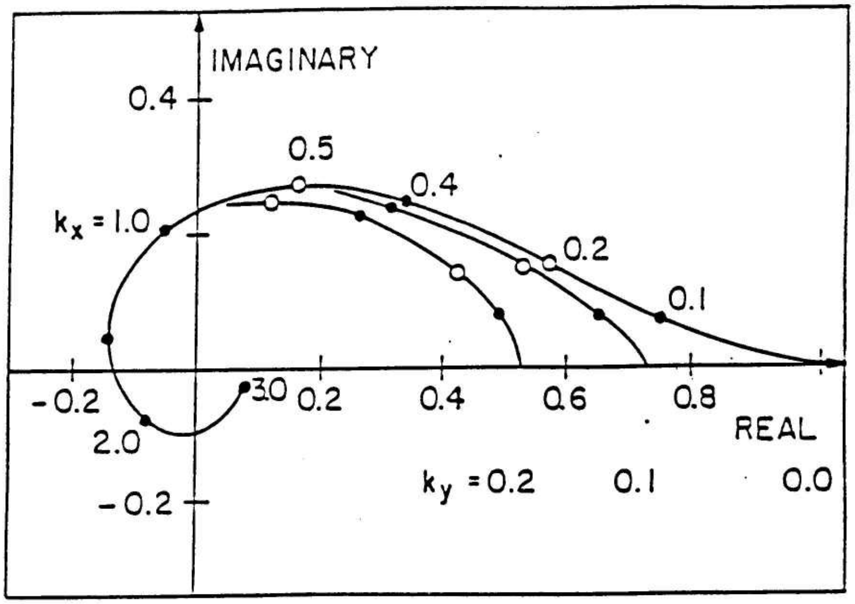

Fig. 13. Phase plane of the function $S(\bar{k}_x,\bar{k}_y)$ for small $\bar{k}_y$ using integral method.

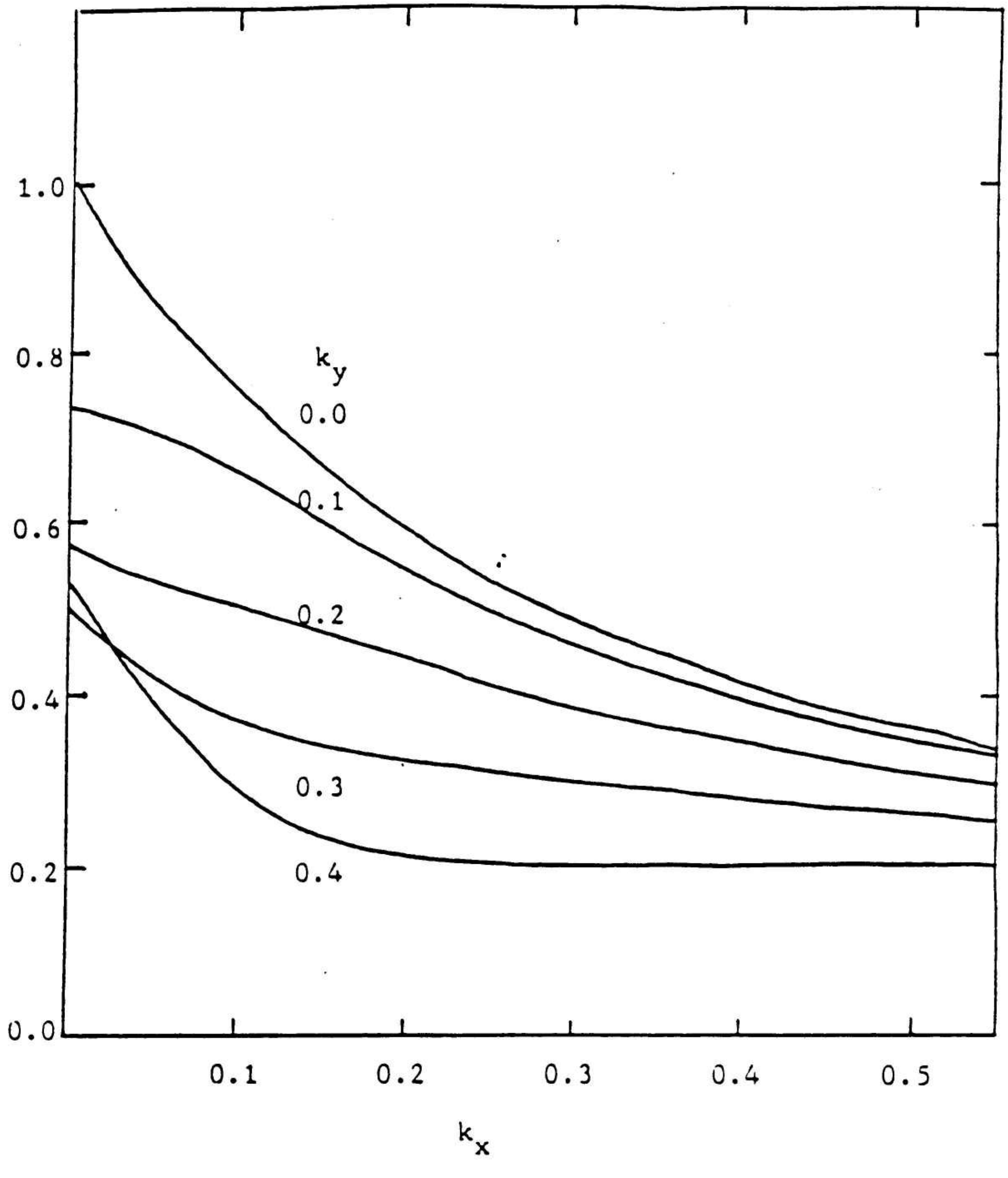

Fig. 14. Amplitude of the function $S(\bar{k}_x,\bar{k}_y)$ for small $\bar{k}_y$ using acceleration potential method.

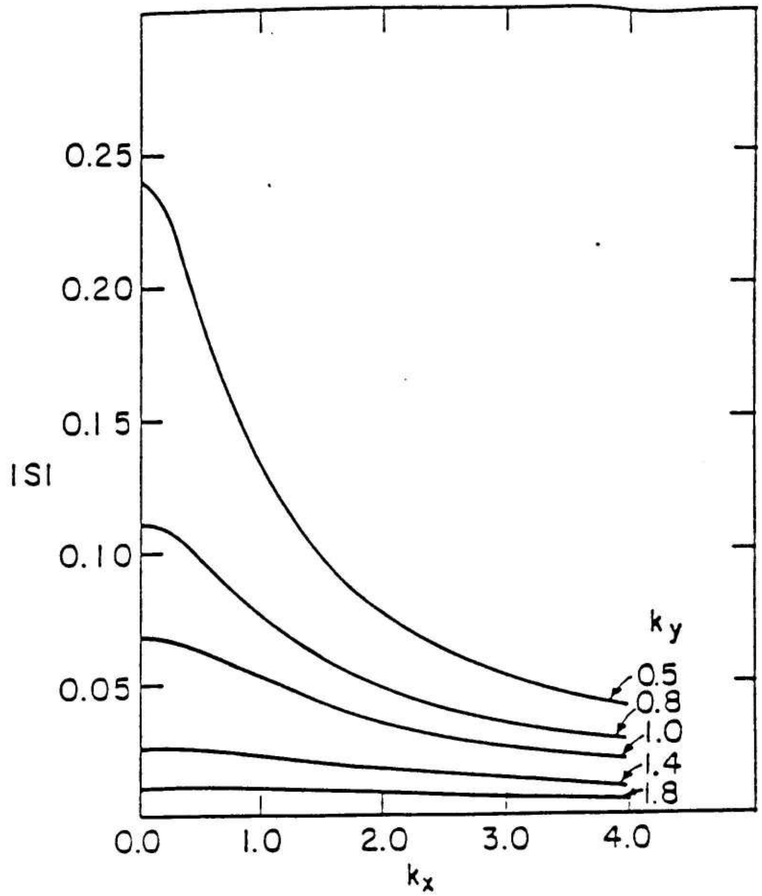

Fig. 15. Amplitude of the function $S(\bar{k}_x,\bar{k}_y)$ for high $\bar{k}_y$.

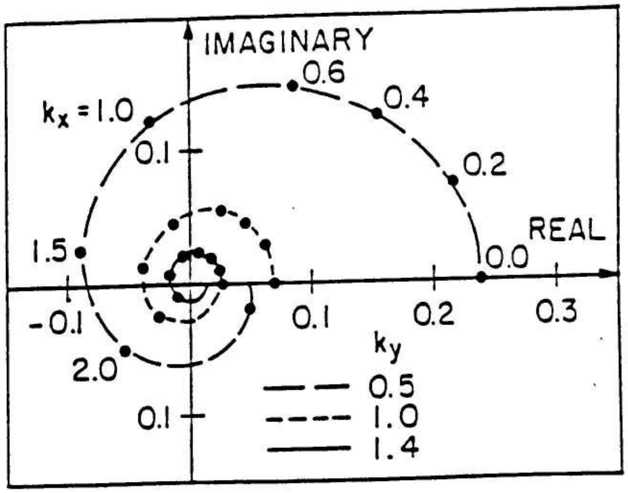

Fig. 16. Phase plane of the function $S(\bar{k}_x,\bar{k}_y)$ for high $\bar{k}_y$.

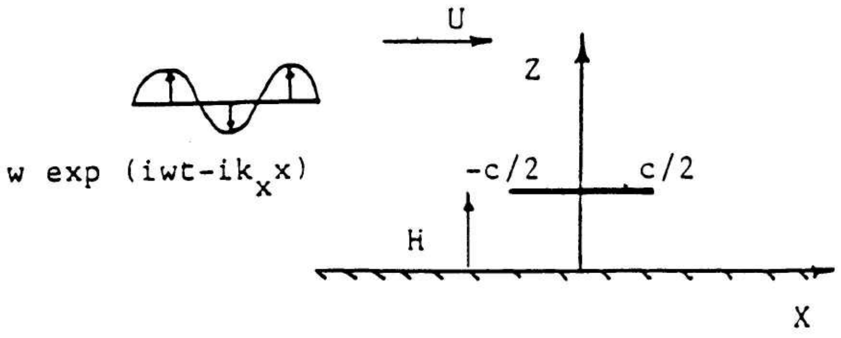

Fig. 17. Interaction of a gust with a plate and a plane.

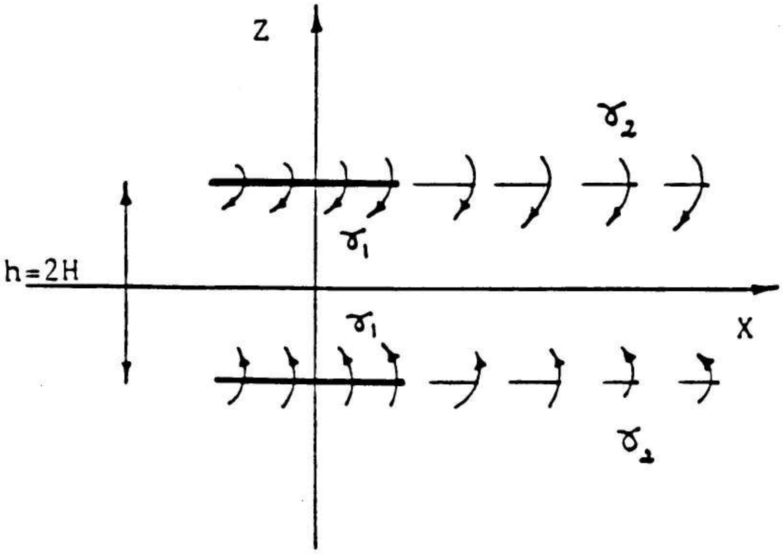

Fig. 18. Vortex sheet representation.

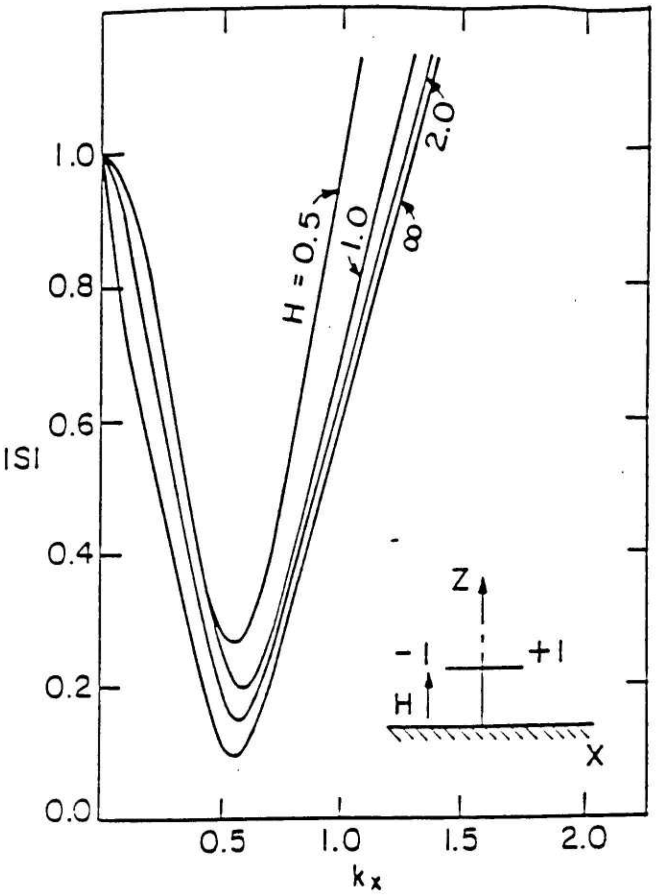

Fig. 19. Amplitude of the function $S(\bar{k}_x, H)$.

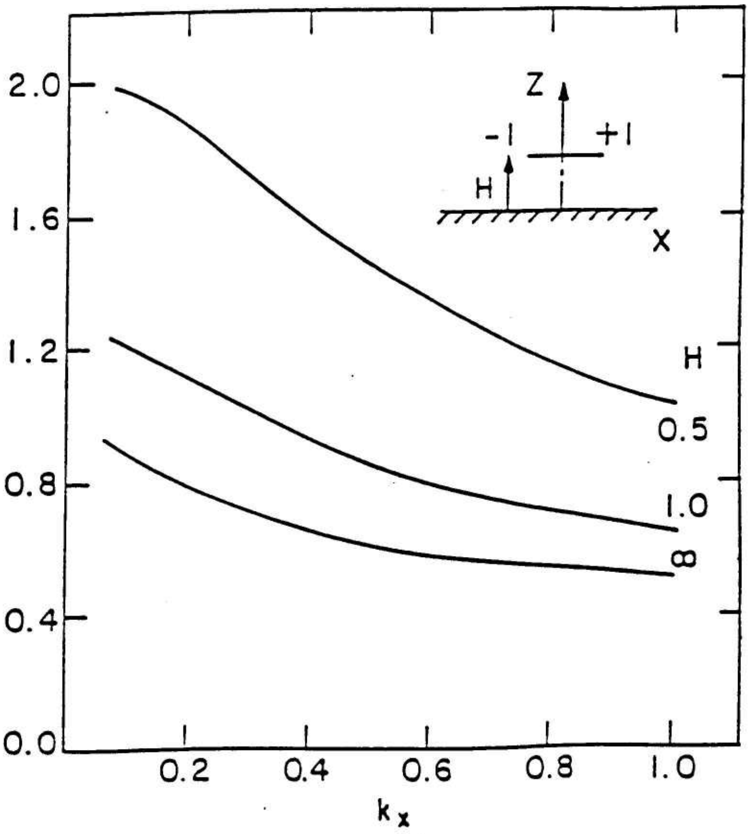

Fig. 20. Amplitude of the circulation given by eq.(135).

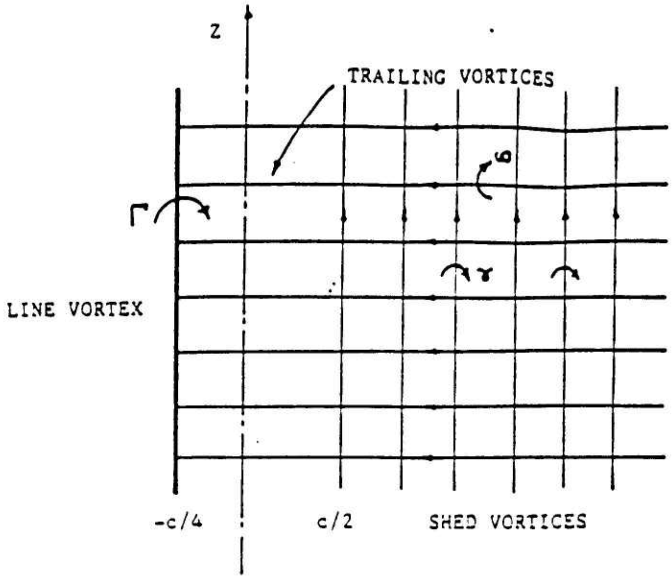

Fig. 21. Approximate vortex sheet representation for the three-dimensional case.

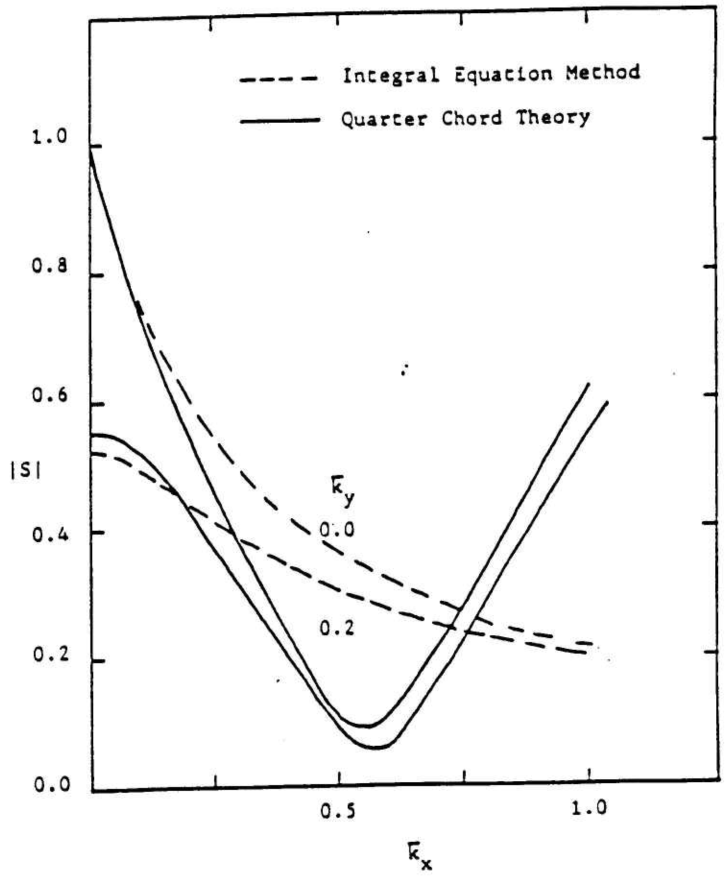

Fig. 22. Amplitude of the function $S(\bar{k}_x, \bar{k}_y)$ using integral method and quarter chord theory method.

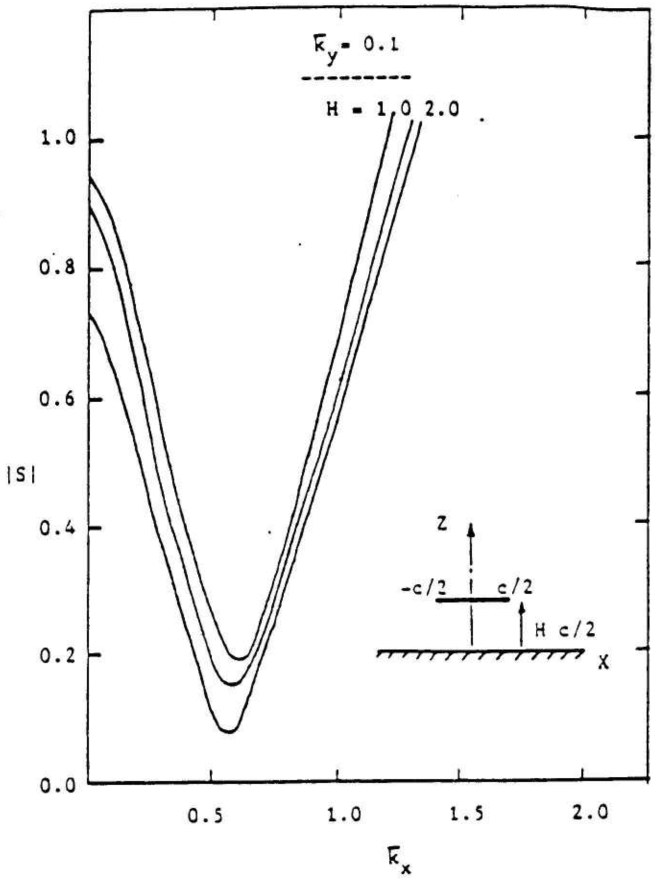

Fig. 23. Amplitude of the function $S(\bar{k}_x,\bar{k}_y,H)$ for $\bar{k}_y=0.1$.

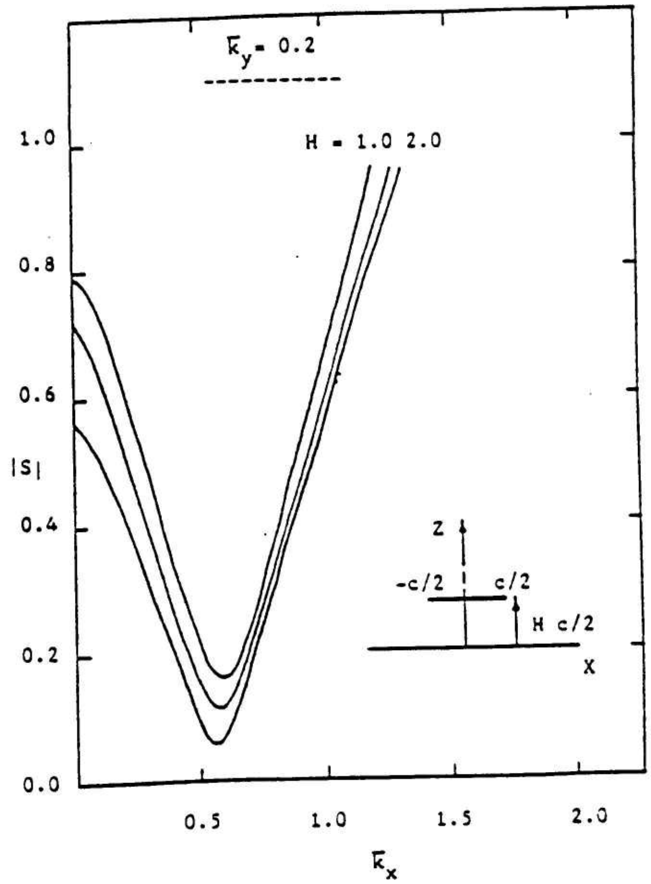

Fig. 24. Amplitude of the function $S(\bar{k}_x,\bar{k}_y,H)$ for $\bar{k}_y=0.2$.

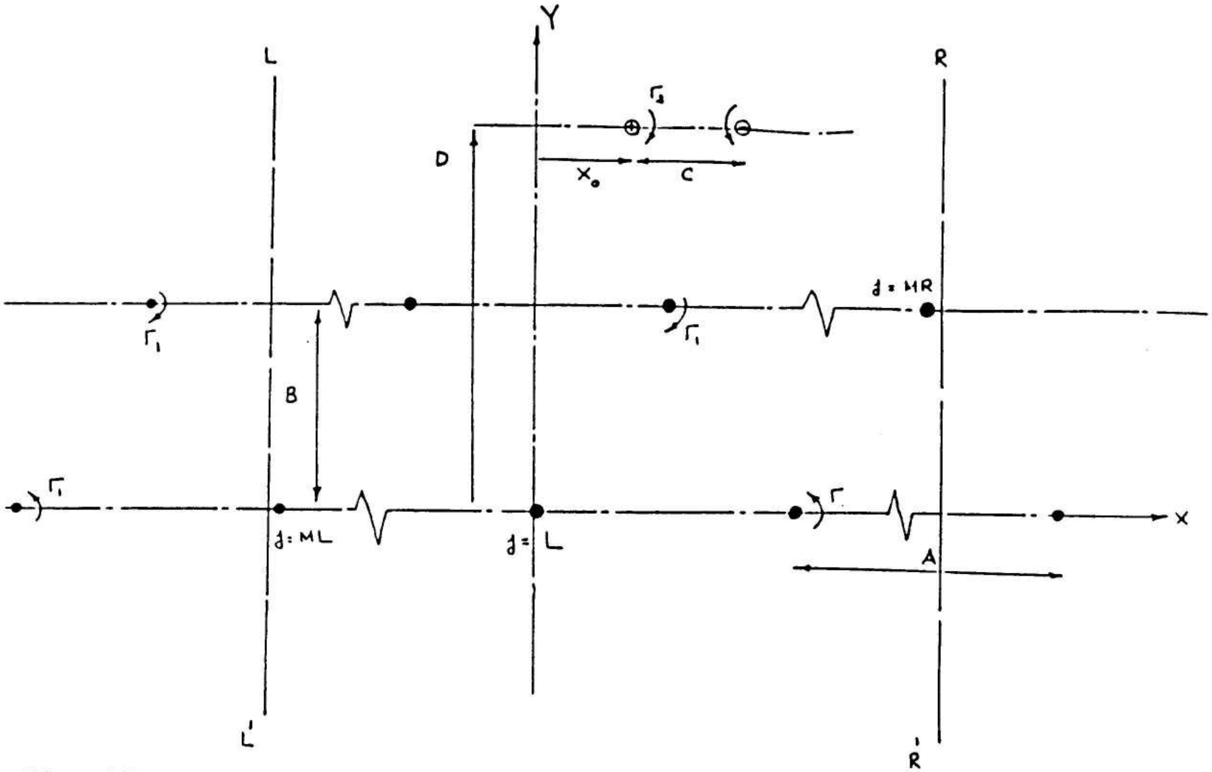

Fig. 25. Vortex street and vortex pair arrangement at time T=0.0.

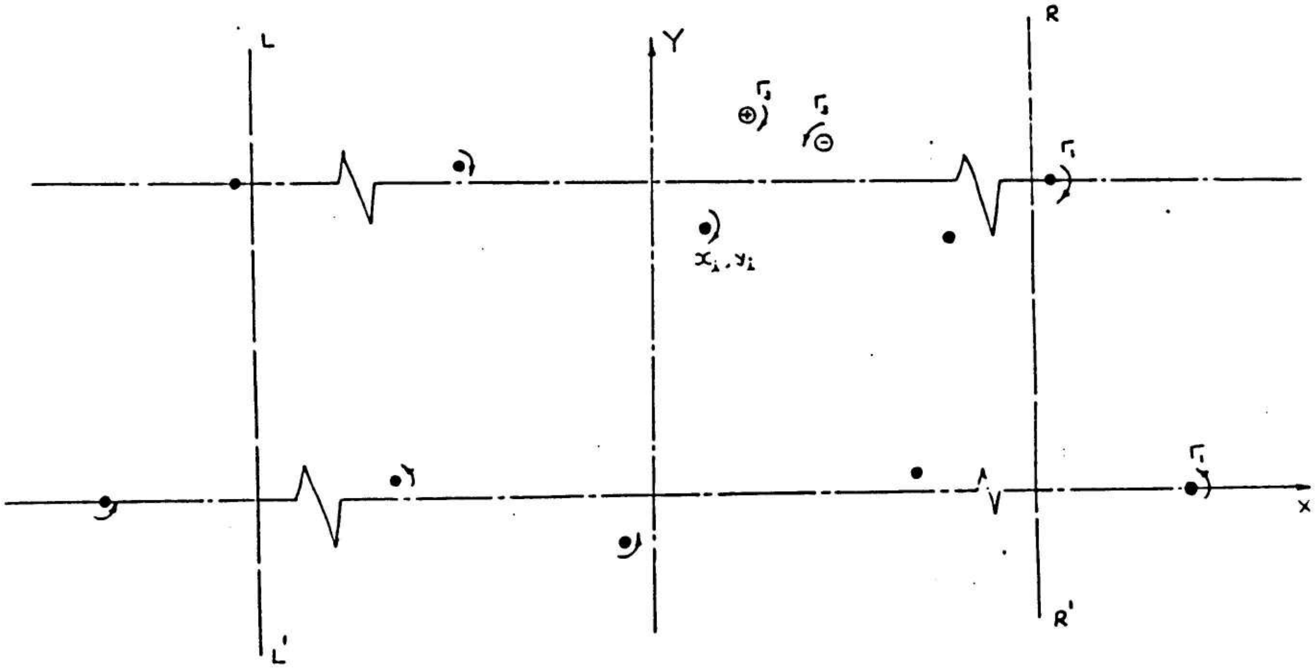

Fig. 26. Disturbed vortex system at a later time T.

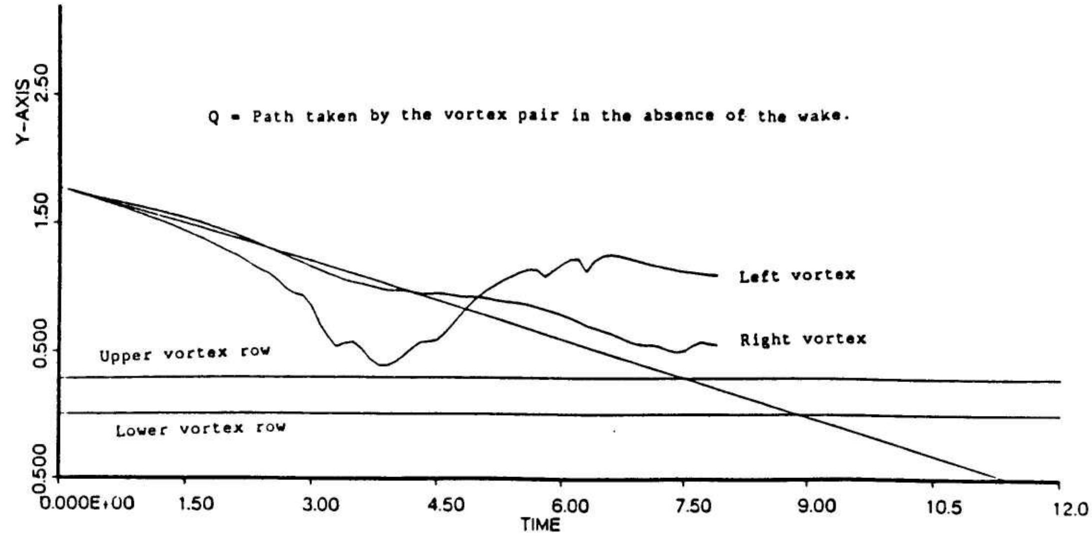

Fig. 27. Position of the vortex pair against time, $\Gamma_2=0.5$, c=2.5.

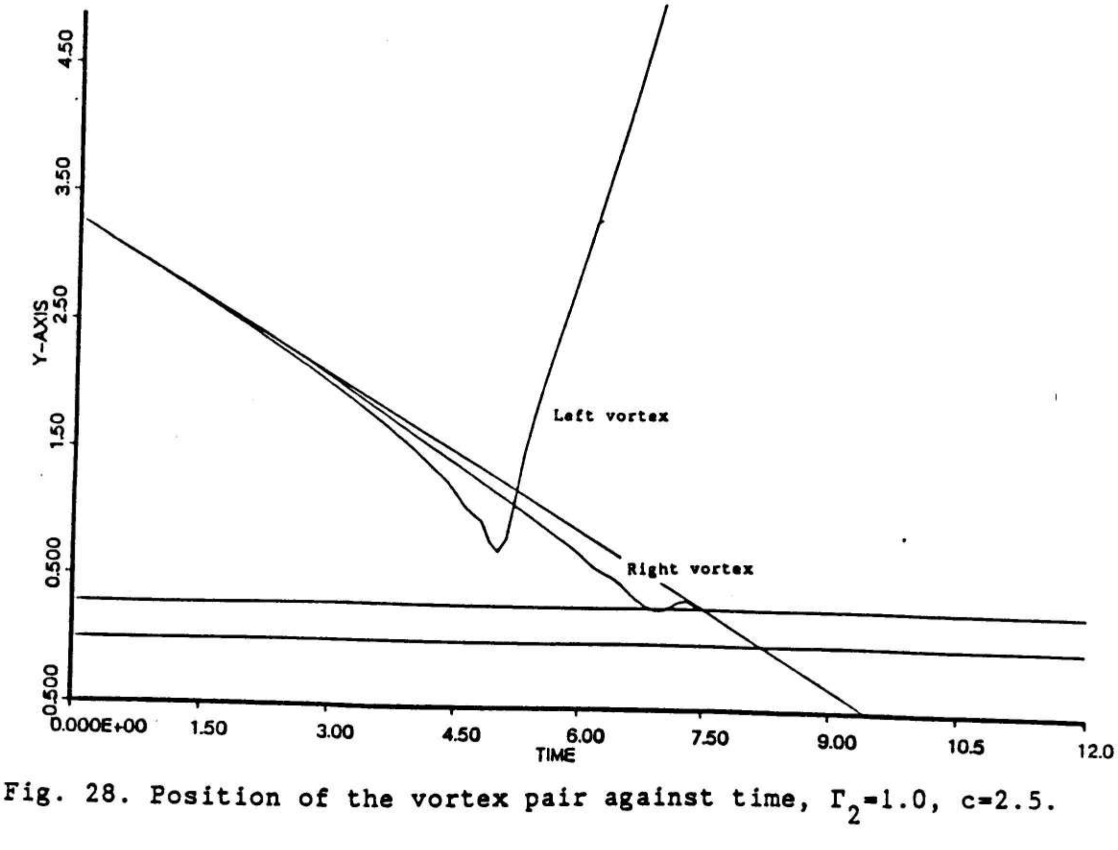

Fig. 28. Position of the vortex pair against time, $\Gamma_2=1.0$, c=2.5.

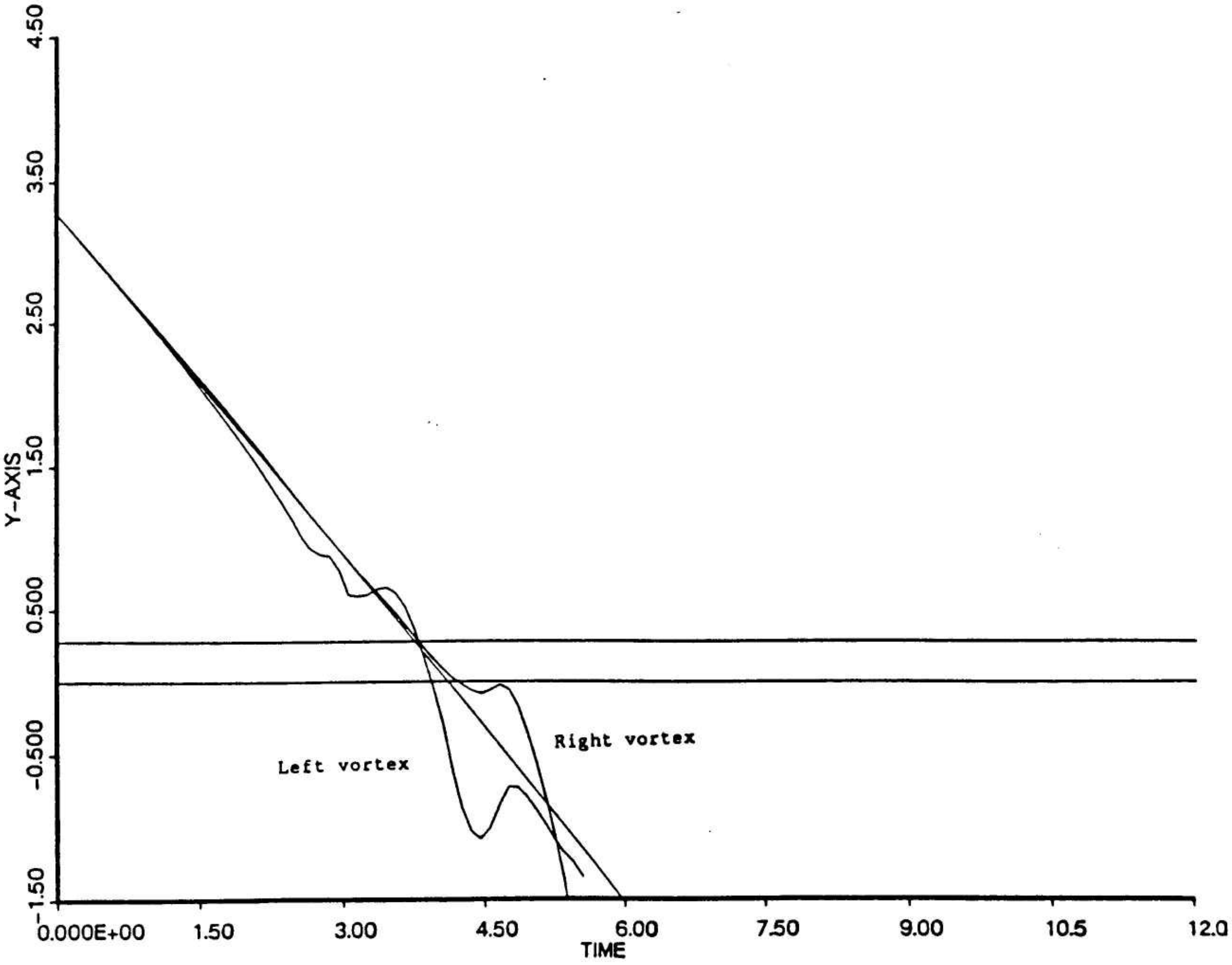

Fig. 29. Position of the vortex pair against time, Γ_2=2.0, c=2.5.

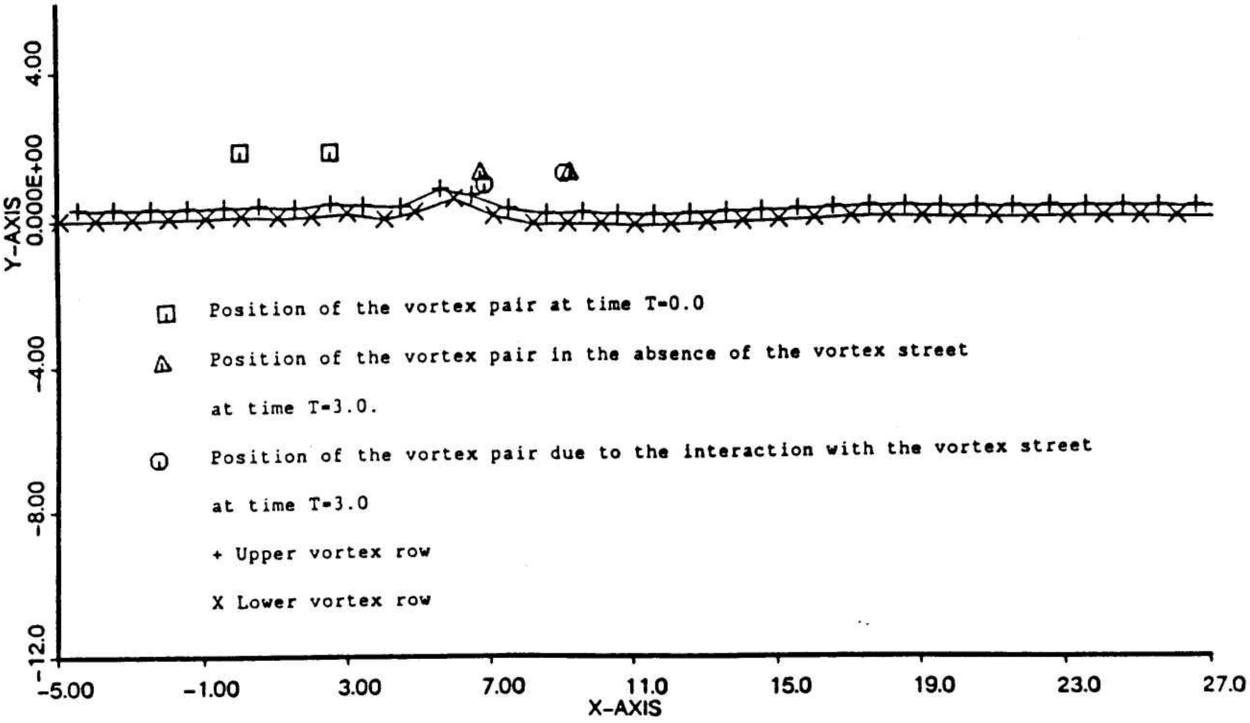

Fig. 30. Positions of the vortex street and the vortex pair at time, T=3.0, Γ_2=0.5, c=2.5.

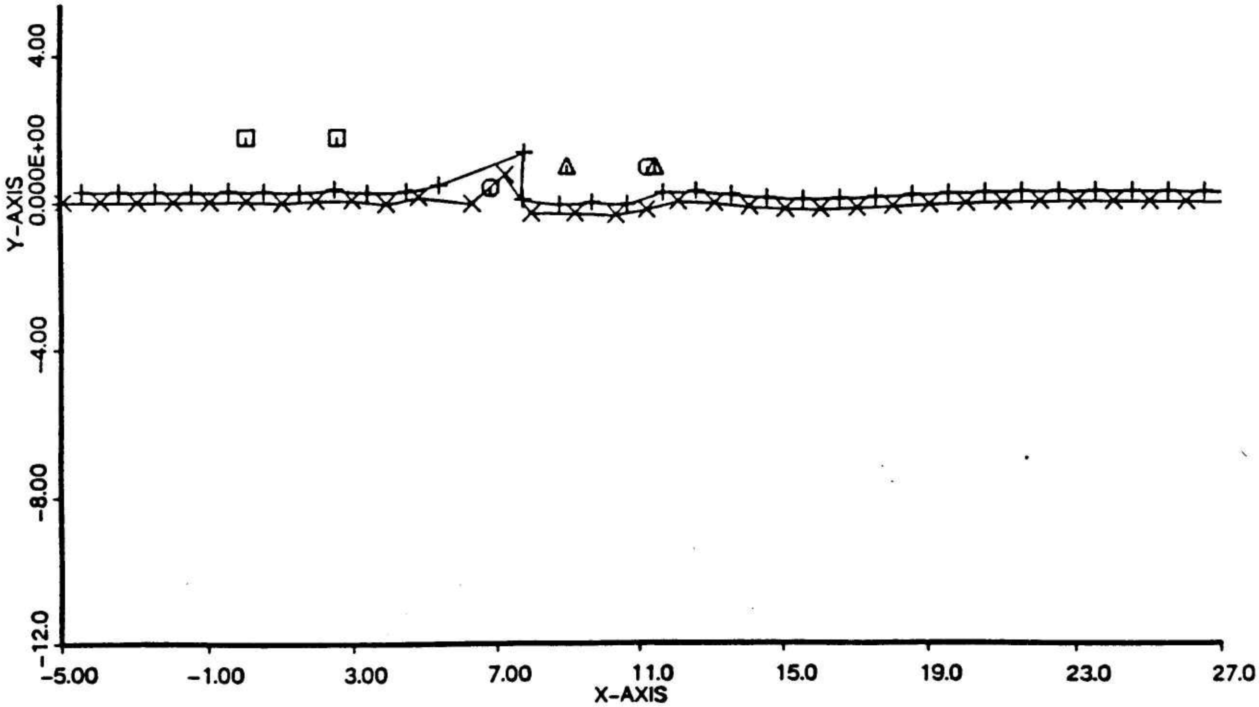

Fig. 31. Positions of the vortex street and the vortex pair at time, T=4.0, Γ_2=0.5, c=2.5.

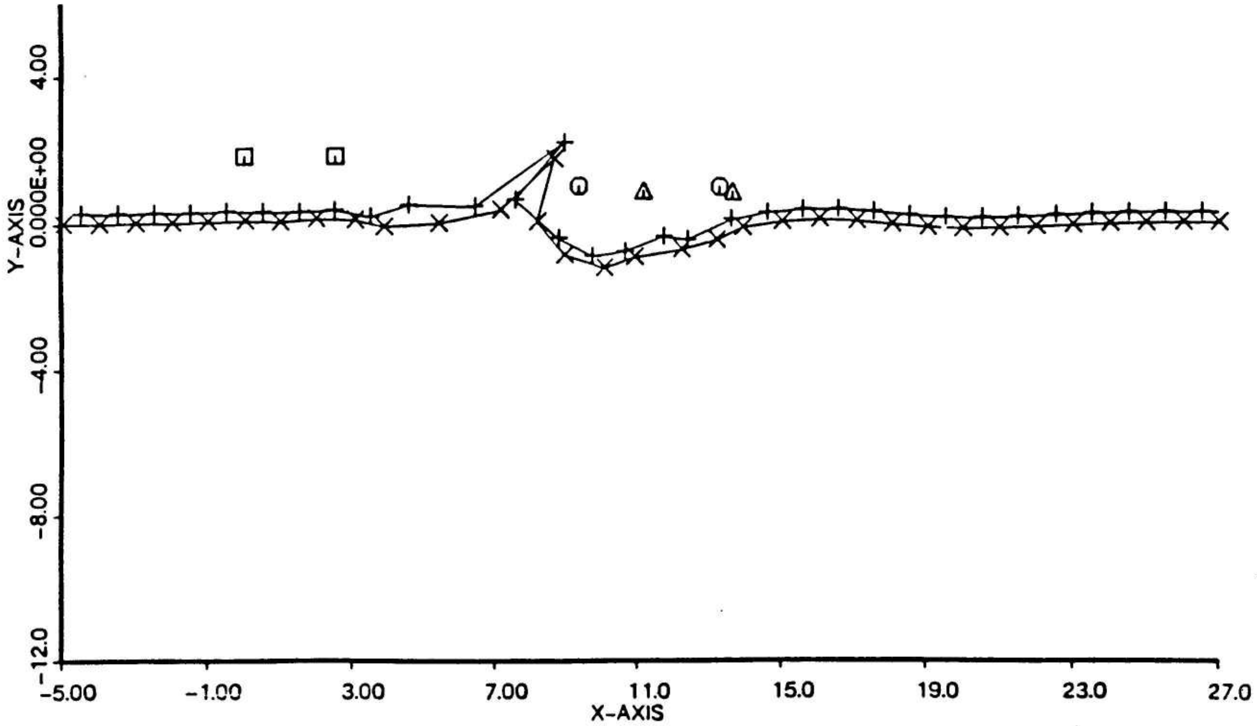

Fig. 32. Positions of the vortex street and the vortex pair at time, T=5.0, Γ_2=0.5, c=2.5.

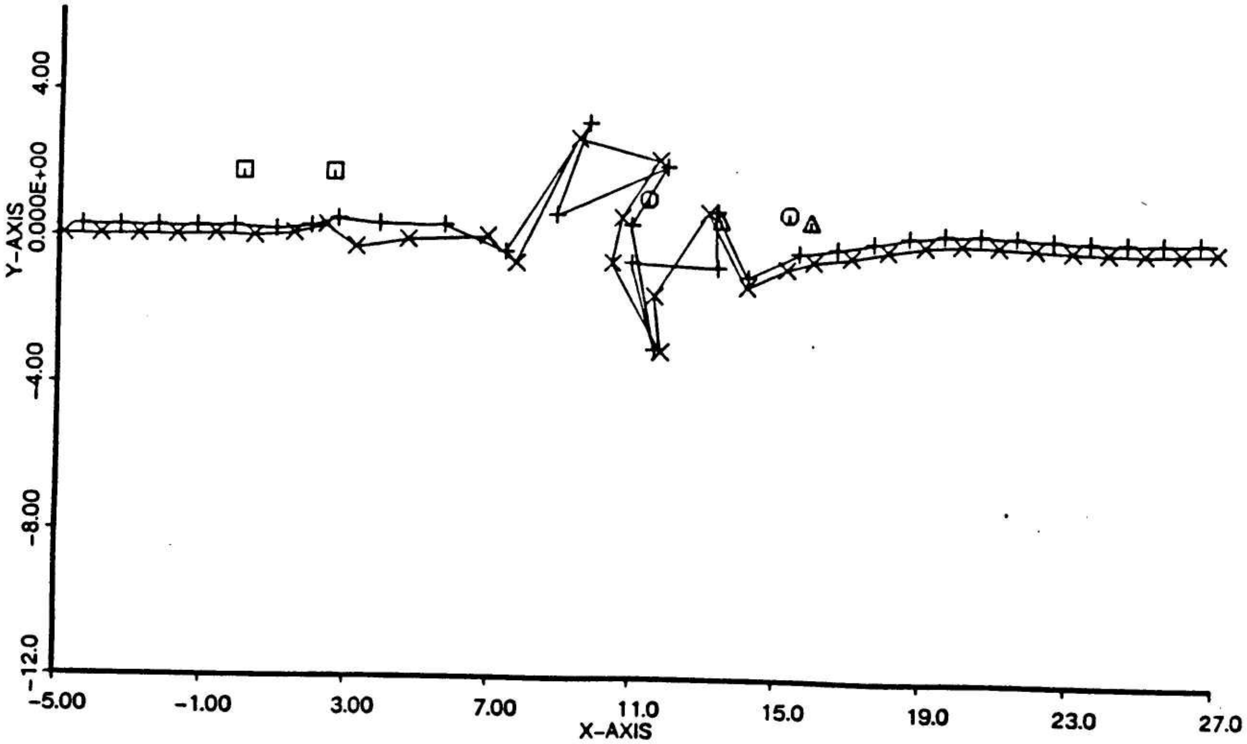

Fig. 33. Positions of the vortex street and the vortex pair at time, T=6.0, Γ_2=0.5, c=2.5.

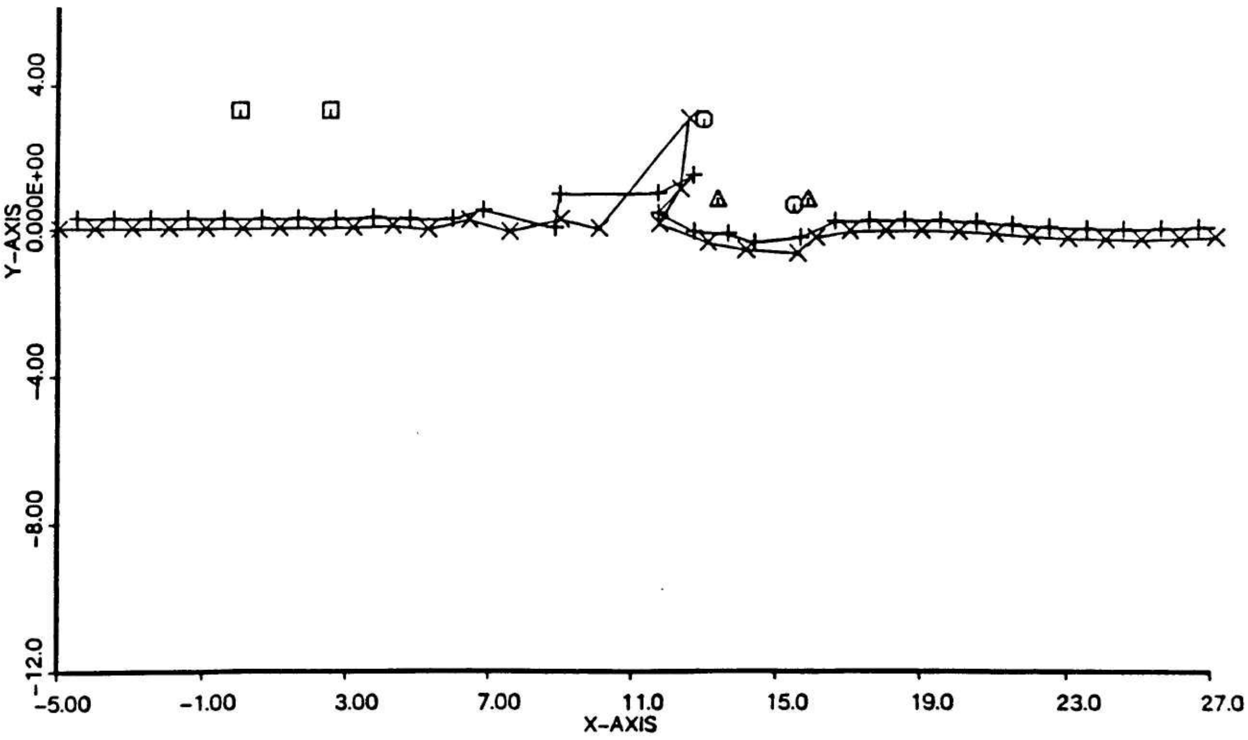

Fig. 34. Positions of the vortex street and the vortex pair at time, T=6.0, Γ_2=1.0, c=2.5.

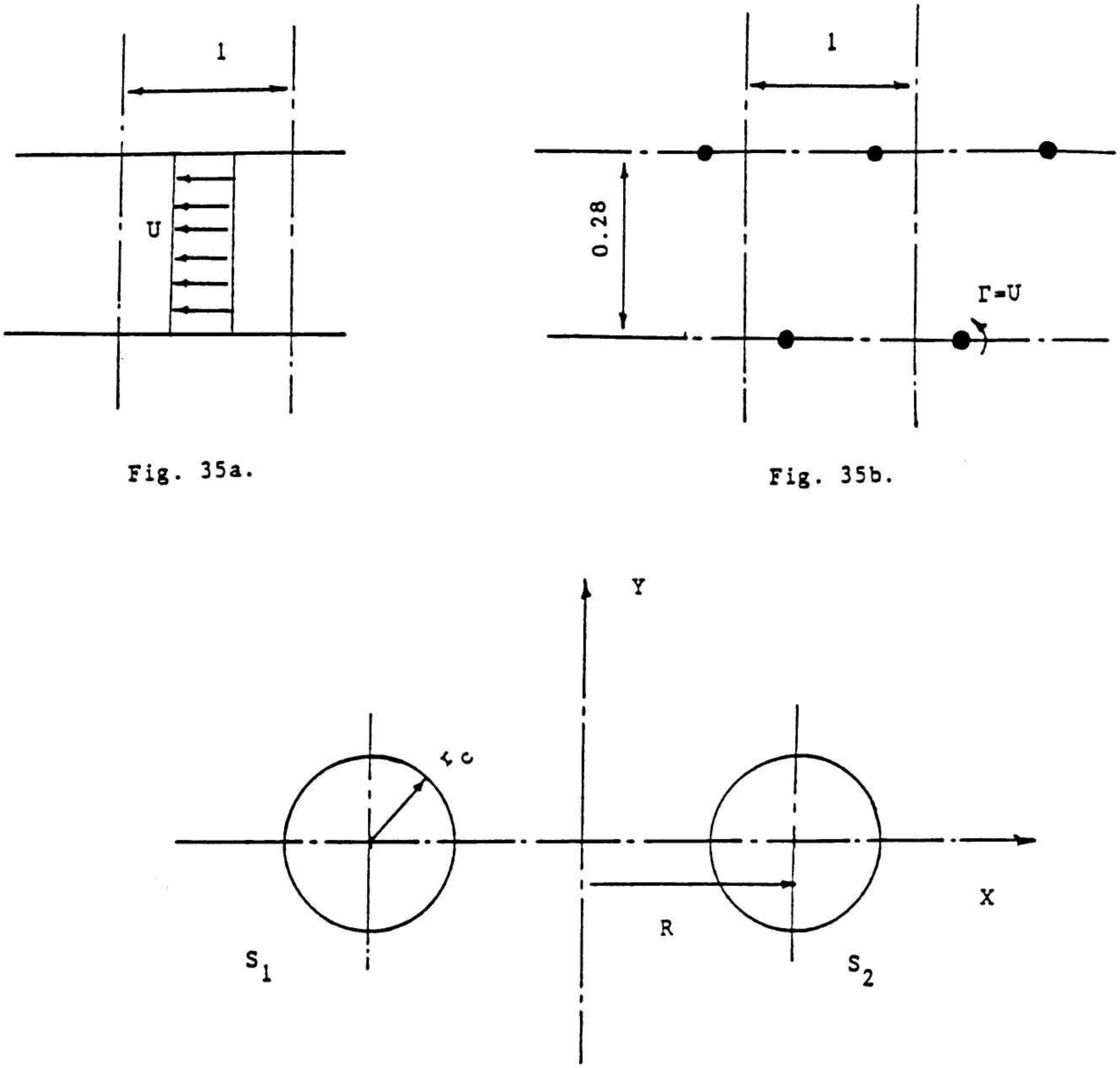

Fig. 35a.

Fig. 35b.

Fig. 35c.

Fig. 35. Wake and the equivalent vortex street arrangement used to determine the core radii.

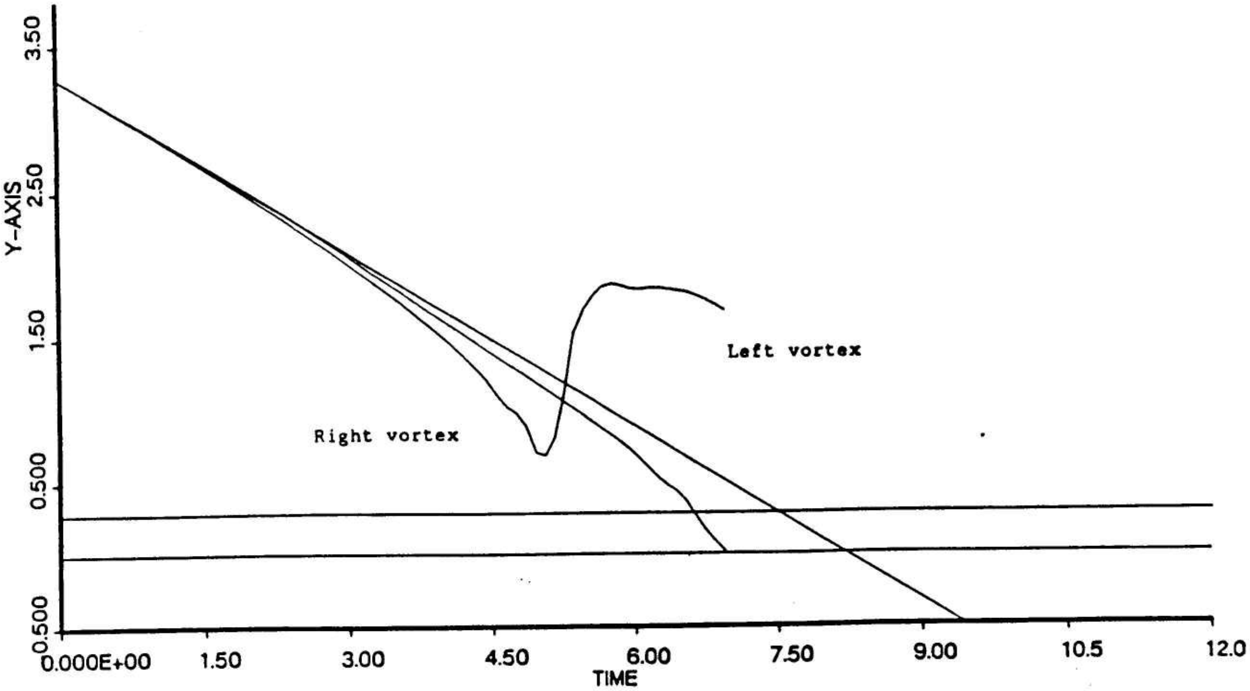

Fig. 36. Position of the vortex pair with core radii against time, $\Gamma_2=1.0$, c=2.5.

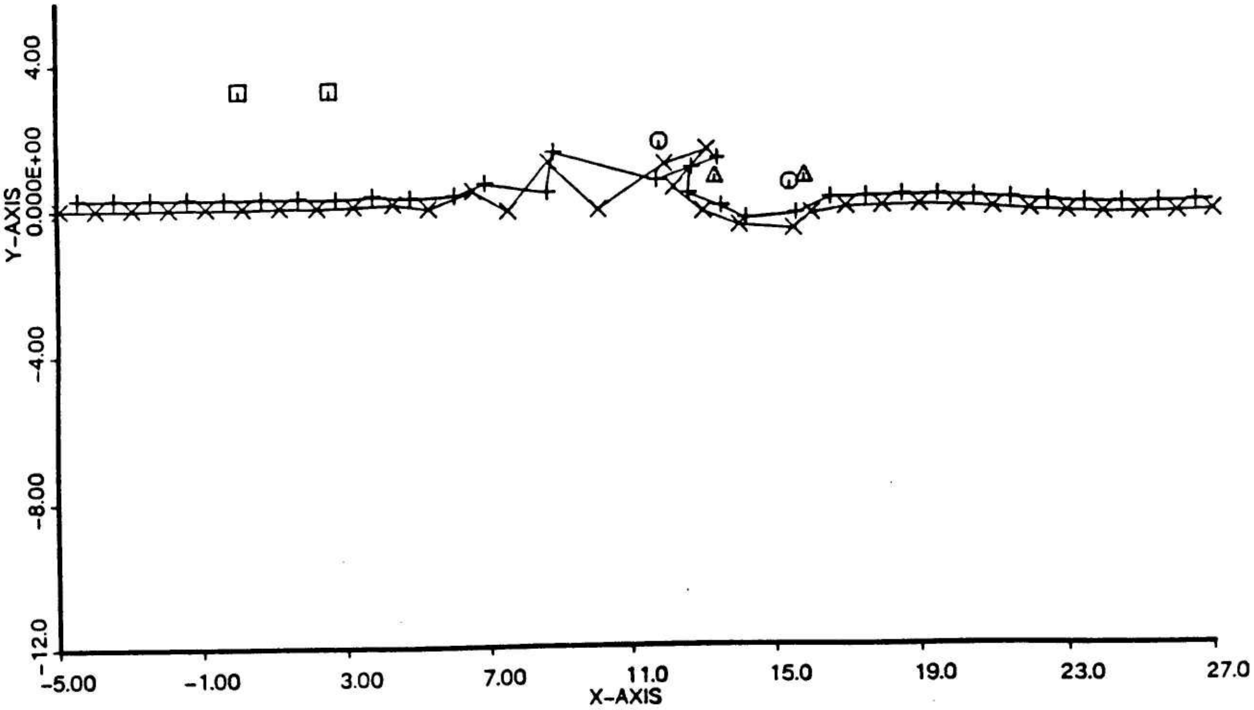

Fig. 37. Positions of the vortex street and the vortex pair with core radii at time, T=6.0, $\Gamma_2=1.0$, c=2.5.

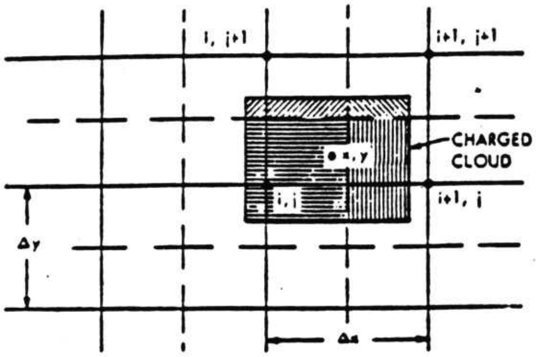

Fig. 38. Cloud located in a grid, with shading showing assignment of density to grid points for CIC method.

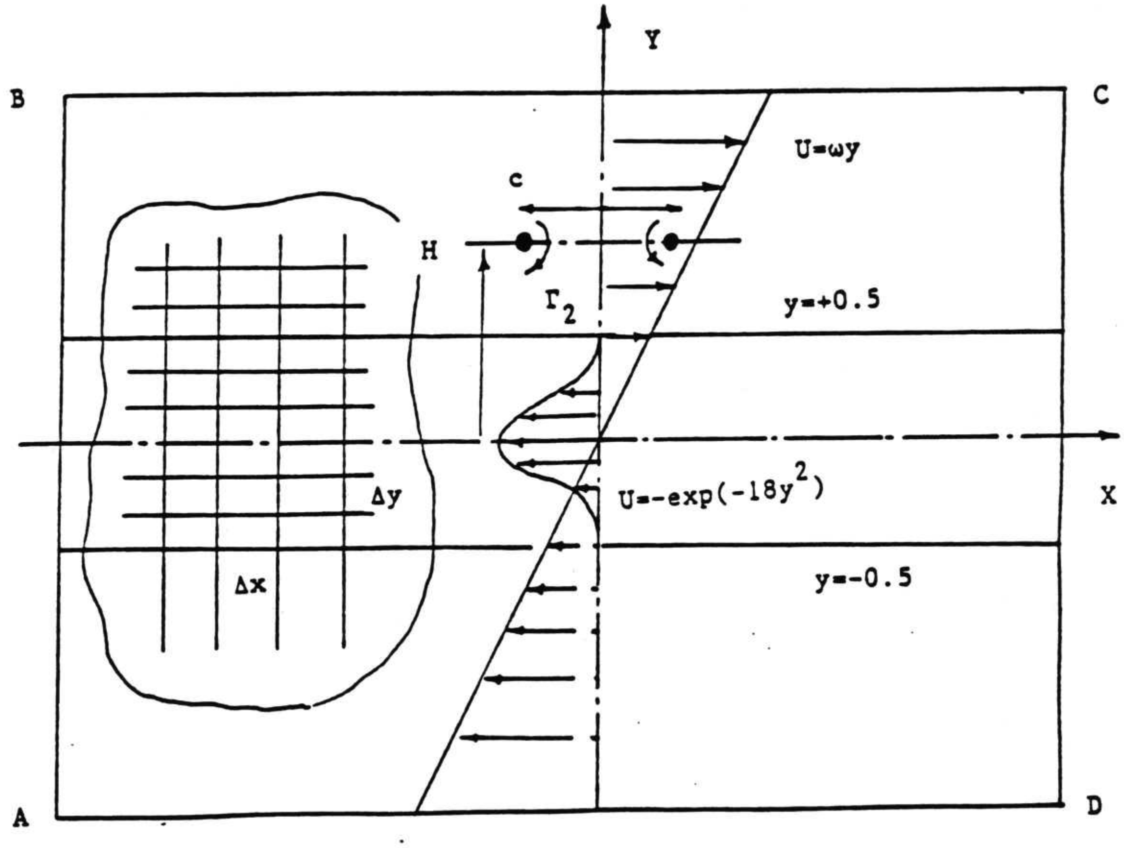

Fig. 39. Initial velocity distribution of the wake and the mean shear. Grid system used for calculations.

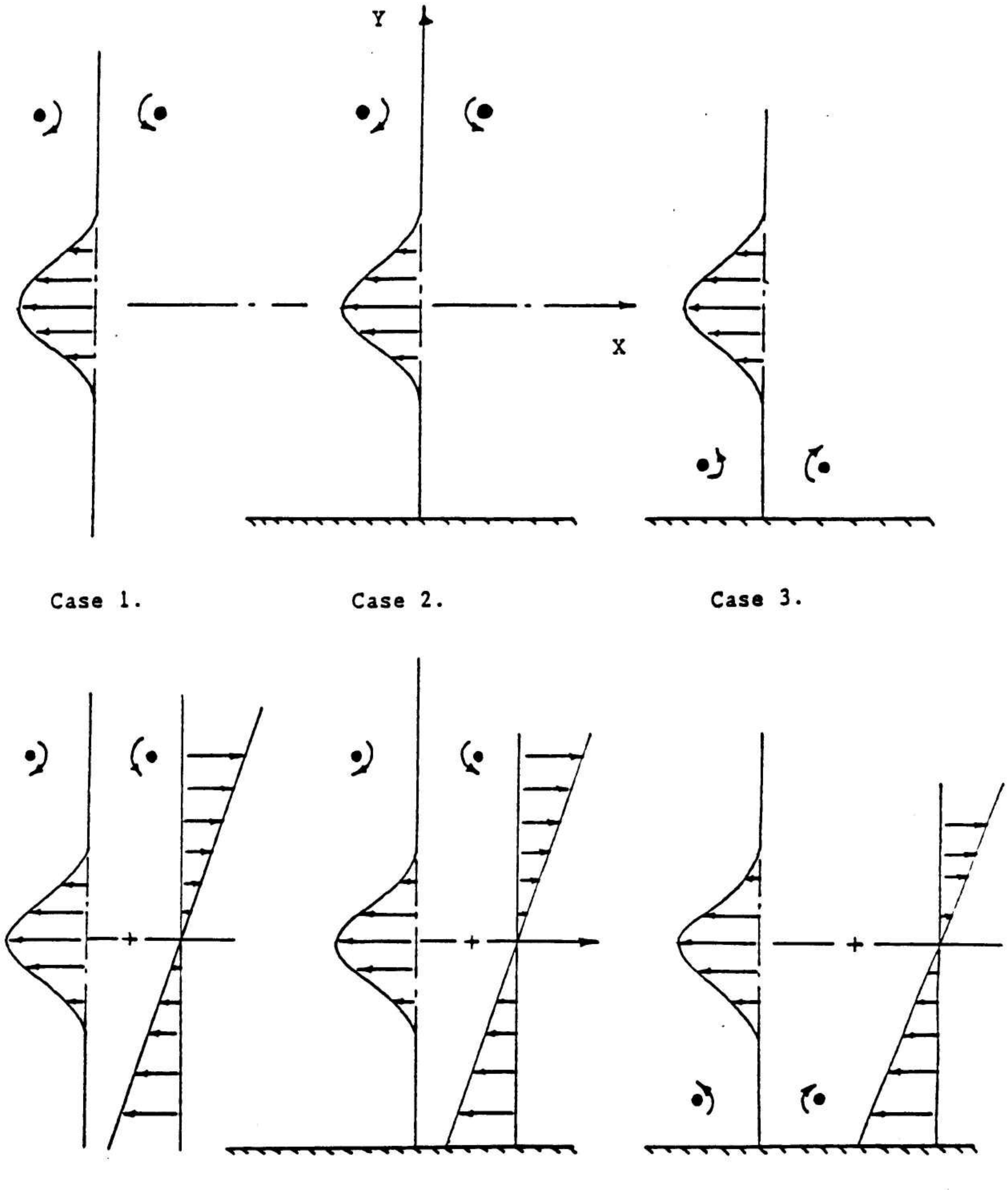

Case 1. Case 2. Case 3.

Case 4. Case 5. Case 6.

Fig. 40. Different cases considered for the numerical experiment.

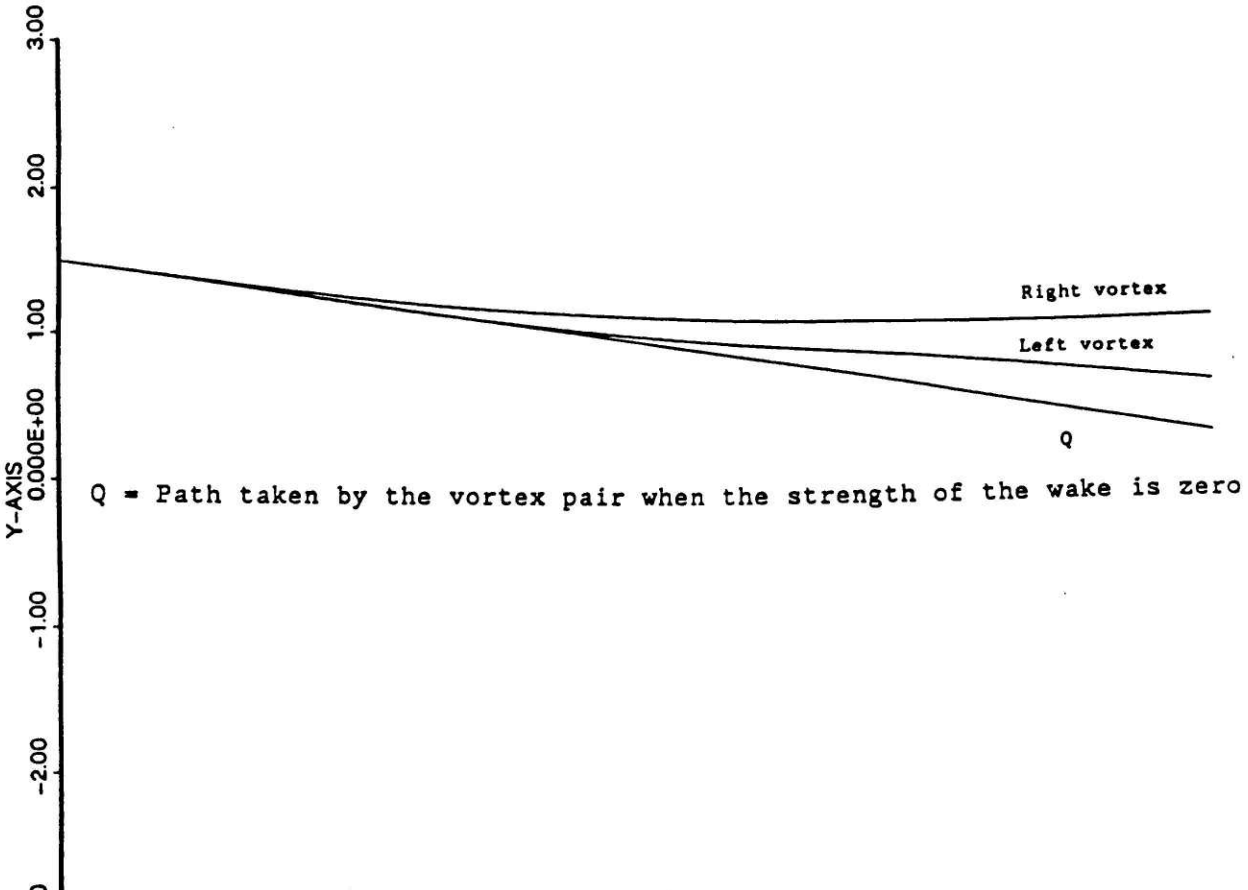

Fig. 41. Y-coordinates of the vortex pair versus time, $\Gamma_2=0.5$, c=1.0 (case 1).

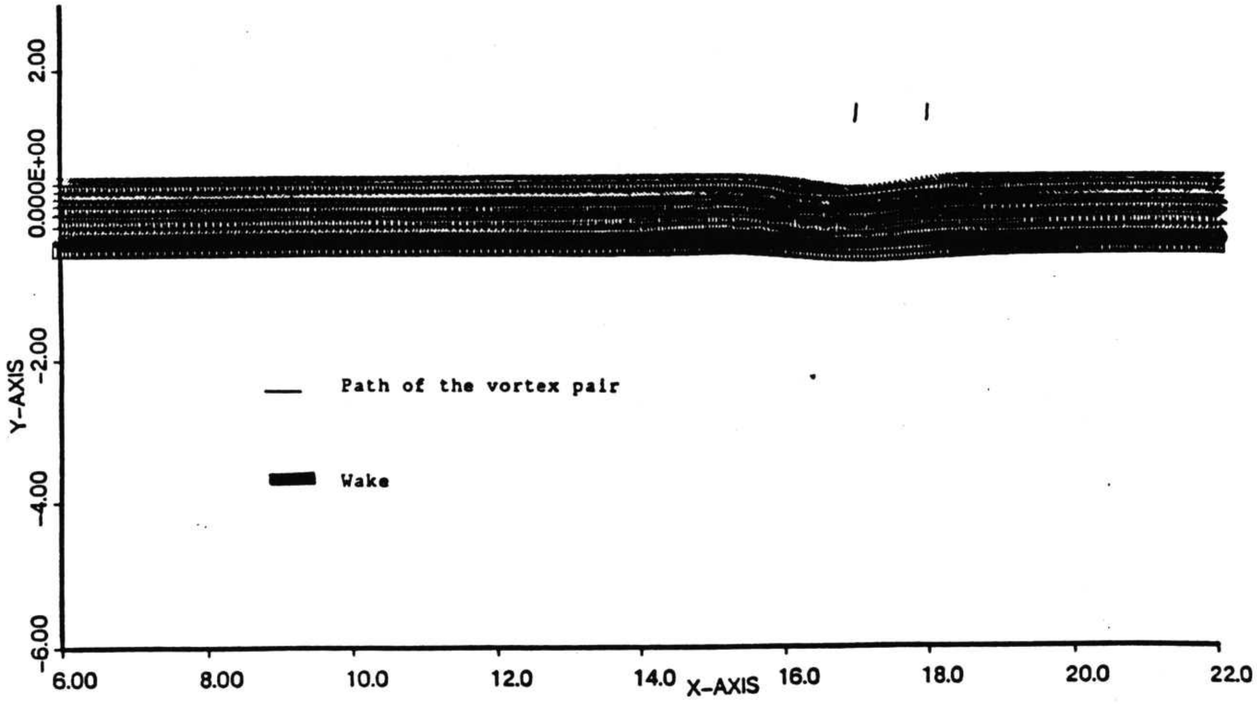

Fig. 42. Disturbed wake and the path of the vortex pair at time, $T=3.0$, $\Gamma_2=0.5$, $c=1.0$ (case 1).

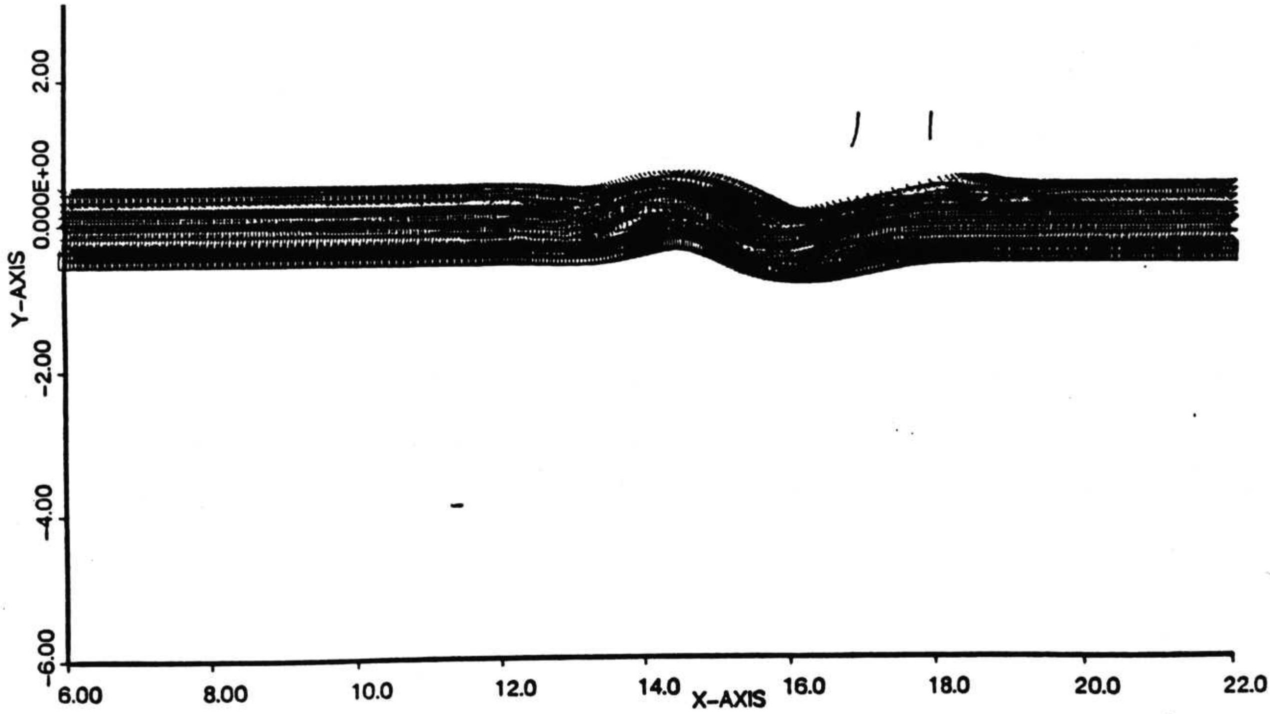

Fig. 43. Disturbed wake and the path of the vortex pair at time, $T=6.0$, $\Gamma_2=0.5$, $c=1.0$ (case 1).

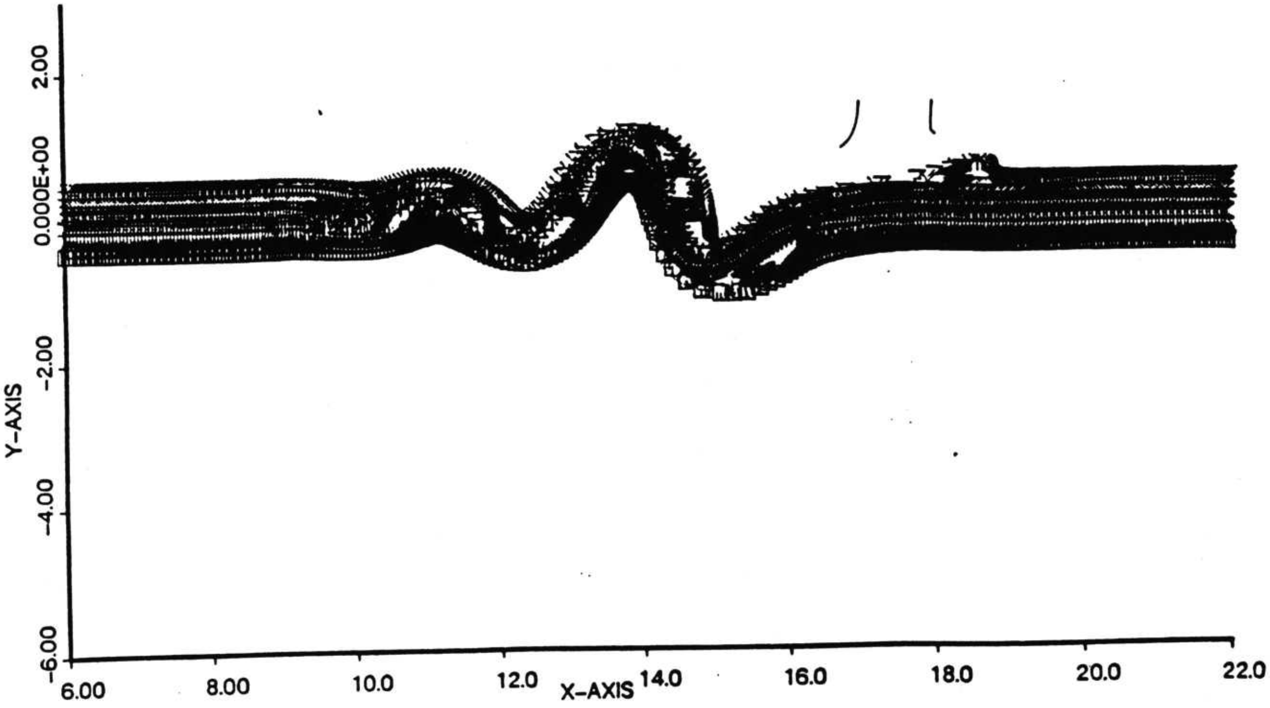

Fig. 44. Disturbed wake and the path of the vortex pair at time, T=9.0, Γ_2=0.5, c=1.0 (case 1).

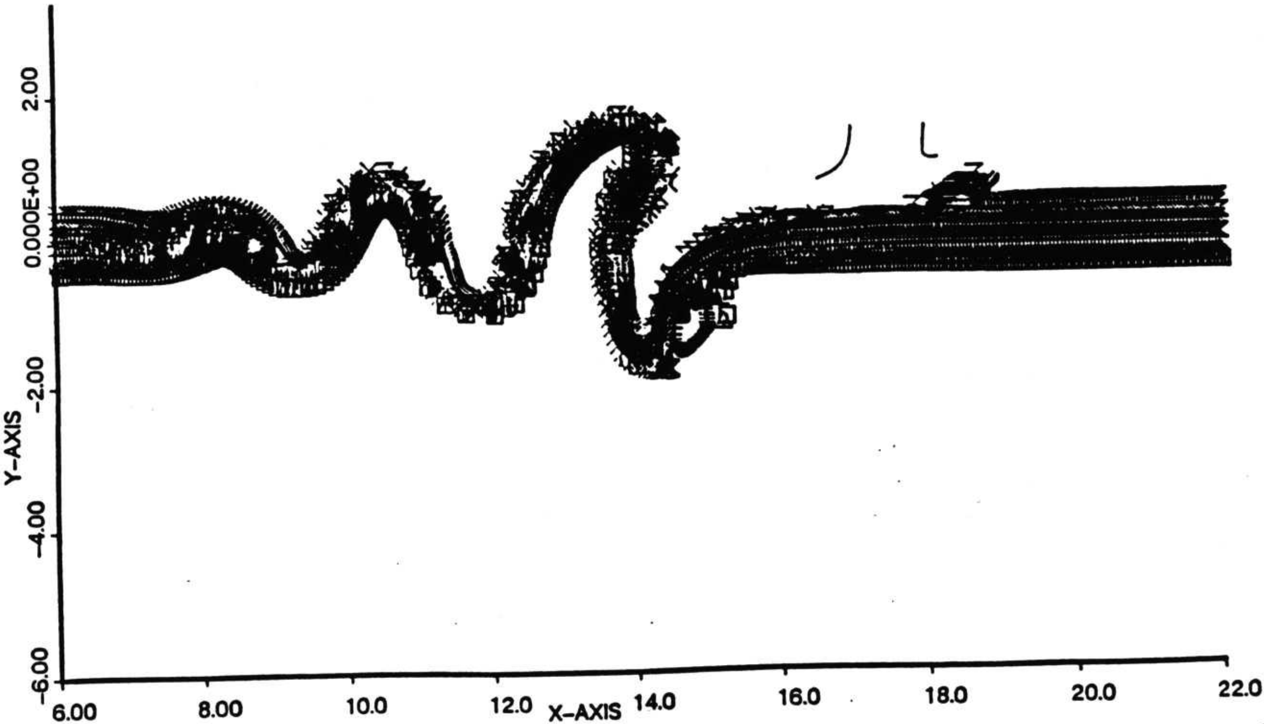

Fig. 45. Disturbed wake and the path of the vortex pair at time, T=12.0, Γ_2=0.5, c=1.0 (case 1).

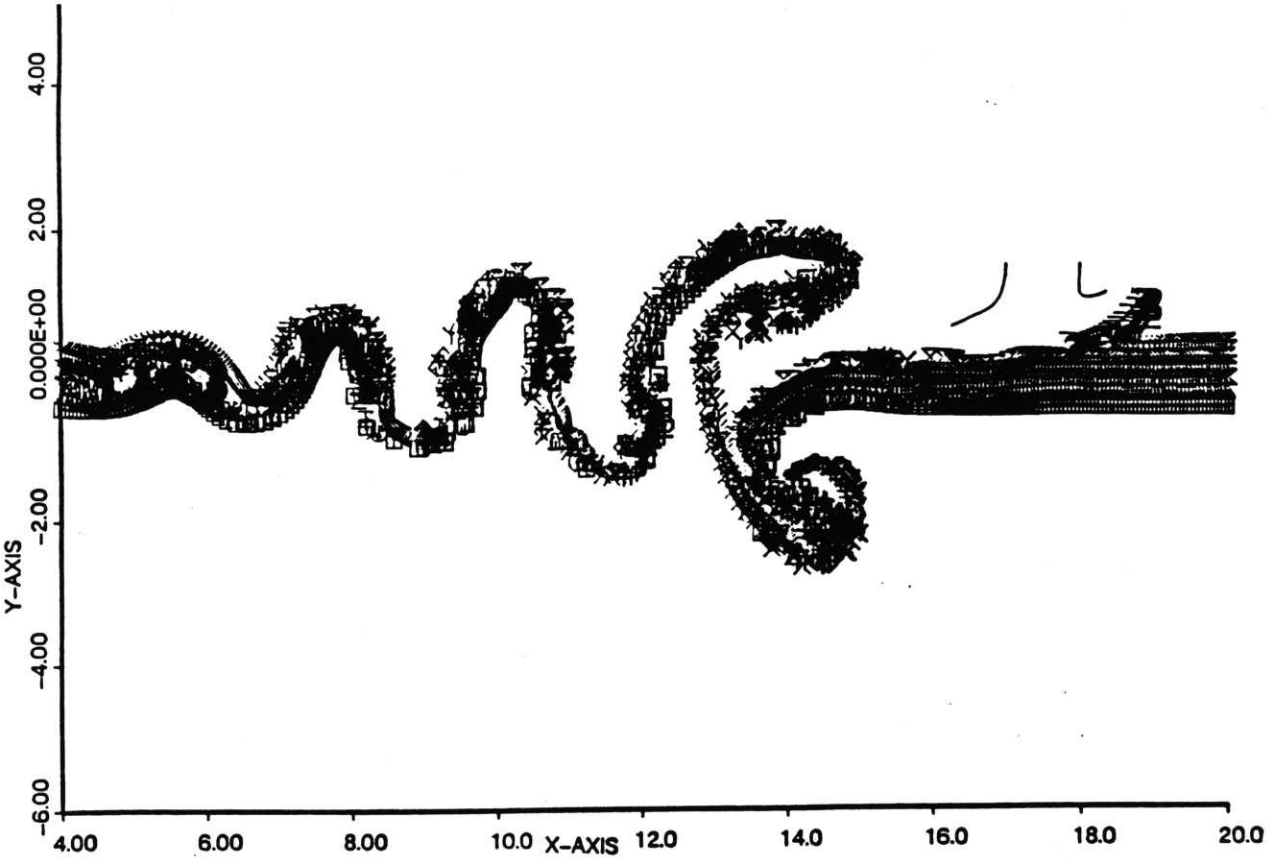

Fig. 46. Disturbed wake and the path of the vortex pair at time, T=15.0, Γ_2=0.5, c=1.0 (case 1).

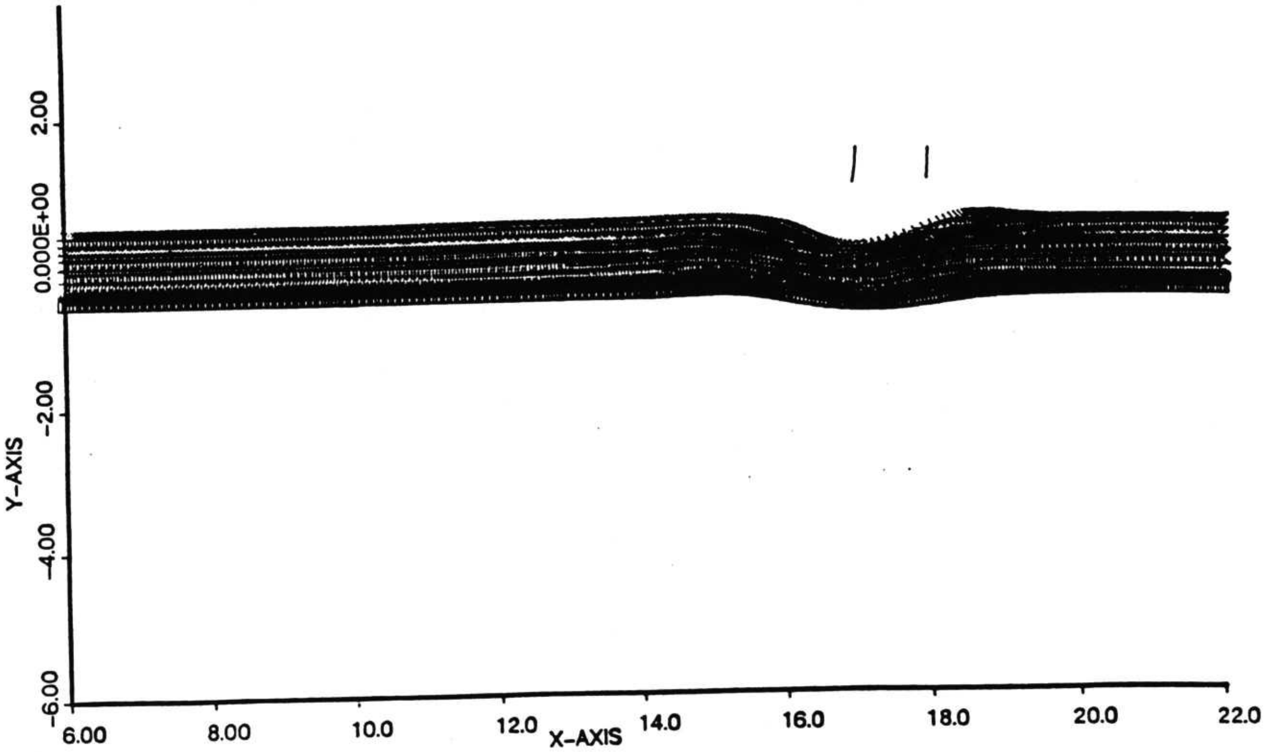

Fig. 47. Disturbed wake and the path of the vortex pair at time, $T=3.0$, $\Gamma_2=1.0$, $c=1.0$ (case 1).

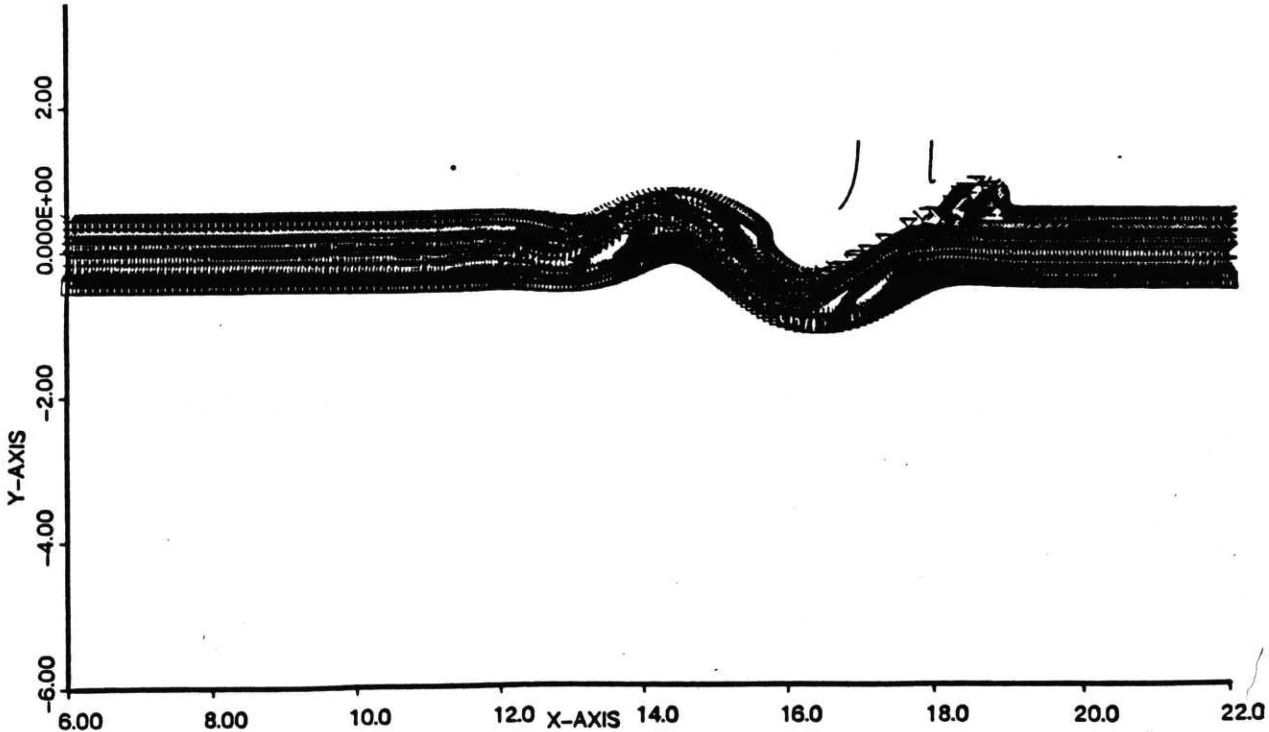

Fig. 48. Disturbed wake and the path of the vortex pair at time, $T=6.0$, $\Gamma_2=1.0$, $c=1.0$ (case 1).

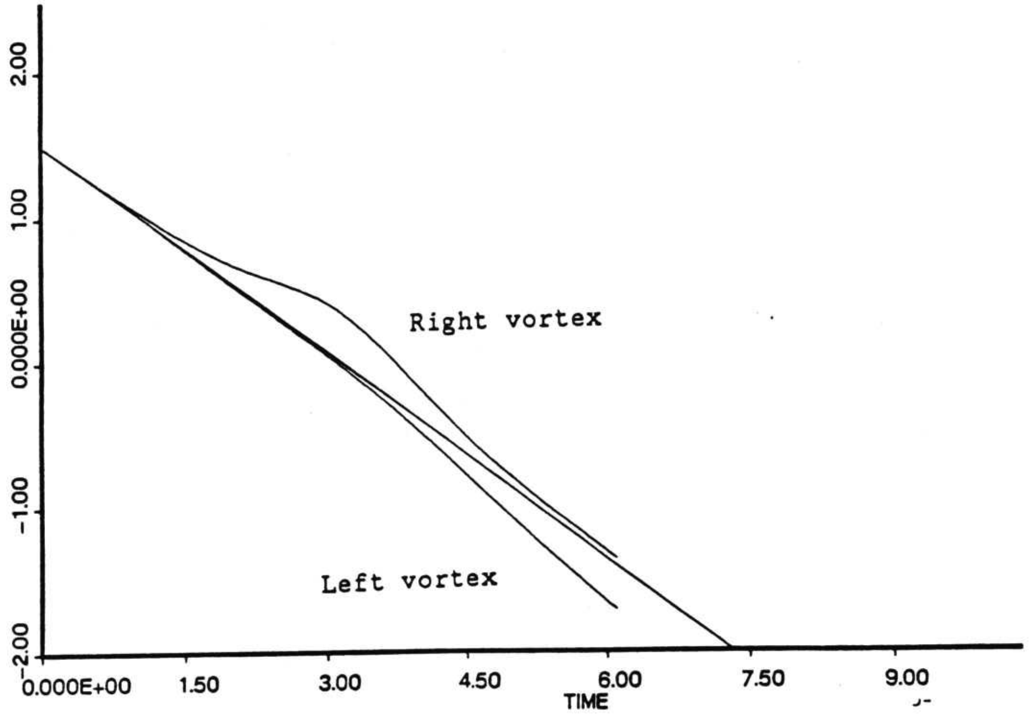

Fig. 49a. Y-coordinates of the vortex pair versus time. $\Gamma_2=3.0$, c=1.0 (case 1).

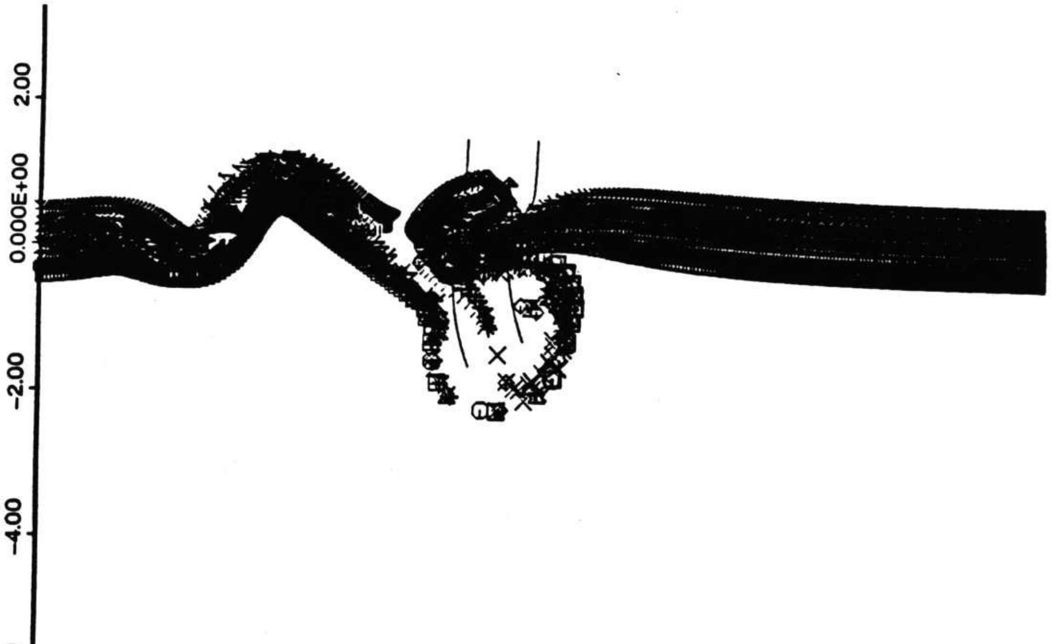

Fig. 49b. Disturbed wake and the path of the vortex pair at time, T=6.0, $\Gamma_2=3.0$, c=1.0 (case 1).

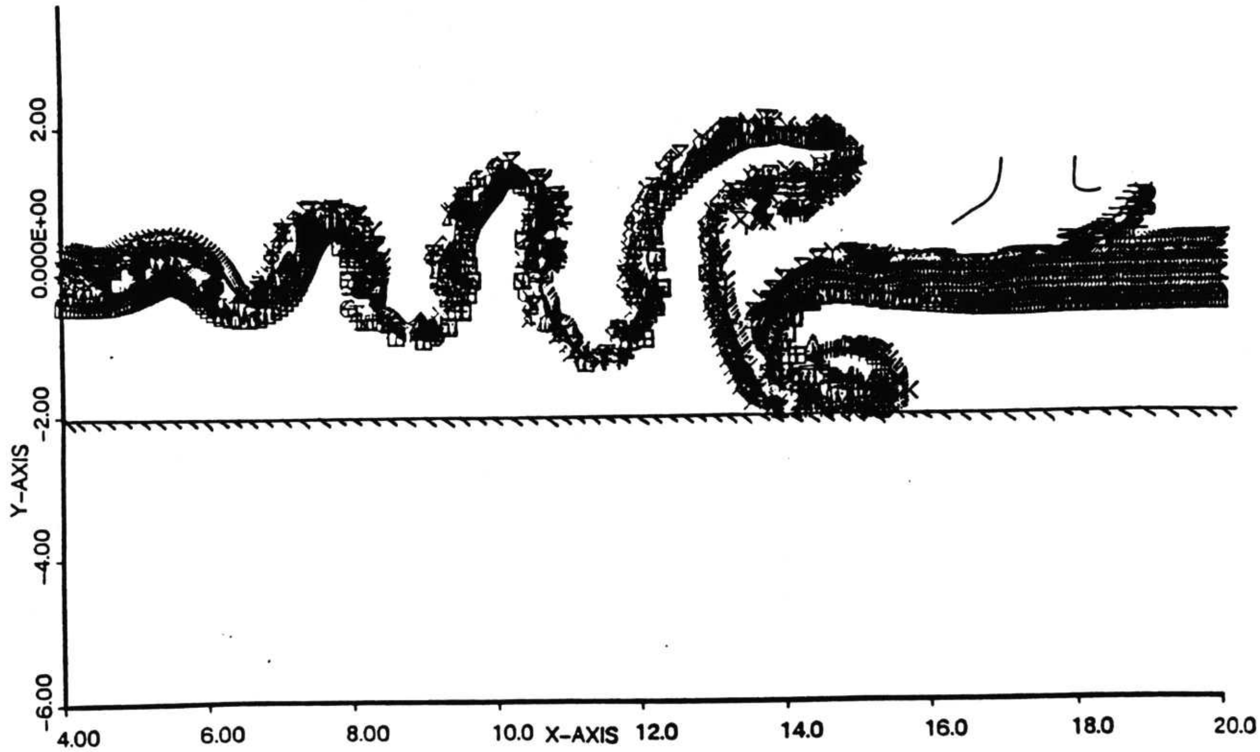

Fig. 50. Disturbed wake and the path of the vortex pair at time, T=15.0, Γ_2=0.5, c=1.0, and with the wall at y=-2.0. (case 2).

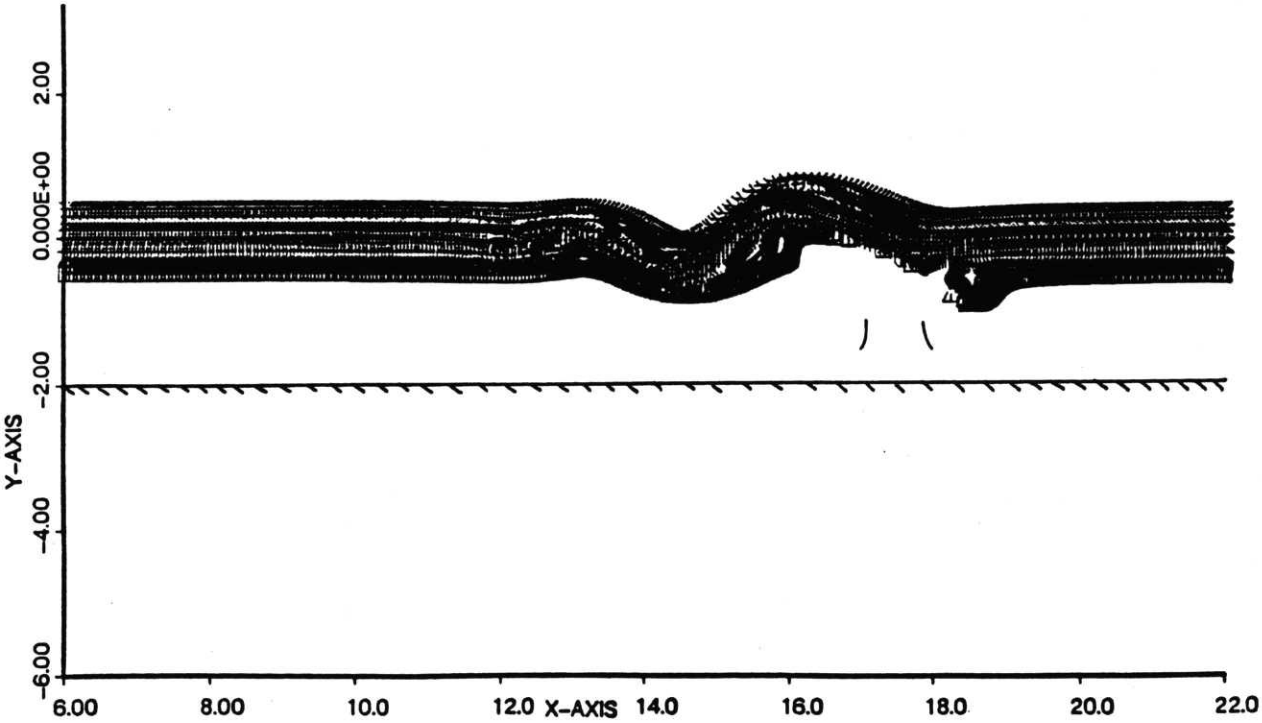

Fig. 51. Disturbed wake and the path of the vortex pair at time, T=6.0, Γ_2=1.0, c=1.0 (case 3).

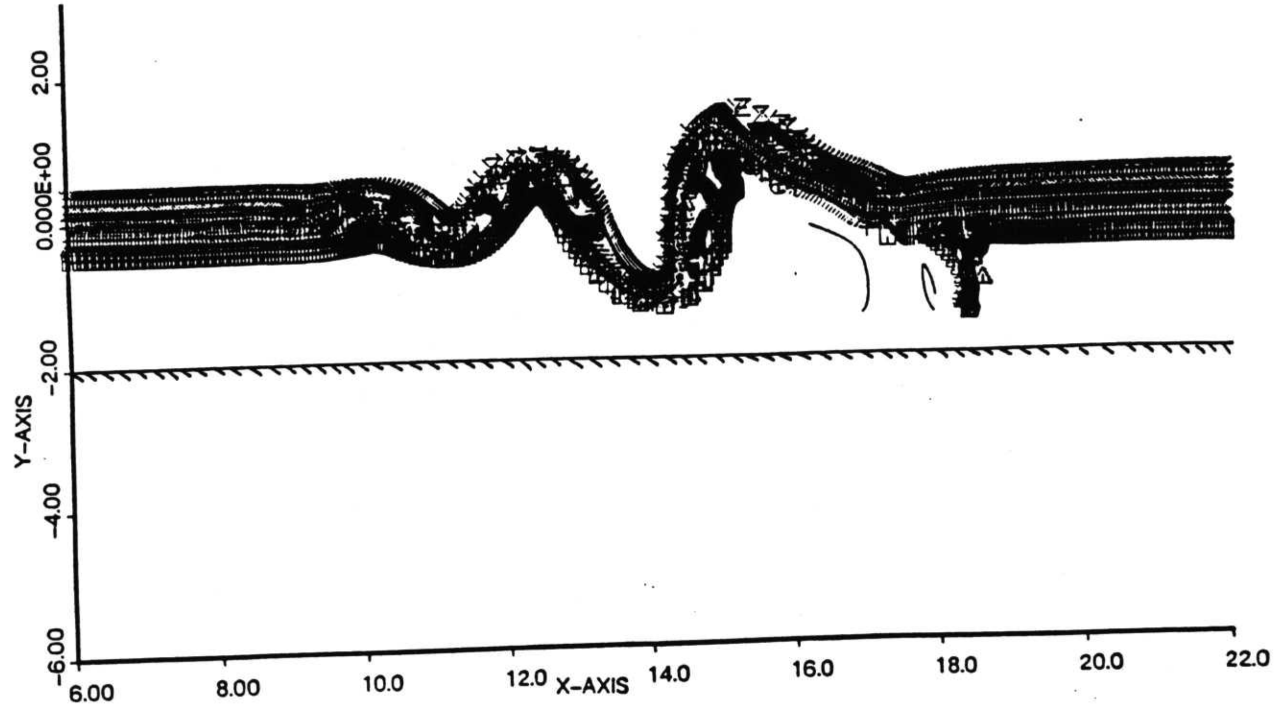

Fig. 52. Disturbed wake and the path of the vortex pair at time, T=9.0, Γ_2=1.0, c=1.0 (case 3).

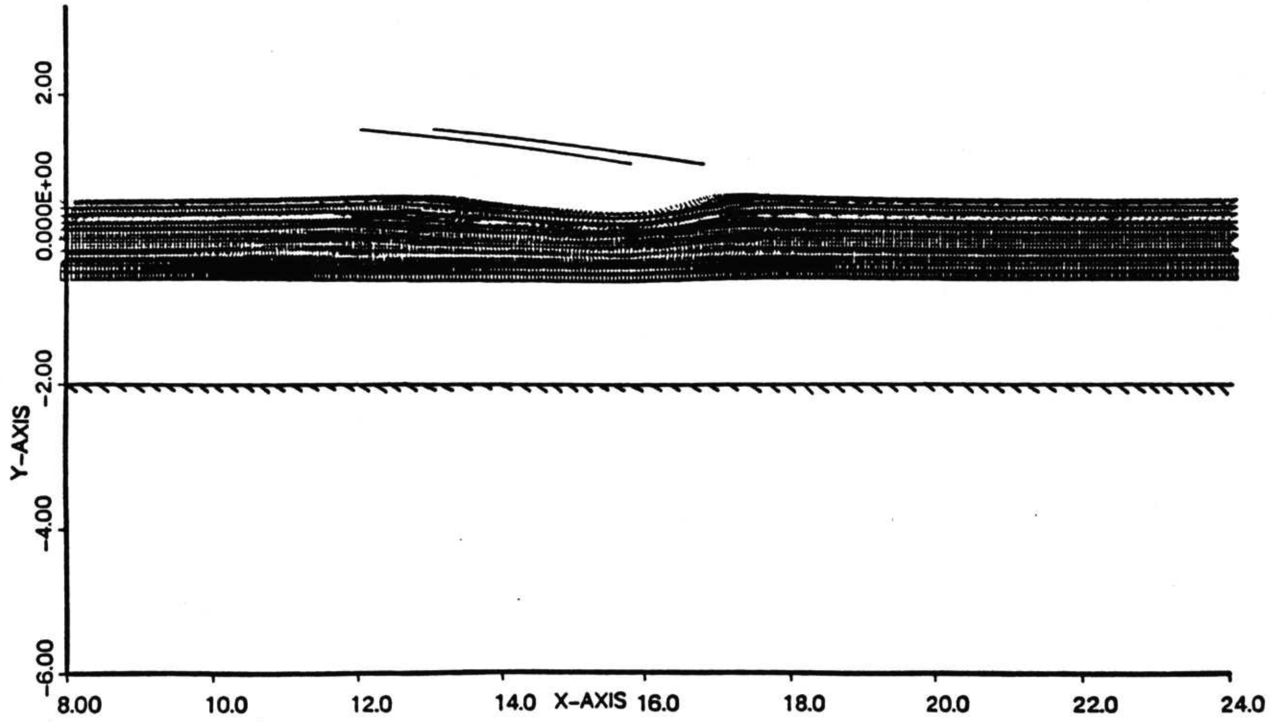

Fig. 53. Disturbed wake and the path of the vortex pair (case 5).T=6.0, Γ_2=0.5, c=1.0,mean shear=0.5, strength of the wake is zero.

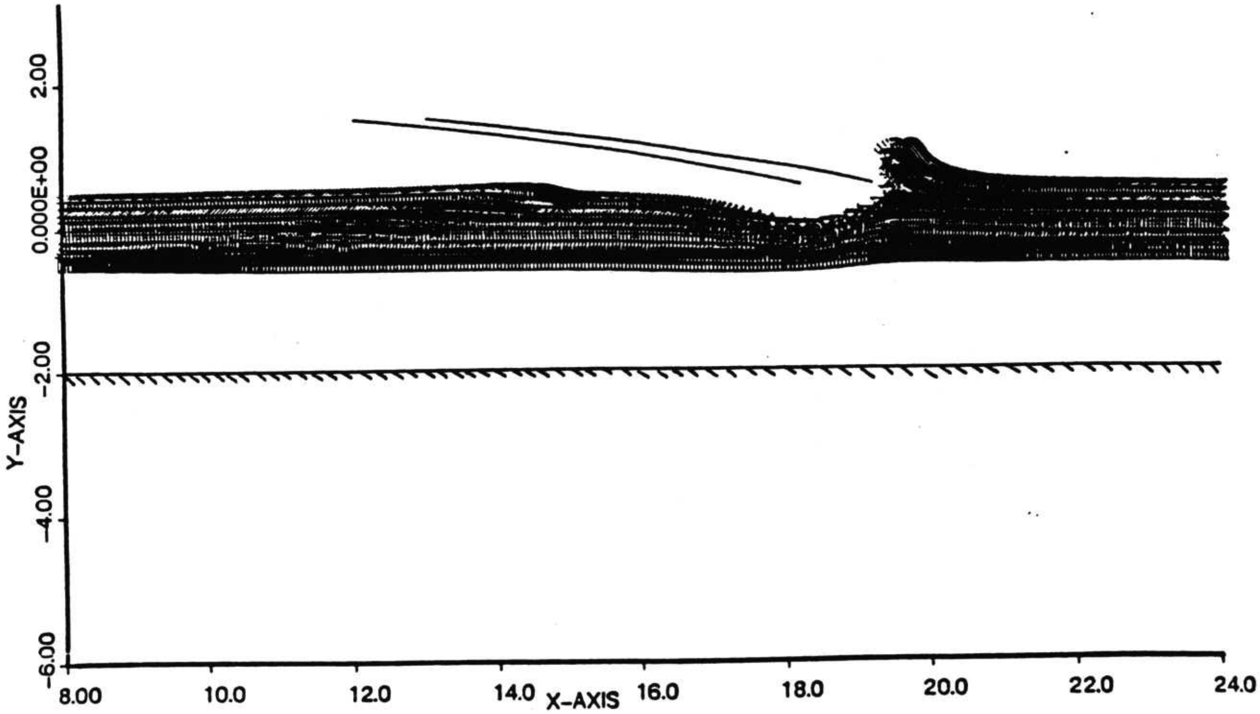

Fig. 54. Disturbed wake and the path of the vortex pair (case 5). T=12.0, Γ_2=0.5, c=1.0, mean shear =0.5, strength of the wake is zero.

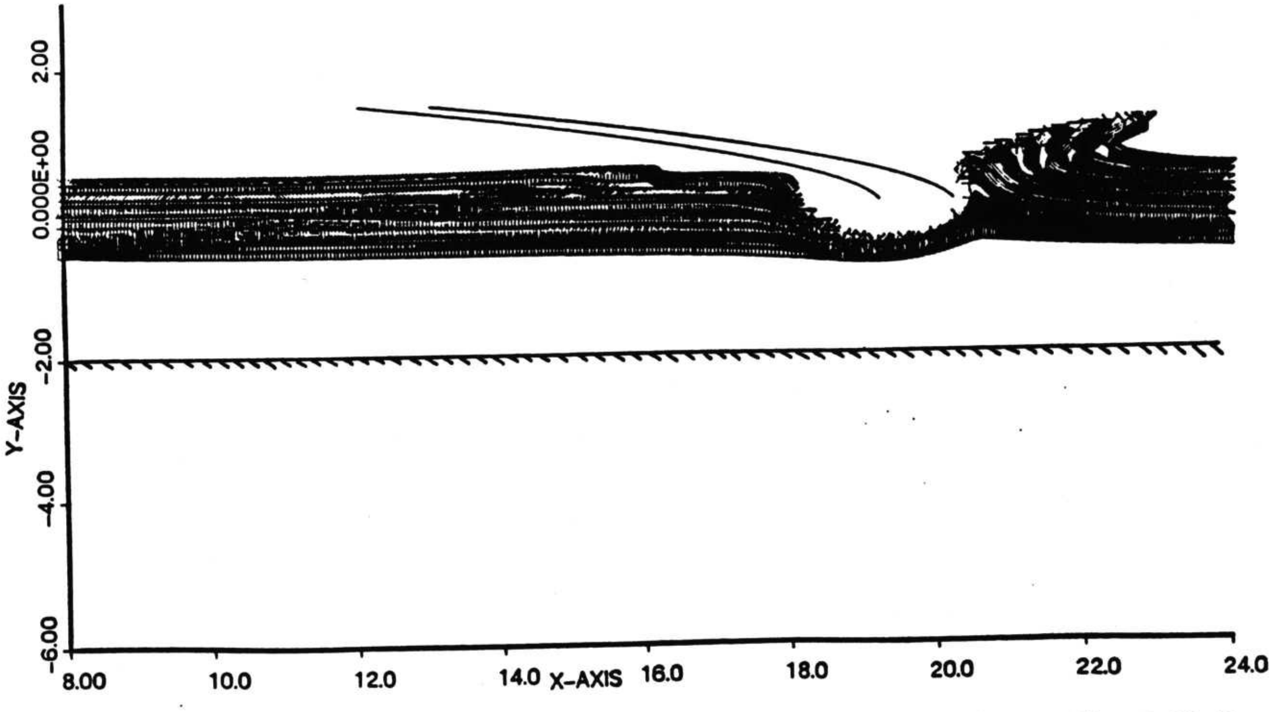

Fig. 55. Disturbed wake and the path of the vortex pair (case 5). T=18.0, Γ_2=0.5, c=1.0, mean shear =0.5, strength of the wake is zero.

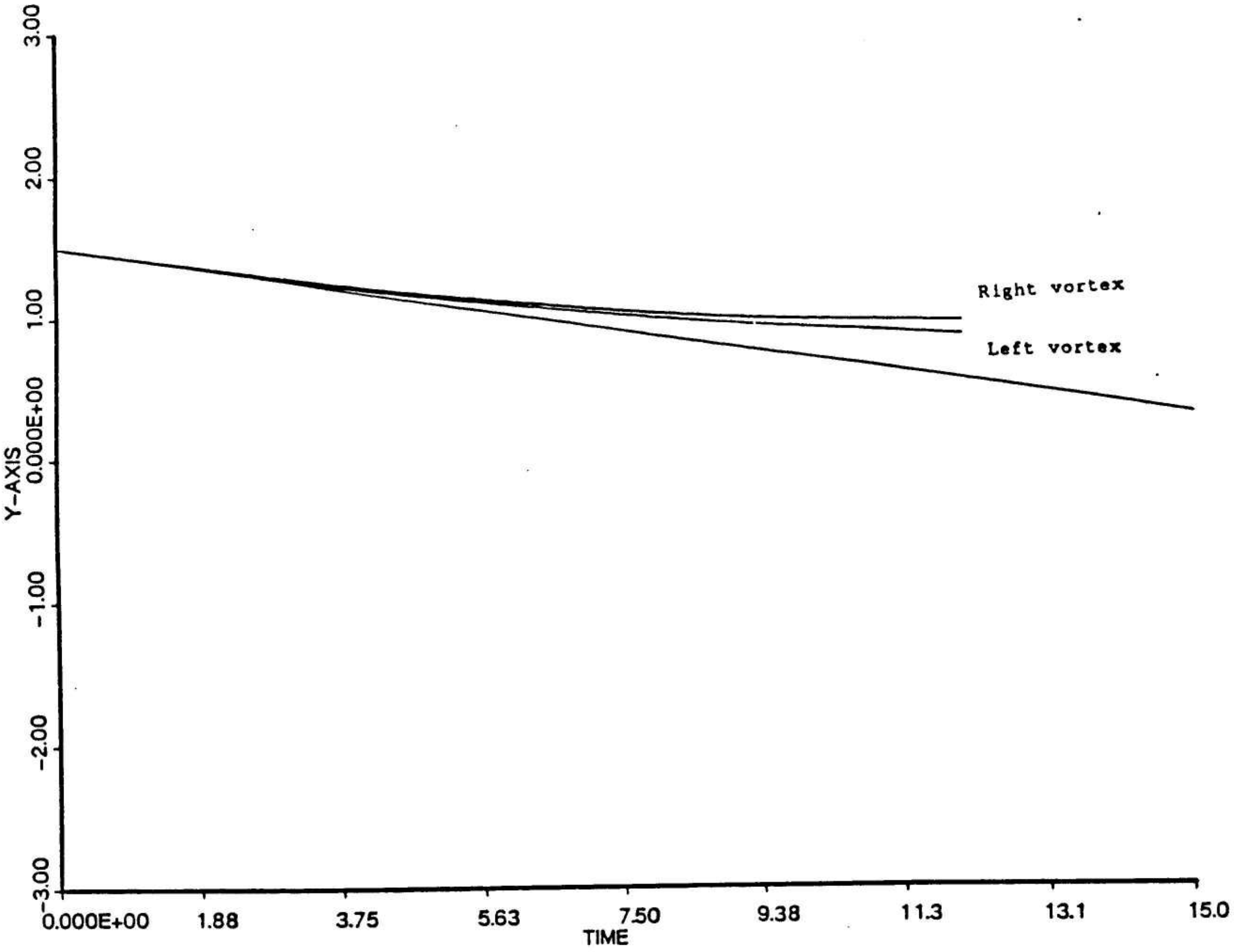

Fig. 56. Y-coordinates of the vortex pair versus time. Γ_2=0.5, c=1.0, mean shear = 0.5 (case 5).

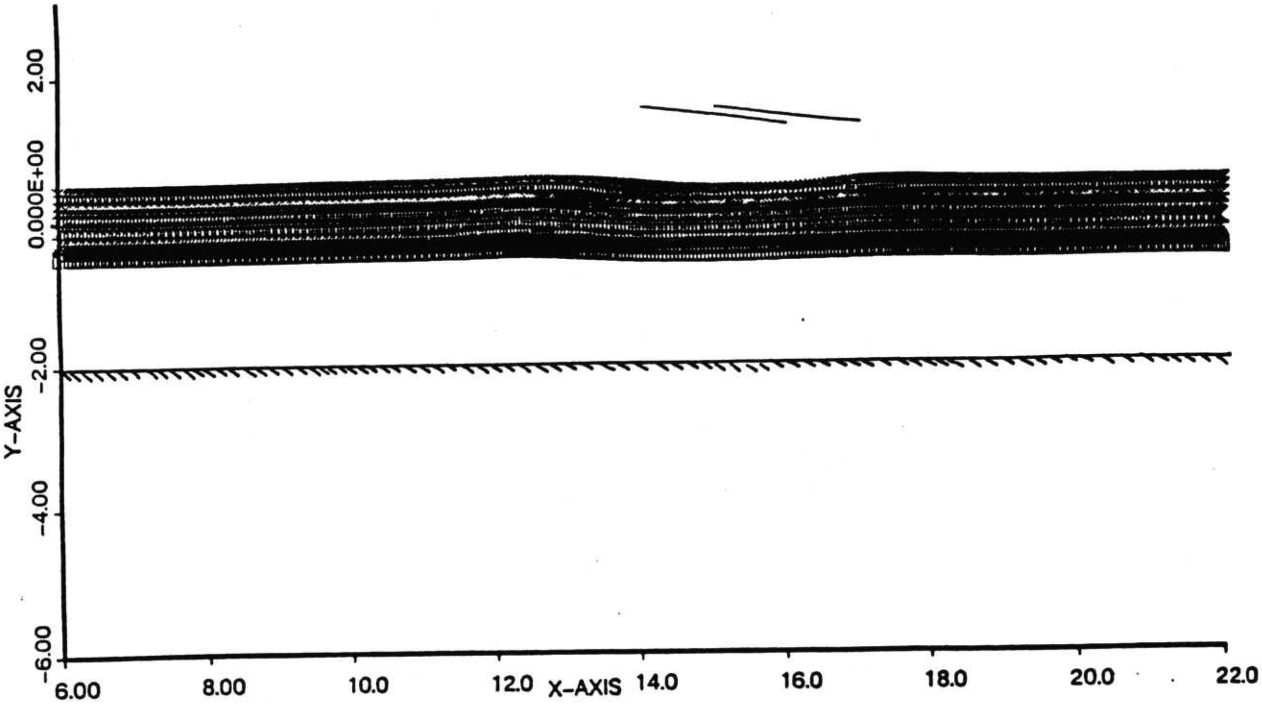

Fig. 57. Disturbed wake and the path of the vortex pair. T=3.0, Γ_2=0.5, c=1.0, mean shear =0.5 (case 5).

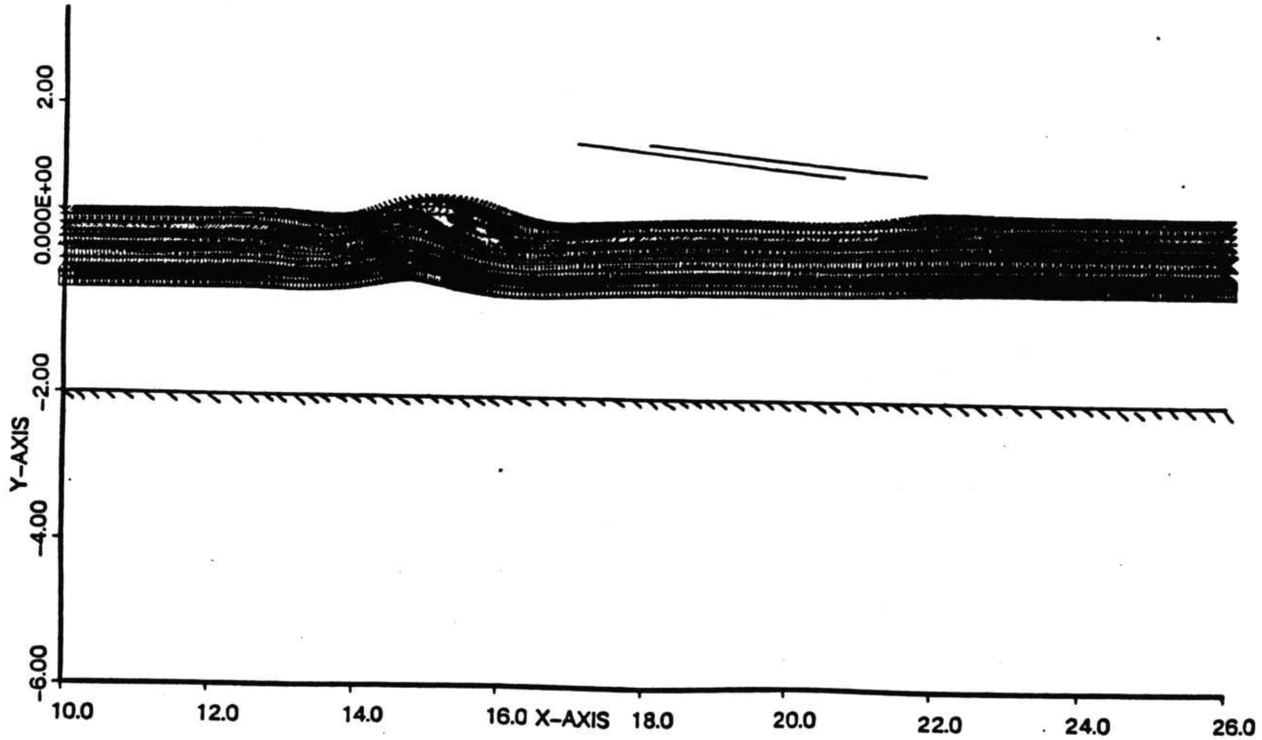

Fig. 58. Disturbed wake and the path of the vortex pair. T=6.0, Γ_2=0.5, c=1.0, mean shear =0.5 (case 5).

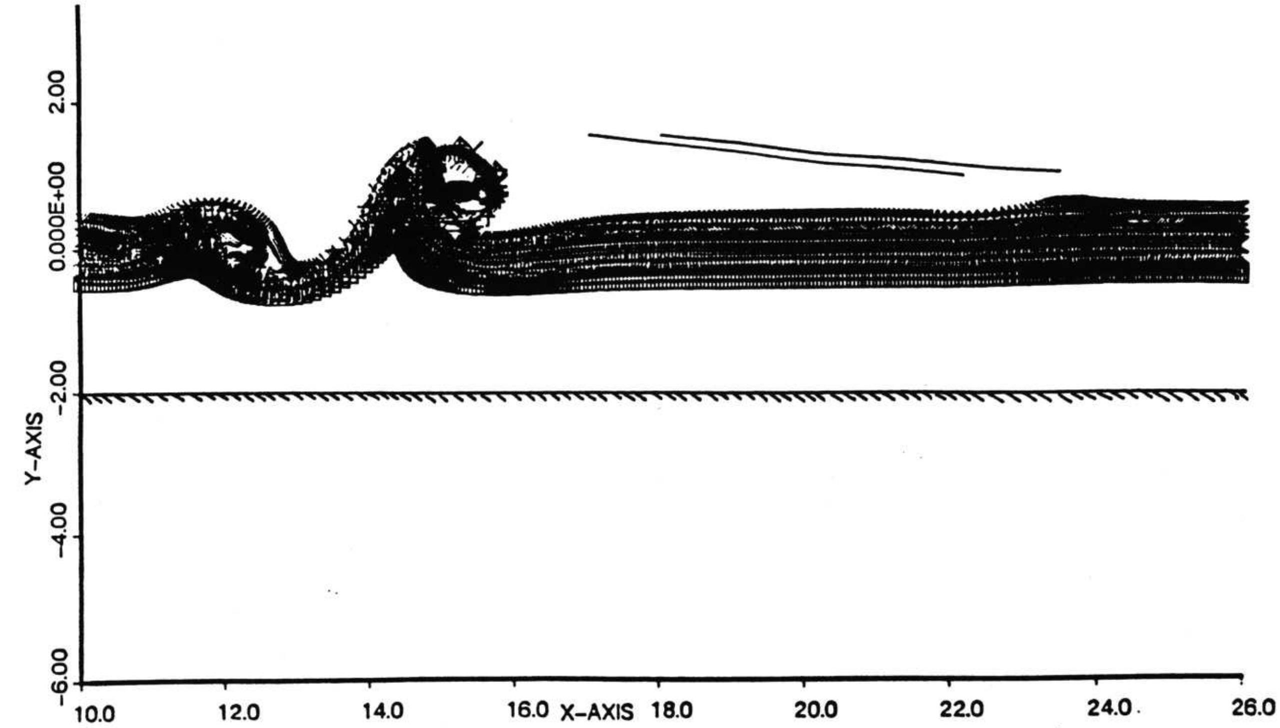

Fig. 59. Disturbed wake and the path of the vortex pair. T=9.0, Γ_2=0.5, c=1.0, mean shear =0.5 (case 5).

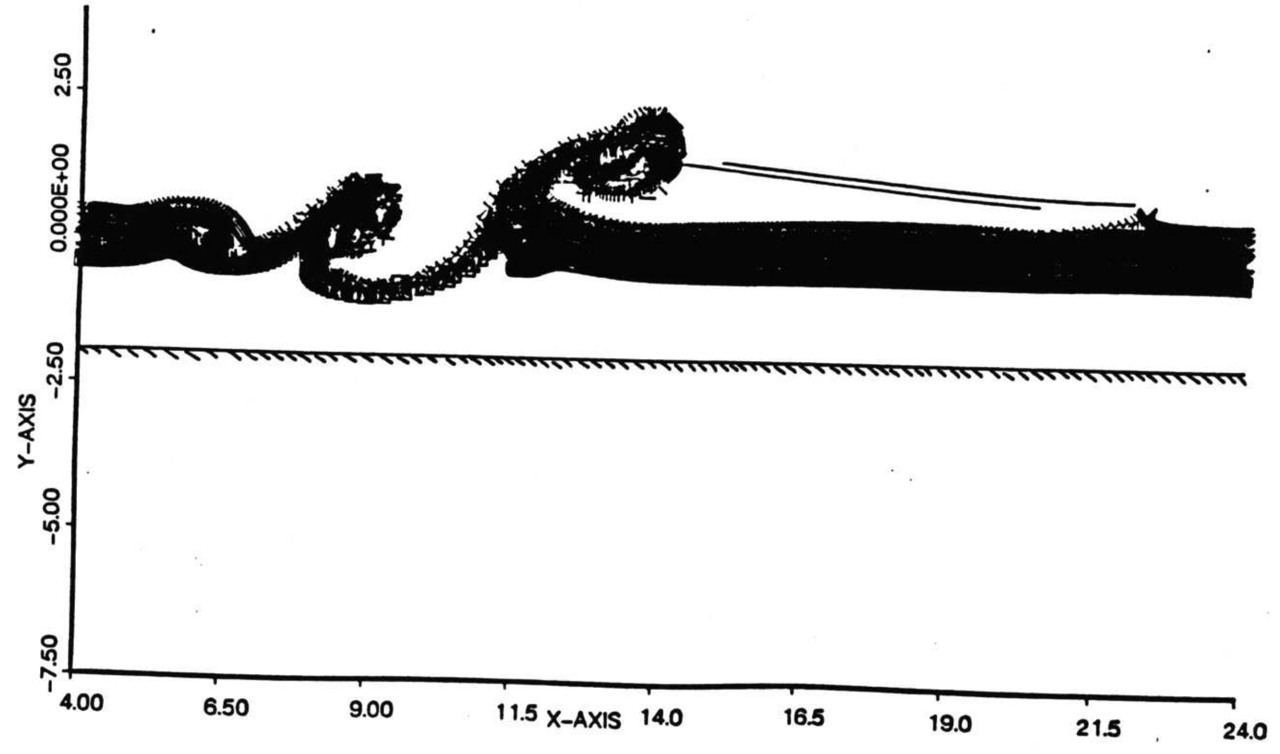

Fig. 60. Disturbed wake and the path of the vortex pair. T=12.0, Γ_2=0.5, c=1.0, mean shear =0.5 (case 5).

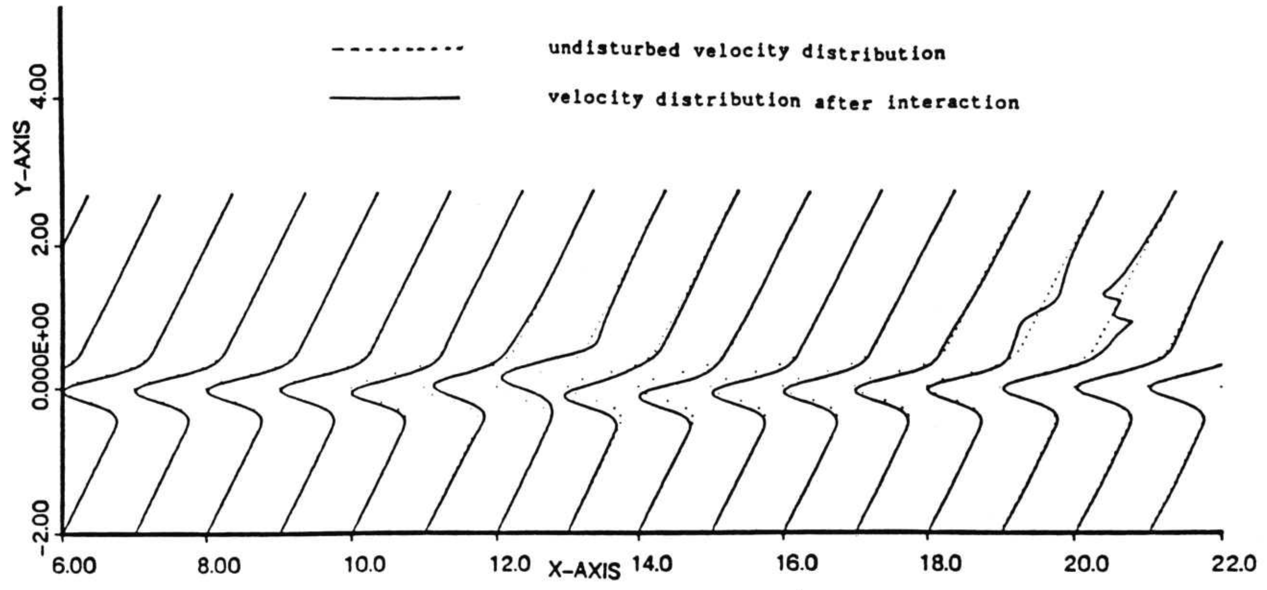

Fig. 61. Streamwise velocity distribution at different sections. T=6.0, Γ_2=0.5, c=1.0, mean shear =0.5, wall at y=-2. (case 5).

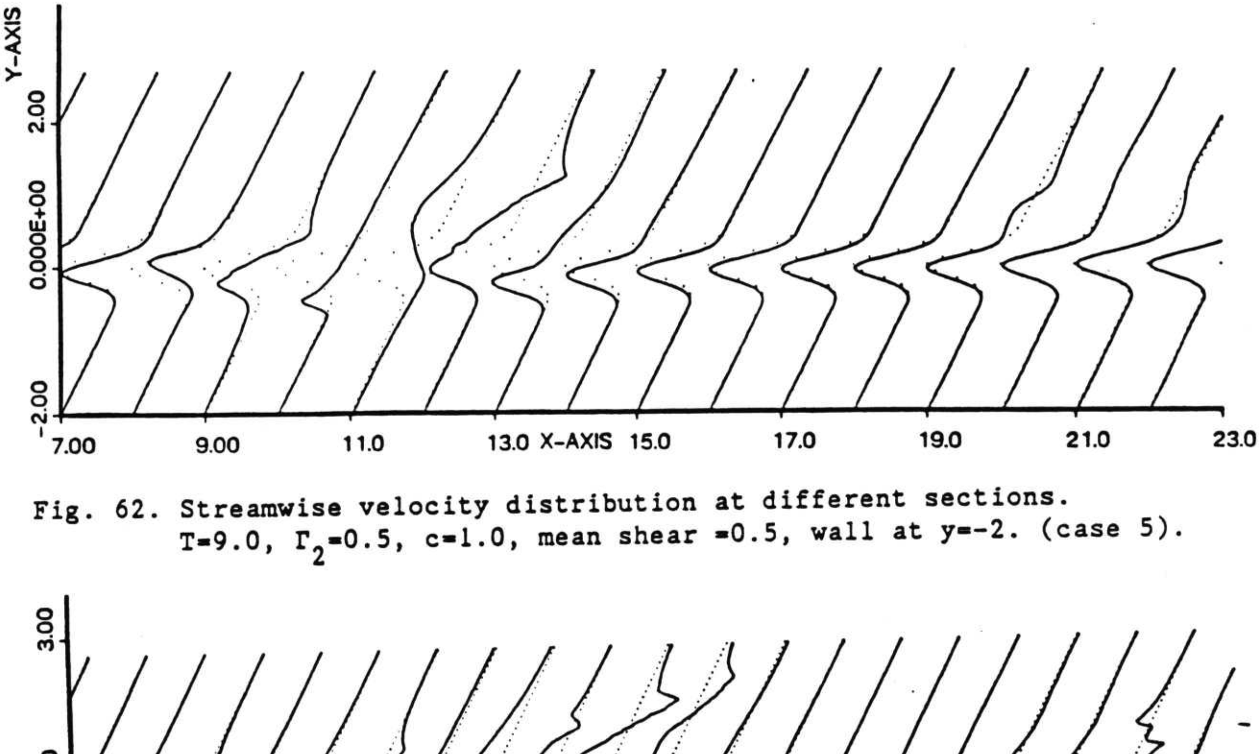

Fig. 62. Streamwise velocity distribution at different sections. T=9.0, Γ_2=0.5, c=1.0, mean shear =0.5, wall at y=-2. (case 5).

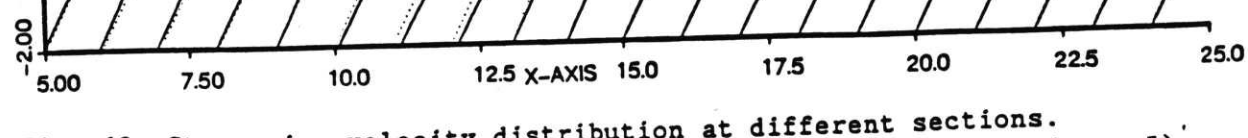

Fig. 63. Streamwise velocity distribution at different sections. T=12.0, Γ_2=0.5, c=1.0, mean shear =0.5, wall at y=-2. (case 5).

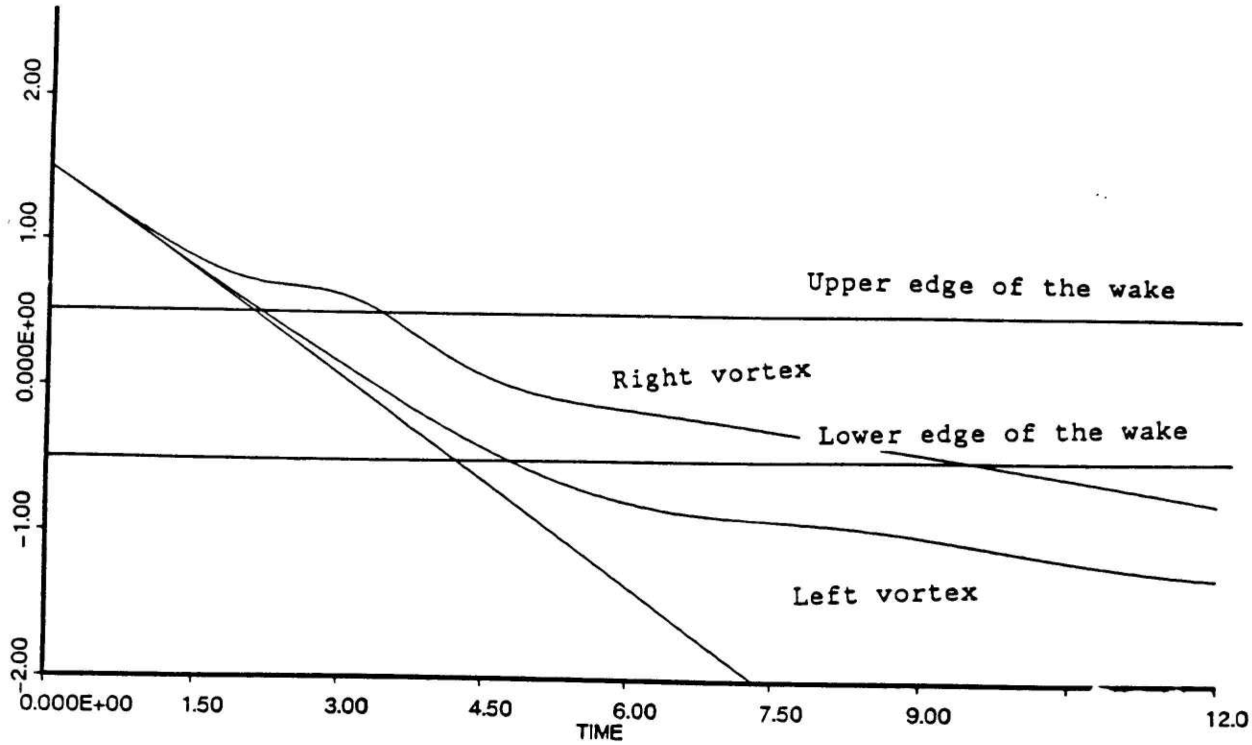

Fig. 63a. Y-coordinate of the vortex pair versus time, Γ_2=3.0, c=1.0, mean shear =0.5 (case 5).

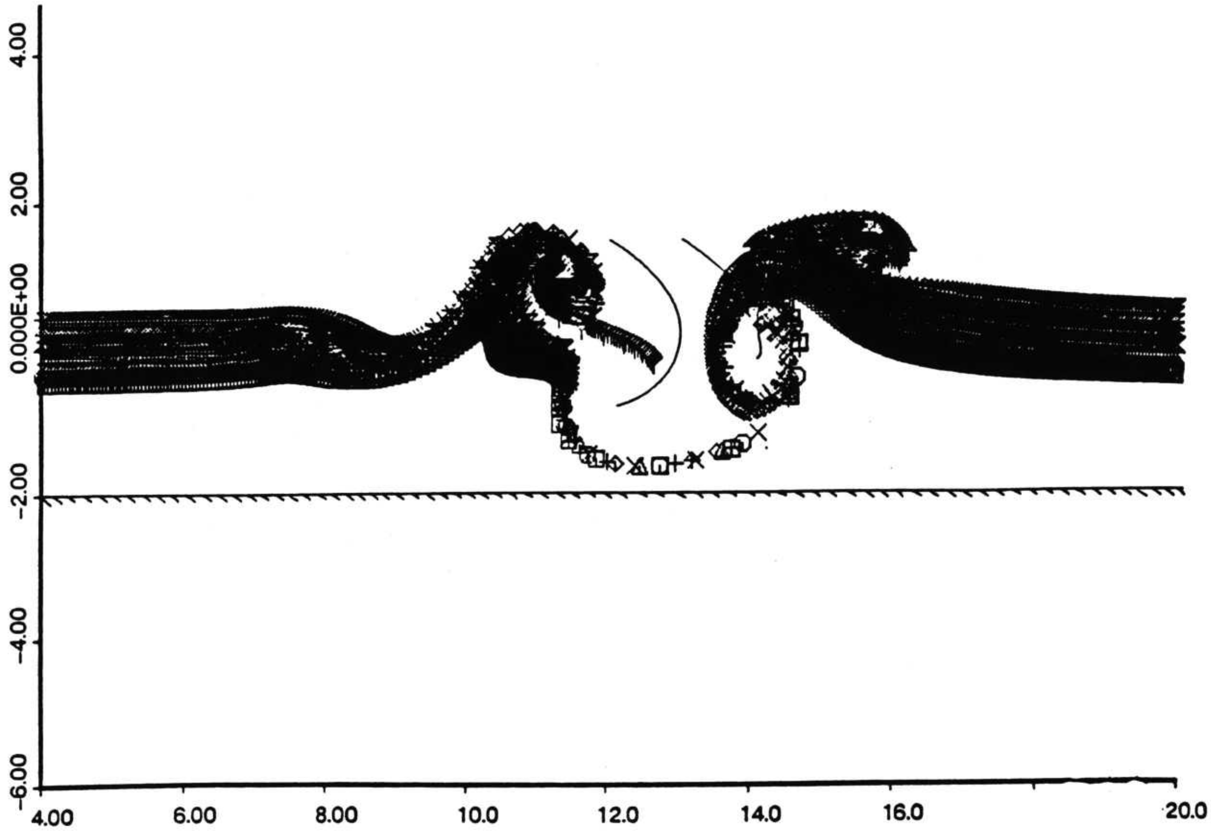

Fig. 63b. Disturbed wake and the path of the vortex pair.
T=6.0, Γ_2=3.0, c=1.0, mean shear =0.5 (case 5).

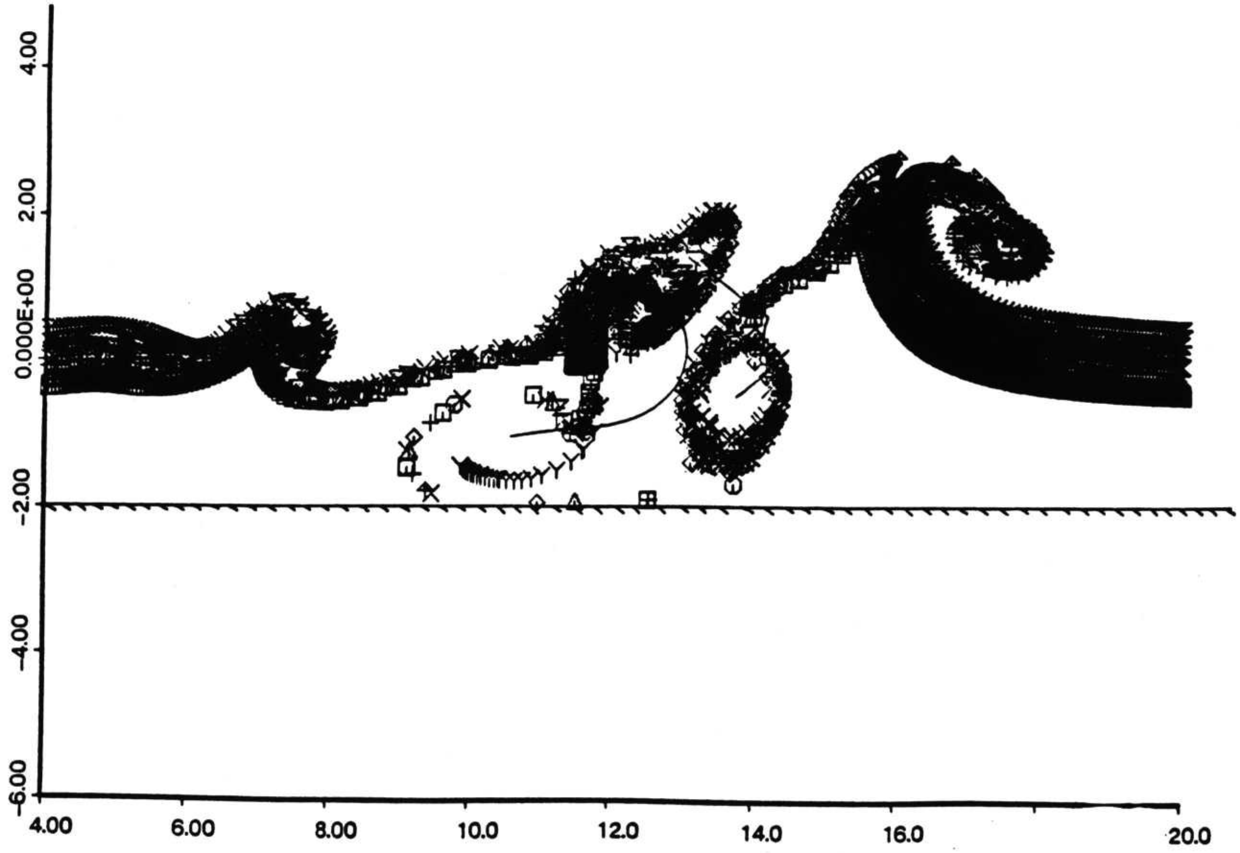

Fig. 63c. Disturbed wake and the path of the vortex pair.
T=9.0, Γ_2=3.0, c=1.0, mean shear =0.5, (case 5).

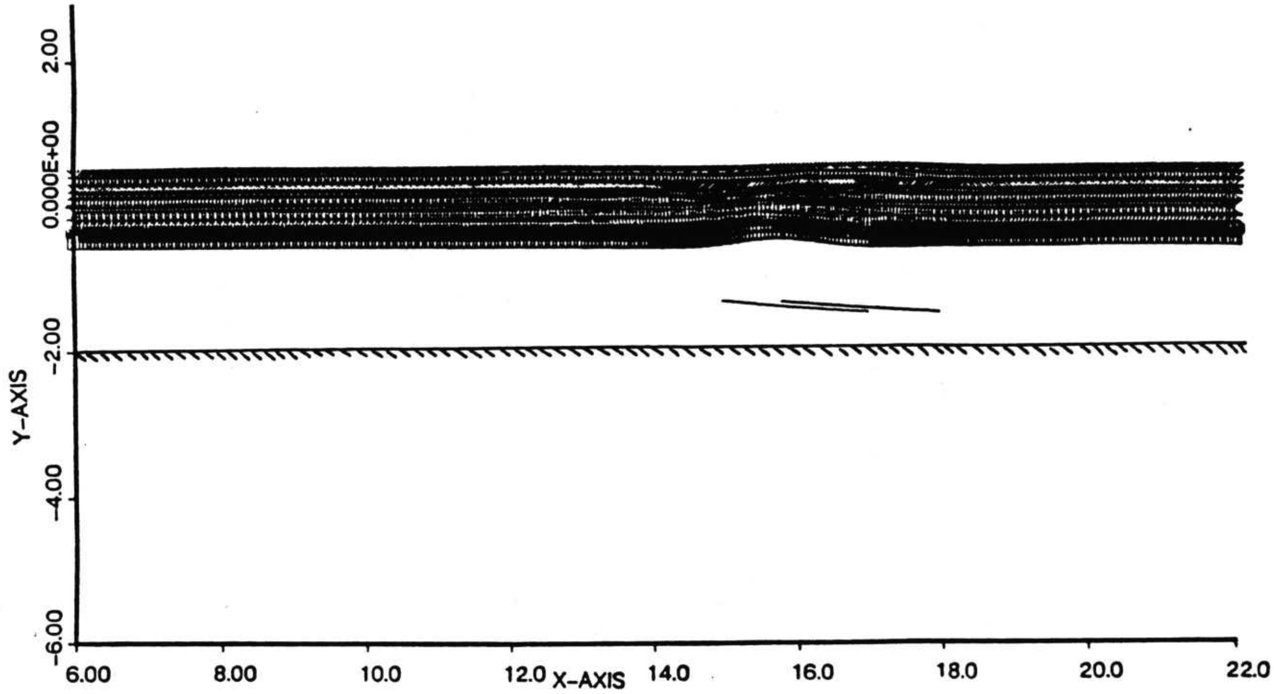

Fig. 64. Disturbed wake and the path of the vortex pair. T=3.0, Γ_2=0.5, c=1.0, mean shear =0.5 (case 6).

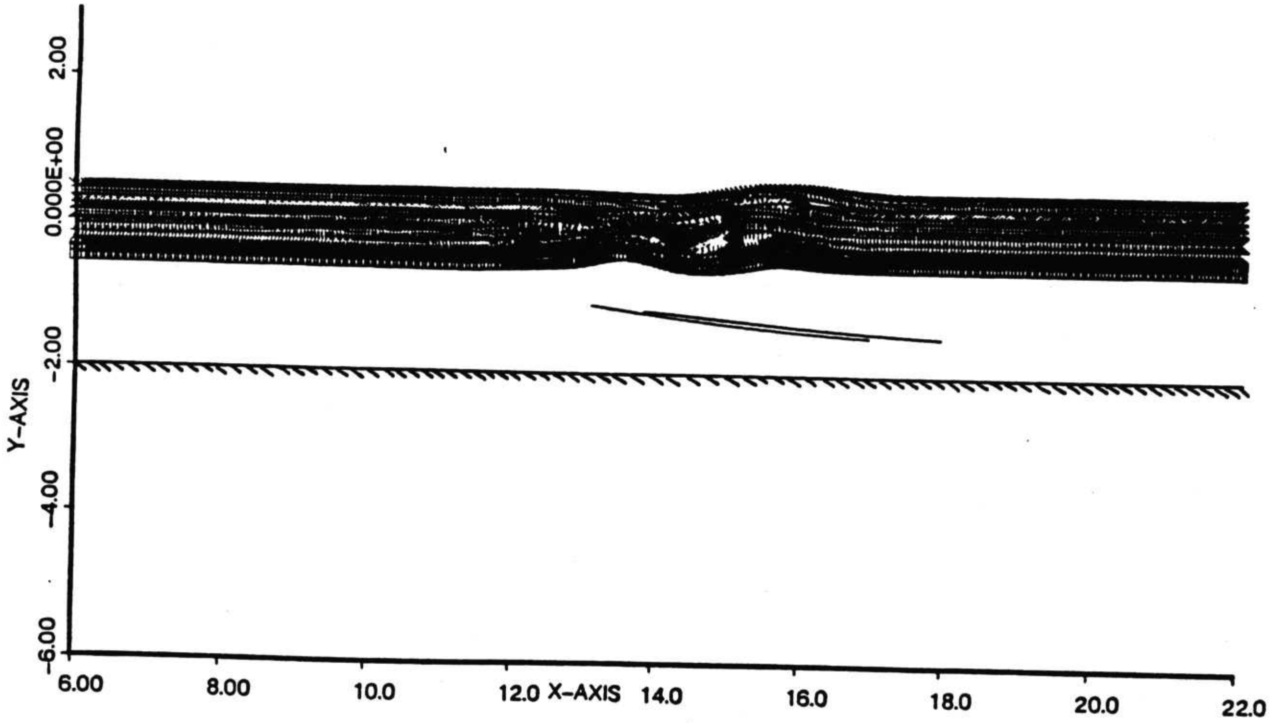

Fig. 65. Disturbed wake and the path of the vortex pair. T=6.0, Γ_2=0.5, c=1.0, mean shear =0.5 (case 6).

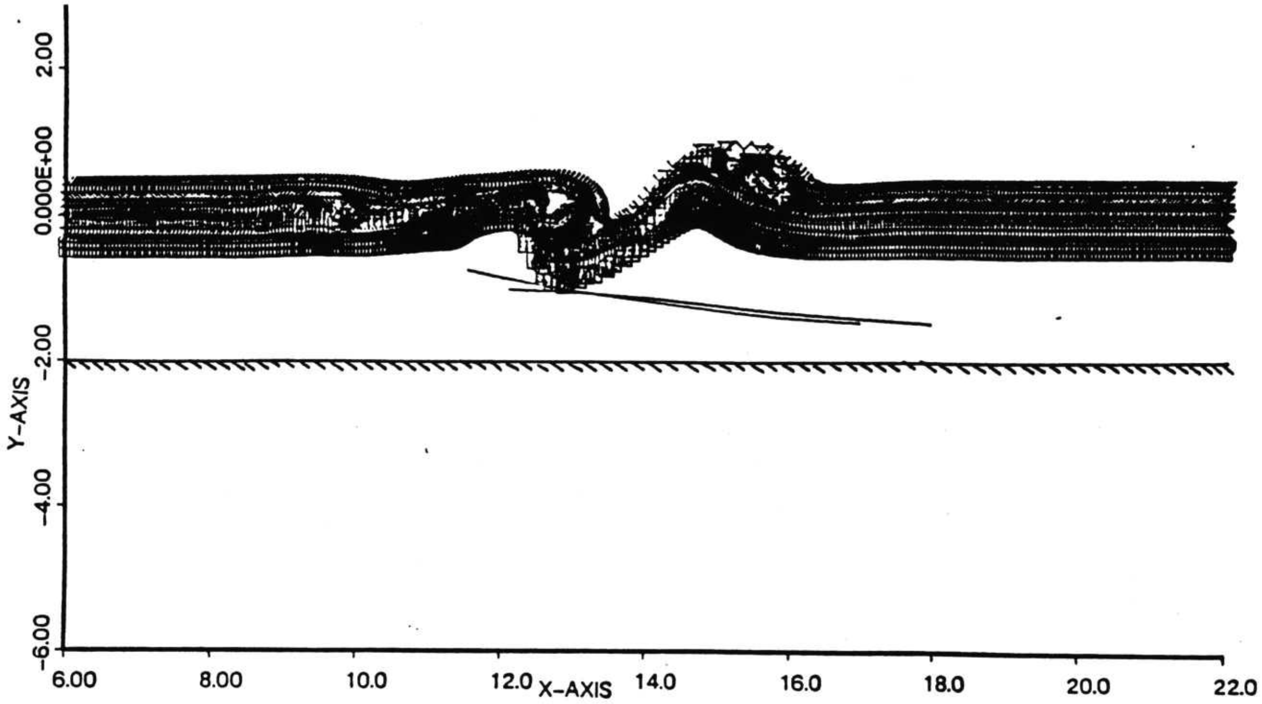

Fig. 66. Disturbed wake and the path of the vortex pair.
T=9.0, Γ_2=0.5, c=1.0, mean shear =0.5 (case 6).

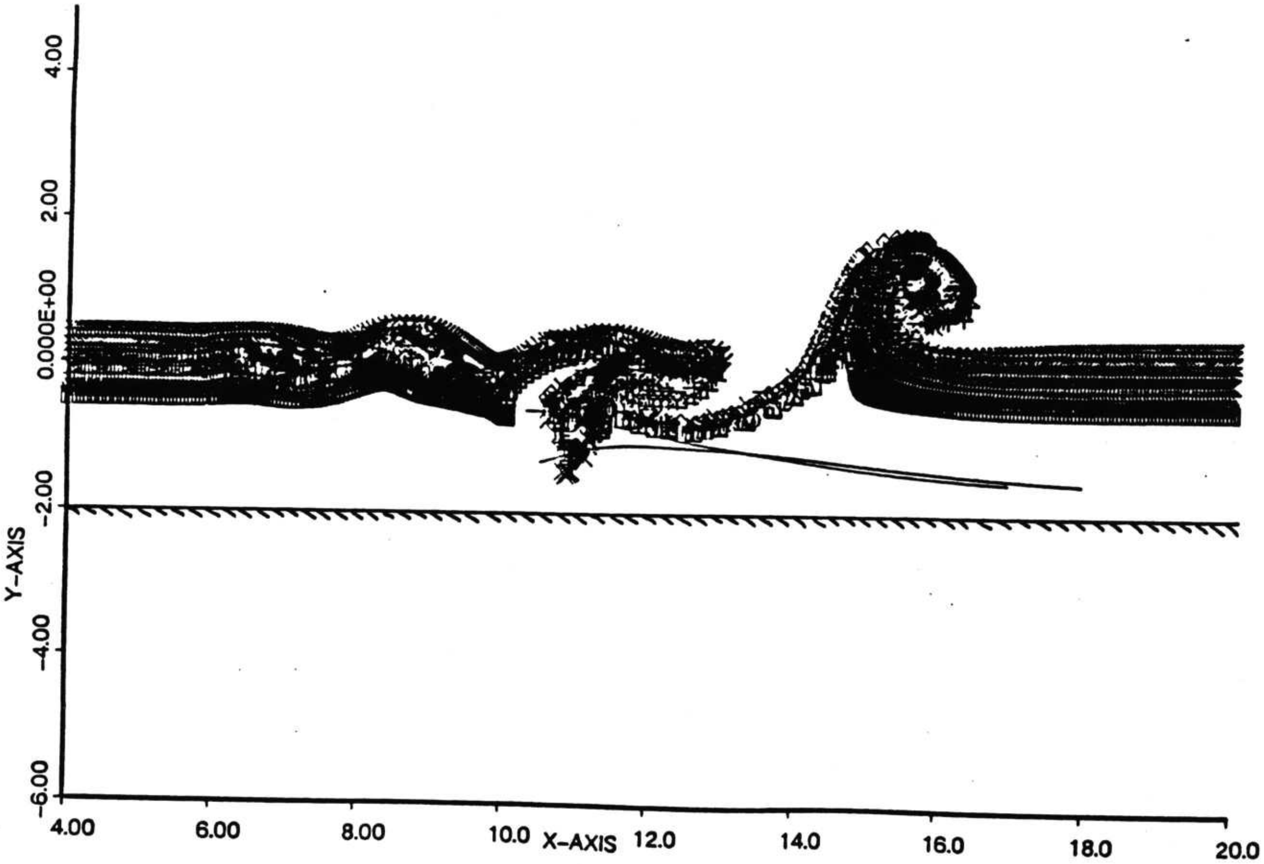

Fig. 67. Disturbed wake and the path of the vortex pair.
T=12.0, Γ_2=0.5, c=1.0, mean shear =0.5 (case 6).

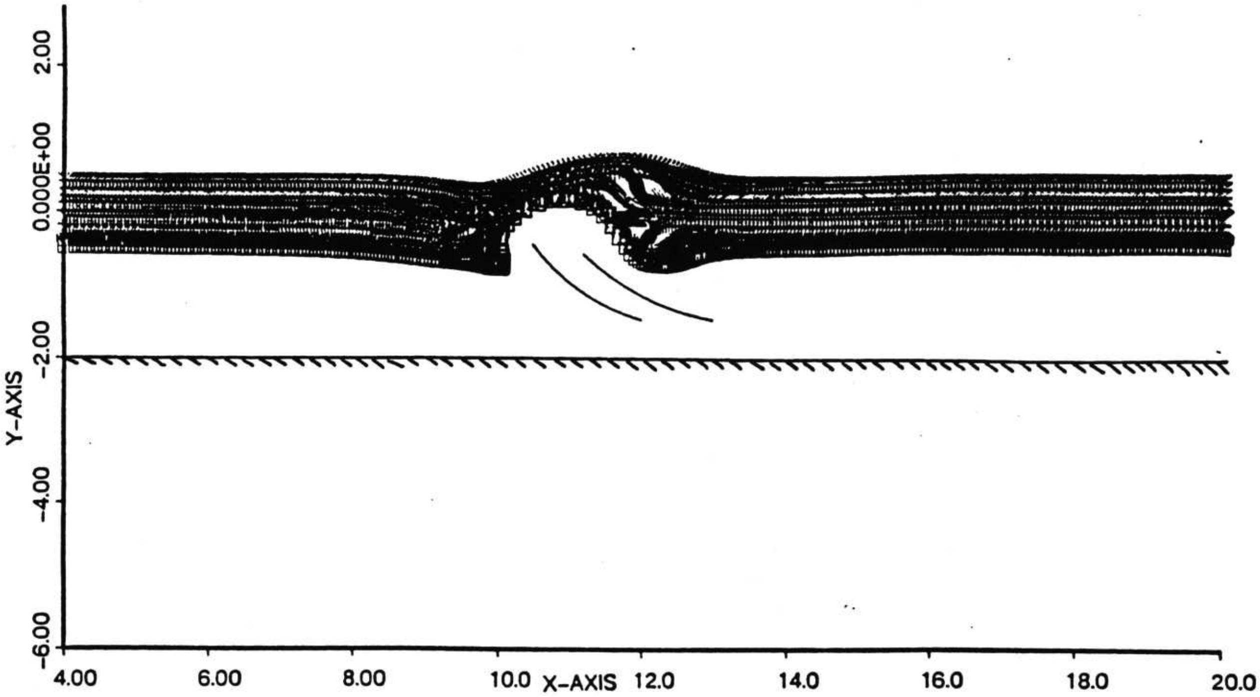

Fig. 68. Disturbed wake and the path of the vortex pair. T=3.0, Γ_2=2.0, c=1.0, mean shear=0.5 (case 6).

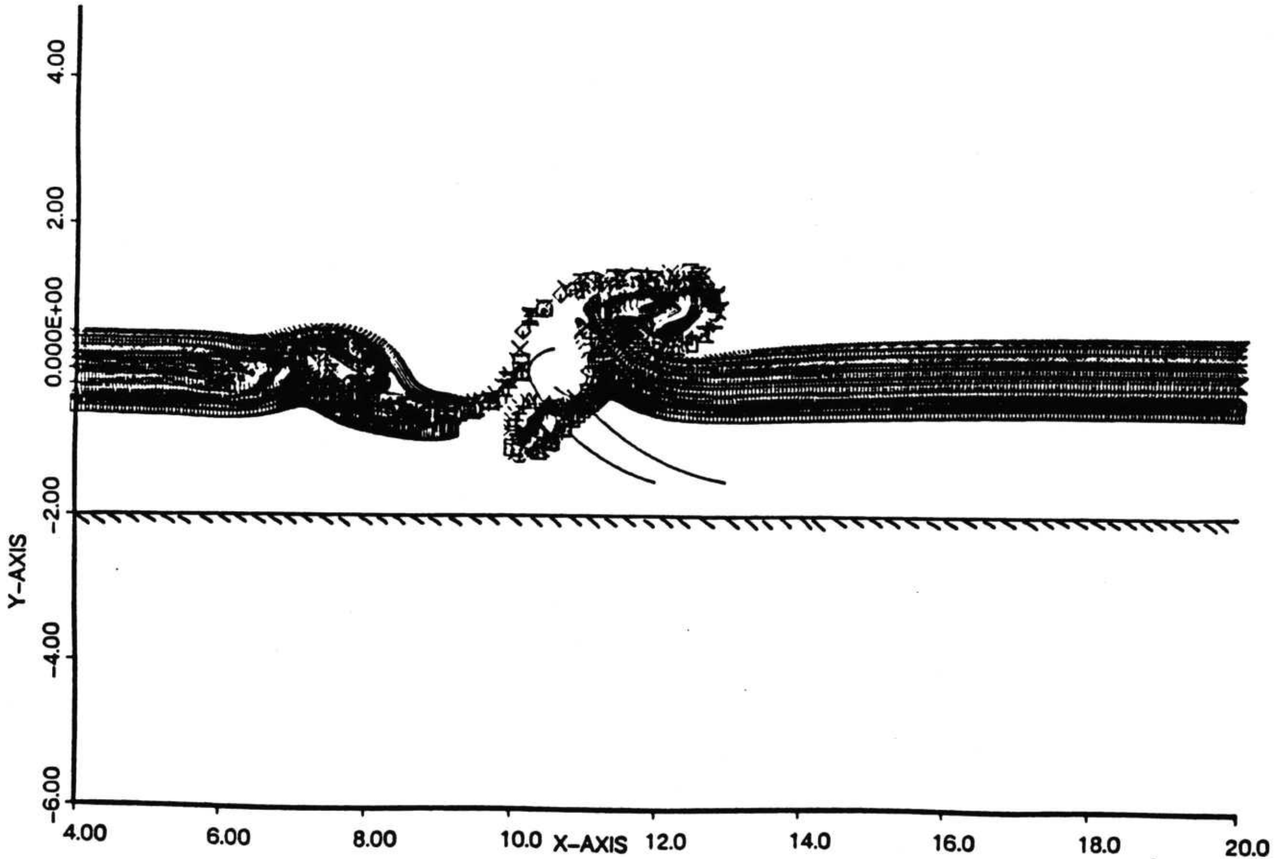

Fig. 69. Disturbed wake and the path of the vortex pair. T=6.0, Γ_2=2.0, c=1.0, mean shear =0.5 (case 6).

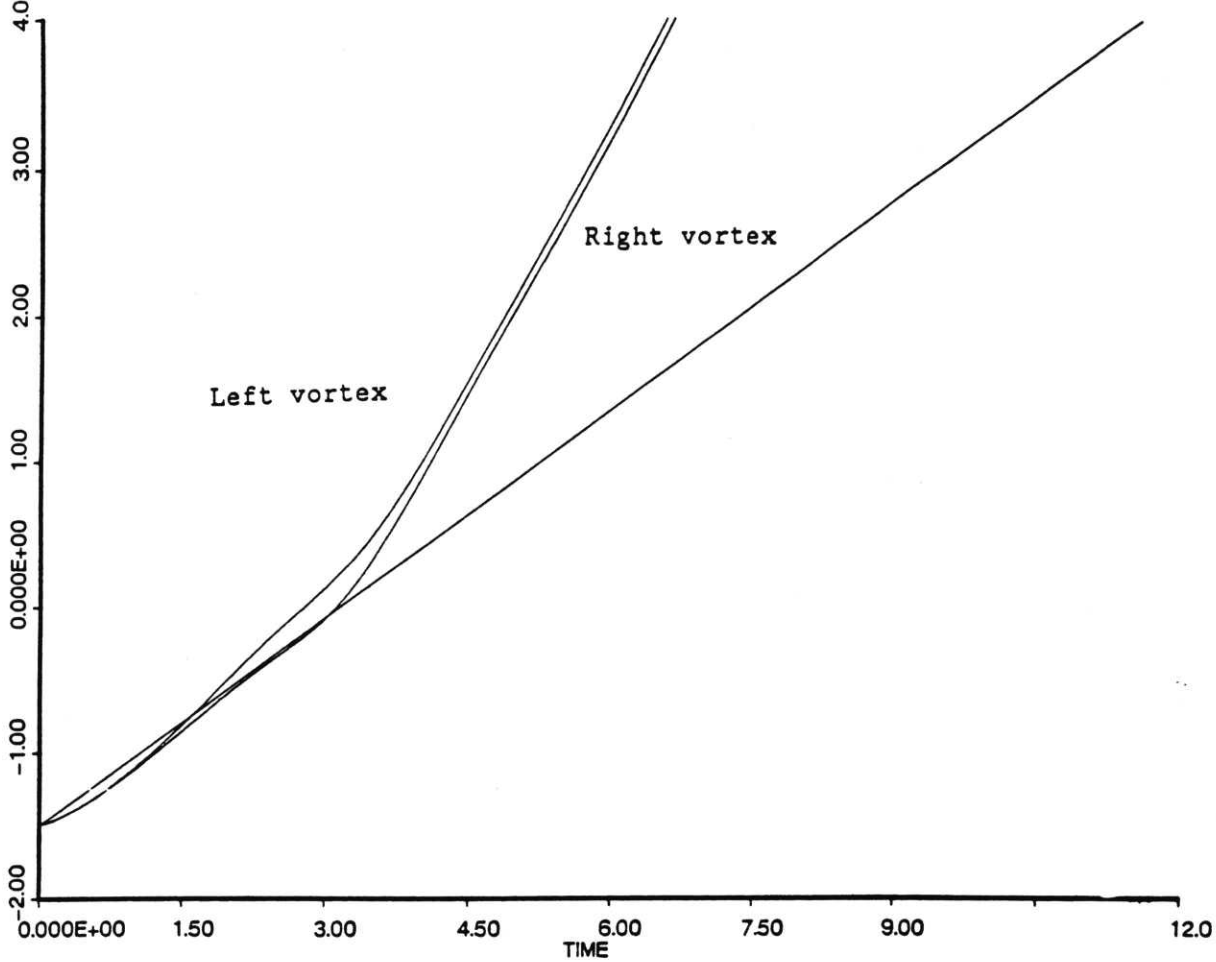

Fig. 69a. Y-coordinate of the vortex pair versus time. Γ_2=3.0, c=1.0, mean shear =0.5 (case 6).

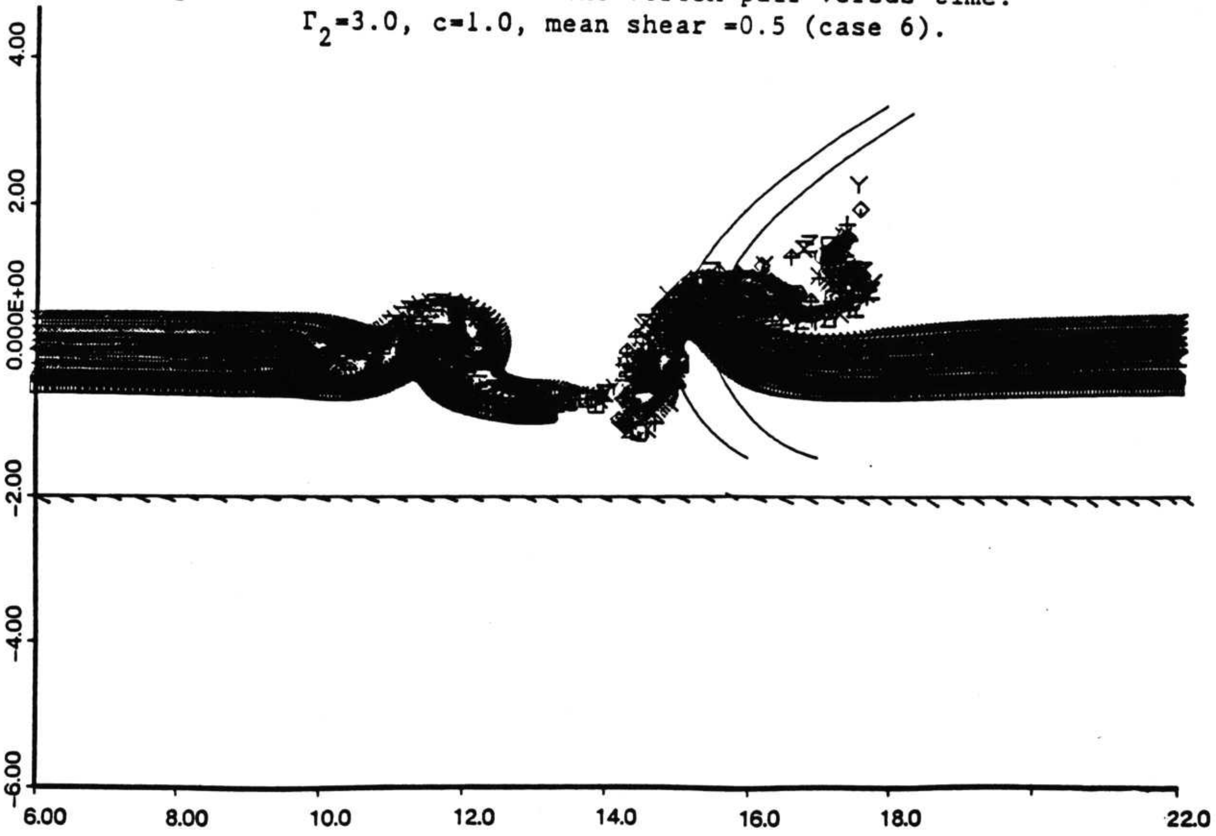

Fig. 69b. Disturbed wake and the path of the vortex pair. T=6.0, Γ_2=3.0, c=1.0, mean shear =0.5 (case 6).

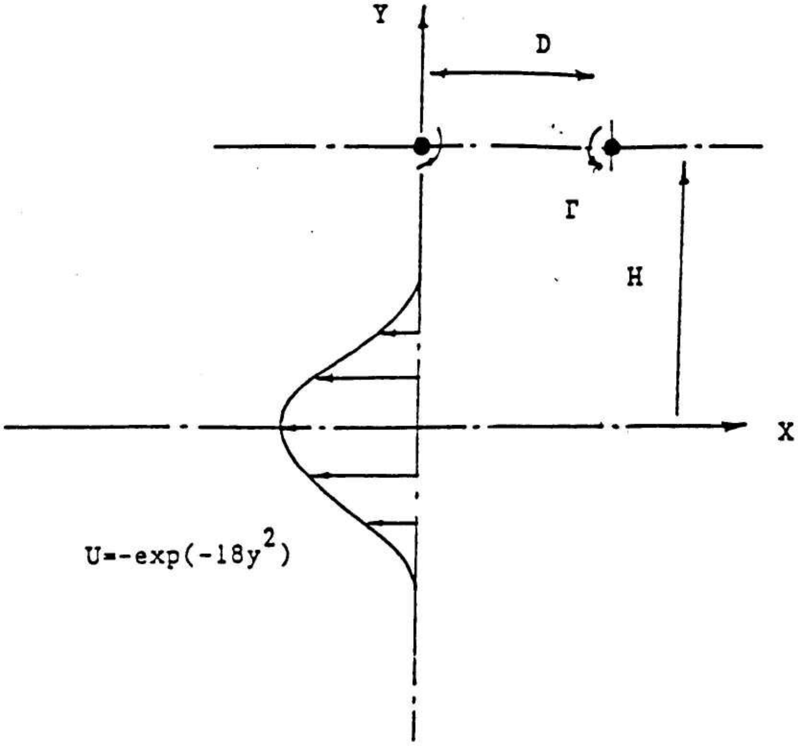

Fig. 70. Velocity profile and vortex locations for the linear theory.

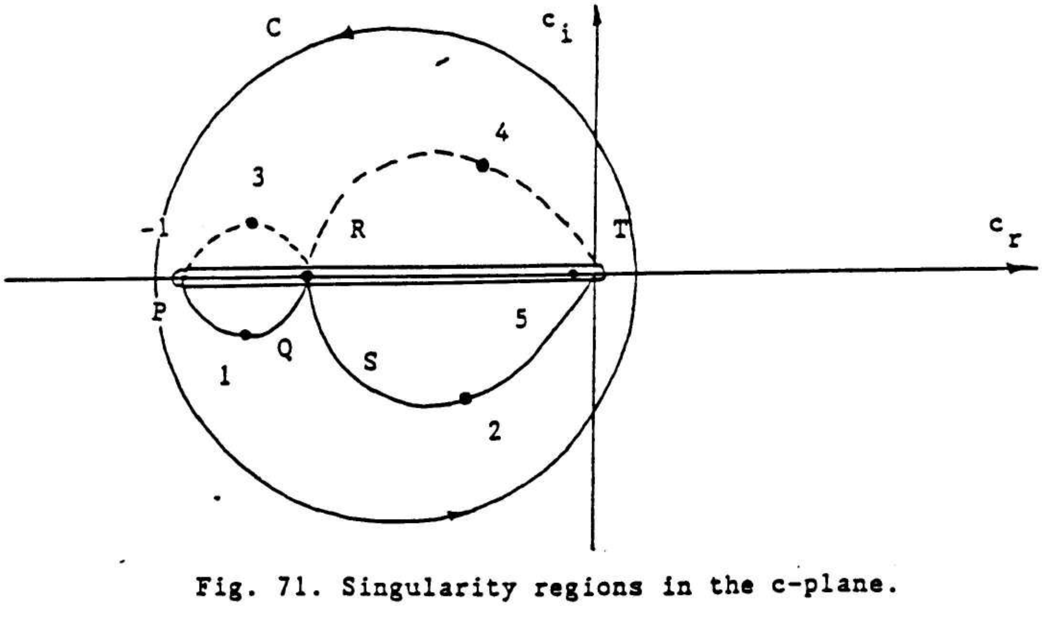

Fig. 71. Singularity regions in the c-plane.

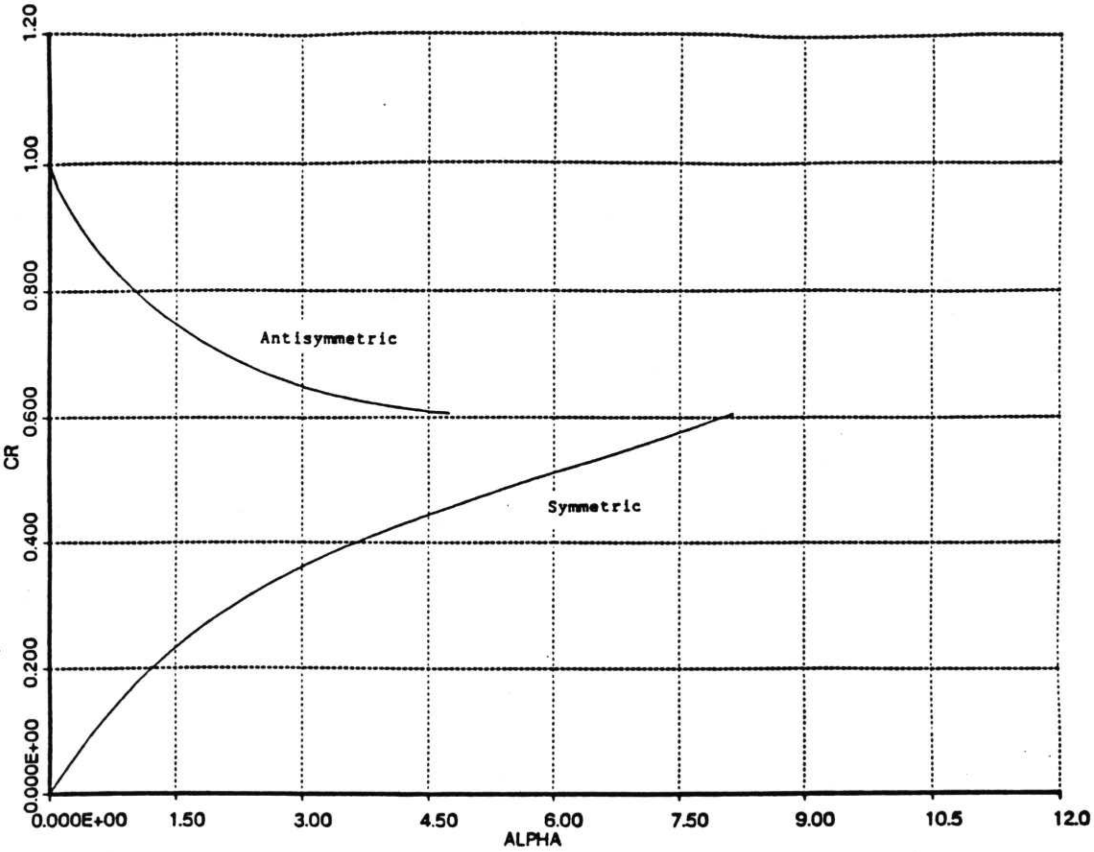

Fig. 72. Eigenvalue diagram for a wake profile $U=\exp(-18y^2)$. Wavenumber versus c_r.

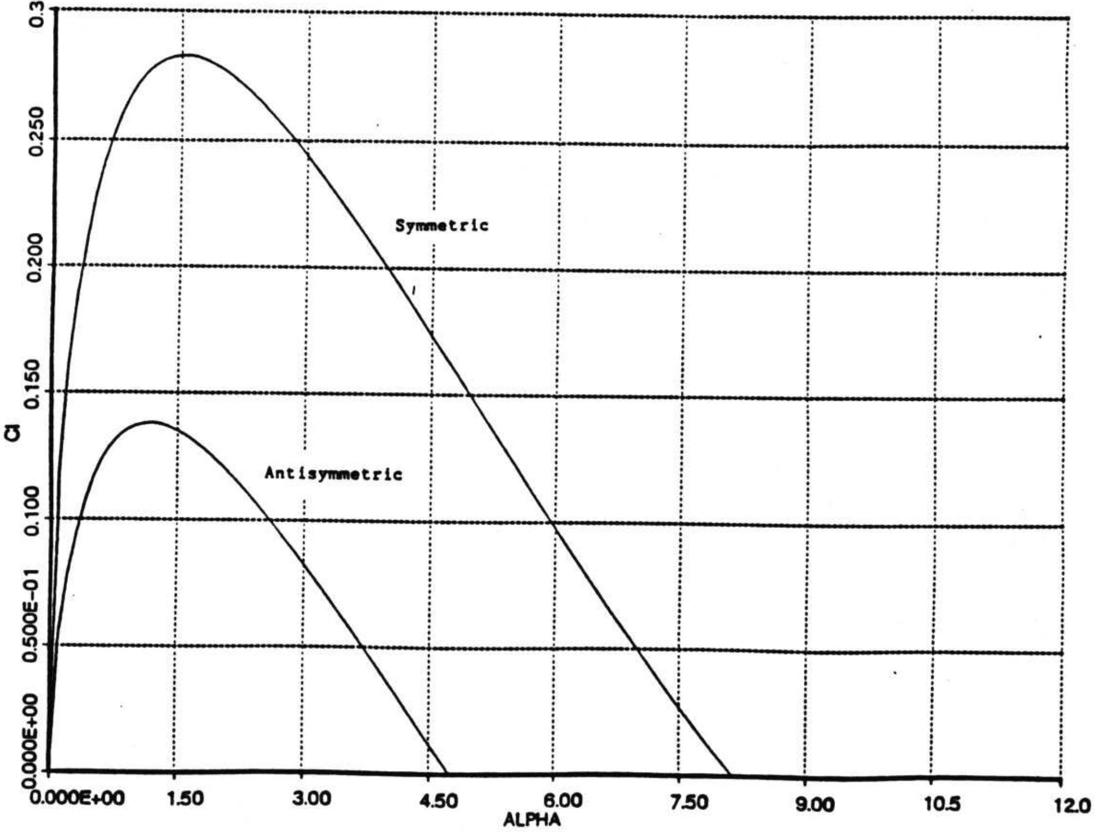

Fig. 73. Wavenumber versus c_i.

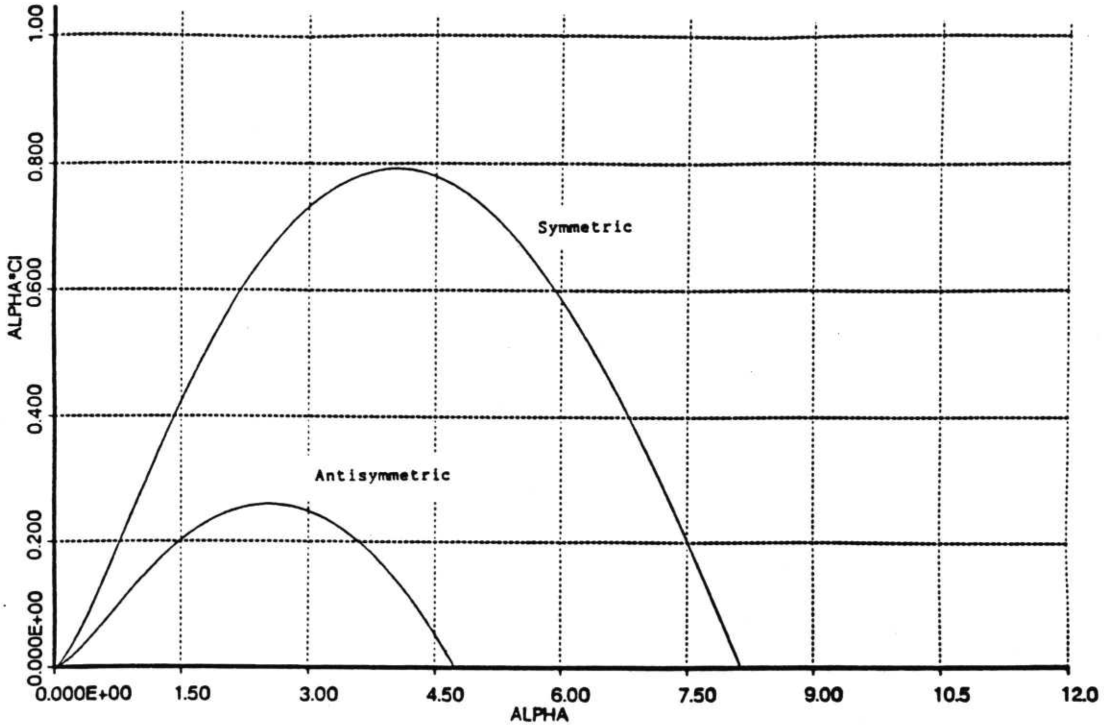

Fig. 74. Wavenumber versus growth rate αc_i.

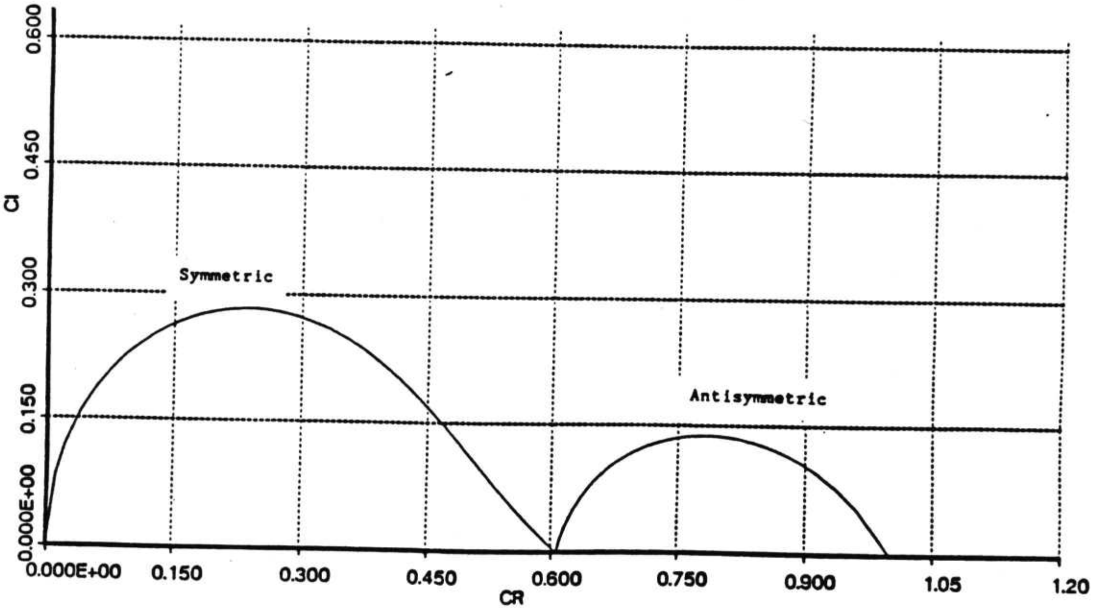

Fig. 75. Real part c_r versus imaginary part c_i.

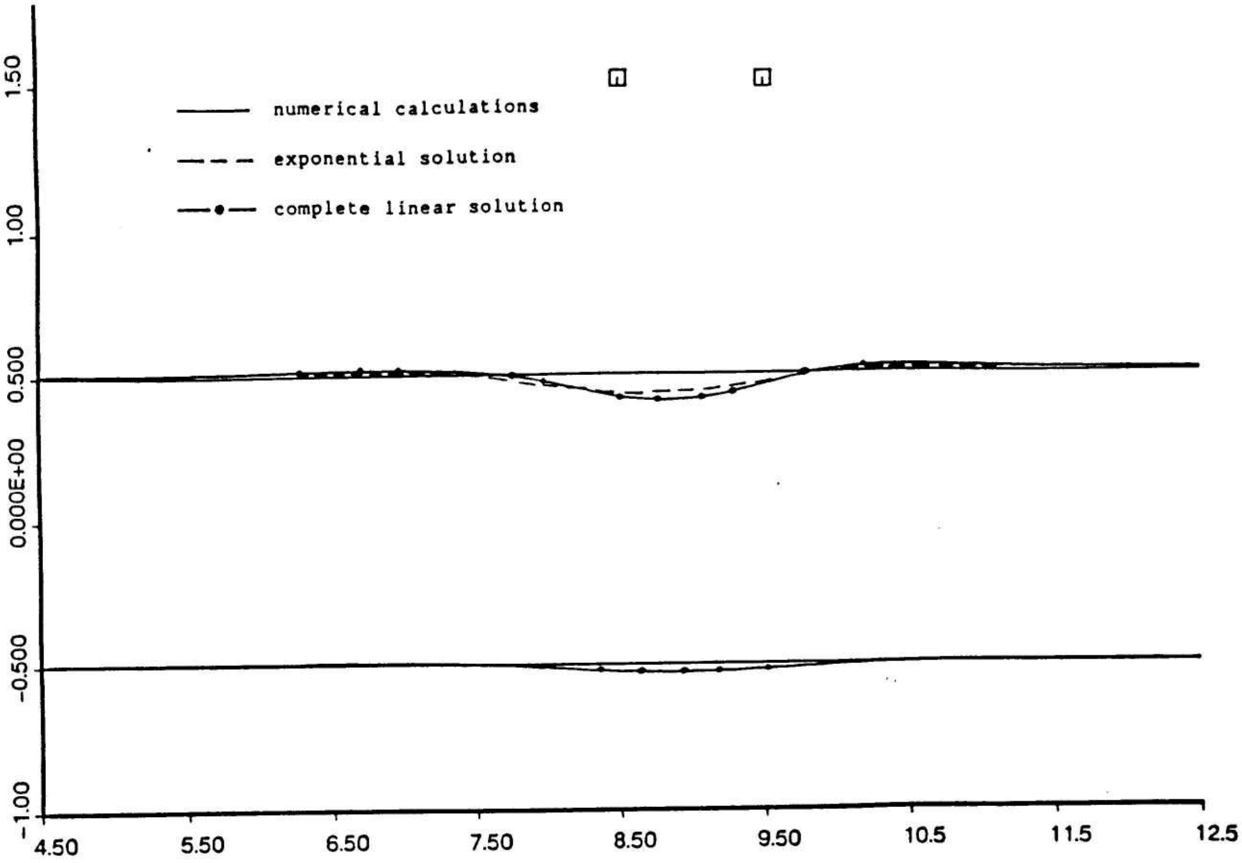

Fig. 76. Comparison between linear theory and CIC method. Time=1.5, Γ_2=0.5, D=1.0.

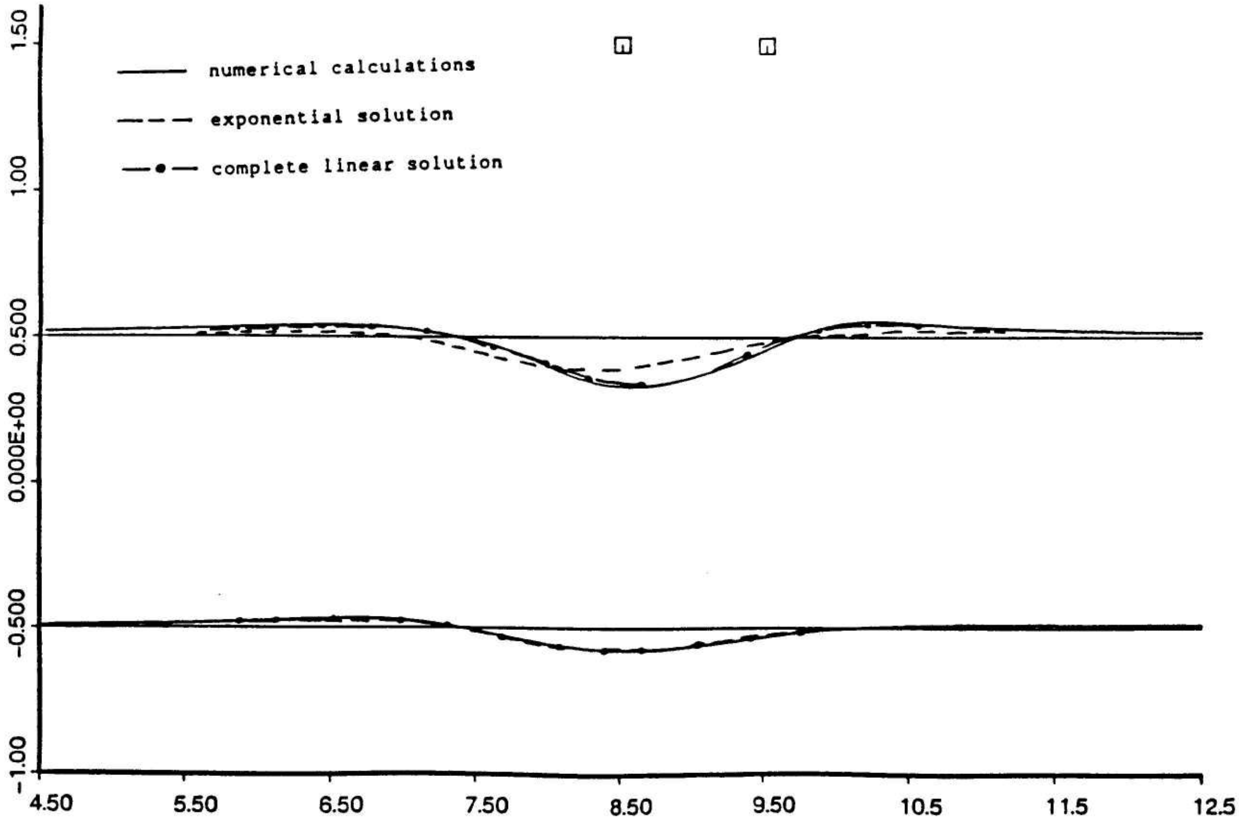

Fig. 77. Comparison between linear theory and CIC method. Time=3.0, Γ_2=0.5, D=1.0.

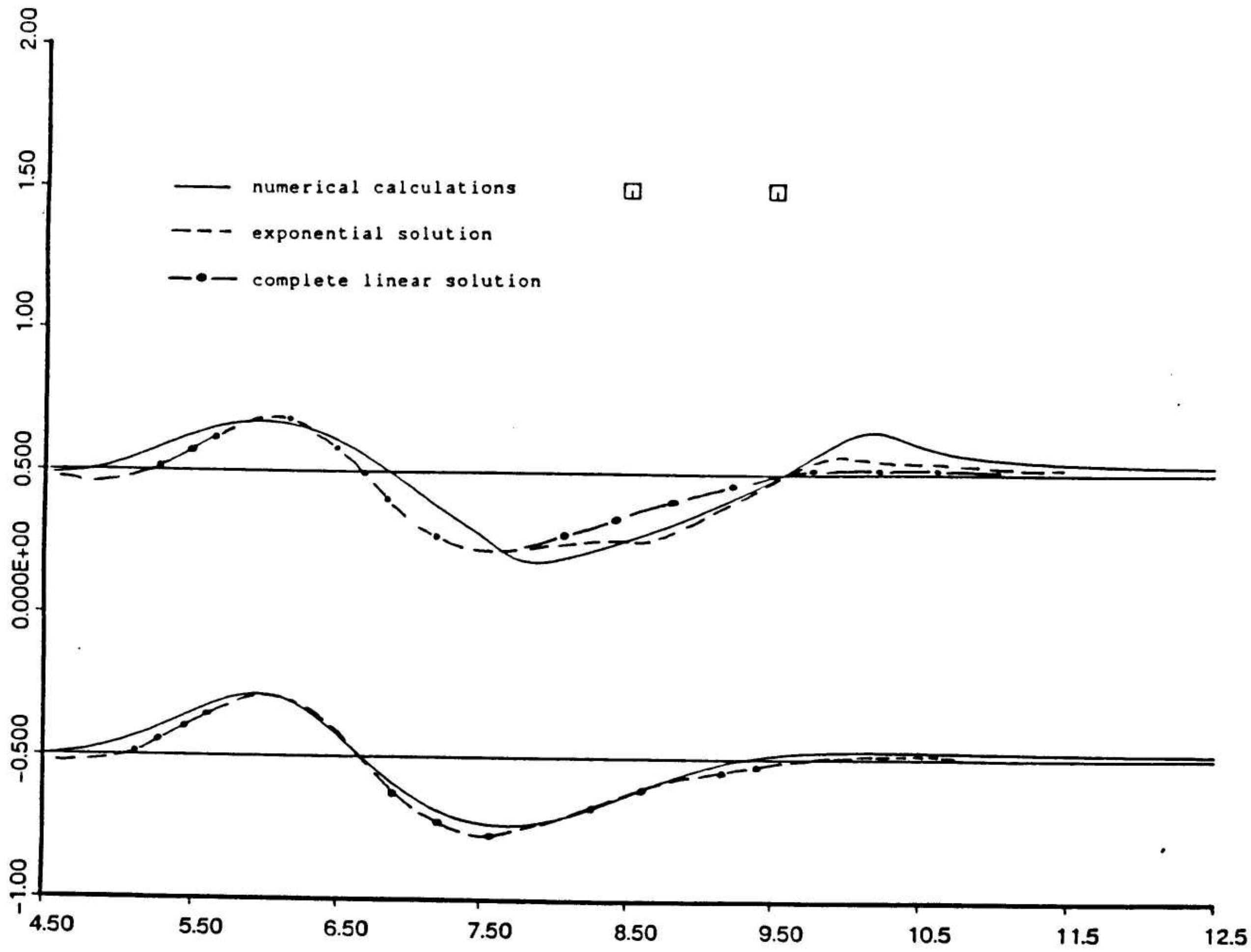

Fig. 78. Comparison between linear theory and CIC method. Time=6.0, Γ_2=0.5, D=1.0.

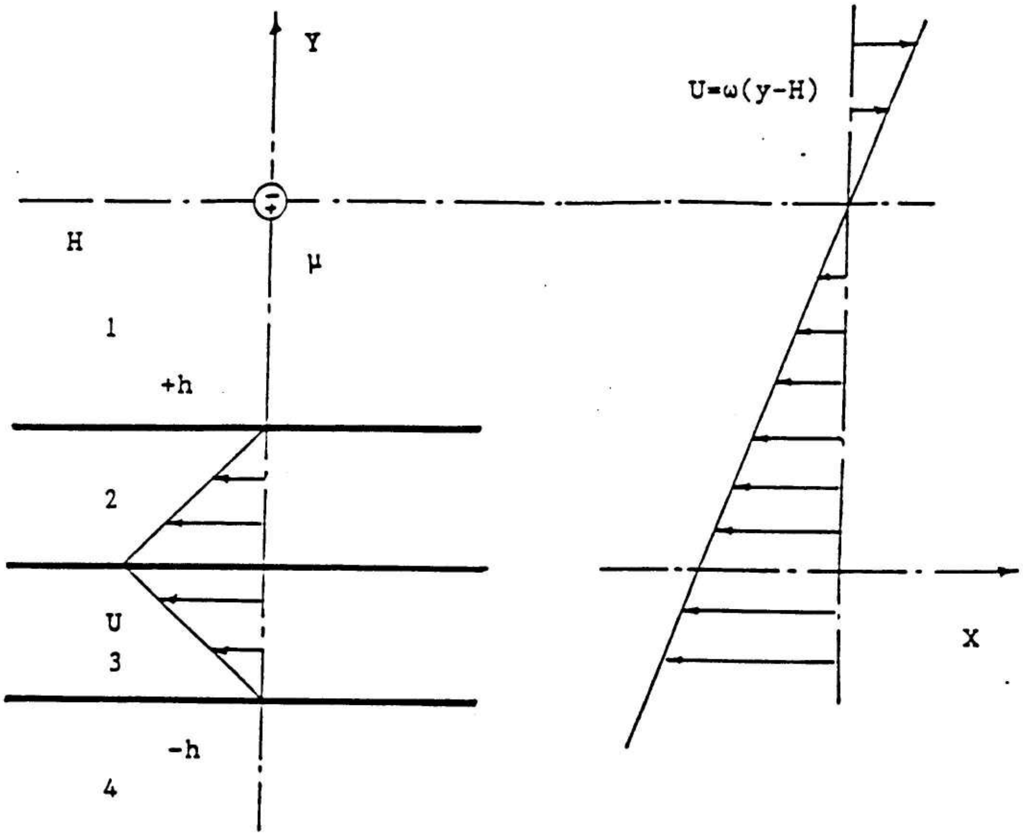

Fig. 79. Flow model for 3-D linear analysis.

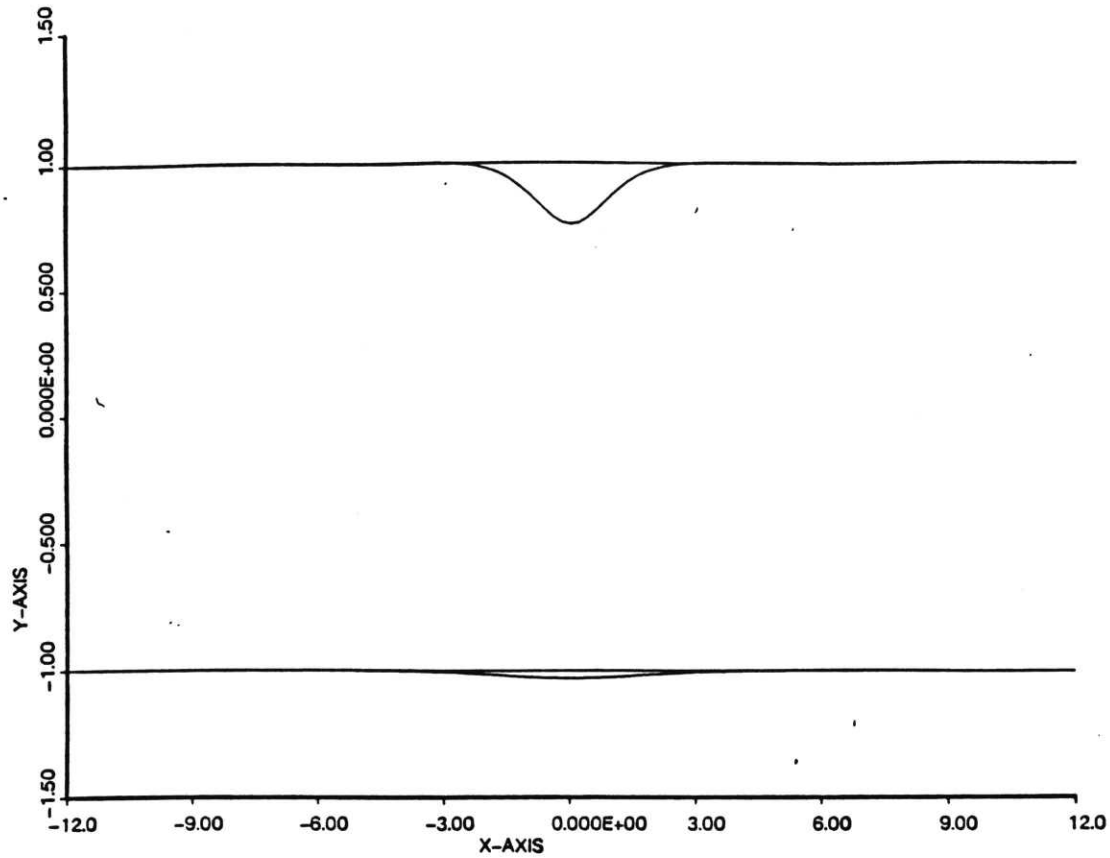

Fig. 80. Upper and lower edges of the wake.
Time=12.0, wake strength=0.0, mean shear=0.0.

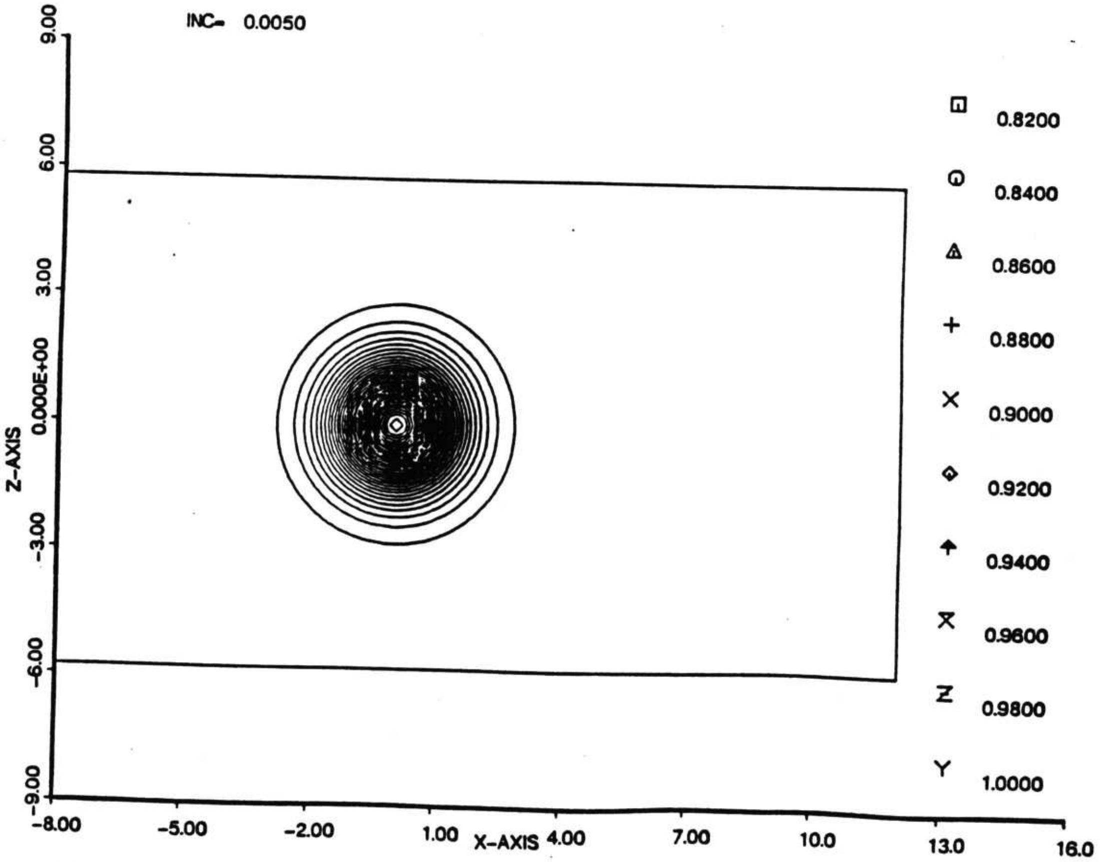

Fig. 81. Contour levels of the upper surface $\eta_a(x,z,t)$.
Time=12.0, wake strength=0.0, mean shear=0.0.

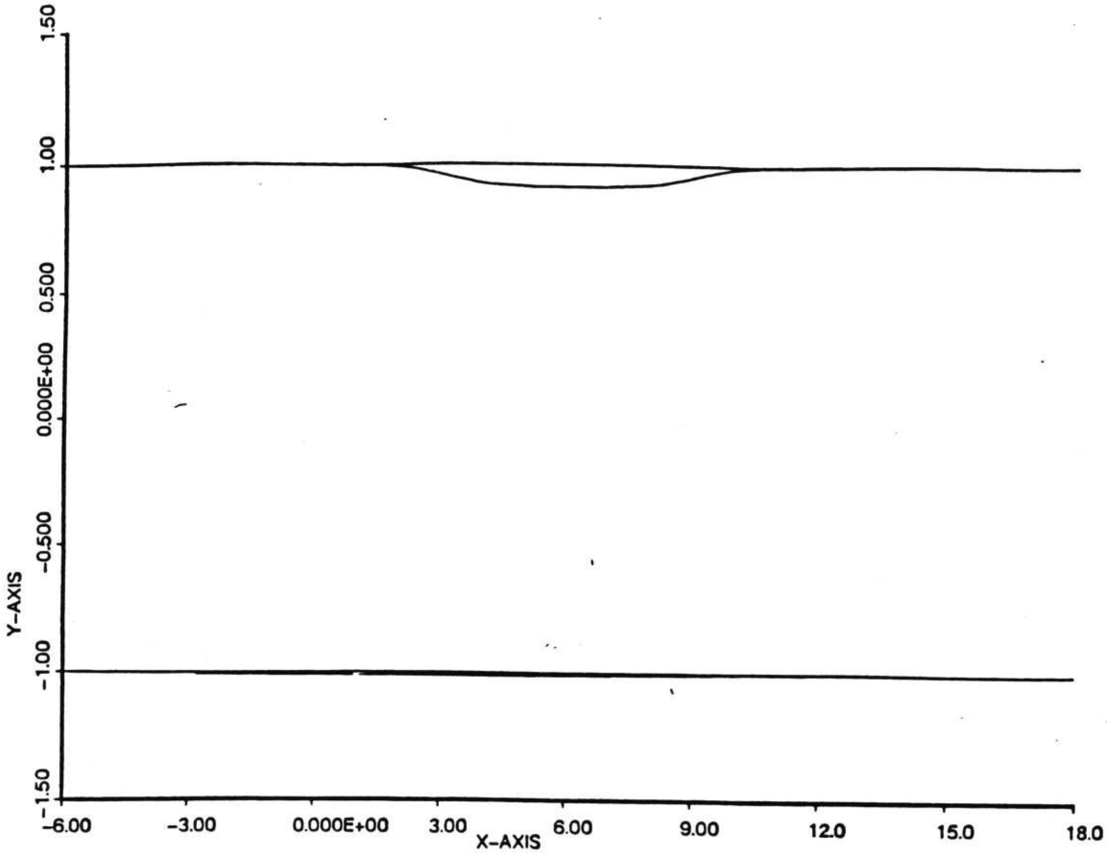

Fig. 82. Upper and lower edges of the wake $\eta_a(x,0,t)$, $\eta_c(x,0,t)$. Time=12.0, wake strength=0.0, mean shear=0.25.

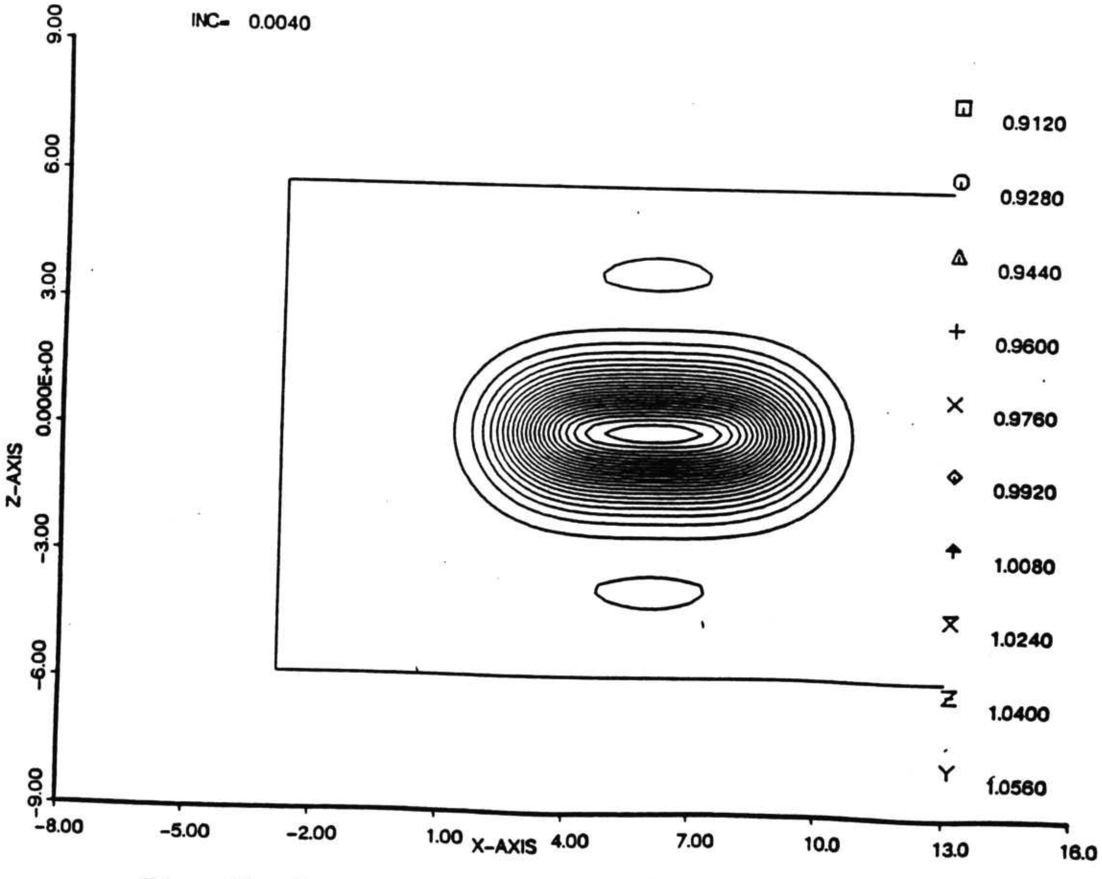

Fig. 83. Contour levels of the upper surface $\eta_a(x,z,t)$. Time=12.0, wake strength=0.0, mean shear=0.25.

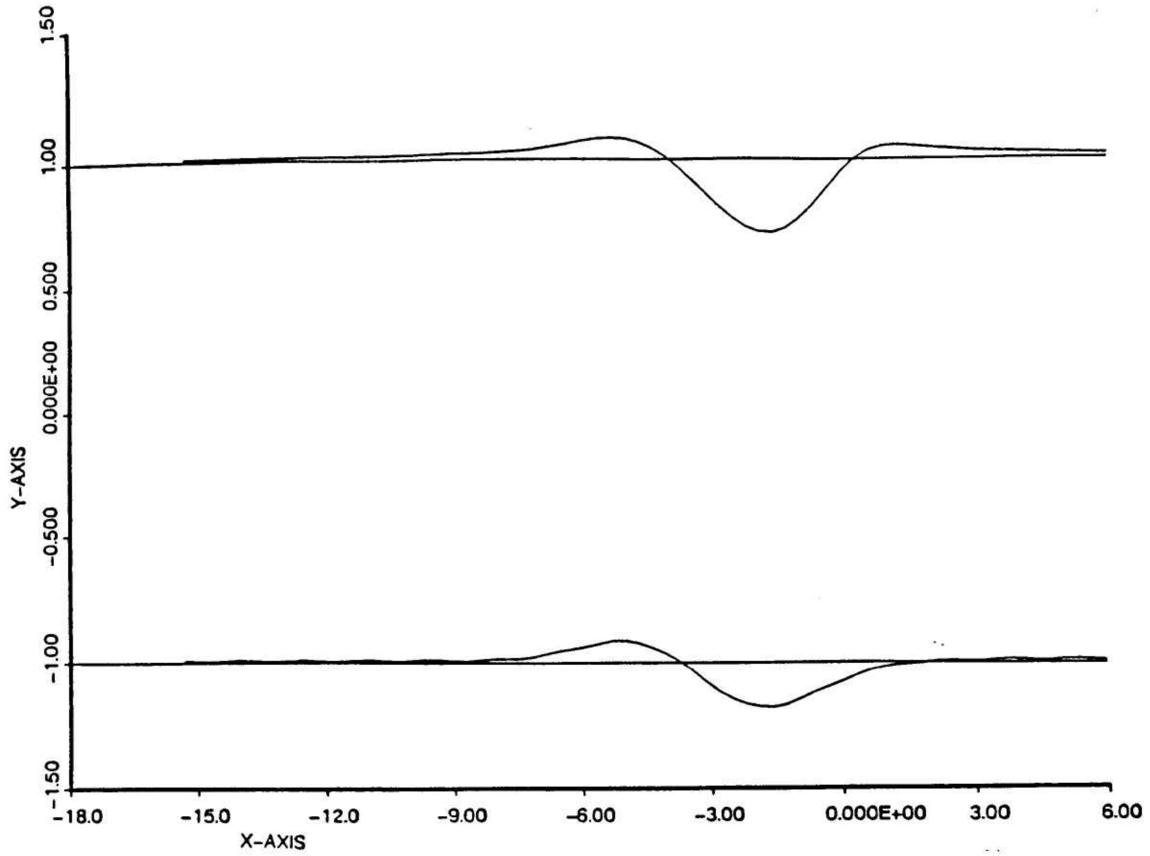

Fig. 84. Upper and lower edges of the wake for the 2-D case. Time=9.0, mean shear=0.0.

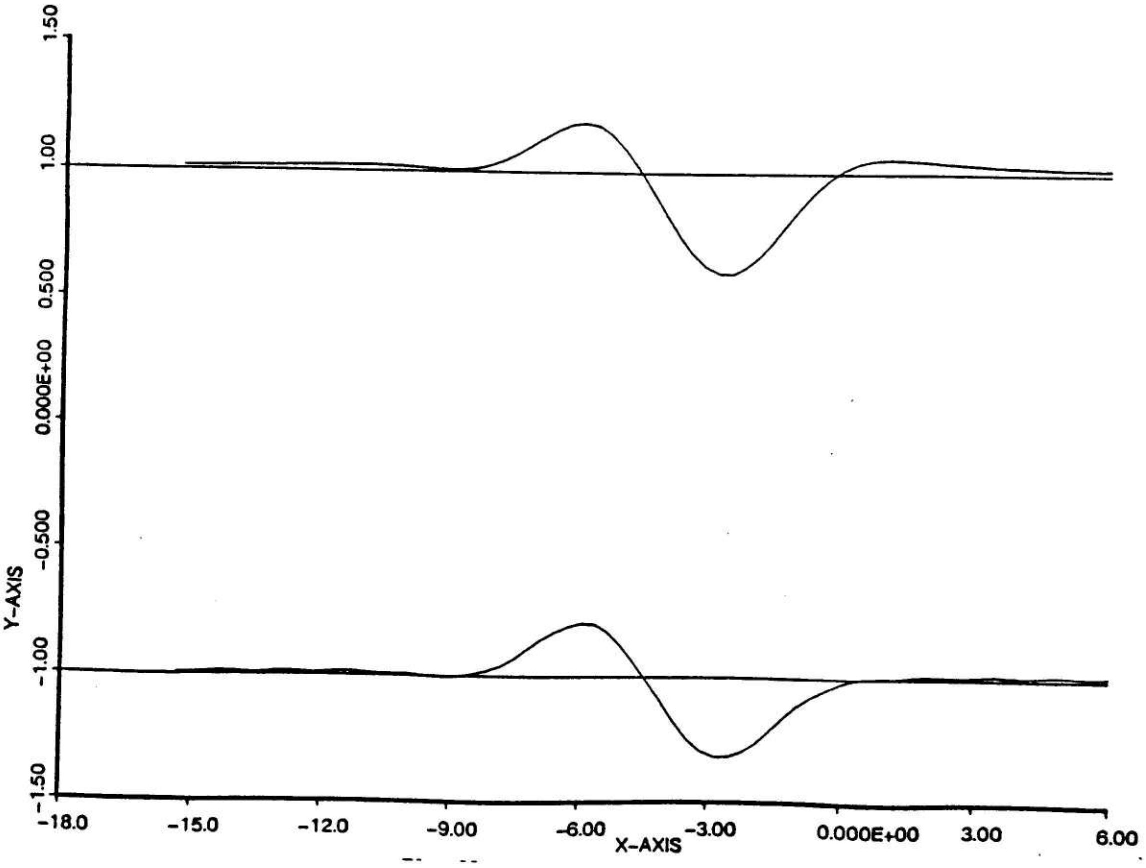

Fig. 85. Upper and lower edges of the wake for the 2-D case. Time=12.0, mean shear=0.0.

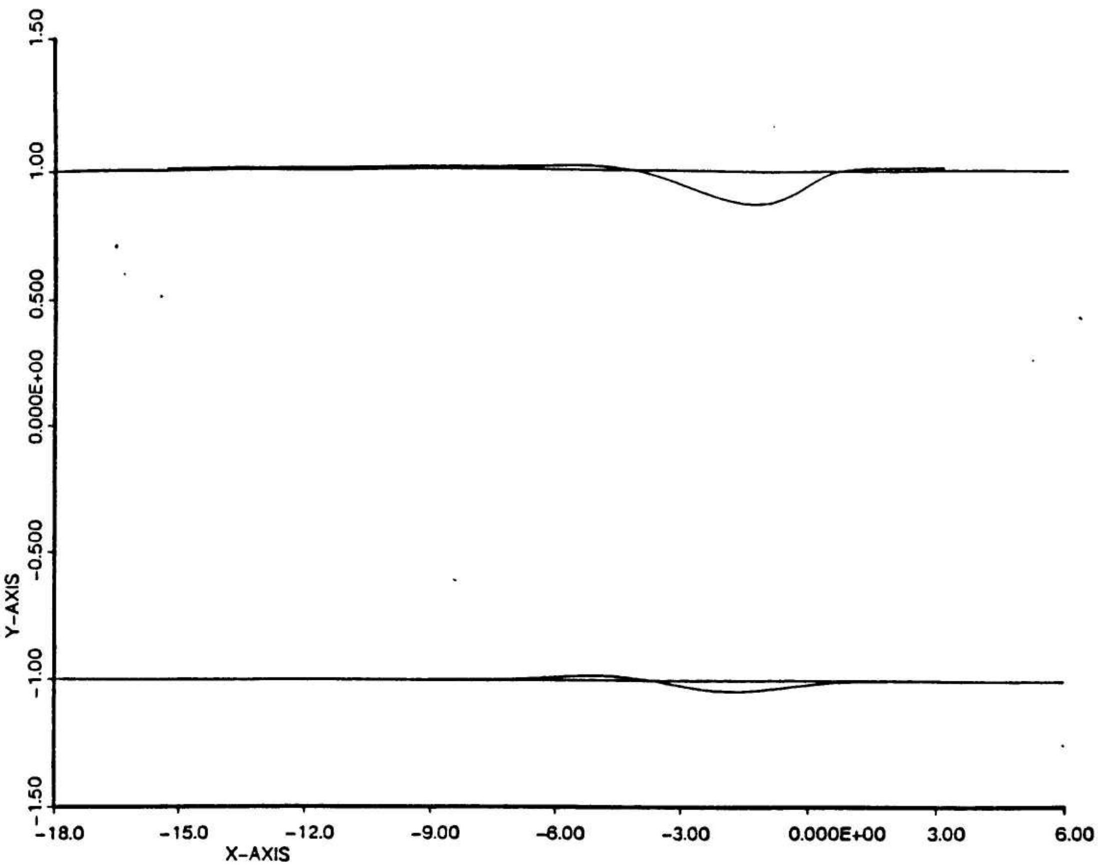

Fig. 86. Upper and lower edges of the wake $\eta_a(x,o,t)$, $\eta_c(x,0,t)$ for the 3-D case. Time=9.0, mean shear=0.0.

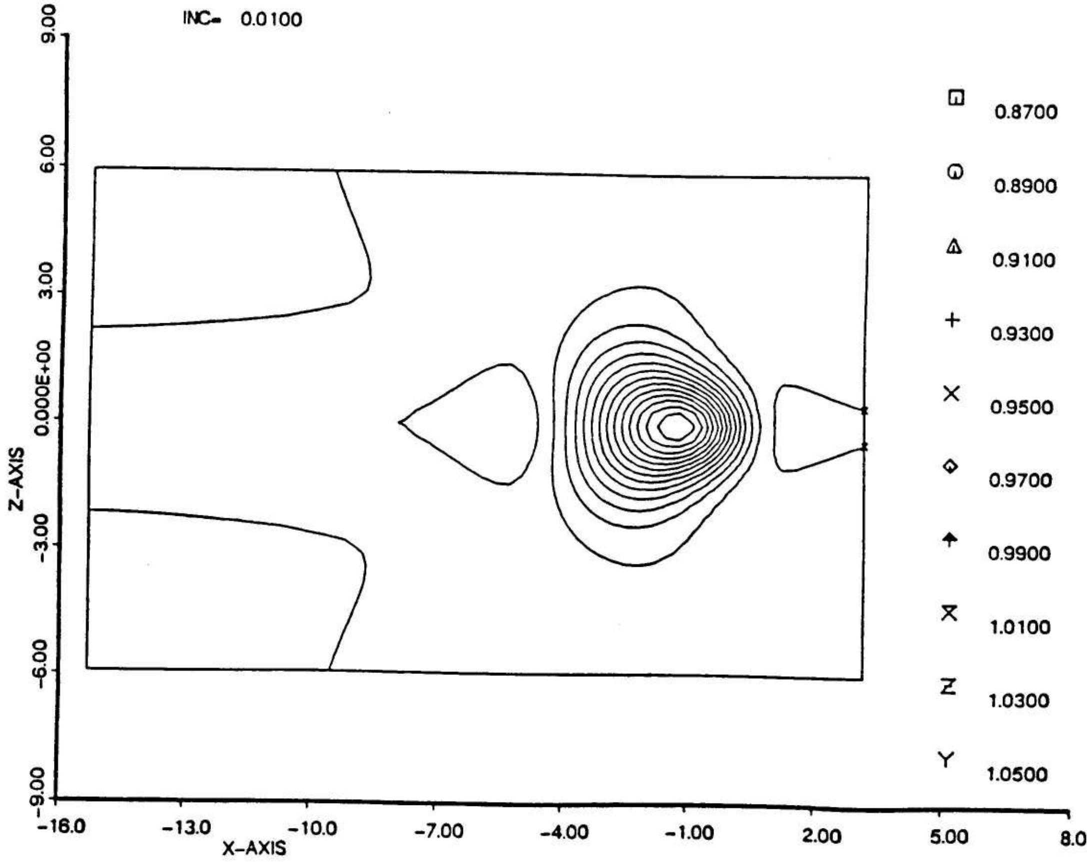

Fig. 87. Contour levels of the upper surface $\eta_a(x,z,t)$. Time=9.0, mean shear=0.0.

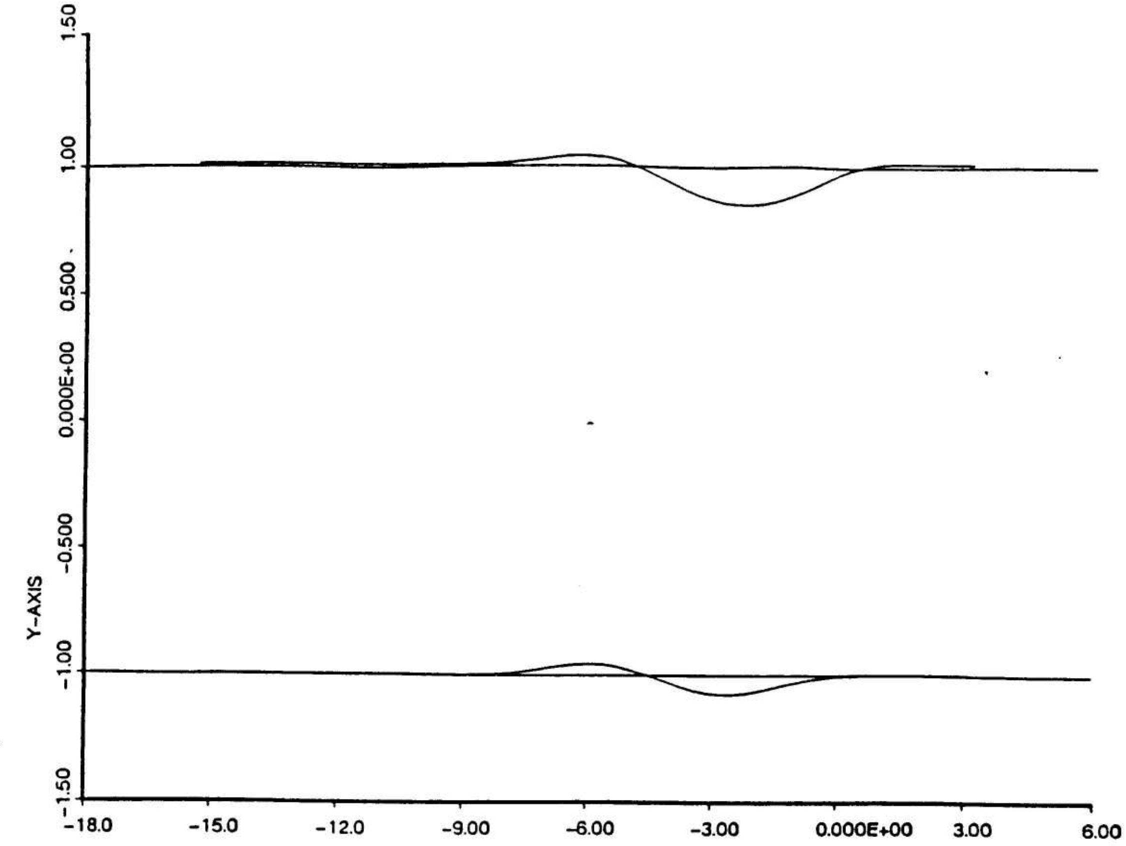

Fig. 88. Upper and lower edges of the wake $\eta_a(x,0,t)$, $\eta_c(x,0,t)$ for the 3-D case. Time=12.0, mean shear=0.0.

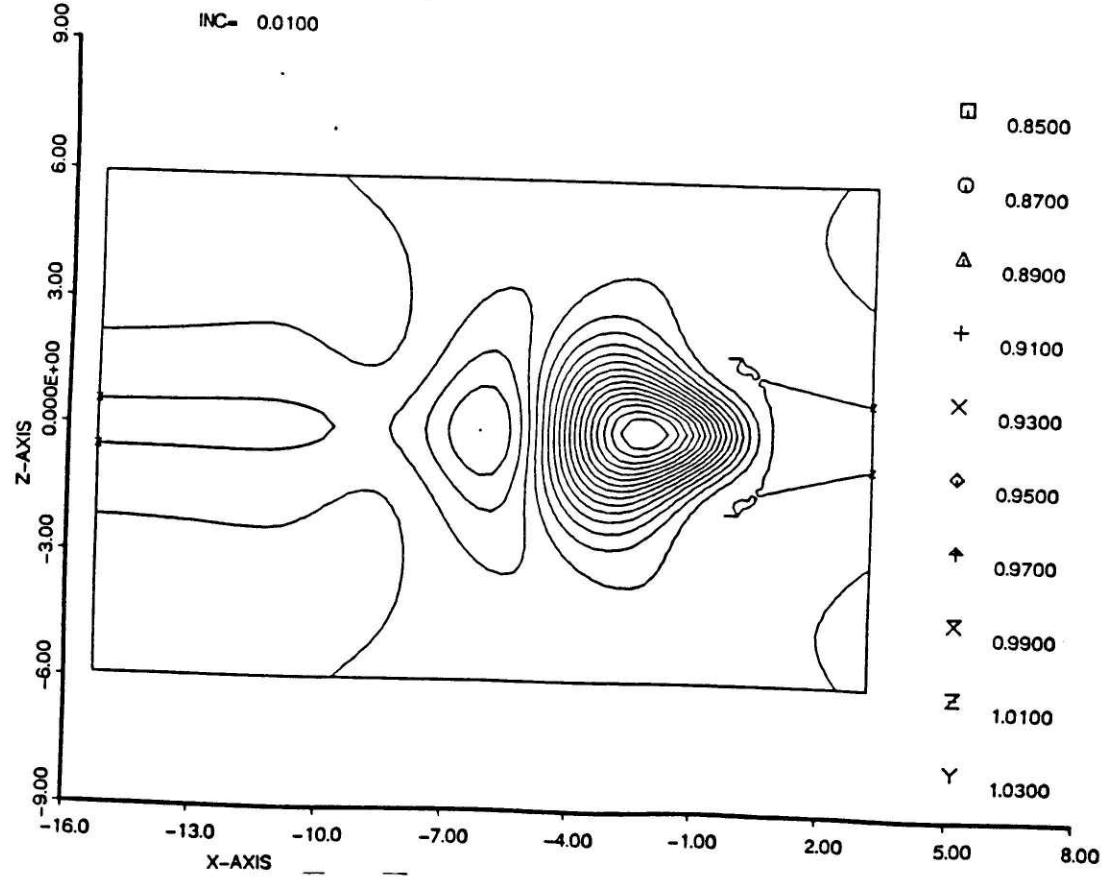

Fig. 89. Contour levels of the upper surface $\eta_a(x,z,t)$. Time=12.0, mean shear=0.0.

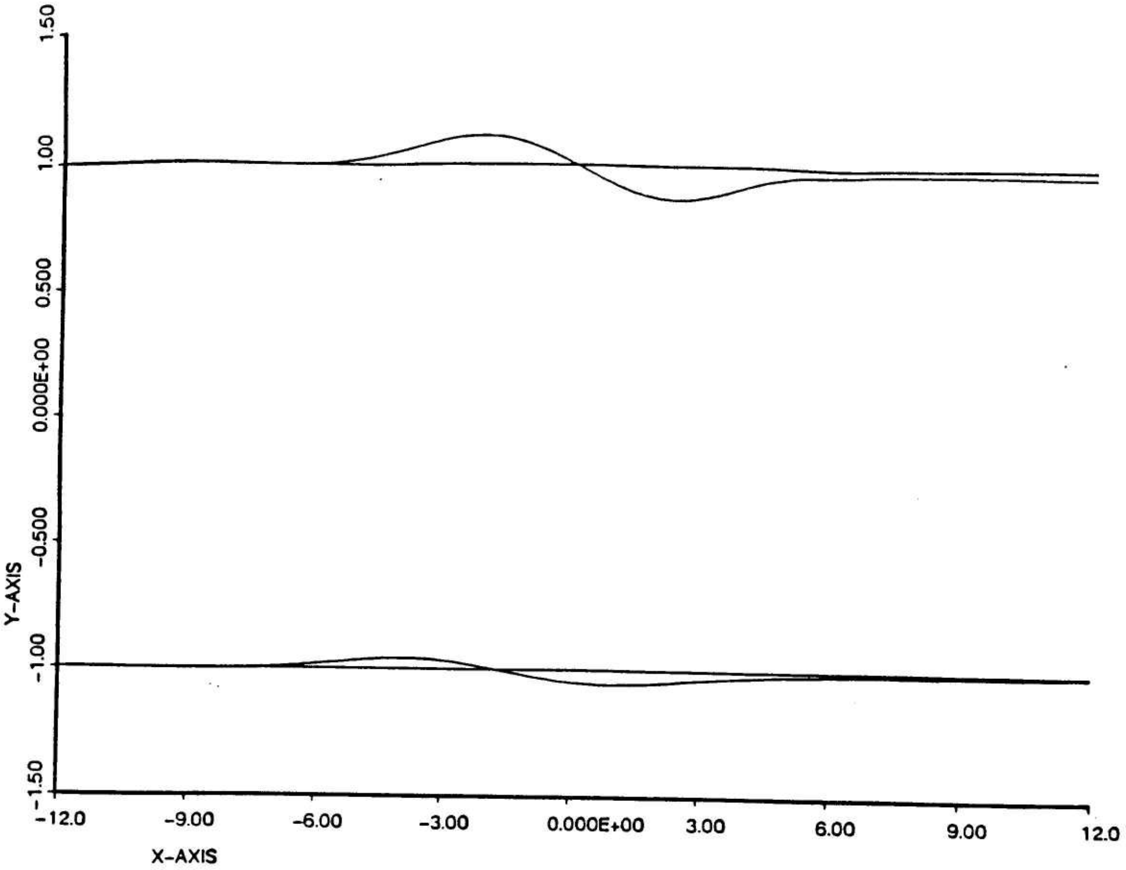

Fig. 90. Upper and lower edges of the wake for the 2-D case. Time=9.0, mean shear=0.5.

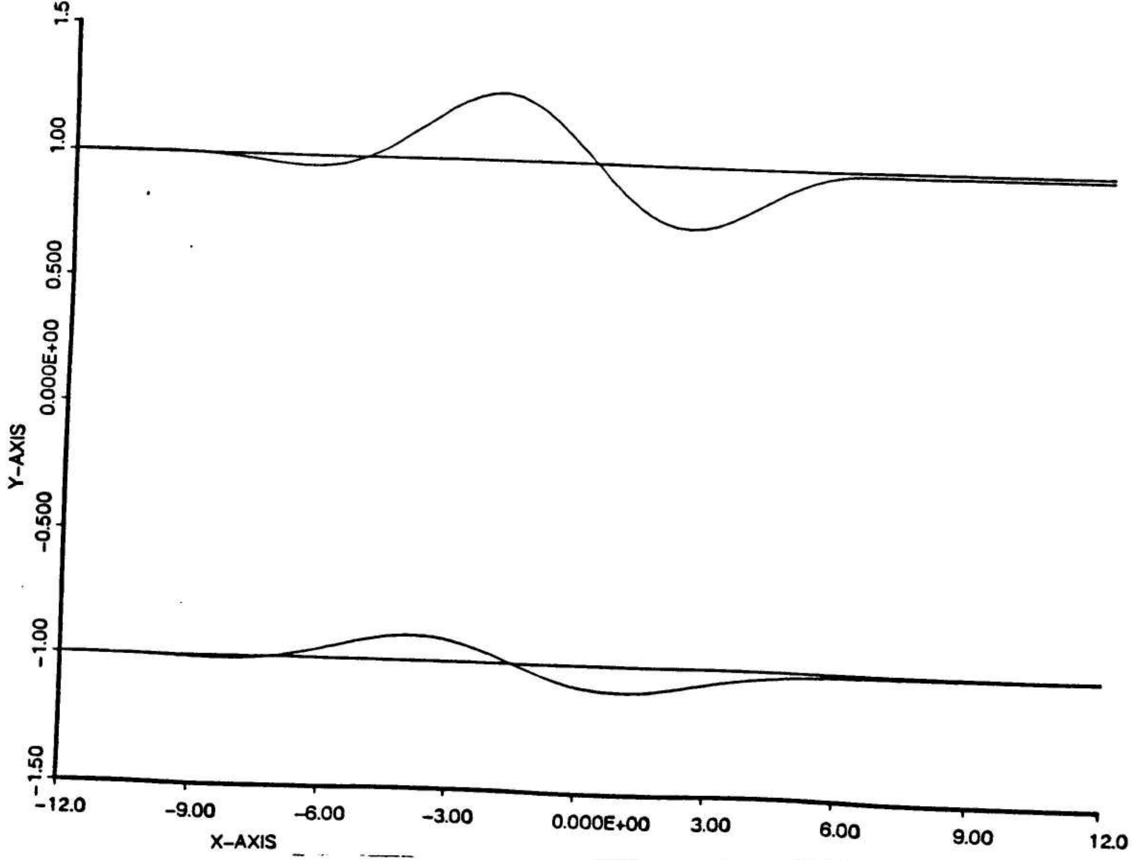

Fig. 91. Upper and lower edges of the wake for 2-D case. Time=12.0, mean shear=0.0.

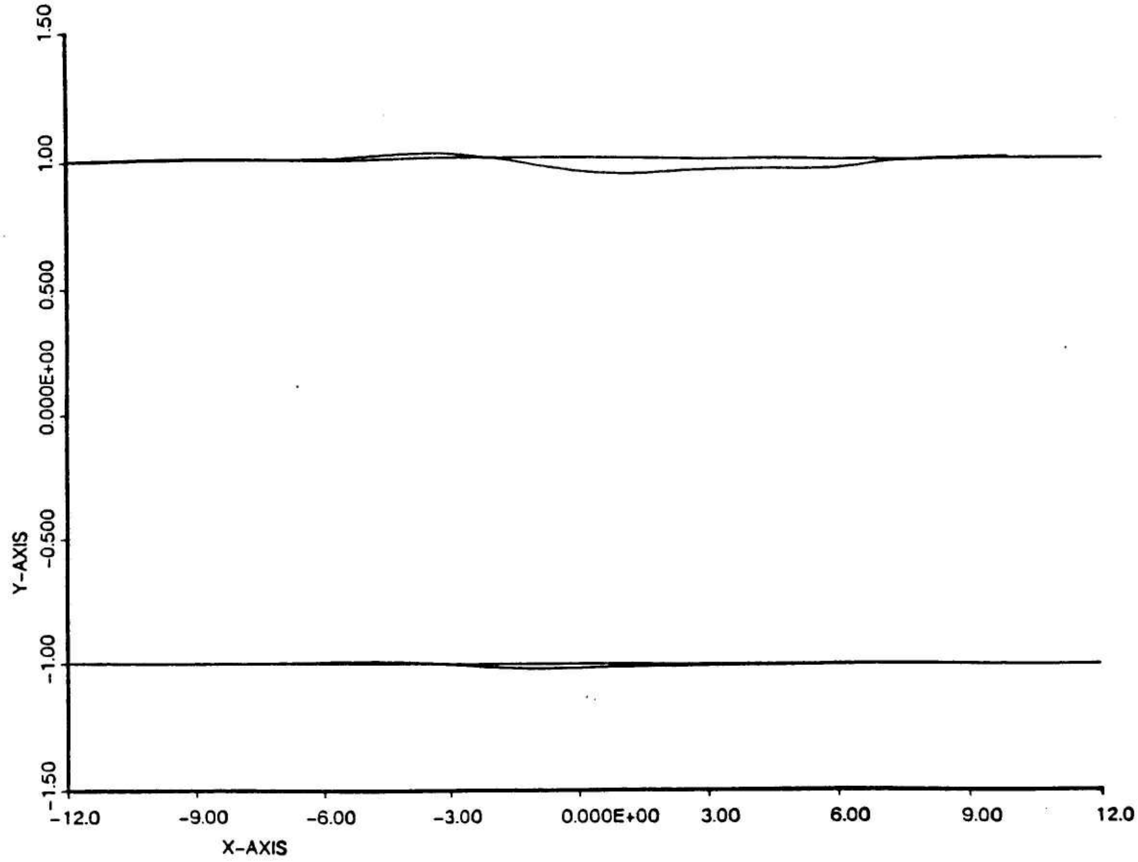

Fig. 92. Upper and lower edges of the wake $\eta_a(x,0,t)$, $\eta_c(x,0,t)$ for the 3-D case. Time=9.0, mean shear=0.25.

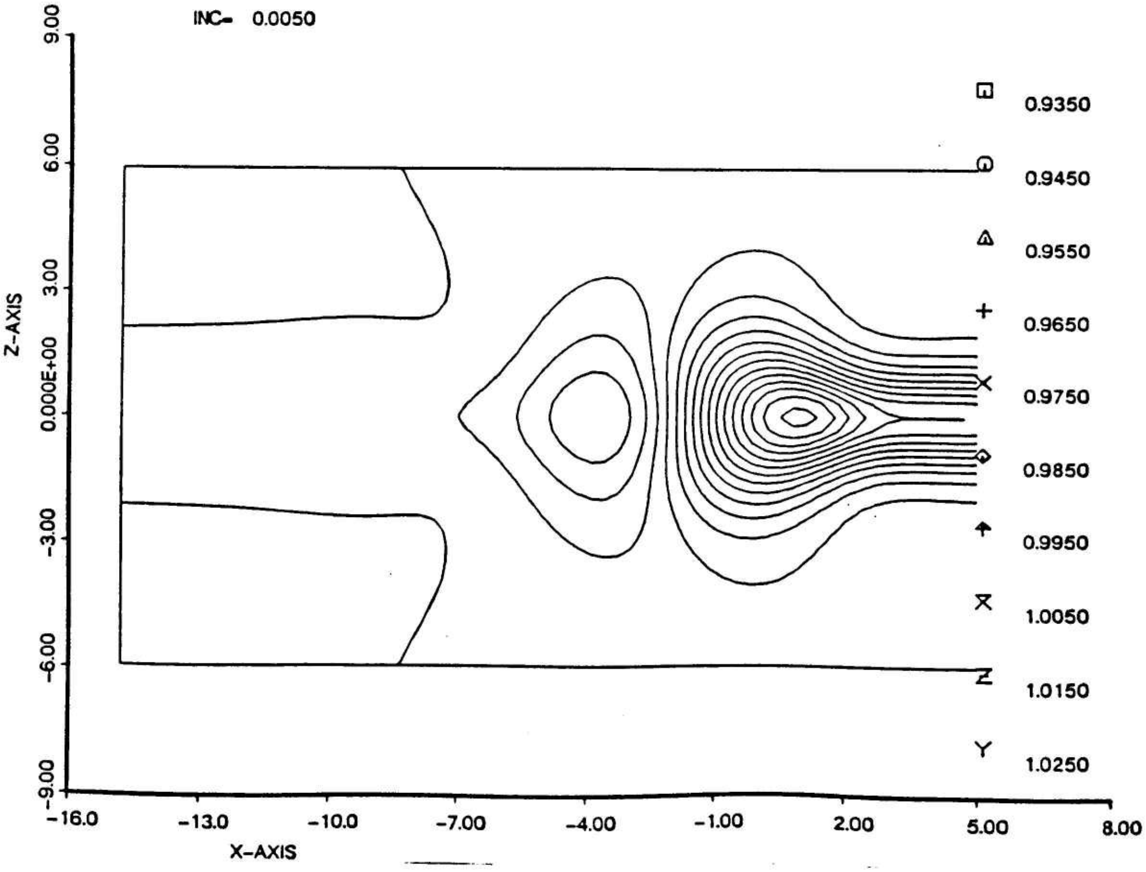

Fig. 93. Contour levels of the upper surface $\eta_a(x,z,t)$. Time=9.0, mean shear=0.25.

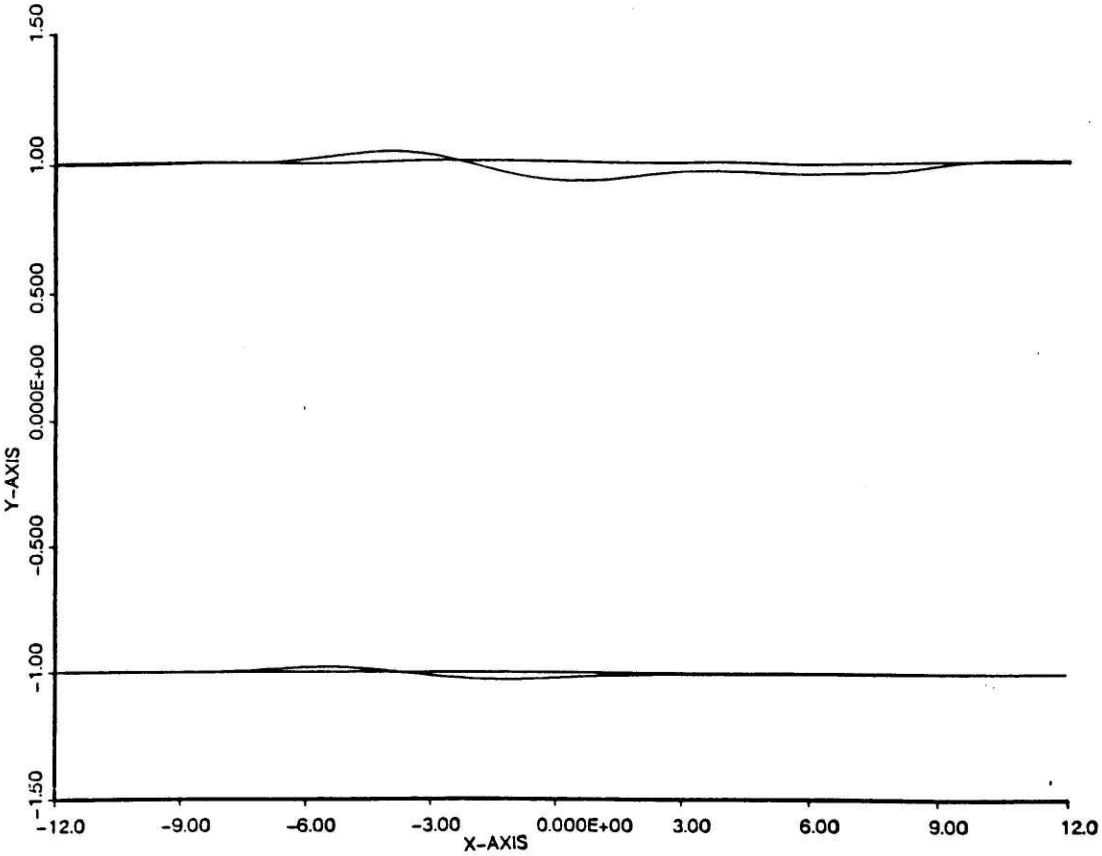

Fig. 94. Upper and lower edges of the wake $\eta_a(x,0,t)$, $\eta_c(x,0,t)$ for the 3-D case. Time=12.0, mean shear=0.25.

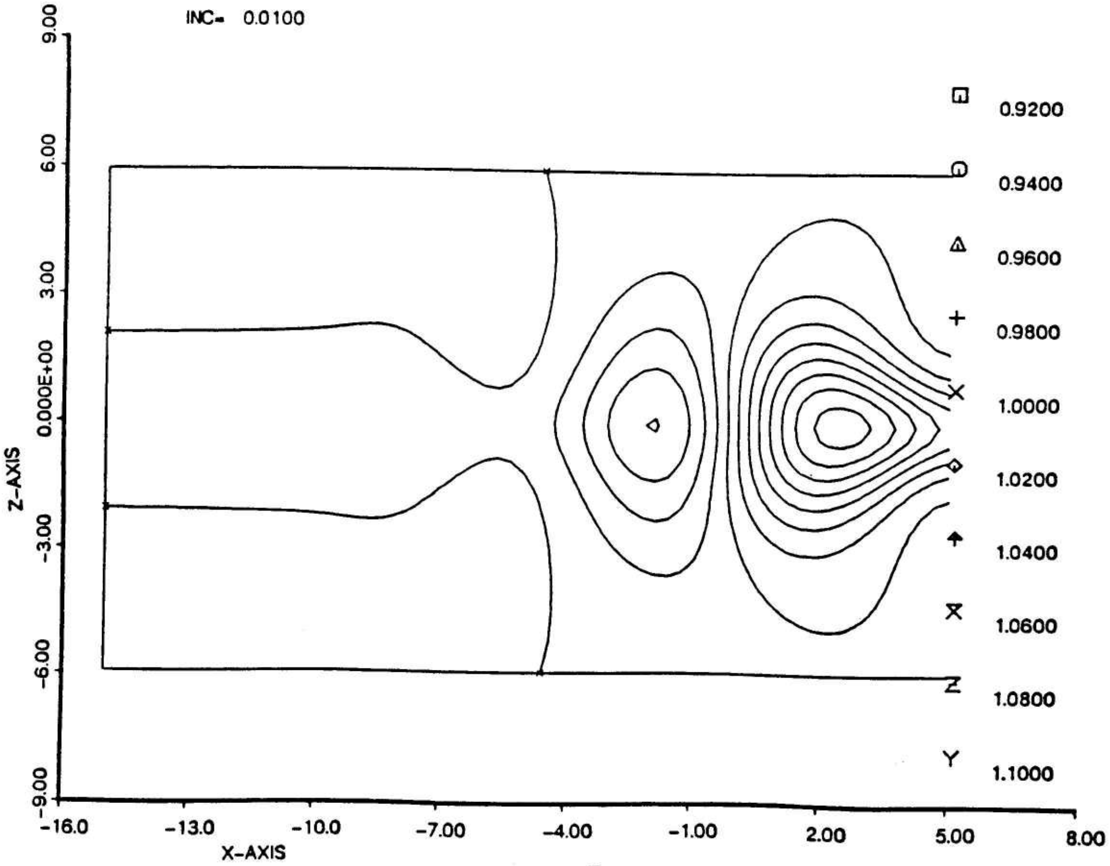

Fig. 95. Contour levels of the upper surface $\eta_a(x,z,t)$. Time=12.0, mean shear=0.25.

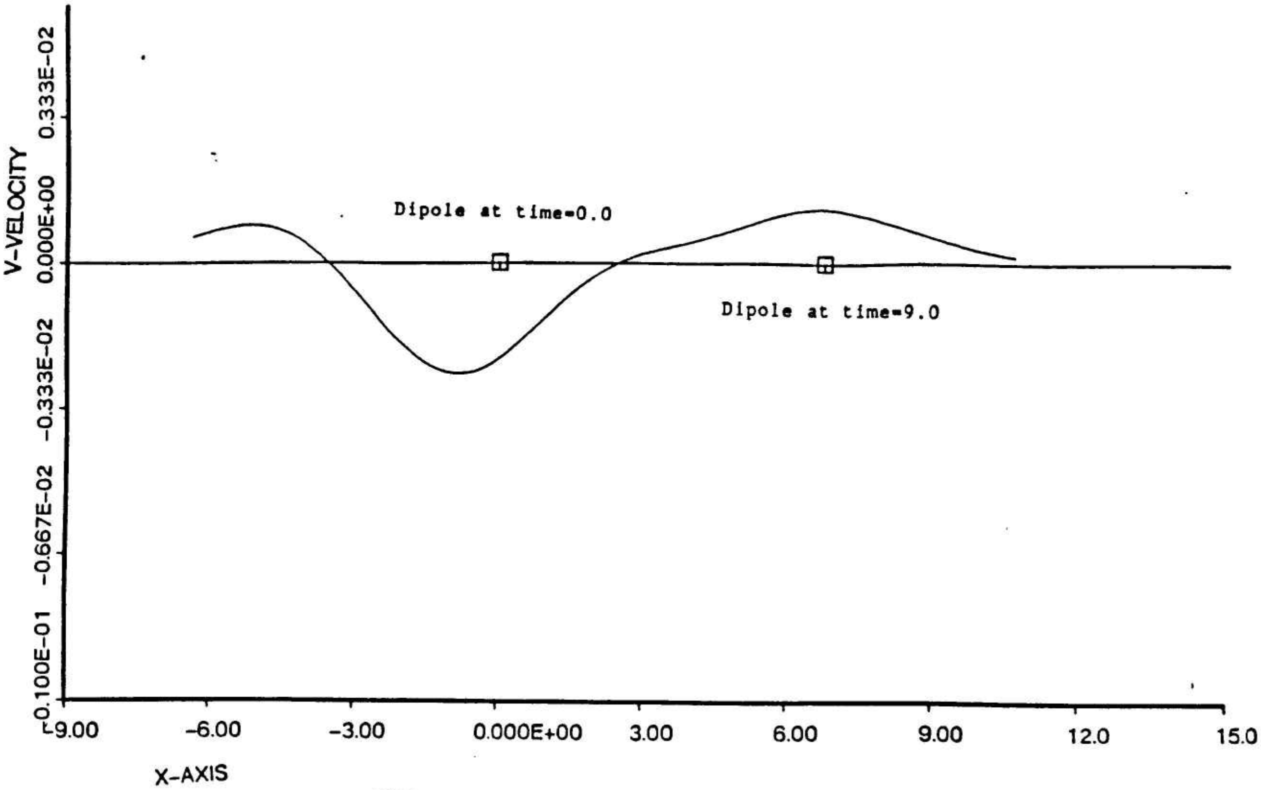

Fig. 96. Normal velocity distribution near the dipole $\bar{v}(x,y=H,0,t)$. Dipole is above the wake. Time=9.0, mean shear=0.25.

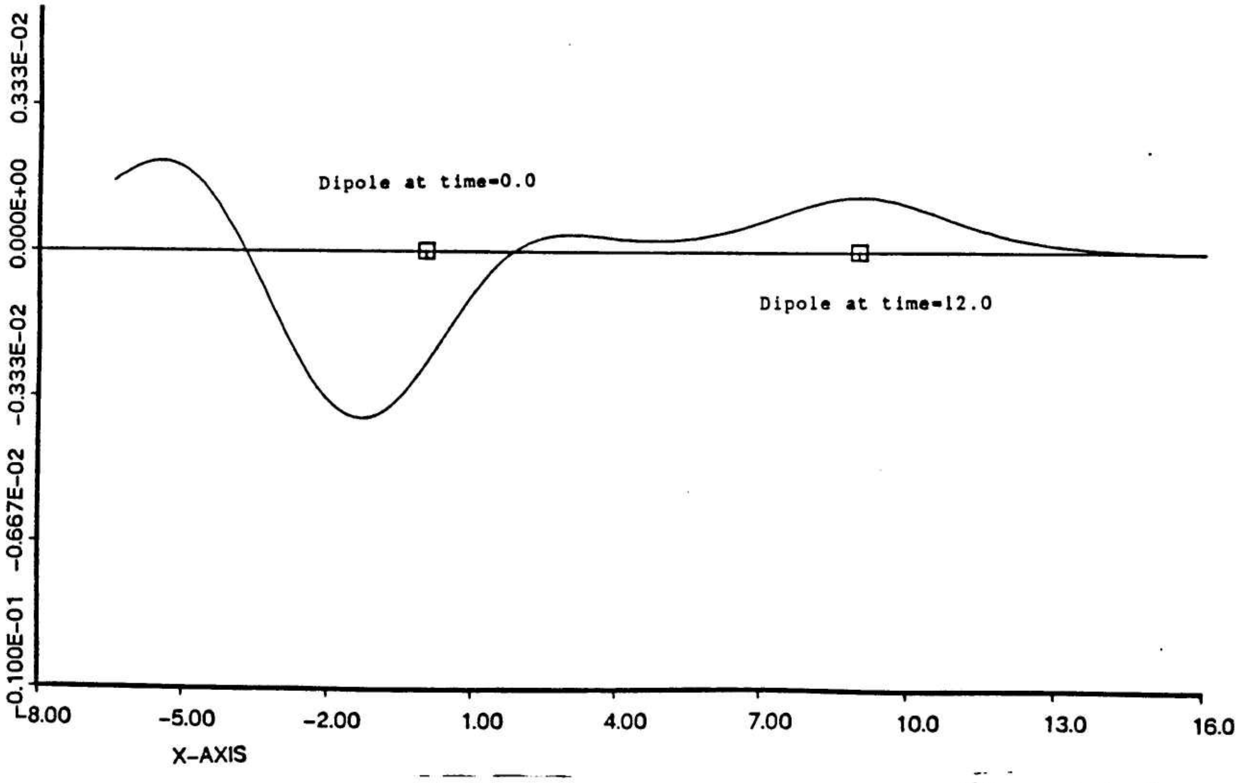

Fig. 97. Normal velocity distribution near the dipole $\bar{v}(x,y=H,0,t)$. Dipole is above the wake. Time=12.0, mean shear=0.25.

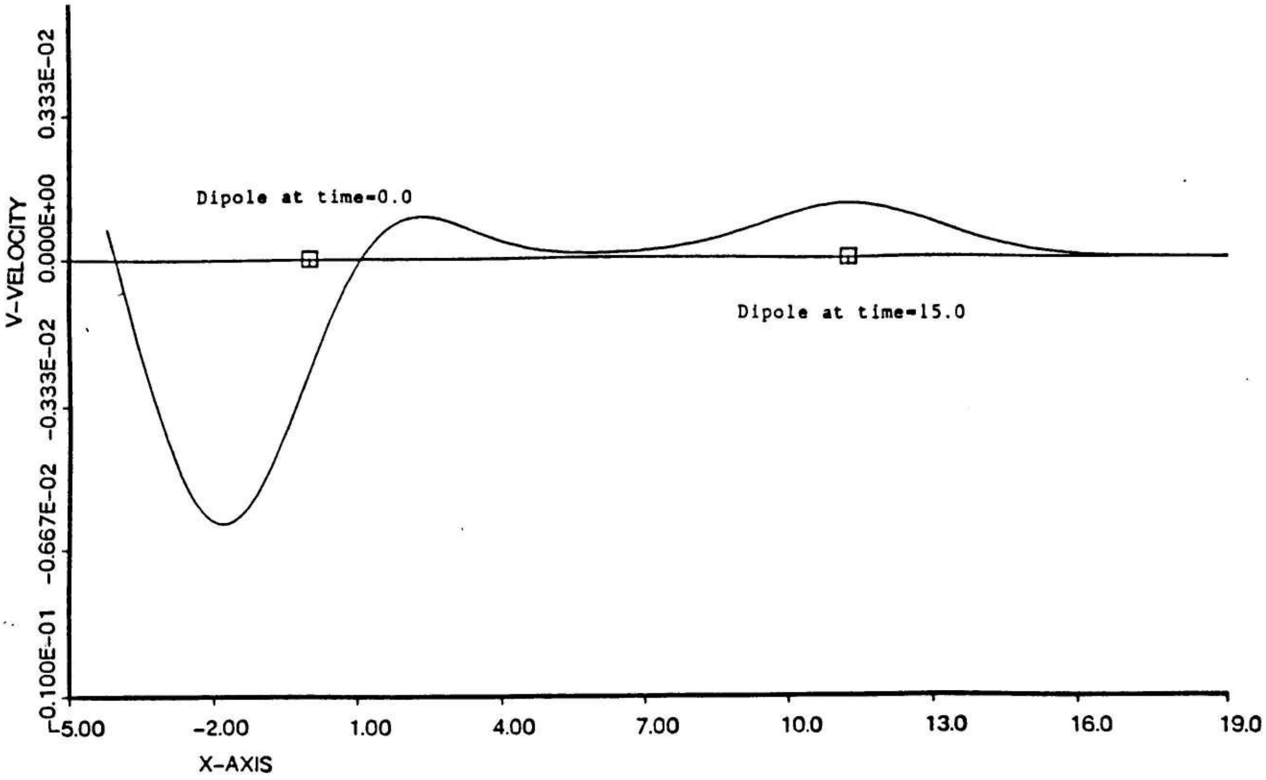

Fig. 98. Normal velocity distribution near the dipole $\bar{v}(x,y=H,0,t)$. Dipole is above the wake. Time=15.0, mean shear=0.25.

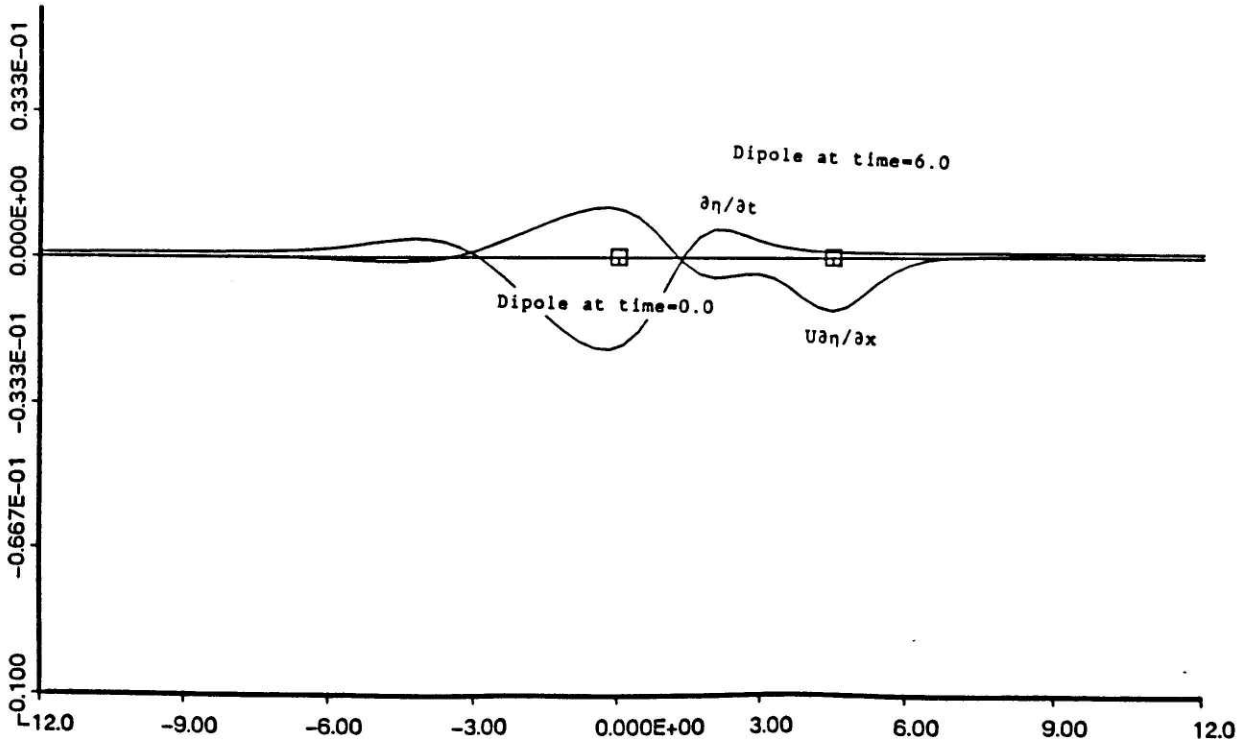

Fig. 99. Source strength distribution at the upper surface. Time=6.0, mean shear=0.25.

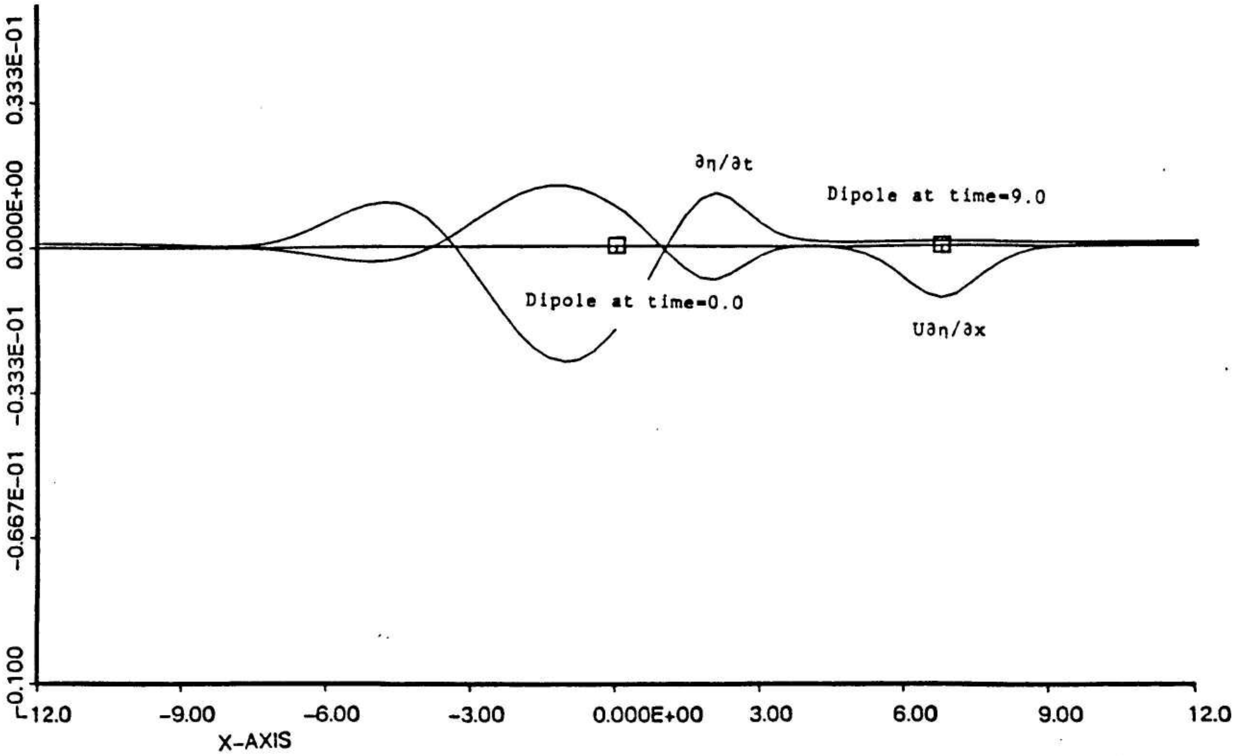

Fig.100. Source strength distribution at the upper surface. Time=9.0, mean shear=0.25.

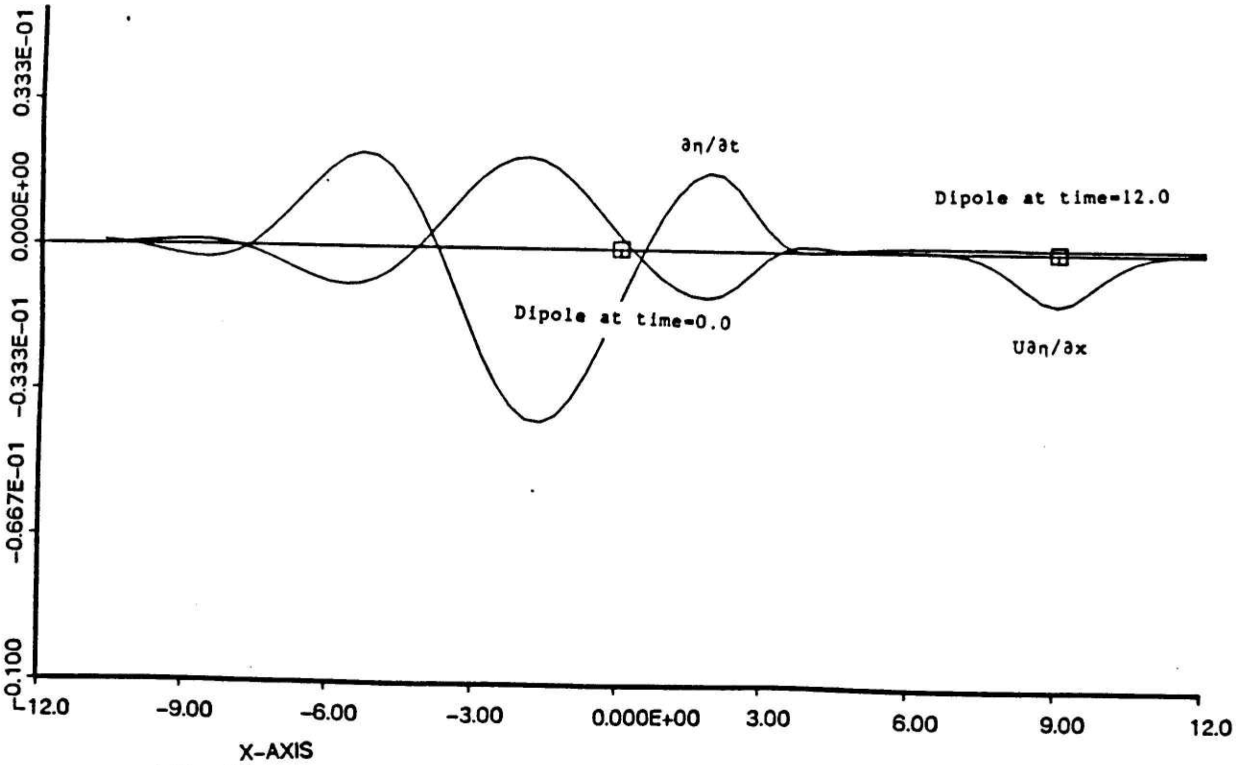

Fig.101. Source strength distributions at the upper surface. Time=12.0, mean shear=0.25.

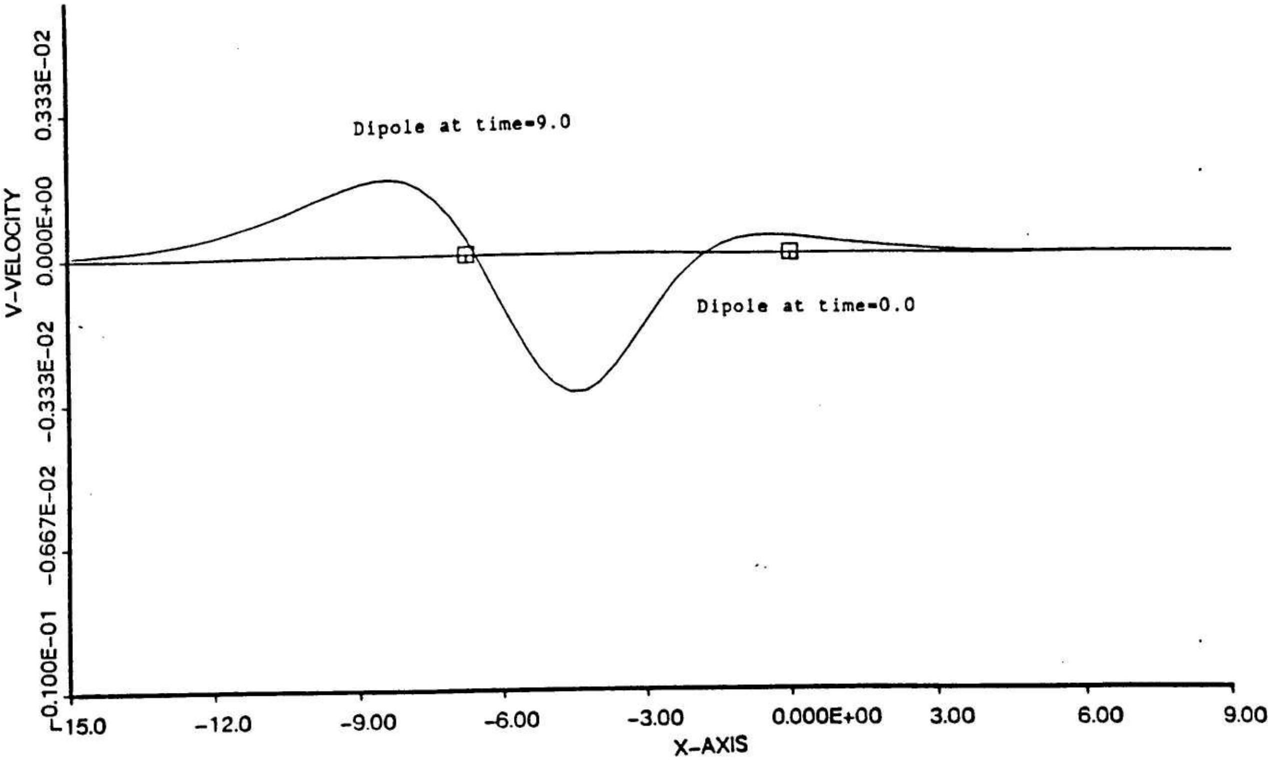

Fig.102. Normal velocity distributions near the dipole $\bar{v}(x,y=H,0,t)$. Dipole is placed below the wake. Time=9.0, mean shear=0.25.

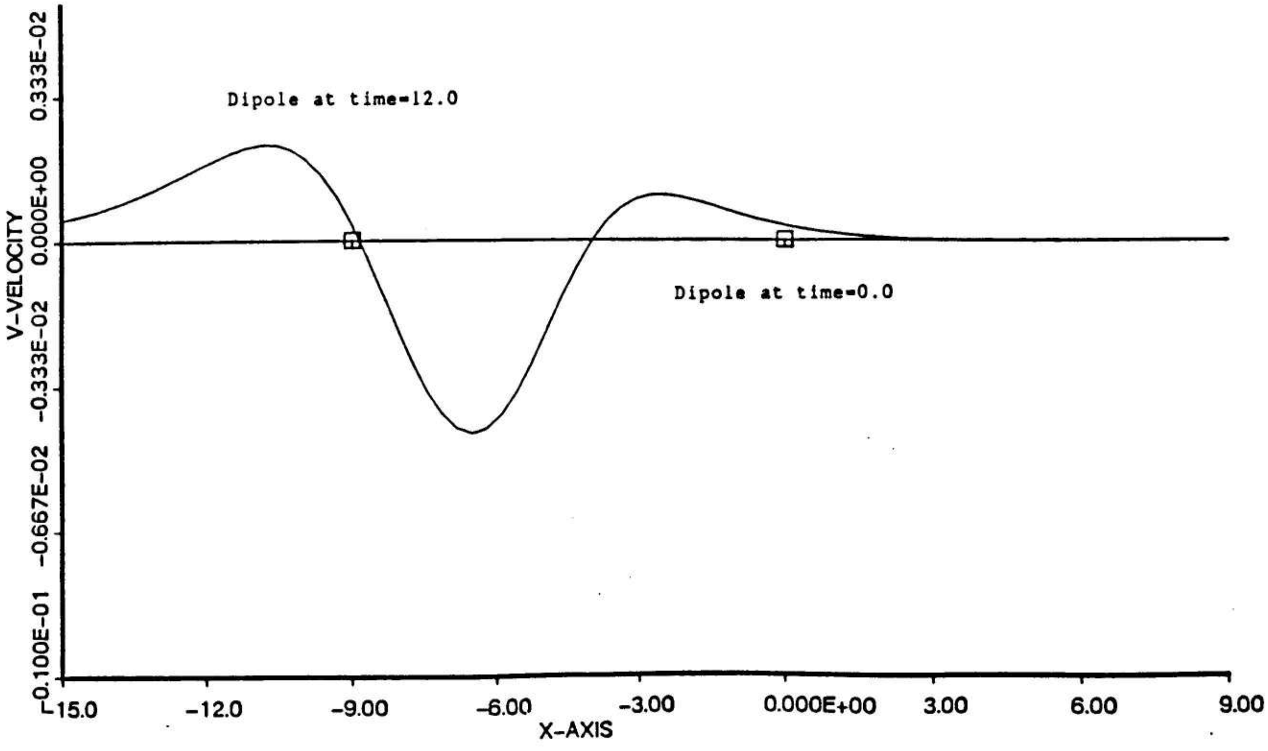

Fig.103. Normal velocity distribution near the dipole $\bar{v}(x,y=H,0,t)$. Dipole is placed below the wake. Time=12.0, mean shear=0.25.

References

Abramowitz,M. and Stegun,I.A. (1970), Handbook of Mathematical Functions, AMS 55, National Bureau of Standards.

Ahmadi, R.A. (1964), "An Asymptotic Unsteady Lifting-Line Theory With Energetics And Optimum Motion of Thrust-Producing Lifting Surfaces " Ph.D Thesis, M.I.T.

Alfredson, P.H. and Johansson, A.V. "Timescales for Turbulent Channel Flow", R. Inst. Tech., Stockholm, Rep. TRITA-MEK-82-11, 1982.

Amiet, R.K. "High Frequency Thin-Airfoil Theory for Subsonic Flow", (1976) AIAA Journal, Vol.14, No.8, pp. 1076-1082.

Anders, J.B., Hefner, J.N. and Bushnell, D.M. "Performance of Large-Eddy Breakup Devices at Post-Transitional Reynolds Numbers", AIAA Paper No. 84-0345.

Anders, J.B. and Watson, R.D. "Airfoil Large-Eddy Breakup Devices for Turbulent Drag Reduction", AIAA-85-0520.

Ashley, H. and Landahl, M.T. (1965), Aerodynamics of Wings and Bodies, Addison-Wesley.

Antonia, R.A. (1972), "Conditionally sampled measurements near the outer edge of a turbulent boundary layer", J. Fluid Mechanics, 56, part 1, pp.

1-18.

Baker, G.R. "The Cloud in Cell Technique Applied to the Roll Up of Vortex Sheets" J. Computational Physics 31, 76-95 (1979).

Bertelrud, A., Truong, T. V. and Avella, F. (1982). "Drag Reduction in Turbulent Boundary Layers Using Ribbons". AIAA 9th Atmospheric Flight Mech. Conf., San Diego, CA. Paper 82-1370.

Betchov, R. and Criminale, Jr. W. (1967) Stability of Parallel Flows, Academic Press, New York.

Birdsall, C.K. and Fuss, D. "Clouds-in-Clouds, Clouds-in-Cells Physics for Many-Body Plasma Simulation", J. Computaional Physics 3, pp. 494-511 (1969).

Blackwelder, R.F. and Eckelmann, H. (1979), "Streamwise vortices associated with the bursting phenomenon", 94, part 3, pp. 577-594.

Blackwelder, R.F. and Haritonidis, H.J. (1983), "Scaling of the bursting frequency in turbulent boundary layers", 132, pp. 87-103.

Blackwelder, R.F. and Kaplan, R.E. (1976), "On the wall structure of the turbulent boundary layer", 76, part 1, pp. 89-112.

Bisplinghoff, R.L., Ashley,H. and Halfman, R.L (1955), Aeroelasticity, Addison-Wesley.

Buneman, O. "Subgrid Resolution of Flow and Force Fields", J. Computational Physics 11, 250-268 (1973).

Bushnell, D.M., "Turbulent Drag Reduction For External Flows", AIAA Paper No. 83-0227.

Chen, C.P. and Blackwelder, R.F. (1978), "Large-scale motion in a turbulent boundary layer: a study using temperature contamination", 89, part 1, pp. 1-31.

Christiansen, J.P. "Numerical Simulation of Hydrodynamics by the Method of Point Vortices", J. Computational Physics 13, pp. 363-379 (1979).

Corino, E.R., and Brodkey,R.S (1969), "A visual investigation of the wall region in turbulent flow", 37, part 1, pp. 1-30.

Corke, T.C., Guezennec, Y. and Nagib, H.M. "Modification in Drag of Turbulent Boundary Layers Resulting from Manipulation of Large-Scale Structures", Progress in Astronautics and Aeronautics, 72, pp. 128, (1979).

De, Z.M. "The Interaction of a Wake with a Boundary Layer", Structure of Complex Turbulent Shear Flow IUTAM Symposium Marseille 1982.

Drazin, P.G. and Reid, W.H. (1981), Hydrodynamic Stability, Cambridge University Press.

Dwight, H.B. (1961), Tables of Integrals and Other Mathematical Data, Macmillan.

Falco, R. "The Production of Turbulence Near a Wall", AIAA Paper No. 80-1356.

Falco, R. "New Results, a Review and Synthesis of the Mechanism of Turbulence Production in Boundary Layers and its Modification", AIAA Paper No. 83-0377.

Filotas, L.T. (1969),"Theory of Airfoil Response in a Gusty Atmosphere. Part I - Aerodynamic Transfer Functions," UTIAS Report No. 139, ctober.

Fromm, J.E. and Harlow, F.H. "Numerical Soluition of the Problem of Vortex Street Development" The Physics of Fluids Vol.4, No.7, July (1963).

Graham, J.M.R. "Similarity rules for thin aerofoil in non-stationary subsonic flows", (1970), J. Fluid Mechanics, 43, part 4, pp.753-766.

Graham, J.M.R. "Lifting Surface Theory for the Problem of an Arbitarily Yawed Sinusoidal Gust Incident on a Thin Aerofoil in Incompressible Flow" Aeronautical Quarterly, Vol XXI, Part 2, pp. 182, May 1970.

Guezennec, Y.C. and Nagib, H.M. (1985). "Documentation of Mechanisms Leading to Net Drag Reduction in Manipulated Boundary Layers". AIAA Paper no. 85-0519.

Head, M.R. and Bandyopadhyay, P. (1981), "New aspects of turbulent boundary-layer structure", 107, pp. 297-338.

Hefner, J.N., Weinstein, L.M. and Bushnell, D.M. "Large-Eddy Breakup Scheme for Turbulent Viscous Drag Reduction", Progress in Astronautics and Aeronautics, 72, pp. 110, (1979).

Hinze, J.O. (1975) Turbulence, McGraw-Hill.

Hockney, R.W., Goel, S.P. and Eastwood, J.W. "Quiet High-Resolution Computer Models of a Plasma", J. Computational Physics 14, 148-158 (1974).

Kim, J. (1985), "Turbulence structures associated with the bursting event", Phy. Fluids 28(1), January .

Kim, H.T., Kline, S.J. and Reynolds, W.C. (1971), "The production of turbulence near a smooth wall in a turbulent boundary layer", 50, part 1, pp. 133-160.

Klebanoff, P.S. "Characteristics of Turbulence in a Boundary Layer With Zero Pressure Gradient", NACA TN. 3178, July 1954.

Kline, S.J., Reynolds, W.C., Schraub, F.A. and Runstadler, P.W. (1967), "The structure of turbulent boundary layers", 30, part 4, pp. 741-773.

Kovasznay, L.S.G. (1970), "The Turbulent Boundary Layers", Annual Review of Fluid Mechanics, 2, pp. 95-112.

Kovasznay, L.S.G., Kibens, V. and Blackwelder, R.F. (1970), "Large-scale motion in the intermittent region of a turbulent boundary layer", 41, part 2, pp. 283-325.

Lamb, H (1932), Hydrodynamics , Dover Publications, New York.

Landahl, M.T. and Henningson, D.S. "The Effects of Drag Reduction Measures on Boundary Layer Turbulence Structure-Implications of an Inviscid Model" AIAA-85-0560.

Leonard, A. "Vortex Methods for Flow Simulation - Review", J. Computational Physics 37, pp. 289-335 (1980).

Leonard, A. "Computing Three-Dimensional Incompressible Flows With Vortex Elements", Ann. Rev. Fluid Mechanics, 1985, 17, 523-559.

Lu, S.S. and Willmarth, W.W. (1973), "Measurements of the structure of the Reynolds stress in a turbulent boundary layer", J. Fluid Mechanics, 60, part 3, pp. 481-511.

Mangus, J.F. "Measurement of Drag and Bursting Frequency Downstream of Tandem Spanwise Ribbons in a Turbulent Boundary Layer", S.M Thesis, M.I.T. (1984).

Mugridge, B.D. "Gust Loading on a Thin Aerofoil", The aeronautical Quarterly, Vol.22, August 1971, pp.301-310.

Mumford, J.C. and Savill, A.M. "Parametric Studies of Flat Plate Turbulence Manipulators Including Direct Drag Results And Laser Flow Visualisation", Paper presented at ASME Symposium on Laminar/Turbulent Boundary Layer: Control, Modification and Marine Applications ETCE Conference, New Orleans, Louisina, February 1984.

Offen, G.R. and Kline, S.J. (1975), "A proposed model of the bursting process in turbulent boundary layers", J. Fluid Mechanics, 70, part 2, pp. 209-228.

Plesniak, M.W. and Nagib, H.M. "Net Drag Reduction in Turbulent Boundary Layers Resulting from Optimized Manipulation", AIAA-85-0518.

Praturi, A.K. and Brodkey, R. (1978), "A stereoscopic visual study of coherent structures in turbulent shear flow", J. Fluid Mechanics, 89, part 2, pp. 251-272.

Rao, K.N., Narasimha, R. and Badri Narayanan, M.A., (1971), "The 'bursting' phenomenon in a turbulent boundary layer" J. Fluid Mechanics, 48, part 2, pp.339-352.

Reissner, E. (1947), "Effect of Finite Span on the Airload Distributions for Oscillating Wings, I - Aerodynamic Theory of Oscillating Wings of Finite Span," NACA TN No. 1194.

Roache, P.J. (1976), Computational Fluid Dynamics, Hermosa-Publishers.

Sahlin, A., Alfredsson H.P. and Johansson, V.A. (1986), "Direct drag measurements for a flat plate with passive boundary layer manipulators", Phy. Fluids 29(3), March.

Sato, H. "An experimental study of non-linear interaction of velocity fluctuations in the transition region of two-dimensional wake", J. Fluid Mechanics,(1970) 44, part 4, pp. 741-765.

Sato, H. and Kuriki, K, "The mechanism of transition in the wake of a thin flat plate placed parallel to a uniform flow", J. Fluid Mechanics, 11, 1961, pp. 321-352.

Schlichting, H., Boundary Layer Theory, McGraw-Hill, New York, 1979

Schwarz, L. (1940), "Berechnung der Druckvertteilung einer harmonisch sich Verformenden Tragflache in ebener Stromung," Luftfahrtforsch., 17, Nr. 11 & 12, December.

Sears, W.R. "Some Aspects of Non-Stationary Airfoil Theory and Its Practical Application", (1941) J. Aeronautical Sciences 8, pp.104.

Smith, C.R. and Metzler, S.P (1983), "The characteristics of low-speed streaks in the near-wall region of a turbulent boundary layer", 129, pp. 27-54.

Swarztrauber, P. and Sweet, R. (1975) "Efficient Fortran Subprograms for the Solution of Elliptic Partial Differential Equations", Technical Note

TN/IA-109, National Center for Atmospheric Research, Boulder, Colorado 80307.

Taneda, S. "Oscillation of the Wake behind a Flat Plate parallel to the flow", J. Physical Society of Japan, Vol.13, No.4, April 1958.

Thomas, A.S.W. and Bull, M.K. (1983), "On the role of wall-pressure fluctuations in deterministic motions in the turbulent boundary layer", 128, pp. 283-322.

Van Dyke, M. (1975), Perturbation Methodsin Fluid Mechanics, Annotated Edition, Parabolic Press, Stanford.

Wallace, J.M., Eckelmann, H. and Brodkey, R.S. (1972), "The wall region in turbulent shear flow", J. Fluid Mechanics, 54, part 1, pp. 39-48.

Watson, G.N. (1966), A Treatise on the Theory of Bessel Functions, Second Edition, Cambridge Univ. Press.

Willmarth, W.W. (1975). Structure of turbulence in boundary Layers. Adv. Appl. Mech. 15, pp. 159.

Willmarth, W.W. and Lu, S.S. (1972), "Structure of the Reynolds stress near the wall", J. Fluid Mechanics, 55, part 1, pp. 65-92.

Yajnik, K.S. and Acharya, M. (1976),"Non-equilibrium Effects in a Turbulent Boundary Layer due to the Destruction of Large Eddies", Structure and

Mechanisms of Turbulence, Vol 1, Lecture Notes in Physics 76 (Springer, New York, 1976), pp.249.

Zabusky, N.J. and Deem, G.S. "Dynamical evolution of two-dimensional unstable shear flows" J. Fluid Mechanics 47, part 2, pp. 353-379, (1971).

APPENDIX A

ⓐ

$$\int_{-1}^{+1} \sqrt{\frac{1+x}{1-x}}\; e^{-i\bar{k}_x x}\, dx = \pi \left\{ J_0(\bar{k}_x) - i\, J_1(\bar{k}_x) \right\}$$

ⓑ

$$\int_{-1}^{+1} \sqrt{\frac{1+x}{1-x}}\; \frac{1}{x-x_1}\, dx = \pi \qquad -1 \leq x_1 \leq 1$$

ⓒ

$$\frac{1}{2\pi} \int_{-1}^{+1} \left\{ \sqrt{\frac{1+x}{1-x}} \int_{-1}^{+1} \frac{\bar{\gamma}(x_1)}{x-x_1}\, dx_1 \right\} dx$$

$$= \frac{1}{2\pi} \int_{-1}^{+1} \bar{\gamma}(x_1) \left\{ \sqrt{\frac{1+x}{1-x}}\; \frac{1}{x-x_1}\, dx \right\} dx_1$$

$$= \frac{1}{2\pi} \int_{-1}^{+1} \bar{\gamma}(x_1)\, dx_1 \cdot \pi$$

$$= \frac{1}{2}\; \frac{\bar{\Gamma}(c/2)}{c/2}$$

ⓒ

$$\int_{-1}^{+1}\sqrt{\frac{1+x}{1-x}}\;\frac{1}{x-x_1}\,dx = \pi\left\{1. - \sqrt{\frac{x_1+1}{x_1-1}}\right\} \qquad 1<x_1<\infty$$

$$\frac{1}{2\pi}\int_{-1}^{+1}\left\{\sqrt{\frac{1+x}{1-x}}\int_{1}^{\infty}\frac{e^{-i\bar{k}_x x_1}}{x-x_1}\,dx_1\right\}dx$$

$$= \frac{1}{2\pi}\int_{1}^{\infty} e^{-i\bar{k}_x x_1}\left\{\int_{-1}^{+1}\sqrt{\frac{1+x}{1-x}}\;\frac{1}{x-x_1}\,dx\right\}dx_1$$

$$= \frac{1}{2\pi}\int_{1}^{\infty} e^{-i\bar{k}_x x_1}\left\{\pi - \pi\sqrt{\frac{x_1+1}{x_1-1}}\right\}dx_1$$

$$= \frac{1}{2}\Bigg\{\frac{e^{-i\bar{k}_x}}{i\bar{k}_x} + \frac{\pi}{2}\Big\{H_1^2(\bar{k}_x) + i\,H_0^2(\bar{k}_x)\Bigg\}$$

ⓓ

$$\int_{-1}^{+1}\sqrt{\frac{1+x}{1-x}}\;\frac{1}{x+x_1}\,dx = \pi\left\{1. - \sqrt{\frac{x_1-1}{x_1+1}}\right\} \qquad 1<x_1<\alpha$$

$$\frac{1}{2\pi}\int_{1}^{\infty} e^{i\bar{k}_x x_1}\, \pi \left\{ 1. - \sqrt{\frac{x_1 - 1}{x_1 + 1}} \right\} dx_1$$

$$= \frac{1}{2} \Big\{ - \frac{e^{i\bar{k}_x}}{i\bar{k}_x} + \frac{\pi}{2} \Big\{ \bar{H}_1^{2}(\bar{k}_x) + i\, \bar{H}_0^{2}(\bar{k}_x) \Big\}$$

APPENDIX B

Consider a vortex sheet with spanwise vorticity of strength $\gamma \exp(-ik_x x)\exp(ik_y y)$ (shed vorticity) and with streamwise vorticity of strength $\delta \exp(-ik_x x)\exp(ik_y y)$ (trailing vorticity), which is positioned in the xy-plane.

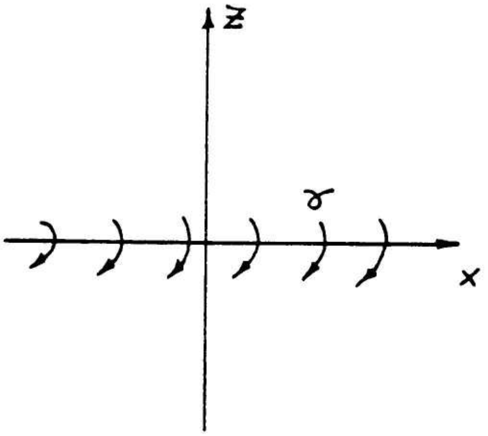

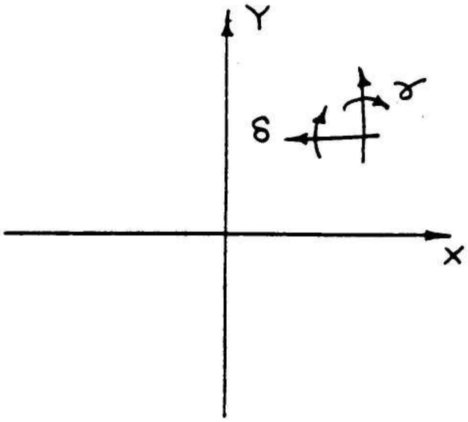

Outside this vortex sheet the flow is governed by the potential equation .

$$\phi_{,xx} + \phi_{,yy} + \phi_{,zz} = 0$$

Assume a solution of the form

$$\phi = f(z) \exp(-ik_x x) \exp(ik_y y) \qquad (B1)$$

hence f(z) satisfies the O.D.E.

$$f''(z) - (k_x^2 + k_y^2) f(z) = 0$$

The solution of this equation is

$$f(z) = A \exp(\sqrt{k_x^2 + k_y^2}\ z) + B \exp(- \sqrt{k_x^2 + k_y^2}\ z)$$

Applying the boundary condition when $|z| \to \infty$, $\phi \to 0$ we have

$$\left.\begin{aligned} f(z) &= A \exp(- \sqrt{k_x^2 + k_y^2}\ z) \quad \text{for } z \geq 0 \\ f(z) &= B \exp(+ \sqrt{k_x^2 + k_y^2}\ z) \quad \text{for } z \leq 0 \end{aligned}\right\} \qquad (B2)$$

Across the vortex sheet streamwise velocity is discontinuous

$$u(x,y,+0)-u(x,y,-0) = \gamma \exp(-ik_x x) \exp(ik_y y)$$

Since $u(x,y,+0) = -u(x,y,-0)$ we obtain

$$\phi,_x(x,y,+0) = \gamma/2 \exp(-ik_x x) \exp(ik_y y)$$

From this relation and eq.(B1) and (B2) we determine A, B and is given by

$$A = i\,\gamma/(2k_x)$$

$$B = -i\,\gamma/(2k_x)\ .$$

Using these values for A and B we obtain the expression for ϕ

$$\phi = i\,|z|/z\ \gamma/(2k_x) \exp(-ik_x x) \exp(ik_y y) \exp(-\sqrt{k_x^2 + k_y^2}\,|z|)$$

If we let $k_y = 0$ we will obtain the results for the two-dimensional case.

APPENDIX C

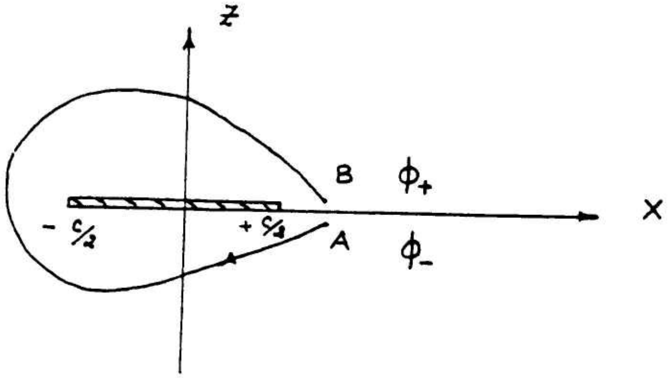

The circulation around the path from A to B is

$$\Gamma(x,y,t) = \int_A^B \vec{u} \cdot d\vec{r}$$

$$= \int_A^B \nabla\phi \cdot d\vec{r}$$

$$= \int_A^B d\phi$$

$$= \phi(x,y,+0,t) - \phi(x,y,-0,t)$$

Since $\phi(x,y,+0,t) = \phi(x,y,-0,t)$

$$\Gamma(x,y,t) = 2\,\phi(x,y,+o,t)$$

When $x = c/2$

$\Gamma(c/2,y,t)$ = circulation around the plate

From eq.(67)

$$\Gamma(c/2,y,t) = Uc/2\ f_2(1)\ \exp(i\omega t)\ \exp(ik_y y) \qquad (C1)$$

$$= 2\ \phi(c/2,y,+0,t)$$

No pressure jump across the wake condition gives

$$\phi(x,y,+0,t) = \phi(c/2,y,+0,t - \frac{x-c/2}{U}) \qquad (C2)$$

From eq.(C1) & (C2) we get

$$\phi(x,y,+0,t) = U/2\ c/2\ f_2(1)\ \exp(ik_x)\ \exp(-ik_x x)\ \exp(ik_y y)\ \exp(i\omega t)$$

From this relation we derive the expression for the vorticity γ_w and δ_w

$$\gamma_w = 2\ \phi,_x(x,y,+0,t)$$

$$= -i\ U\ k_x\ f_2(1)\ \exp(ik_x)\ \exp(-ik_x x)\ \exp(ik_y y)\ \exp(i\omega t)$$

$$\delta_w = 2\ \phi,_y(x,y,+0,t)$$

$$= -i\ U\ k_y\ f_2(1)\ \exp(ik_x)\ \exp(-ik_x x)\ \exp(ik_y y)\ \exp(i\omega t)$$

APPENDIX D

ⓐ

$$\int_{-\infty}^{\infty} \frac{e^{i\bar{k}_y\eta}\,(x-\xi)}{\left\{(x-\xi)^2+\eta^2\right\}^{3/2}}\,d\eta \;=\; 2\bar{k}_y\, K_1\left\{\bar{k}_y|x-\xi|\right\}\,\mathrm{sgn}($$

ⓑ

$$\int_{-\infty}^{\infty} \frac{e^{i\bar{k}_y\eta}\,\eta}{\left\{(x-\xi)^2+\eta^2\right\}^{3/2}}\,d\eta \;=\; 2i\,\bar{k}_y\, K_0\left\{\bar{k}_y|x-\xi|\right\}$$

ⓒ

$$\int_{\xi=1}^{\infty}\int_{\eta=-\infty}^{\infty} \frac{e^{-i\bar{k}_x\xi}\,e^{i\bar{k}_y\eta}\,\eta}{\left\{(x-\xi)^2+\eta^2\right\}^{3/2}}\,d\eta \;=\; 2i\,\bar{k}_y\int_{\xi=1}^{\infty} e^{-i\bar{k}_x\xi}\,K_0\{\bar{k}_y(\xi-$$

ⓓ

$$\int_{\xi=1}^{\infty}\int_{\eta=-\infty}^{+\infty} \frac{e^{-i\bar{k}_x\xi}\,e^{i\bar{k}_y\eta}\,(x-\xi)}{\left\{(x-\xi)^2+\eta^2\right\}^{3/2}}\,d\eta \;=\; -2\bar{k}_y\int_{\xi=1}^{\infty} K_1\left\{\bar{k}_y(\xi-x)\right\} e^{-i\bar{k}_x\xi}$$

If we change the variables in the last two expressions (c) , (d) with $\xi' = \xi - 1$, we obtain

$$2i\bar{k}_y \int_{\xi=1}^{\infty} e^{-i\bar{k}_x \xi} K_0\left\{\bar{k}_y(\xi - x)\right\} d\xi = 2i\bar{k}_y e^{i\bar{k}_x} \int_{\xi'=0}^{\infty} e^{-i\bar{k}_x \xi'} K_0\left\{\bar{k}_y(\xi' - x + 1)\right\}$$

$$-2\bar{k}_y \int_{\xi=1}^{\infty} e^{-i\bar{k}_x \xi} K_1\left\{\bar{k}_y(\xi - x)\right\} d\xi = -2\bar{k}_y e^{-i\bar{k}_x} \int_{\xi'=0}^{\infty} e^{-i\bar{k}_x \xi'} K_1\left\{\bar{k}_y(\xi' - x + 1)\right\} d\xi$$

Substituting these results in the eq.(70) we obtain

$$-\frac{w(\bar{k}_x, \bar{k}_y)}{U} e^{i\bar{k}_x x} = -\frac{\bar{k}_y}{2\pi} \int_{-1}^{+1} f_1(\xi) K_1\left\{\bar{k}_y |x - \xi|\right\} \operatorname{sgn}(x - \xi)\, d\xi$$

$$-\frac{\bar{k}_y^2}{2\pi} \int_{-1}^{+1} f_2(\xi) K_0\left\{\bar{k}_y |x - \xi|\right\} d\xi$$

$$-\frac{i\bar{k}_x \bar{k}_y f_2(1)}{2\pi} \int_{\xi'=0}^{\infty} e^{-i\bar{k}_x \xi'} K_1\left\{\bar{k}_y(\xi' + 1 - x)\right\} d\xi'$$

$$- \frac{\bar{k}_y^{2} \, f_2(1)}{2\pi} \int_{\xi'=0}^{\infty} e^{-i\bar{k}_x \xi'} \, K_0 \left\{ \bar{k}_y \left(\xi' + 1 - x \right) \right\} d\xi' \qquad (D1)$$

Consider the integral

$$I_1 = \int_{\xi'=0}^{\infty} e^{-i\bar{k}_x \xi'} \, K_1 \left\{ \bar{k}_y \left(\xi' + 1 - x \right) \right\} d\xi'$$

$$= - \int_{\xi'=0}^{\infty} e^{-i\bar{k}_x \xi'} \, K_0' \left\{ \bar{k}_y \left(\xi' + 1 - x \right) \right\} d\xi$$

$$= \frac{K_0 \left\{ \bar{k}_y (1 - x) \right\}}{\bar{k}_y} - \frac{i\bar{k}_x}{\bar{k}_y} \int_{0}^{\infty} e^{-i\bar{k}_x \xi'} \, K_0 \left\{ \bar{k}_y \left(\xi' + 1 - x \right) \right\} d\xi$$

We modify this equation to another form

$$I_2 = \int_0^\infty e^{-\iota \bar{k}_x \xi'} K_0\left\{\bar{k}_y(\xi'+1-x)\right\} d\xi'$$

$$= \int_{-(1-x)}^\infty e^{-\iota \bar{k}_x \xi'} K_0\left\{\bar{k}_y(\xi'+1-x)\right\} d\xi'$$

$$- \int_{1-x}^\infty e^{-\iota \bar{k}_x \xi'} K_0\left\{\bar{k}_y(\xi'+1-x)\right\} d\xi'$$

$$= Q\, e^{\iota \bar{k}_x} e^{-\iota \bar{k}_x x} - e^{\iota \bar{k}_x (1-x)} \int_0^{(1-x)} e^{-\iota \bar{k}_x \xi} K_0\left\{\bar{k}_y \xi\right\} d\xi$$

where

$$Q = \int_0^\infty e^{-\iota \bar{k}_x \xi} K_0\left\{\bar{k}_y \xi\right\} d\xi .$$

and it is given by

$$Q = \frac{1}{\left\{ \bar{k}_x^{\,2} + \bar{k}_y^{\,2} \right\}^{1/2}} \left\{ \frac{\pi}{2} - i \log_e \frac{\bar{k}_x + \sqrt{\bar{k}_x^{\,2} + \bar{k}_y^{\,2}}}{\bar{k}_y} \right\}$$

With the substitution of these results into eq.(D1) it takes the form

$$- \frac{w(\bar{k}_x, \bar{k}_y)}{U} e^{i \bar{k}_x x} = - \frac{\bar{k}_y}{2\pi} \int_{-1}^{+1} f_1(\xi) \, K_1\left\{ \bar{k}_y |x-\xi| \right\} \operatorname{sgn}(x-\xi) \, d\xi$$

$$- \frac{\bar{k}_y^{\,2}}{2\pi} \int_{-1}^{+1} f_2(\xi) \, K_0\left\{ \bar{k}_y |x-\xi| \right\} d\xi$$

$$- \frac{f_2(1)}{2\pi} \left\{ \bar{k}_x^{\,2} + \bar{k}_y^{\,2} \right\} Q \, e^{i \bar{k}_x} \, e^{-i \bar{k}_x x}$$

$$+ \frac{f_2(1)}{2\pi} \left\{ \bar{k}_x^{\,2} + \bar{k}_y^{\,2} \right\} e^{i \bar{k}_x (1-x)} \int_0^{(1-x)} e^{-i \bar{k}_x \xi} \, K_0\left\{ \bar{k}_y \xi \right\} d\xi$$

$$- \frac{i \bar{k}_x}{2\pi} f_2(1) \, K_0\left\{ \bar{k}_y (1-x) \right\}$$

APPENDIX E

Evaluation of $$\frac{\partial}{\partial z}\int_{-\infty}^{0}\frac{z\,e^{j k_x \xi}}{\xi^2+z^2}\,d\xi$$ when $z \longrightarrow 0$

$$\int_{-\infty}^{0}\frac{z\,e^{j k_x \xi}}{\xi^2+z^2}\,d\xi \;=\; \frac{j}{2}\int_{0}^{\infty}\frac{e^{-j\xi_1}}{\xi_1+j z_1}\,d\xi \;-\; \frac{j}{2}\int_{0}^{\infty}\frac{e^{-j\xi_1}}{\xi_1-j z_1}\,d\xi_1$$

$$z_1 = k_x z \qquad\qquad \xi_1 = \omega \xi .$$

Consider these integrals seperately

$$I_1 = \int_{0}^{\infty}\frac{e^{-j\xi_1}}{\xi_1+j z_1}\,d\xi_1$$

Let

$$t = j(\xi_1 + j z_1) = -z_1 + j\xi_1$$

$$I_1 = e^{-z_1}\int_{-z_1}^{-z_1+j\infty}\frac{e^{-t}}{t}\,dt .$$

$$\frac{\partial I_1}{\partial z_1} = -e^{-z_1}\int_{-z_1}^{-z_1+j\infty}\frac{e^{-t}}{t}\,dt \qquad - \frac{1}{z_1}$$

We can write this integral as

$$\frac{\partial I_1}{\partial z_1} = -e^{-z_1}\left\{\times\!\!\!\!\!\int_{-z_1}^{z_1}\frac{e^{-t}}{t}\,dt + \int_{\frown}\frac{e^{-t}}{t}\,dt + \int_{z_1}^{\infty}\frac{e^{-t}}{t}\,dt\right\} - \frac{1}{z_1}$$

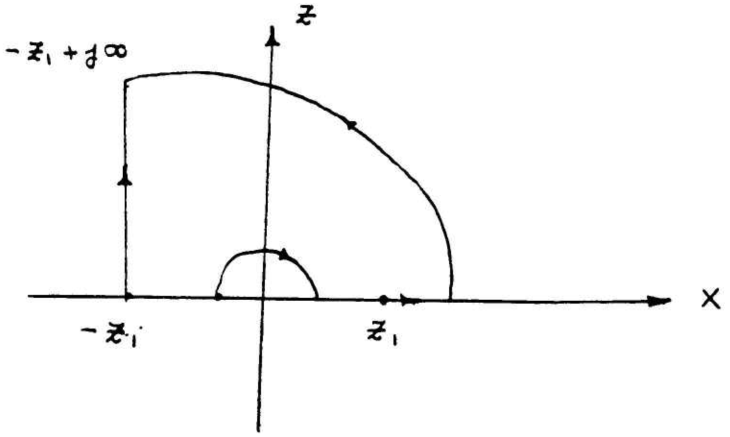

The second integral is

$$I_2 = \int_0^{\infty}\frac{e^{-j\xi_1}}{\xi_1 - jz_1}\,d\xi_1$$

$$= e^{z_1}\int_{z_1}^{z_1+j\infty}\frac{e^{-t}}{t}\,dt$$

$$\frac{\partial I_2}{\partial z_1} = e^{z_1} \int_{z_1}^{z_1 + j\infty} \frac{e^{-t}}{t}\, dt \quad - \frac{1}{z_1}$$

$$= e^{z_1} \int_{z_1}^{\infty} \frac{e^{-t}}{t}\, dt \quad - \frac{1}{z_1}$$

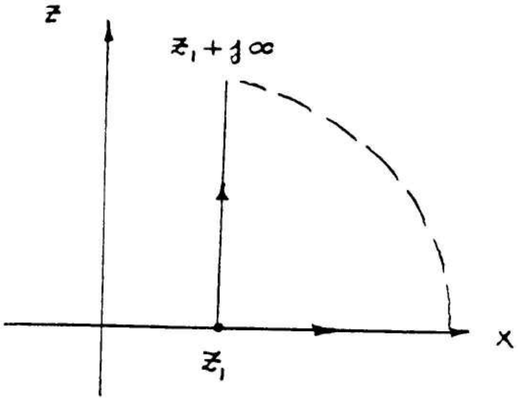

$$\frac{\partial I_1}{\partial z_1} - \frac{\partial I_2}{\partial z_2} = -\left(e^{z_1} + e^{-z_1}\right) \int_{z_1}^{\infty} \frac{e^{-t}}{t}\, dt \quad - e^{-z_1} \int_{\frown} \frac{e^{-t}}{t}\, dt$$

$$- e^{-z_1} \int\!\!\!\!\!\times_{-z_1}^{z_1} \frac{e^{-t}}{t}\, dt \,.$$

When $z_1 \longrightarrow 0$

$$\int_{z_1}^{\infty} \frac{e^{-t}}{t}\, dt = -\left\{ \gamma + \ln z_1 \right\}$$

$$= -\left\{ \gamma + \ln k_x z \right\}$$

$$\not\int_{-z_1}^{z_1} \frac{e^{-t}}{t}\, dt \longrightarrow 0$$

$$\int_{-z_1}^{z_1} \frac{e^{-t}}{t}\, dt \longrightarrow -\pi j$$

Therefore when $z \longrightarrow 0$

$$\frac{\partial I_1}{\partial z_1} - \frac{\partial I_2}{\partial z_1} = 2 \left\{ \gamma + \ln k_x z + \frac{\pi}{2} j \right\}$$

$$\frac{\partial}{\partial z} \int_{-\infty}^{0} \frac{z\, e^{j k_x \xi}}{\xi^2 + z^2}\, d\xi \longrightarrow j k_x \left\{ \gamma + \log k_x z + \frac{\pi}{2} j \right\}$$

APPENDIX F

$$\frac{\partial^2}{\partial z^2}\left\{\frac{1}{(\rho^2+r^2)^{1/2}}\right\} = \frac{3z^2}{(\rho^2+r^2)^{5/2}} - \frac{1}{(\rho^2+r^2)^{3/2}}$$

$$-\frac{\partial^2}{\partial z^2}\int_0^\infty \frac{e^{-jk_x\rho}}{\{\rho^2+r^2\}^{1/2}}\,d\rho = \int_0^\infty \frac{\cos k_x\rho}{\{\rho^2+r^2\}^{3/2}}\,d\rho - 3z^2\int_0^\infty \frac{\cos k_x\rho}{\{\rho^2+r^2\}^{5/2}}\,d\rho$$

$$-j\int_0^\infty \frac{\sin k_x\rho}{\{\rho^2+r^2\}^{3/2}}\,d\rho + 3jz^2\int_0^\infty \frac{\sin k_x\rho}{\{\rho^2+r^2\}^{5/2}}\,d\rho$$

Evaluation of these integrals

$$K_\nu(xz) = \frac{\Gamma(\nu+\frac{1}{2})\,(2z)^\nu}{\pi^{1/2}\,x^\nu}\int_0^\infty \frac{\cos xt}{\{t^2+z^2\}^{\nu+\frac{1}{2}}}\,dt$$

ⓐ $\nu = 0$

$$\int_0^\infty \frac{\cos k_x\rho}{\{\rho^2+r^2\}^{1/2}}\,d\rho = K_0(k_x r)$$

ⓑ $\nu = 1$

$$\int_0^\infty \frac{\cos k_x \varrho}{\left\{ \varrho^2 + \tau^2 \right\}^{3/2}} \, d\varrho = \frac{k_x}{\tau} K_1 (k_x \tau)$$

ⓒ $\nu = 2$

$$\int_0^\infty \frac{\cos k_x \varrho}{\left\{ \varrho^2 + \tau^2 \right\}^{5/2}} \, d\varrho = \frac{k_x^2}{3 \tau^2} K_2 (k_x \tau)$$

$$I_{-\nu} (x z) - L_\nu (x z) = \frac{2 \left(\frac{x}{2} \right)^\nu}{\sqrt{\pi} \; \Gamma \left(\nu + \frac{1}{2} \right) z^\nu} \int_0^\infty \sin x t \; \left(z^2 + t^2 \right)^{\nu - \frac{1}{2}} dt$$

ⓐ $\nu = -1$

$$\int_0^\infty \frac{\sin k_x t}{\left\{ t^2 + \tau^2 \right\}^{3/2}} \, dt = - \frac{\pi k_x}{2 z} \left\{ I_1 (k_x \tau) - L_{-1} (k_x \tau) \right\}$$

$$L_{-1} = L_1 + \frac{2}{\pi}$$

$$\int_0^\infty \frac{\sin k_x t}{\left\{t^2 + r^2\right\}^{3/2}}\, dt = -\frac{\pi}{2}\,\frac{k_x}{r}\left\{ I_1(k_x r) - L_1(k_x r)\right\} + \frac{k_x}{r}$$

ⓑ $\nu = -2$

$$\int_0^\infty \frac{\sin k_x \xi}{\left\{\xi^2 + r^2\right\}^{5/2}}\, d\xi = \frac{\pi}{6}\,\frac{k_x^2}{r^2}\left\{ I_2(k_x r) - L_{-2}(k_x r)\right\}$$

$$L_{-2} = L_2 + \frac{2 k_x r}{3\pi} - \frac{2}{\pi k_x r}$$

$$\int_0^\infty \frac{\sin k_x \xi}{\left\{\xi^2 + r^2\right\}^{5/2}}\, d\xi = \frac{\pi k_x^2}{6 r^2}\left\{ I_2(k_x r) - L_2(k_x r)\right\} - \frac{k_x^3}{9 r} + \frac{k_x}{3 r^3}$$

$$-\frac{\partial^2}{\partial z^2}\int_0^\infty \frac{e^{-j k_x \xi}}{\left\{r^2+\xi^2\right\}^{1/2}}\,d\xi \;=\; \frac{k_x}{r}\,K_1(k_x r) - \frac{z^2 k_x^2}{r^2}\,K_2(k_x r)$$

$$+\,j\,\frac{\pi}{2}\,\frac{k_x}{r}\left\{I_1(k_x r) - L_1(k_x r)\right\} - \frac{j k_x}{r}$$

$$+\,j\,\frac{\pi}{2}\,\frac{k_x^2 z^2}{r^2}\left\{I_2(k_x r) - L_2(k_x r)\right\}$$

$$-\,\frac{j z^2 k_x^3}{3r} + \frac{j z^2 k_x}{r}$$

APPENDIX G

ⓐ

$$W^{01} = - \int_{0}^{\infty} \frac{j k_x}{\left\{ z^2 + Y^2 \right\}} \cos k_y \eta \, d\eta + j k_x z^2 \int_{0}^{\infty} \frac{\cos k_y \eta}{\left\{ z^2 + \eta^2 \right\}^{3/2}} d\eta$$

$$= - j k_x K_0 (k_y z) + j k_x k_y z \, K_1 (k_y z)$$

when $z \longrightarrow 0$

$$K_0 (k_y z) \sim - \left\{ \gamma + \ln \frac{k_y z}{2} \right\} + O (z^2 \log z)$$

$$K_1 (k_y z) \sim \frac{1}{k_y z} + O (z^2 \log z)$$

$$W^{01} \sim j k_x \left\{ \gamma + \ln \frac{k_y}{2} + \ln z + 1 \right\} .$$

ⓑ

$$W^{02} = k_x \int_0^\infty \frac{\cos k_y Y \; K_1(k_x r)}{\{\eta^2 + z^2\}^{1/2}} \, d\eta \; - z^2 k_x^2 \int_0^\infty \frac{\cos k_y \eta \; K_2(k_x r)}{\{\eta^2 + z^2\}} \, d\eta$$

When $z \longrightarrow 0$ this integral has a singularity at $\eta = 0$.
Therefore we divide this integral into two parts

$$\int_0^\infty \{ \quad \} d\eta = \int_0^\varepsilon \{ \quad \} d\eta + \int_\varepsilon^\infty \{ \quad \} d\eta$$

where $1 >> \varepsilon >> z$. Consider the first integral

$$k_x \int_0^\infty \frac{\cos k_y Y \; K_1(k_x r)}{\{\eta^2 + z^2\}^{1/2}} \, d\eta \sim \int_0^\varepsilon \frac{1}{\eta^2 + z^2} \, d\eta$$

$$\sim \frac{\pi}{2} \cdot \frac{1}{z}$$

$$k_x^2 z^2 \int_0^\varepsilon \frac{\cos k_y \eta \; K_2(k_x r)}{\eta^2 + z^2} \sim 2 z^2 \int_0^\varepsilon \frac{1}{\{Y^2 + z^2\}^2} \, d\eta$$

$$\sim \frac{1}{\varepsilon} + \frac{\pi}{2} \cdot \frac{1}{z}$$

Consider the second integral

$$k_x \int_{\varepsilon}^{\infty} \frac{\cos k_y \eta \;\; K_1(k_x r)}{\left\{\eta^2 + z^2\right\}^{1/2}} \, d\eta \quad \sim \quad k_x \int_{\varepsilon}^{\infty} \frac{\cos k_y \eta \;\; K_1(k_x \eta)}{\eta} \, d\eta \, .$$

$$k_x^2 z^2 \int_{\varepsilon}^{\infty} \frac{\cos k_y \eta \;\; K_2(k_x r)}{\left\{\eta^2 + z^2\right\}} \, d\eta \quad \sim \quad k_x^2 z^2 \int_{\varepsilon}^{\infty} \frac{\cos k_y \eta \;\; K_2(k_x \eta)}{\eta^2} \, d\eta$$

$$\sim \quad 0 \, .$$

Adding these two integrals we obtain

$$w^{02} \quad = \quad k_x \int_{\varepsilon}^{\infty} \frac{\cos k_y \eta \;\; K_1(k_x \eta)}{\eta} \, d\eta \quad - \quad \frac{1}{\varepsilon} \, .$$

ⓒ

$$W^{03} = j\, k_x \, \frac{\pi}{2} \int_0^\infty \frac{\cos k_y \eta}{r} \left\{ I_1(k_x r) - L_1(k_x r) \right\} d\eta$$

$$+ \; j\, k_x^2 \, z^2 \cdot \frac{\pi}{2} \int_0^\infty \frac{\cos k_y \eta}{r^2} \left\{ I_2(k_x r) - L_2(k_x r) \right\} d\eta$$

For small arguments

$$I_1(t) - L_1(t) \sim \frac{t}{2}$$

$$I_2(t) - L_2(t) \sim \frac{t^2}{8}$$

hence

$$\frac{I_1(k_x r) - L_1(k_x r)}{r} \sim \frac{I_1(k_x Y) - L_1(k_x Y)}{Y}$$

$$\frac{I_2(k_x r) - L_2(k_x r)}{r^2} \sim \frac{I_2(k_x y) - L_2(k_x Y)}{Y^2}$$

When $z \longrightarrow 0$

$$w^{03} = j\, k_x \frac{\pi}{2} \int_0^{\infty} \frac{\cos k_y \eta}{\eta} \left\{ I_1(k_x \eta) - L_1(k_x \eta) \right\} d\eta$$

ⓓ

$$w^{04} = - j \frac{k_x^3 z^2}{3} \int_0^{\infty} \frac{\cos k_y \eta}{r}\, d\eta$$

$$= - j \frac{k_x^3 z^2}{3} K_0(k_y z)$$

when $z \longrightarrow 0$

$$w^{04} \sim O(z^2 \log z).$$

APPENDIX H

ⓐ Consider the function

$$F = k_x \int_{\varepsilon}^{\infty} \frac{\cos k_y \eta \; K_1(k_x \eta)}{\eta} \, d\eta \; - \; \frac{1}{\varepsilon}$$

Let

$$I = \int_{\varepsilon}^{\infty} \frac{\cos k_y \eta \quad K_1(k_x \eta)}{\eta} \, d\eta$$

$$= \int_{\varepsilon k_x}^{\infty} \frac{\cos a\eta \quad K_1(\eta)}{\eta} \, d\eta$$

$$a = \frac{k_y}{k_x}$$

$$\frac{dI}{da} = \int_{\varepsilon k_x}^{\infty} \sin a\eta \quad K_0'(\eta) \, d\eta .$$

$$= K_0(\eta) \sin \eta a \Big|_{\varepsilon k_x}^{\infty} - a \int_{\varepsilon k_x}^{\infty} \cos a\eta \, K_0(\eta) \, d\eta$$

$$= - a \cdot \frac{\pi}{2} \frac{1}{\sqrt{1 + a^2}}$$

Integrating

$$I = - \frac{\pi}{2} \sqrt{1 + a^2} + \text{const.}$$

when $a = 0$ $\qquad I = \int_{\varepsilon k_x}^{\infty} \frac{K_1(\eta)}{\eta} \, d\eta \, .$

$$I = \frac{\pi}{2} - \frac{\pi}{2} \sqrt{1 + a^2} + \int_{\varepsilon k_x}^{\infty} \frac{K_1(\eta)}{\eta} \, d\eta$$

$$F = - \frac{\pi}{2} k_x \left\{ \sqrt{1 + a^2} - 1 \right\} + k_x \left\{ \int_{\varepsilon k_x}^{\infty} \frac{K_1(\eta)}{\eta} \, d\eta - \frac{1}{\varepsilon k_x} \right\}$$

$$\int_{\varepsilon k_x}^{\infty} \frac{K_1(\eta)}{\eta}\, d\eta \quad - \quad \frac{1}{\varepsilon k_x} \quad = \; - \pi/2 .$$

$$F \; = \; - \frac{\pi}{2} \; k_x \sqrt{1 + a^2}$$

ⓑ

$$\int_{0}^{\infty} \frac{\cos a\eta}{\eta} \left\{ I_1(\eta) - L_1(\eta) \right\} d\eta$$

$$= \frac{2}{\pi} \left\{ \sqrt{1 + a^2} \;\log \frac{1 + \sqrt{1 + a^2}}{a} \; - 1 \right\}$$

APPENDIX L

$$I = \frac{1}{\pi} \int_0^\infty \frac{d\rho}{\sqrt{2+\rho}\,\sqrt{\rho}}\; e^{-2\rho \bar{k}_y} \int_0^\infty \frac{e^{-q\lambda}}{(\rho+q)} \sqrt{q}\; dq$$

Using the result

$$\int_0^\infty \frac{e^{-q\lambda}}{(\rho+q)} \sqrt{q}\; dq = \sqrt{\frac{\pi}{\lambda}} - \sqrt{\rho}\,\pi\, e^{\rho\lambda} \operatorname{erfc}\sqrt{\lambda\rho}$$

we obtain

$$I = \frac{1}{\sqrt{\pi\lambda}} \int_0^\infty \frac{d\rho}{\sqrt{2+\rho}}\; \frac{e^{-2\rho\bar{k}_y}}{\sqrt{\rho}}\; d\rho - \int_0^\infty \frac{e^{-\mu\rho}}{\sqrt{2+\rho}} \operatorname{erfc}\sqrt{\lambda\rho}\; d\rho$$

With the following result

$$\int_0^\infty \frac{d\rho}{\sqrt{2+\rho}}\; \frac{e^{-2\rho\bar{k}_y}}{\sqrt{\rho}}\; d\rho = e^{2\bar{k}_y} \int_1^\infty \frac{e^{-2\bar{k}_y t}}{\sqrt{t^2-1}}\; dt = e^{2\bar{k}_y} K_0(2\bar{k}_y)$$

we obtain

$$I = \frac{1}{\sqrt{\pi\lambda}}\; e^{2\bar{k}_y} K_0(2\bar{k}_y) - C$$

where $$C = \int_0^\infty \frac{e^{-\mu\rho}}{\sqrt{2+\rho}} \operatorname{erfc}\sqrt{\lambda\rho}\; d\rho .$$

APPENDIX J

Strength of the trailing and the shed vortices in the upper plate wake (Fig.10) is given by eq.(65 & 66)

$$\gamma_w = -i\bar{k}_x U_\infty f_2(1)\exp(i\bar{k}_x)\exp(-ik_x x)\exp(ik_y y)\exp(i\omega t)$$

$$\delta_w = i\bar{k}_y U_\infty f_2(1)\exp(i\bar{k}_x)\exp(-ik_x x)\exp(ik_y y)\exp(i\omega t) \qquad (J1)$$

From Biot-Savart law, the induced normal velocity due to this vortex sheet at the 3/4 chord point is

$$w\left(\frac{1}{2}, z\right) = -\frac{1}{4\pi} f_2(1) \int_{-\infty}^{\infty} \frac{e^{i\bar{k}_y \eta}}{\left\{1 + z^2 + \eta^2\right\}^{3/2}}\, d\eta$$

$$+ \frac{i\bar{k}_x f_2(1) e^{i\bar{k}_x}}{4\pi} \int_{\xi=1}^{\infty} \int_{\eta=-\infty}^{\infty} \frac{e^{-i\bar{k}_x \xi}\, e^{i\bar{k}_y \eta} \left(\frac{1}{2} - \xi\right)}{\left\{\left(\frac{1}{2} - \xi\right)^2 + \eta^2 + z^2\right\}^{3/2}}\, d\xi\, d\eta$$

$$+ \frac{i\bar{k}_y f_2(1) e^{i\bar{k}_x}}{4\pi} \int_{\xi=-\frac{1}{2}}^{\infty} \int_{\eta=-\infty}^{\infty} \frac{e^{-i\bar{k}_x \xi}\, e^{i\bar{k}_y \eta}\, d\xi\, d\eta}{\left\{\left(\frac{1}{2} - \xi\right)^2 + \eta^2 + z^2\right\}^{3/2}} \qquad (J2)$$

Evaluating the η integrals and simplifying it we obtain

$$w\left(\tfrac{1}{2}, z\right) = -\frac{1}{2\pi} f_2(1) \frac{1}{1+z^2}$$

$$-\frac{\bar{k}_x^2+\bar{k}_y^2}{2\pi} f_2(1) e^{i\frac{\bar{k}_x}{2}} \int_0^\infty e^{-i\bar{k}_x t} K_0\left\{\bar{k}_y\sqrt{t^2+z^2}\right\} dt$$

$$+\frac{\bar{k}_x^2 f_2(1) e^{i\frac{\bar{k}_x}{2}}}{2\pi} \int_0^{\frac{1}{2}} e^{-i\bar{k}_x t} K_0\left\{\bar{k}_y\sqrt{t^2+z^2}\right\} dt$$

$$-\frac{\bar{k}_y^2 f_2(1) e^{i\frac{\bar{k}_x}{2}}}{2\pi} \int_{-1}^0 e^{-i\bar{k}_x t} K_0\left\{\bar{k}_y\sqrt{t^2+z^2}\right\} dt$$

$$-\frac{i\bar{k}_x}{2\pi} f_2(1) K_0\left\{\bar{k}_y\sqrt{\tfrac{1}{2}^2+z^2}\right\} \qquad J3$$

When z = 0, we obtain the induced velocity due to the upper plate and is given by

$$\frac{W_{IN})_{UPPER}}{U_\infty} = -\frac{f_2(1)}{2\pi}\left\{1 + 2\bar{k}_y^2 e^{i\frac{\bar{k}_x}{2}} E1 + \bar{k}_x^2 e^{i\frac{\bar{k}_x}{2}} E2\right.$$

$$\left. - \bar{k}_y^2 e^{i\frac{\bar{k}_x}{2}} E3 + i\bar{k}_x K_0\left(\frac{\bar{k}_y}{2}\right)\right\} \qquad J4$$

$$\frac{W_{IN})_{UPPER}}{U_\infty} = -\frac{f_2(1)}{2\pi} \, R1 \tag{J5}$$

where

$$E1 = \int_0^\infty \cos \bar{k}_x t \; K_0\{\bar{k}_y t\}\, dt = \frac{\pi}{2} \frac{1}{\sqrt{\bar{k}_x^2 + \bar{k}_y^2}} \tag{J6}$$

$$E2 = \int_{\frac{1}{2}}^\infty e^{-i\bar{k}_x t} \; K_0\{\bar{k}_y t\}\, dt \tag{J7}$$

$$E3 = \int_1^\infty e^{i\bar{k}_x t} \; K_0\{\bar{k}_y t\}\, dt \tag{J8}$$

Substituting for z = h and changing the sign we obtain the induced velocity due to the lower plate and is given by

$$\frac{W_{IN})_{LOWER}}{U_\infty} = \frac{f_2(1)}{2\pi} \left\{ \frac{1}{1+h^2} + \left(\bar{k}_x^2 + \bar{k}_y^2\right) e^{i\frac{\bar{k}_x}{2}} F1 - \bar{k}_x^2 e^{i\frac{\bar{k}_x}{2}} F2 \right.$$

$$\left. + \bar{k}_y^2 \, e^{i\frac{\bar{k}_x}{2}} F3 + i\bar{k}_x \, K_0\left\{\bar{k}_y \sqrt{\tfrac{1}{2}^2 + h^2}\right\} \right] \tag{J9}$$

$$\frac{W_{IN})_{LOWER}}{U_\infty} = \frac{f_2(1)}{2\pi} \, R2 \tag{J10}$$

where

$$F1 = \int_0^{\infty} e^{-i\bar{k}_x t} K_0\left\{ \bar{k}_y \sqrt{t^2+h^2} \right\} dt$$

$$= \frac{\pi}{2} \frac{1}{\sqrt{\bar{k}_x^2 + \bar{k}_y^2}} e^{-h\sqrt{\bar{k}_x^2 + \bar{k}_y^2}} - i \int_0^{\infty} \sin \bar{k}_x t \; K_0\left\{ \bar{k}_y \sqrt{t^2+h^2} \right\} dt$$

$$F2 = \int_0^{\frac{1}{2}} e^{-i\bar{k}_x t} K_0\left\{ \bar{k}_y \sqrt{t^2+h^2} \right\} dt$$

$$F3 = \int_0^{1} e^{i\bar{k}_x t} K_0\left\{ \bar{k}_y \sqrt{t^2+h^2} \right\} dt \qquad (J11)$$

Equating the total induced velocity to the negative of the gust velocity we obtain an expression for $f_2(1)$.

$$-\frac{w}{U_\infty} e^{-i\frac{\bar{k}_x}{2}} = -\frac{f_2(1)}{2\pi} R1 + \frac{f_2(1)}{2\pi} R2 \qquad (J12)$$

hence

$$f_2(1) = \frac{w}{U_\infty} \frac{2\pi e^{-i\frac{\bar{k}_x}{2}}}{R1 - R2} \qquad (J13)$$

All the integrals involed in R1 & R2 are evaluated numerically.

APPENDIX K

In this section we will derive the solution of the eq.(168), using Green's function method.

$$\frac{d^2\bar{v}}{dy^2} - k^2\bar{v} - \frac{\bar{v}}{U-c}\frac{d^2U}{dY^2} = \delta(Y-H) \qquad (K1)$$

Let G(y,k,c,H) be the solution of this equation, hence

$G^-(y,k,c,H) = A\,\psi_1 + B\,\psi_2$ for $y<H$

$G^+(y,k,c,H) = C\,\psi_1 + D\,\psi_2$ for $y>H$.

(K2)

The boundary conditions are

(1) $G' - k\,G = 0;\ y \to -\infty$

$G' + k\,G = 0;\ y \to +\infty$

(2) $G^+(y=H,k,c,H) = G^-(y=H,k,c,H)$

(3)

$$\frac{d}{dY}G^+(y,k,c,H)\Big|_{y=H} - \frac{d}{dY}G^{-1}(Y,k,c,H)\Big|_{y=H} = 1.$$

Applying these boundary conditions to eq.(K2) and using the definition for ψ_1 and ψ_2 from eq.(169), we get

B=C=0

$$A = \frac{\psi_2(H)}{\psi_1(H)\,\psi_2'(H) - \psi_2(H)\,\psi_1'(H)} \qquad (K3)$$

$$B = \frac{\psi_1(H)}{\psi_1(H)\,\psi_2'(H) - \psi_2(H)\,\psi_1'(H)} \qquad (K4)$$

Substituting for $\psi_1(H)$ and $\psi_2(H)$ from eq.(169) gives

$$\begin{aligned} &\psi_1(H)\,\psi_2'(H) - \psi_2(H)\,\psi_1'(H) \\ &= \Big\{ \big(\phi_1'(-\infty) - |k|\,\phi_1(-\infty)\big)\big(\phi_2'(+\infty) + |k|\,\phi_2(+\infty)\big) \\ &\quad - \big(\phi_1'(+\infty) + |k|\,\phi_1(+\infty)\big)\big(\phi_2'(+\infty) - |k|\,\phi_2(+\infty)\big)\Big\} \\ &\quad \Big\{ \phi_1(H)\,\phi_2'(H) - \phi_1'(H)\,\phi_2(H) \Big\} \end{aligned} \qquad (K5)$$

Noting that the Wronskian of the eq.(K1) is independent of y, we have

$$\phi_1(H)\,\phi_2'(H) - \phi_1'(H)\,\phi_2(H) = 1.$$

From eqs. (K3-K6) we obtain

$$G(y, k, c, H) = -\frac{\psi_2(H)\,\psi_1(Y)}{2\left(\phi_1'(+\infty) + |k|\,\phi_1(+\infty)\right)\left(\phi_2'(+\infty) + |k|\,\phi_2(+\infty)\right)}$$

$$y < H$$

$$= -\frac{\psi_2(Y)\,\psi_1(H)}{2\left(\phi_1'(+\infty) + |k|\,\phi_1(+\infty)\right)\left(\phi_2'(+\infty) + |k|\,\phi_2(+\infty)\right)}$$

$$y > H.$$

Appendix J

From eq.(181) we get the following equations for the velocity field $\bar{v}$.

Region (1)

$$\bar{v} = A\ e^{-\alpha y}. \tag{L1}$$

Region (2)

$$\bar{v} = B\ e^{-\alpha y} + C\ e^{+\alpha y}. \tag{L2}$$

Region (3)

$$\bar{v} = D\ e^{-\alpha y} + E\ e^{+\alpha y}. \tag{L3}$$

Region (4)

$$\bar{v} = F\ e^{+\alpha y}. \tag{L4}$$

Kinematic boundary condition eq. (183) yields

at surface 'a'

$$\eta_a\ ik_x\ (w(h-H)-c) = A\ e^{-\alpha h} - v_{0a}/cik_x.$$

$$\eta_a\ ik_x\ (w(h-H)-c) = B\ e^{-\alpha h} + C\ e^{+\alpha h} - v_{0a}/cik_x.$$

at surface 'b'

$$\eta_b \; ik_x \; (-wH-U-c) = B + C - v_{0b}/cik_x .$$

$$\eta_b \; ik_x \; (-wH-U-c) = D + E - v_{0b}/cik_x .$$

at surface 'c'

$$\eta_c \; ik_x \; (w(-h-H)-c) = D \; e^{+\alpha h} + E \; e^{-\alpha h} - v_{0c}/cik_x$$

$$\eta_c \; ik_x \; (w(-h-H)-c) = F \; e^{-\alpha h} - v_{0c}/cik_x .$$

From the above equations we determine A,B,C,D,E,F.

$$A \, e^{-\alpha h} = - \; \tilde{\eta}_a \left\{ c + w(H-h) \right\} \iota k_x + \frac{\tilde{v}_{oa}}{c \iota k_x} \qquad (L5)$$

$$B = - \frac{\iota k_x \left\{ \tilde{\eta}_b (wH+c+U) e^{\alpha h} - \tilde{\eta}_a \left(w(H-h)+c \right) \right\}}{e^{\alpha h} - e^{-\alpha h}} + \frac{\tilde{v}_{ob} e^{\alpha h} - \tilde{v}_{ob}}{c \iota k_x \{ e^{\alpha h} - e^{-\alpha}}$$

(L6

$$C = \frac{\iota k_x \left\{ \tilde{\eta}_b (wH+U+c) \; e^{-\alpha h} - \tilde{\eta}_a (c+w(H-h)) \right\}}{e^{\alpha h} - e^{-\alpha h}} - \frac{\tilde{v}_{ob} e^{-\alpha h} - \tilde{v}_{oa}}{c \iota k_x \{ e^{\alpha h} - e^{-\alpha}}$$

(L7)

$$D = \frac{\iota k_x \left\{ \tilde{\eta}_b (wH + c + U)\, e^{-\alpha h} - \tilde{\eta}_c (w(H+h) + c) \right\}}{e^{\alpha h} - e^{-\alpha h}} - \frac{\tilde{V}_{ob}\, e^{-\alpha h} - \tilde{V}_{oc}}{c \iota k_x \{ e^{\alpha h} - e^{-\alpha h} \}} \tag{L8}$$

$$E = - \frac{\iota k_x \left\{ \tilde{\eta}_b (wH + c + U)\, e^{\alpha h} - \tilde{\eta}_c (w(H+h) + c) \right\}}{e^{\alpha h} - e^{-\alpha h}} + \frac{\tilde{V}_{ob}\, e^{\alpha h} - \tilde{V}_{oc}}{c \iota k_x \{ e^{\alpha h} - e^{-\alpha h} \}} \tag{L9}$$

$$F e^{-\alpha h} = \frac{\tilde{V}_{oc}}{c \iota k_x} - \tilde{\eta}_c \{ w(H+h) + c \} \iota k_x \tag{L10}$$

Applying eq.(182) to the pressure boundary conditions at the interfaces we get

at surface 'a'

$$- \iota k_x (w(H-h) - c)\{-\alpha A e^{-\alpha h}\} + \iota k_x A e^{-\alpha h} w + \frac{w(h-H)}{c} \frac{\partial \tilde{V}_{oa}}{\partial y}$$

$$- \frac{\tilde{V}_{oa}}{c} w = - \iota k_x (w(h-H) - c)\left(-\alpha B e^{-\alpha h} + c \alpha e^{\alpha h}\right)$$

$$+ \iota k_x \left(B e^{-\alpha h} + c e^{\alpha h}\right)\left(\frac{U}{h} + w\right) + \frac{w(h-H)}{c} \frac{\partial \tilde{V}_{oa}}{\partial y} - \frac{\tilde{V}_{oa}}{c} \left(\frac{U}{h} + w\right.$$

at surface 'b'

$$-\iota k_x\left(-WH-U-c\right)\left(-\alpha B+C\alpha\right)+\iota k_x\left(B+C\right)\left(\frac{U}{h}+W\right)$$

$$+\frac{1}{c}\left(-U-Wh\right)\frac{\partial\tilde{V}_{ob}}{\partial y}-\frac{\tilde{V}_{ob}}{c}\left(\frac{U}{h}+W\right)=$$

$$-\iota k_x\left(-WH-U-c\right)\left(-\alpha D+E\alpha\right)$$

$$+\iota k_x\left(-\frac{U}{h}+W\right)\left(D+E\right)+\left(-U-WH\right)\frac{1}{c}-\frac{\partial\tilde{V}_{ob}}{\partial y}+\frac{\tilde{V}_{ob}}{c}\left(\frac{U}{h}-W\right)$$

at surface 'c'

$$-\iota k_x\left(W\left(-h-H\right)-c\right)\left(-\alpha D e^{\alpha h}+E\alpha e^{-\alpha h}\right)$$

$$+\iota k_x\left(D e^{\alpha h}+E e^{-\alpha h}\right)\left(-\frac{U}{h}+W\right)$$

$$+\frac{W\left(-h-H\right)}{c}\frac{\partial\tilde{V}_{oc}}{\partial y}-\frac{\tilde{V}_{oc}}{c}\left(W-\frac{U}{h}\right)=-\iota k_x\left(W\left(-h-H\right)-c\right)F\alpha e^{-\alpha}$$

$$+\iota k_x F e^{-\alpha h}W+\frac{W\left(-h-H\right)}{c}\frac{\partial\tilde{V}_{oc}}{\partial y}-\frac{\tilde{V}_{oc}}{c}W$$

Substituting for A,B,C,D,E,F from the eqs. (L5-L8) we obtain three simultaneous equations for η_a, η_b and η_c.

In region (1)

$$\bar{v} = A\, e^{-\alpha y}.$$

Substituting for A from eq.(L5) we obtain

$$\bar{V} = -\, e^{-\alpha(y-h)} \left\{ \frac{\mu}{2}\, \frac{\alpha\, e^{-\alpha(H-h)}}{c\,i\,k_x} + \tilde{\eta}_a\, i\,k_x\, \big(w(H-h) + c\big) \right\}$$